IAEA TECDOC SERIES

IAEA-TECDOC-1978

Structural Materials for Heavy Liquid Metal Cooled Fast Reactors

Proceedings of a Technical Meeting

IAEA
International Atomic Energy Agency

STRUCTURAL MATERIALS FOR HEAVY LIQUID METAL COOLED FAST REACTORS

The following States are Members of the International Atomic Energy Agency:

AFGHANISTAN
ALBANIA
ALGERIA
ANGOLA
ANTIGUA AND BARBUDA
ARGENTINA
ARMENIA
AUSTRALIA
AUSTRIA
AZERBAIJAN
BAHAMAS
BAHRAIN
BANGLADESH
BARBADOS
BELARUS
BELGIUM
BELIZE
BENIN
BOLIVIA, PLURINATIONAL STATE OF
BOSNIA AND HERZEGOVINA
BOTSWANA
BRAZIL
BRUNEI DARUSSALAM
BULGARIA
BURKINA FASO
BURUNDI
CAMBODIA
CAMEROON
CANADA
CENTRAL AFRICAN REPUBLIC
CHAD
CHILE
CHINA
COLOMBIA
COMOROS
CONGO
COSTA RICA
CÔTE D'IVOIRE
CROATIA
CUBA
CYPRUS
CZECH REPUBLIC
DEMOCRATIC REPUBLIC OF THE CONGO
DENMARK
DJIBOUTI
DOMINICA
DOMINICAN REPUBLIC
ECUADOR
EGYPT
EL SALVADOR
ERITREA
ESTONIA
ESWATINI
ETHIOPIA
FIJI
FINLAND
FRANCE
GABON
GEORGIA
GERMANY
GHANA
GREECE
GRENADA
GUATEMALA
GUYANA
HAITI
HOLY SEE
HONDURAS
HUNGARY
ICELAND
INDIA
INDONESIA
IRAN, ISLAMIC REPUBLIC OF
IRAQ
IRELAND
ISRAEL
ITALY
JAMAICA
JAPAN
JORDAN
KAZAKHSTAN
KENYA
KOREA, REPUBLIC OF
KUWAIT
KYRGYZSTAN
LAO PEOPLE'S DEMOCRATIC REPUBLIC
LATVIA
LEBANON
LESOTHO
LIBERIA
LIBYA
LIECHTENSTEIN
LITHUANIA
LUXEMBOURG
MADAGASCAR
MALAWI
MALAYSIA
MALI
MALTA
MARSHALL ISLANDS
MAURITANIA
MAURITIUS
MEXICO
MONACO
MONGOLIA
MONTENEGRO
MOROCCO
MOZAMBIQUE
MYANMAR
NAMIBIA
NEPAL
NETHERLANDS
NEW ZEALAND
NICARAGUA
NIGER
NIGERIA
NORTH MACEDONIA
NORWAY
OMAN
PAKISTAN
PALAU
PANAMA
PAPUA NEW GUINEA
PARAGUAY
PERU
PHILIPPINES
POLAND
PORTUGAL
QATAR
REPUBLIC OF MOLDOVA
ROMANIA
RUSSIAN FEDERATION
RWANDA
SAINT LUCIA
SAINT VINCENT AND THE GRENADINES
SAMOA
SAN MARINO
SAUDI ARABIA
SENEGAL
SERBIA
SEYCHELLES
SIERRA LEONE
SINGAPORE
SLOVAKIA
SLOVENIA
SOUTH AFRICA
SPAIN
SRI LANKA
SUDAN
SWEDEN
SWITZERLAND
SYRIAN ARAB REPUBLIC
TAJIKISTAN
THAILAND
TOGO
TRINIDAD AND TOBAGO
TUNISIA
TURKEY
TURKMENISTAN
UGANDA
UKRAINE
UNITED ARAB EMIRATES
UNITED KINGDOM OF GREAT BRITAIN AND NORTHERN IRELAND
UNITED REPUBLIC OF TANZANIA
UNITED STATES OF AMERICA
URUGUAY
UZBEKISTAN
VANUATU
VENEZUELA, BOLIVARIAN REPUBLIC OF
VIET NAM
YEMEN
ZAMBIA
ZIMBABWE

The Agency's Statute was approved on 23 October 1956 by the Conference on the Statute of the IAEA held at United Nations Headquarters, New York; it entered into force on 29 July 1957. The Headquarters of the Agency are situated in Vienna. Its principal objective is "to accelerate and enlarge the contribution of atomic energy to peace, health and prosperity throughout the world''.

IAEA-TECDOC-1978

STRUCTURAL MATERIALS FOR HEAVY LIQUID METAL COOLED FAST REACTORS

PROCEEDINGS OF A TECHNICAL MEETING

INTERNATIONAL ATOMIC ENERGY AGENCY
VIENNA, 2021

COPYRIGHT NOTICE

For further information on this publication, please contact:

Nuclear Power Technology Development Section
International Atomic Energy Agency
Vienna International Centre
PO Box 100
1400 Vienna, Austria
Email: Official.Mail@iaea.org

Printed by the IAEA in Austria
September 2021

IAEA Library Cataloguing in Publication Data

Names: International Atomic Energy Agency.
Title: Structural materials for heavy liquid metal cooled fast reactors : proceedings of a technical meeting / International Atomic Energy Agency.
Description: Vienna : International Atomic Energy Agency, 2021. | Series: IAEA TECDOC series, ISSN 1011–4289 ; no. 1978 | Includes bibliographical references.
Identifiers: IAEAL 21-01446 | ISBN 978-92-0-128821-9 (paperback : alk. paper) | ISBN 978-92-0-128721-2 (pdf)
Subjects: LCSH: Nuclear reactors — Materials. | Liquid metal cooled reactors. | Fast reactors.

FOREWORD

The compatibility of structural materials, such as steels with lead and lead–bismuth eutectic, poses a significant challenge in the development of heavy liquid metal cooled fast reactors. Factors including very high temperatures, high fast neutron flux, high irradiation exposure and corrosiveness create an extreme environment for materials in advanced reactor systems. In order to develop innovative nuclear energy systems, it is crucial that liquid coolants be compatible with structural materials and that appropriate structural materials for advanced reactor concepts be selected. The safety, feasibility and optimization of innovative nuclear systems depend on the capability of the selected materials to withstand expected operating conditions.

To understand the status of research and development in this area and to provide a forum to exchange information on related topics, the IAEA organized a Technical Meeting on Structural Materials for Heavy Liquid Metal Cooled Fast Reactors in October 2019. A total of 15 peer reviewed papers were presented during the meeting, which was divided into three sessions: (i) heavy liquid metal compatibility with structural materials: phenomena, modelling and operational experience; (ii) corrosion mitigation measures: coating, new structural materials, environmental conditioning; and (iii) qualification programmes of structural materials for heavy liquid metal fast reactors. Three group discussions — on outstanding research challenges, new materials and coating techniques and industrialization — provided a sound understanding of the most relevant topics in this area. This publication presents the proceedings, summaries and conclusions of the meeting and the papers presented at the event.

The IAEA expresses its appreciation to all contributors to this publication. The IAEA officers responsible for this publication were V. Kriventsev and C. Batra of the Division of Nuclear Power.

EDITORIAL NOTE

This publication has been prepared from the original material as submitted by the contributors and has not been edited by the editorial staff of the IAEA. The views expressed remain the responsibility of the contributors and do not necessarily represent the views of the IAEA or its Member States.

Neither the IAEA nor its Member States assume any responsibility for consequences which may arise from the use of this publication. This publication does not address questions of responsibility, legal or otherwise, for acts or omissions on the part of any person.

The use of particular designations of countries or territories does not imply any judgement by the publisher, the IAEA, as to the legal status of such countries or territories, of their authorities and institutions or of the delimitation of their boundaries.

The mention of names of specific companies or products (whether or not indicated as registered) does not imply any intention to infringe proprietary rights, nor should it be construed as an endorsement or recommendation on the part of the IAEA.

The authors are responsible for having obtained the necessary permission for the IAEA to reproduce, translate or use material from sources already protected by copyrights.

The IAEA has no responsibility for the persistence or accuracy of URLs for external or third party Internet web sites referred to in this publication and does not guarantee that any content on such web sites is, or will remain, accurate or appropriate.

CONTENTS

1. INTRODUCTION

1.1.BACKGROUND

The innovative technology of fast reactors offers several advantages, such as higher utilization of the natural uranium, reduction of highly radioactive minor actinides and the ability to operate in a closed fuel cycle. The fast neutron spectrum allows fast reactors to increase the energy yield from natural uranium by a factor of sixty to seventy compared to the thermal spectrum reactors. This increased yield would allow for a sustainable fuel supply for nuclear power programmes that would last for thousands of years based on proven uranium resources as well as for a significant improvement of nuclear waste management. Since the beginning of the nuclear era, sodium has been used in nuclear reactors due to its attractive physical properties, such as high thermal conductivity and relatively high boiling temperature, and also because sodium is a very weak moderator and weak absorber of neutrons. Sodium technology has reached its maturity and has more than 500 reactor-years of operation experience. However, sodium reacts aggressively with water and air oxygen, and thus requires special measures and designs of the heat removal systems to avoid sodium contact with water and prevent sodium fires. To overcome these challenges, other coolants are considered as alternatives. Fast reactors cooled by heavy liquid metals (HLM), such as lead or lead-bismuth eutectic (LBE) alloy also offers improved safety and reliability, as the coolant does not react chemically with water and air, and has a high boiling temperature and other attractive thermo-physical properties. This allows smaller dimensions of the reactor vessel, excludes the need for an intermediate circuit, and reduces the size of the reactor unit, which has a significant impact on economics of the construction. The deployment of the HLM cooled fast reactors could be an attractive benefit for the growing energy sector. The main structural materials used today in fast reactors are mostly stainless steels and various steel alloys. The heavy liquid metal coolants, such as lead and LBE have the ability to dissolve oxygen. With this in mind, by controlling the oxygen concentration in the liquid metal, a protective oxide film can be formed on the steel surface. These oxide films serve as a protection from the dissolution of the steel. State-of-the-art research focuses on new materials such as oxide dispersion strengthened (ODS) steels, refractory alloys, SiC ceramic matrix composites, MAX phase materials and coated materials. Various phenomena affect the properties and behaviour of steels during exposure to heavy liquid metals, including the dissolution of steel alloy elements, liquid metal embrittlement, non-passivating oxidation and others. Corrosion and degradation of standard steels have two major consequences on the operation of lead and lead-bismuth cooled fast reactors (LFRs): the loss of material owing to corrosion affects the integrity of structures and components, and the release of corrosion products in the coolant and formation of solid oxides that could lead to the blockage of the coolant circulation.

One of the main goals of the scientific community focused on LFRs is to explore and identify mitigation strategies that can reduce the degradation of materials in operation in order to ensure the safety and efficiency of the nuclear system. The mitigation measures should be based on a deep understanding of the physical phenomena and processes causing changes in the materials' properties. The major mitigation measures include HLM environmental control (e.g. operating at low temperature, active control of oxygen concentration or employment of corrosion inhibitors), the adoption of surface engineering solutions (such as protective coatings), and the development of innovative materials capable of withstanding harsh HLM environments.

Operation under controlled oxygen concentration and at low temperatures (below 450–480°C) has proven to be efficient against corrosion issues. However, experiments performed at higher temperatures have shown that oxygen control is less effective, and strong corrosion(depending on the steel type and experimental conditions) can occur as the temperature increases.

Several researchers consider using coatings on standard steels as the most viable solution in the short term having as advantage the use of materials with known properties and qualified for neutron irradiation.

The development of innovative materials (corrosion resistant to HLM) is a promising option to combat degradation phenomena in the long term. Alumina-forming austenitic (AFA) steels have shown very good performance in HLM environment compared to the standard steels or high-entropy alloys, as they have some unique compositions, microstructures and engineering properties. However, physics-based experimental validation is required to develop modelling tools able to simulate and analyse the long-term behaviour of materials in HLM when exposed to corrosive environments and/or irradiation.

In addition, fast-evolving HLM technologies require the establishment of a standardized procedures to perform corrosion and mechanical tests, as well as to assess the performance of manufactured materials in various shapes. The assessment of mechanical properties of materials in liquid metal and coated steels under irradiation is also a high priority; these properties should be measured in the relevant ranges of temperature, neutron fluence, stresses and HLM flow velocity for the different components.

Taking recent developments into consideration, and in order to identify gaps and needs, the IAEA Technical Working Group on Fast Reactors (TWG-FR) recommended a Technical Meeting on this topic. The technical meeting on *Structural Materials for Heavy Liquid Metal Cooled Fast Reactors* was held in Vienna in October 2019, addressing the IAEA Member States' expressed need for information exchange on projects and programs in the field, as well as for the identification of priorities based on the analysis of technology gaps to be covered through research and development (R&D) activities to be carried out at the international level under the IAEA's aegis. This document provides the summary of the technical sessions as well as full papers submitted and presented at the meeting. The papers have been peer reviewed.

1.2.OBJECTIVE

The purpose of the meeting was to discuss experiences, innovations, and technological challenges related to structural materials proposed for advanced reactors cooled by lead and lead-bismuth eutectic. The meeting provided a forum to promote and facilitate the exchange of information on structural materials for HLM cooled reactors at the national and international levels and to present and discuss the current status of R&D in this field. The objective of this document is to provide to the Member States a reference, summarizing the work presented, including the full contributions, by the participants.

1.3.SCOPE

This TECDOC presents the Proceedings of the Technical Meeting on Structural Materials for Heavy Liquid Metal Cooled Fast Reactors, which was held in October 2019 in Vienna. The document compiles summaries of the technical sessions, group discussions and includes the full peer-reviewed papers that were submitted to and presented at the meeting.

1.4.STRUCTURE

Section 1 provide the introduction to the document. Section 2 summarizes the technical/meeting session and discussions from the technical meeting. Section 3 provides a summary of group discussion and Section 4 highlights main summary and conclusions from the meeting. Full papers submitted to the meeting are also included in this document, categorized by technical sessions.

2. SUMMARY OF MEETING SESSIONS

2.1. SESSION I: HLM COMPATIBILITY WITH STRUCTURAL MATERIALS: PHENOMENA, MODELLING AND OPERATIONAL EXPERIENCE

K. Tucek (European Commission, Joint Research Centre),

Session I discussed aspects related to the structural material compatibility with HLM, specifically what concerns the involved phenomena, performed modelling and experimental activities, as well as acquired out-of-pile operational experience. The Session included six presentations from four IAEA Member States and one International Organisation (European Commission, Joint Research Centre/JRC).

The first presentation of A. Hojná (CVR, Czech Republic) provided a very comprehensive overview of experimental assessments of the structural material compatibility of T91 ferritic martensitic steel and 15-15Ti austenitic steel with lead and lead-bismuth eutectic (LBE), forming also an important contribution to the discussion on the involved degradation phenomenology (in particular, the mechanism of crack initiation). The crack initiation tests verified the immunity of 15-15Ti to liquid metal embrittlement (LME) and environmentally assisted cracking (EAC),) and showed the sensitivity of T91 steel to LME/EAC with tendency to crack initiation in contact with liquid lead at 350-400 °C and liquid LBE at 300°C at stresses above ultimate tensile strength (UTS) and high plastic deformation. Based on the new and past research experience is stated that the T91 steel can be sensitive to LME/EAC in low flow HLM, but only beyond design loads of operation of Gen IV systems' components.

Two presentations were further given by RATEN ICN (Romania), reporting on R&D activities in support of the FALCON (Fostering ALfred CONstruction) Consortium and the deployment of the European demonstrator of the LFR technology (the Advanced Lead Fast Reactor European Demonstrator - ALFRED). The first presentation delivered by D. Gugiu (a neutronic study of refractory metals –Vanadium and Molybdenum alloys) envisaged to be used as alternative fuel cladding materials for the ALFRED reactor. The key observations are that the molibden alloys, especially Mo-Re alloys can significantly affect the neutron economy of the reactor when used as fuel pins cladding. Due to the microstructural changes that were observed the use Mo-Re alloys with high rhenium concentrations in neutron environments is not recommended. The use of vanadium results in an increase of the reactivity, but this effect could be managed by control rods or through changing the fissile enrichment during the design phase. The proposal for further studies of formation of gaseous elements with irradiation and increase of chromium was made.) In the second presentation, A. Nitu reported on the development of experimental capabilities for mechanical testing in molten lead at RATEN ICN, including the discussion of results of preliminary tensile tests conducted in-situ on 316L-grade austenitic steel.

The fourth presentation of V. Slugeň (Slovak University of Technology) explained benefits and challenges related to the use of positron annihilation spectroscopy (PAS) to study vacancy type defects induced by irradiation. The corrosion behaviour of steam generator tubes and related experimental activities supporting the ongoing construction licensing of the BREST-OD-300 LFR demonstrator in the Russian Federation were then comprehensively discussed by K. Shutko (NIKIET). The main conclusion here is that the material of heat exchanger tubes (EP302M stainless steel) demonstrates adoptable corrosion and corrosion-mechanical behavior for providing reliable stem generator (SG) designed service life of 30 years. In this context, the dual/combined aspects of steam corrosion and lead corrosion were addressed in relation to the

advanced austenitic steel (EP302M) considered for BREST-OD-300. Lastly, the sixth presentation of K. Tuček (EC/JRC) described development and acceptance testing of a new experimental facility for performing mechanical tests in molten lead in oxygen-controlled environment at temperatures up to 650 °C, and reported on outcomes of the first campaign of slowstrain rate tensile (SSRT) tests of T91 in oxygen-depleted lead environment. It shows that the ductility of T91 does not decrease compared to the reference tests in argon, meaning no LME effect occurred under these conditions. Further tests are recommended to make a conclusion about T91 susceptibility to LME in liquid lead.

Two special presentations were also made during this session, one presentation on the status of the IAEA CRP on fuel materials for fast reactors and other on IAEA publication rules and guidelines.

2.2.SESSION II: CORROSION MITIGATION MEASURES: COATING, NEW STRUCTURAL MATERIALS, ENVIRONMENTAL CONDITIONING

P. Szakalos (KTH), A. Weisenburger (KIT)

Eight presentations have been provided in the session highlighting different aspects of corrosion and corrosion mitigation strategies. Two presentations focused on corrosion of conventional ferritic/ martensitic and austenitic steels at different conditions. One of these presented the innovative steam generator design concept for the micro-modular LFR. The newly designed double walled layer functionally graded cellular (FGC) tubes were introduced and it was determined that the 316L austenitic steel is suitable for the lead-bismuth side. While the other proposed the addition of silicon for corrosion mitigation(Si-containing stainless steel and oxide dispersion strengthened-China low activation martensitic (ODS-CLAM) steel proposed by The Institute of Nuclear Energy Safety Technology, Chinese Academy of Sciences - INEST, CAS). The results revealed that the corrosion resistance with the addition of silicon gained a considerable improvement. Three presentations addressed the development of alumina-forming austenitic (AFA) steels; the first presented the results of corrosion resistance of AFA alloy. It was proven that the AFA alloy has promising corrosion behavior and mechanical properties compared with the AISI316L reference material. Thus, AFA steels could be suitable cladding materials used in in liquid lead at elevated temperatures. Other two presentations addressed high- entropy alloys (HEA) The use of Cr-Fe-Mn-Ni high entropy alloys with the lead melts can be recommended to a temperature of 500 ºC. By optimizing the HEA's composition and by adding additional alloys the operating temperature can be increased. The second presentation showed that elements like niobium or yttrium act either as a principal element (Nb in HEA) or as a minor additions (AFA) and can have a positive effect on the alumina scale formation in molten lead at elevated temperatures. The application of surface alloying was part of a combined presentation. One presentation highlights the use of nano-ceramic coatings in lead environment, proving that the coating guarantees the suppression of the permeation of tritium through the structural steel. Also, the chemical stability was verified, no delamination and no reduction of the thickness of the coating were observed. The other discussed the corrosion mitigation strategies induced by the impurities in the fuel. It was shown that the carbon impurities presented in the composition of the fuel can affect the condition of the steel cladding, mostly in the low temperature part of the temperature range. The possible way to reduce this effect is to block carbon penetration into the shell by adding into its composition an effective carbide former. This can suppress intergranular corrosion of steel cladding.

2.3.SESSION III: QUALIFICATION PROGRAMMES OF STRUCTURAL MATERIALS FOR HLM FAST REACTORS

B. Long (CIAE), E. Stergar (SCK•CEN)

In Session III, five presentations reviewed materials and their selection during the design stage in heavy liquid metal cooled nuclear systems such as MYRRHA, CiADS, ALFRED and SVBR-100. R&D on the application of structural and functional materials as well as possible co ating technologies has been discussed. Contributions came from Belgium (MYRRHA), Italy (ALFRED), Russia (SVBR-100) and China (CiADS).

In the first presentation, Z.G. Wang presented the R&D efforts around the silicon containing ferritic martensitic SIMP steel. This presentation was followed by an overview of the MYRRHA materials research program by E. Stergar and a presentation of S. Bassini about the materials qualification program for the ALFRED reactor. Their research shows that during the short-term exposure of AFA steels in liquid lead the corrosion resistance is very high. The long-term corrosion tests are yet to be done. A. Dedul gave some insights in the materials R&D and licensing processes of SVBR-100. The session was concluded with a presentation by B. Long about the status of the heavy liquid metal corrosion research in the China Institute of Atomic Energy (CIAE). The results show that austenitic stainless steel exhibits a good corrosion resistance under 400 ºC in liquid LBE, while ferritic/martensitic (FM) T91 steel has a slightly better corrosion resistance. And that FM T91 has excellent resistance to lead and bismuth corrosion below 550 ºC.

3. SUMMARY OF GROUP DISCUSSIONS

3.1.GROUP DISCUSSION I: OUTSTANDING RESEARCH CHALLENGES

K. Tucek (European Commission, Joint Research Centre), M. Vanazzi (CNCT)

Following the first portion of Session I, meeting participants discussed outstanding research challenges related to structural materials for HLM-cooled fast reactors. The discussion identified main structural materials currently used by the individual reactor concepts, together with reference temperature ranges of their application. It also identified further R&D needs, specifically: (i) materials qualification for the high-temperature operation; (ii) supporting pre-normative R&D; and (iii) development of representative design rules, as well as assessment and test procedures for improved standardization. In this context, the participants specifically highlighted a short-term need for an improved assessment of safety margins and related damage criteria for a robust safety demonstration of accident prevention. A general lack of fast neutron spectrum irradiation facilities to representatively qualify materials and components was also noted during the discussion. In support to the safety demonstration and licensing, the participants additionally recommended an establishment of an expert group to collect and assess available material performance data of candidate structural materials for HLM-cooled reactor concepts.

3.2.GROUP DISCUSION II: NEW MATERIALS AND COATING TECHNIQUES

P. Szakalos (KTH), A. Weisenburger (KIT)

There are several highly promising new materials and coating technologies available now based on alumina, either as self-healing alumina forming alloys or as coatings. Corrosion resistance and mechanical properties are very promising, however significant research work still needs to be done before commercialization. One specific FeCrAl-materials – Fe-10Cr-4Al-RE is already produced in the 10-ton scale. The view of the regulators was asked, and both argue that each technology has to demonstrate that in case of failure, no severe consequences will occur. In addition, the chemistry of the liquid metal has to be always considered, because it can accelerate or mitigate any corrosion attack. Self-healing of scales would be a preferable option, however in the field of accident tolerant fuel (ATF) even companies consider now the use of coatings for surface protection. Participants discussed technologies and materials. However, several of the considered mitigation techniques require significant further research and time before being fully deployable.

3.3.GROUP DISCUSSION III: INDUSTRIALIZATION

E. Stergar (SCK•CEN)

The group discussion was dedicated to the readiness of different new and innovative materials classes for potential use in heavy metal cooled reactors. Beside further developments of the 'classic' austenitic and ferritic/martensitic steels, optimized alumina forming steels have shown very favorable corrosion properties in heavy liquid metals. Nevertheless, other materials properties such as creep or their behavior in irradiation environment still have to be investigated.

In the discussion it was also pointed out that it is not always clear what type of information is required by the authorities to qualify a new material for use in a (new) nuclear system. Here it was pointed out that a common guideline, technical note, or the like identifying the actual expectations of the authorities towards the materials performance could be very beneficial.

During the discussion it also became clear that progress in materials development is very often determined by industry. If there is a significant direct economic benefit, then the developments (and licensing) are typically faster.

4. CONCLUSIONS

The following conclusions were discussed and agreed by the meeting participants:

Conclusions:

— At this meeting, a broad range of structural materials issues have been covered under the technical topics with a focus on structural material compatibility with HLM (phenomena, modelling and experimental activities), on corrosion mitigation measures (coating, surface engineering, environmental conditioning) as well as on new materials and coating techniques;
— For high temperature applications – there are concerns over durability, incomplete testing standards, etc.;
— As consequence, further needed R&D efforts have been identified regarding materials qualification for the high-temperature operation, as well as in the development of representative design rules and in the assessment and test procedures for improved standardisation;
— Participants have agreed and emphasized that there are already low temperature applications materials that can be explored and utilized;
— New materials and coating technologies based on alumina (as self-healing alumina forming alloys or as coatings) have been developed and are available, their corrosion and mechanical properties being very promising;
— It has been agreed that some of the discussed mitigation measures (new materials and coatings) require significant further research and time for qualification before commercialization;
— The technological readiness of various new and innovative materials for use in heavy metal cooled reactors has been addressed at large extent leading to the conclusion that optimized alumina forming steels show very favourable corrosion properties in heavy liquid metals, however some other properties (e.g., creep) or their behaviour under irradiation still require additional investigations;
— The issue of new material qualification for the use in new, innovative nuclear systems should be approached in a more comprehensive way able to harmonize the requirements of the regulatory bodies.

Possible Future Work:

— A study to address material science issues having impact on safety assessment regarding LFRs should be formulated and proposed;
— It is advised to organize a special technical session devoted to LFR materials at the FR21 conference; meeting participants are encouraged to submit papers;
— It is advised to invite a group of experts to voluntarily gather, compile and assess data about the existing ASS, FSS and advanced steels. The group could identify materials behaviour at high temperatures, radiation, etc. in order to draw the conclusions for improvements in testing standards, safety demonstration, data quality and further provide suggestions regarding long-term R&D agendas;
— To consider introducing a sub-group within the IAEA Technical Working Group on Fast Reactors (TWG-FR) either on: LFR, or on Structural Materials for Innovative Fast Reactors, or on Structural Materials for LFRs.
— To harmonize the knowledge, expertise and methodologies for proper data/results interpretation of corrosion testing;

— It is advised to take an action to address the need of fast reactor irradiation facilities for qualification of new structural materials at the international level.

ABBREVIATIONS

AFA	alumina-forming austenitic
ALFRED	Advanced Lead Fast Reactor European Demonstrator
ATF	accident tolerant fuel
CLAM	China Low Activation Martensitic
CIAE	China Institute of Atomic Energy
EAC	environmentally assisted cracking
EC/JRC	European Commission, Joint Research Centre
FALCON	fostering ALFRED construction
FGC	functionally graded cellular
F/M	ferritic/martensitic
HEA	high entropy alloys
HLM	heavy liquid metal
INEST CAS	Institute of Nuclear Energy Safety Technology, Chinese Academy of Sciences
LBE	lead bismuth eutectic
LME	liquid metal embrittlement
LFR	lead/LBE cooled fast reactors
ODS	oxide dispersed steel
PAS	positron annihilation spectroscopy
SG	steam generator
SIMP	Si containing ferritic martensitic steel
SSRT	slow strain rate tensile
TWG-FR	technical working group on fast reactors
UTS	ultimate tensile strength

PAPERS PRESENTED AT THE MEETING

SESSION I: HLM COMPATIBILITY WITH STRUCTURAL MATERIALS: PHENOMENA, MODELLING AND OPERATIONAL EXPERIENCE

KINETICS AND MECHANISM OF CRACK INITIATION OF LIQUID METAL EMBRITTLEMENT

The second level of the Environmentally Assisted Cracking understanding

A. HOJNÁ
Centrum výzkumu Řež s. r. o.
Řež/Husinec, Czech Republic
Email: anna.hojna@cvrez.cz

P. HALODOVÁ, L. ROZUMOVÁ, F. DI GABRIELE, M. CHOCHOLOUŠEK
Centrum výzkumu Řež s. r. o.
Řež/Husinec, Czech Republic
Email: anna.hojna@cvrez.cz

Abstract

The performance of two candidate structural materials T91 and 15-15Ti steel subjected to testing in HLM is discussed, with the focus on the description of degradation mechanism and kinetics connected to the phenomenon of Liquid Metal Embrittlement (LME). To summarize basic findings the paper traces the path to understanding of the degradation mechanism for two candidate structural materials in contact with Heavy Liquid Metals, HLM, a review of the present knowledge is presented. Considering Liquid Metal Embrittlement sensitivity as the first level assessment of the degradation, kinetics and initiation conditions belong to the second level, which means the understanding. Numerous experiments were carried out in liquid lead, Pb, and lead bismuth eutectic, LBE, at different temperatures and loading modes. Unlike the austenitic stainless steel 15-15Ti, the sensitivity to LME was found for the ferritic-martensitic steel T91 when in contact with HLM. Although higher crack growth rates are measured, the growth is stable, therefore kinetics is rather an EAC phenomenon than embrittlement. Moreover, this characteristic, together with the absence of HLM penetration in the steel and the observation of cleavage-like fracture, suggests that the adsorption based mechanism is in place.

1. INTRODUCTION

Qualification of structural materials in Heavy Liquid Metals (HLM) is a key issue in the development of HLM-cooled nuclear reactors [1, 2, 3]. Potential degradation (in absence of irradiation) includes general and local corrosion, environmentally assisted cracking (EAC) and embrittlement.

Embrittlement is generally considered as liquid metal atom's penetration /diffusion into bulk material, affecting the material mechanical behaviour. The phenomenon called Liquid Metal Embrittlement (LME) is typically associated with the risk of premature unstable fracture of components in contact with liquid metals. Historically, for structural materials in HLM, the LME was associated with the observation of the ductility trough, i.e. the decrease of ductility of tensile test specimen in contact with HLM, in relation to temperature and strain rate. Specifically, for T91 steel in lead, between 350 and 425 °C [4, 5] and for T91 in lead-bismuth eutectic (LBE) between 160 and 425 °C [4,6]. However, presence of Pb/Bi atoms inside the material has not been directly verified.

The explanation of the ductility trough was ambiguous. The observed effect can be explained by LME as well as EAC. One can consider that multiple EAC cleavage-like cracks initiating from the surface being in contact with HLM and their growing would also decrease the specimen elongation. The cleavage-like facets have been observed in many dedicated tests [4-15]. In addition, two facts supporting the idea of EAC have been shown for T91 steel recently.

Firstly, it was shown that the degradation disappeared if the surface was cleaned from the liquid PbBi after 1000 hour exposure at 500 °C with low oxygen [16]. Secondly, it was observed that the liquid metal atoms did not penetrate into bulk, but only locally into plastic deformed regions of the steel [17]. Based on recent studies, the degradation of the structural materials in HLM, which was attributed to LME, is better to consider as a special case of EAC, i.e. LME/EAC.

In the present understanding, the controlling factor of the LME/EAC degradation is likely the adsorption of liquid metal on a bare metal surface [18]. The key effects supporting the hypothesis are the followings: (i) the sensitivity to cracking decreases with increasing temperature, being the highest above the melting point (LBE: 127 °C, Pb: 328 °C); (ii) the crack propagation is faster than the diffusion rate of the heavy metal atoms; and (iii) wetting is the precondition for cracking [19].

In the 90's, the ferritic martensitic steel T91 (9%Cr-1Mo-0.4Mn-0.2Si-0.2V-0.1Ni) was selected as one of the candidate materials for internal structural components of future lead fast reactors and Accelerator Driven Systems (ADS), because of its very good behaviour under irradiation. The induced radioactivity is estimated to be about half of the one of austenitic stainless steels used for the nuclear reactor cores at present. Moreover, T91 is known for its very good resistance to swelling and for the very small transition temperature shift after high level irradiation, which is requested for the GIV reactor core materials. However, the position of T91 on the list of the candidate materials is now being questioned owing to many laboratory data indicating its sensitivity to LME in HLM [4-15]. The effect was misinterpreted as embrittlement, as mentioned above. Moreover, the findings were based only on those laboratory tests examining T91 behaviour in very extreme conditions that are not relevant for estimated normal operating conditions. It could be considered only for accidental conditions. In design, applied loads remain elastic, i.e. well below the yield strength, in normal operation regime. It is likely, that the issue of LME/EAC occurrence when addressed within these allowable operating stresses could have a completely different outcome.

At the present, the 15-15Ti austenitic steel (15%Cr-15Ni-1.6Mn-1.5Mo-0.8Si-0.4Ti) is considered as an alternative material for the fuel cladding mainly because the steel should not be susceptible to LME. However, the 15-15Ti would have several times higher swelling, when irradiated at high dose, in comparison to ferritic-martensitic steels. With respect to higher Ni and Mo contents, higher induced radioactivity is estimated and due to high Ni solubility in liquid metals corrosion resistance is limited.

To verify materials' performance in HLM under stress, two-level experimenting is usually performed. On the first level the material's sensitivity to cracking is tested; on the second level more understanding and description of the degradation is required. In previous experiments, the mechanical testing in contact with liquid LBE and Pb had been performed and the role of oxide rupture causing wetting, as the cracking precursors, had been discussed. This study intends to advance to the second level, by summarizing the sensitivity test results and following up to provide an insight into the conditions for crack initiating and development in HLM.

2. EXPERIMENTAL

2.1. **Materials**

The ferritic-martensitic steel T91 (Grade 91 Class 2/S50460) of composition 8.895 wt. % Cr, 0.889% Mo, 0.401% Mn, 0.235% Si, 0.121% Ni, 0.202% V, 0.080% Cu, 0.048%N, 0.019% P, 0.010% Al, 0.102% C, bal. Fe, was produced by Industeel, ArcelorMittal group for the

EUROTRANS/DEMETRA project. The material was normalized at 1150 °C for 15 min with subsequent water cooling to room temperature and finally annealed at 770 °C for 45 min, then slowly cooled in the air. The material was provided in plate of 15 mm thickness. The microstructure consists of lath martensite with original austenitic grains of 20 μm average size. The mechanical properties yield strength (YS) and UTS respectively were 503 MPa and 621 MPa respectively at 300 °C.

The austenitic Ti-stabilized stainless steel 15-15Ti (1.4970) of composition 15.95% Cr, 15.40% Ni, 1.20% Mo, 1.49% Mn, 0.52% Si, 0.44%Ti, 0.026% Cu, 0.036% V, 0.023 Al, 0.1% C, bal. Fe was provided by SCK•CEN in form of a cylindrical billet of 12cm in diameter, after solution annealing. The microstructure exhibited a non-uniform grain size, which ranges from 19 to 67 μm.

2.2. **Specimens**

Several types of specimens were used for the tests described. All the specimen types are listed in Table 1

TABLE 1. SUMMARY OF ALL TYPES OF TEST SPECIMENS (DIMENSIONS IN MM)

Specimen type (dimensions)	Loading	Applied displacement rate	Reference
Flat coupon (1×5 × 22)	Three point bend	Static	20-23
Notched round bar (Ø4 × 20)	Tensile	Slow, quasi-static	13, 14
Smooth round bar (Ø4 × 20)	Tensile	Slow, quasi-static	9, 13, 14
Flat tapered platelet (3×4-6.4 × 26)	Tensile	Slow, quasi-static (R0, R2)	20, 21, 23
RCT (thickness 6, 8; Ø 15.5, 20)	Tensile & Bend	Slow, quasi-static	24, 25
CT (thickness 12.5, width 25)	Tensile & Bend	Slow, quasi-static	26, 27

2.3. **Test technique**

For static exposure flat coupons were pre-loaded in a test holder by three-point bent to deflection calculated according to ISO 7539-2 standard: $y = \sigma \times H^2/(6 \times E \times t)$, where σ is the applied stress at test temperature, H is the span, E is the Young module and t is the coupon thickness. The pre-stress of 80 to 110 % of YS was applied. The holder was then inserted into the static tank, or into the slow flow COLONRI I loop referred elsewhere [9,20].

Slow Strain Rate (SSRT) and Constant Extension Rate (CERT) tests were applied [9,13,14,16,24]. Three displacement rates R0, R1 and R2, respectively 2×10^{-4}, 2×10^{-6} and 2×10^{-8} m/s, were used. For smooth and notched specimens, the respective strain rates were 1×10^{-2}, 1×10^{-4} and 1×10^{-6} 1/s. For tapered specimens, R2 corresponds to strain rate of 1×10^{-6} s^{-1} at the minimum cross section.

J integral test: Compact tension (CT) specimens were exposed to LBE in the static cell mounted on a tensile machine. Initially, pre-exposure to molten LBE bubbled with Ar-6% H_2 was carried out at about 450 °C for 20 h, in order to reach oxygen content below 10^{-6} wt. % before loading. Then, the temperature was decreased to 350 °C and after 2 h of stabilization the cyclic loading was applied for pre-cracking.
Afterwards, the specimen was unloaded and J integral test performed with 0.2 mm/min stroke rate. After test, each specimen was broken to open. The J integral data were evaluated according to the ASTM E 1820.

2.4. **Environment**

The mechanical tests in liquid Pb/LBE were performed in HLM systems built on various testing machines. Older HLM systems use one vessel where the preparation of HLM (melting and oxygen setting by Ar/H_2 gas bubbling) was carried out in the presence of the specimen [9,13,14,16,24]. Newer HLM systems were based on the two-vessel concept, where the first vessel served for the preparation of HLM and the second one for the testing of the specimen [21-23]. The oxygen content was measured in both vessels using oxygen sensors (e.g. Bi/Bi_2O_3). In the Pb/LBE was maintained dissolved O content of about 1×10^{-6} wt. % and one day exposure preceded the load application.

2.5. **Post-test evaluation**

After exposure, specimens were at first observed by microscopic techniques for crack occurrence. Then, cross and longitudinal section samples were prepared for investigation. If remaining Pb/PbBi obscured the observation, the specimens were chemically cleaned through immersing in a solution of H_2O_2, CH_3COOH and CH_3CH_2OH (in the 1:1:1 ratio). The specimen surface was observed and analysed using scanning electron microscopes (SEM) MIRA3 GMU SEM and a dual beam focussed ion beam scanning electron microscopes (FIB-SEM) system LYRA3 GMU (TESCAN).

3. RESULTS I - SENSITIVITY TO LME/EAC CRACKING IN HLM

Sensitivity of materials to cracking in environment is usually studied performing SSRT testing in contact with the environment. The testing had been performed and results had been referred elsewhere [4-9, 13, 14]. The effect of environment on material performance in mechanical testing is usually most clear from values of the elongation (A) and the reduction of area (RA). A decrease of A and RA indicates sensitivity to EAC.

3.1. **T91 & liquid LBE**

Experimental data of A and RA for T91 in air and LBE, obtained from SSRT performed at R1 and R2 strain rates are shown in Fig. 1. Average values of three tests at each temperature are reported. The presence of LME/EAC was indicated at 300 °C in R1 and R2 tests. In case of R2, RA decreased from 75% in air to 51% in environment. LME/EAC cleavage-like facets were observed on the fracture surface and were deeper in the slower than in the faster tests (Fig. 2) [9].

3.2. **T91 & liquid Pb**

Experimental data of A and RA for T91 in air and Pb, gathered from SSRT performed with smooth bar specimens at R1 and R2 strain rates at several temperatures, are summarized in Fig. 3. SEM observation of the specimens' fracture surface revealed fully ductile fracture modes in air and Pb environments.

At the same time, CERTs performed with notched specimens resulted in LME/EAC initiation and growth [13, 14]. The crack initiated from the notch root, acting as stress concentrator, whereas the ligament was exposed to ultimate tensile strength (UTS) of the steel. To show the sensitivity in the graph of Fig. 3, an apparent elongation A* (final elongation/gauge length in %) was used. A lower A* in Pb compared to air is clear at 350 °C. The LME/EAC sensitivity at 300 – 400 °C was verified by SEM observation of the cleavage-like facets on the fracture surface of notched specimens.

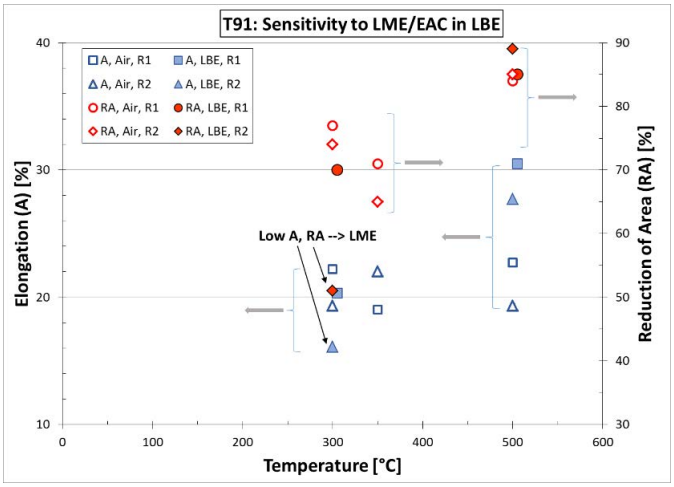

FIG.1. Results of SSRT of T91 in liquid LBE and in air at two strain rates, R2<R1. The graphs of elongation and reduction of area versus temperature show a decrease of A and RA values in LBE at 300 °C compared to air.

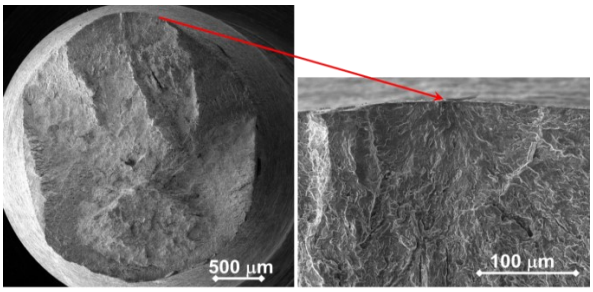

FIG.2. SSRT in LBE at 300 °C at R2- T91 fracture appearance showing cleavage-like facets around the surface being in contact with LBE, indication of LME/EAC (reproduced from Ref. [9] with permission courtesy of Elsevier).

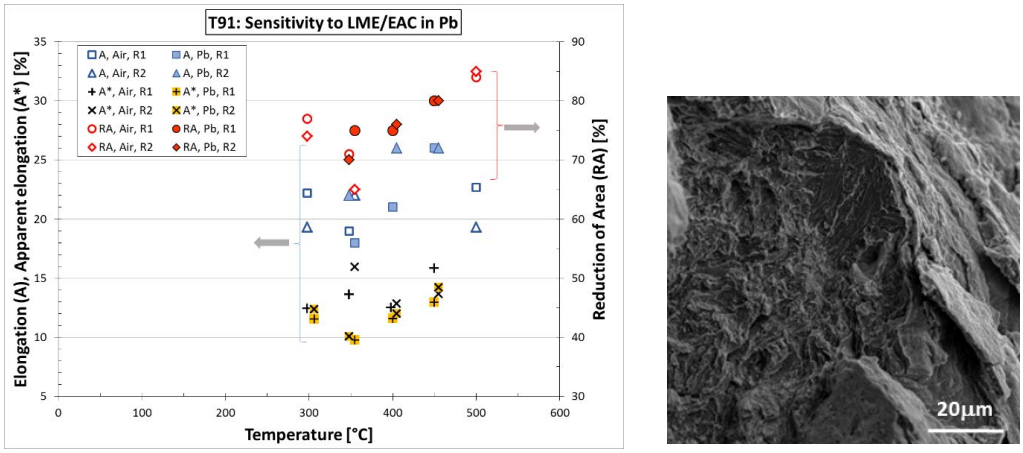

FIG. 3. Results of SSRT of T91 in liquid Pb and in air at R2<R1: The graphs of A elongation and RA reduction of area of the smooth specimens versus temperature, which do not show decrease of A, RA values in Pb, and A apparent elongation of the notched ones, which show decrease in Pb at 350 °C. Note, that the tests at 300 °C marked Pb were performed in air with specimens pre-wetted by Pb. SEM image shows the cleavage-like crack from the notch*

4. RESULTS II - CONDITIONS FOR LME/EAC CRACKING IN HLM: INITIATION

To study conditions necessary for materials to initiate cracking in HLM, static tests were carried out on pre-stressed coupons and CERTs with tapered specimens in contact with liquid LBE and Pb [21-23, 29]. Series of static exposure tests were performed to study whether the combined effect of long-term contact with environment and stress close to the yield strength (YS) could stimulate the crack initiation. In CERTs, the principle is based on the fact that the cracking process is accelerated with applied strain rate. Moreover, the tapered shape of the specimen gauge length has the advantage of applying a range of stresses with one load, which can be used for threshold stress assessment.

4.1. **T91 & liquid LBE**

T91 coupons pre-stressed up to 1.1 YS were exposed to LBE at 350 °C for 500, 1000 and 2000 hours. After exposure, a double-layer oxide about 2 μm thick was observed, after 1000 and more hours. However, no tendency to oxide failure was detected. Consequently, no LME/EAC crack was observed in any of the bent coupons.

CERT testing of T91 tapered specimens was performed in LBE at 300 °C with R0, R1 and R2 test rates. Reference tests were carried out in air. Figure 4 shows the test curves of the slowest test rate R2 (2×10^{-8} m/s).

The stress-displacement curves show distinctive oscillations in air as well as in HLM, indication of the dynamic strain ageing (DSA) effect.

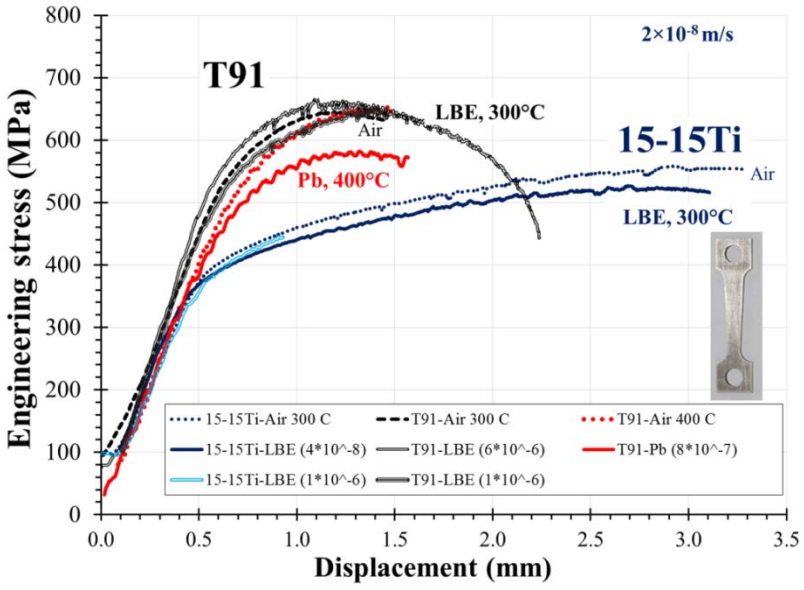

FIG.4. CERTs at R2: Stress at minimum cross section of the tapered specimens vs. displacement curves. The most of tests were stopped at maximum load; only one test at LBE went until rupture. The number in bracket stands for oxygen content in wt. %.

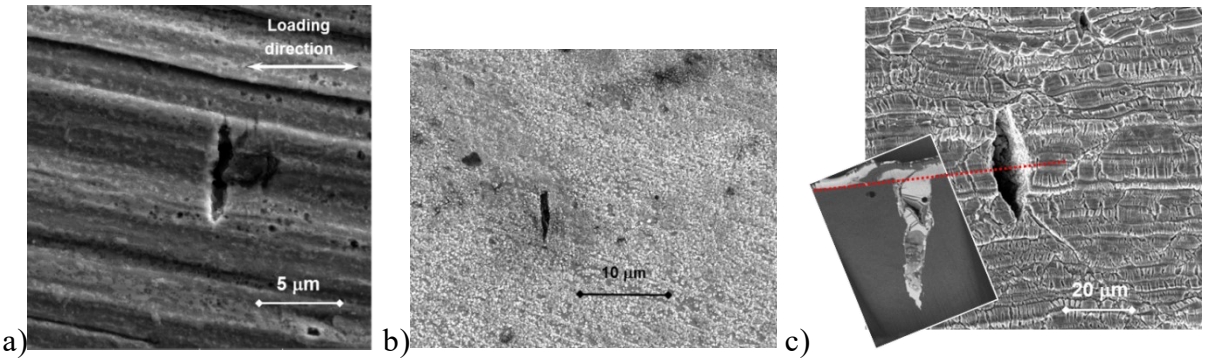

FIG. 5. LME/EAC initiation on the surface of T91 tapered specimens after CERTs in LBE & 300 °C: a) b) short cracks observed at the minimum cross section in tests stopped at maximum load; c) about 25 µm long crack, at the minimum cross section, in test to rupture including image of FIB cross-cut marked by dashed line [28]. Reprinted from [21] with permission courtesy from Elsevier.

After CERTs, out of 5 specimens tested by R2, LME/EAC degradation was identified only in 3 and in each case with a single crack on the flat surface [21]. One short crack per specimen was observed in the region of maximum plastic strain and stress (Fig. 5). Using FIB it was found that one LBE/EAC crack about 25 µm long on the surface was 46 µm deep (Fig. 5c), filled with Pb and Bi and exhibit partly inter-lath path [28]. Energy-dispersive X-ray spectroscopy (EDS) analysis of the lift-out lamella confirmed the presence of Pb and Bi only along the crack walls and inside the crack tip. No Pb or Bi penetrated into the bulk metal. Besides the open cracks, numerous shallow cracks, limited to the oxide layer, manifested the stress surface interaction in LBE.

4.2. **T91 & liquid Pb**

T91 coupons pre-stressed up to 1.1 YS were exposed to liquid Pb at 400 °C for 500 and 1000 hours. After the exposure, double-layer oxide development up to 5 µm was observed after 1000 and more hours. However, no tendency to oxide failure was detected. Consequently, there was no observation of LME/EAC in the bend coupons.

The post-test observation of CERTs highlighted the 2 µm protective double-layer oxide (Fig. 6) built on the tapered specimen surfaces. The outer oxide structure was Fe-O and the inner one consisted of Cr-Fe-O. When loads were applied up to the maximum, only the surface oxide was damaged (Fig. 6b) and very fine superficial cracks in the oxide appeared. LME/EAC cracking was not observed.

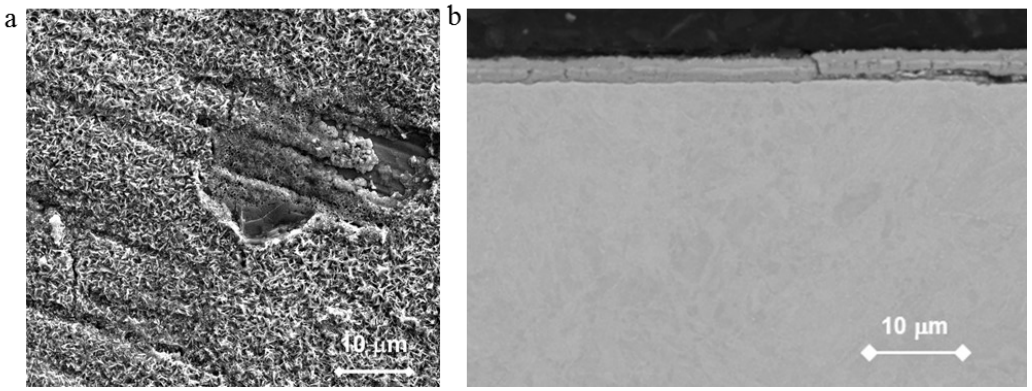

FIG. 6. Surface of T91 after CERT in Pb & 400 °C: (a) the outer oxide layer after chemical removal of Pb; (b) cross section.

4.3. **Initiation of LME/EAC of T91 in HLM - summary**

Based on the SSRT and CERT data, conditions of LME/EAC initiation occurred when: plastic strain > 1.3% and stress> 645 MPa, i.e. about the UTS [21-23]. Moreover, in tests of T91 in liquid lead at 400 °C, the load level applied was sufficient to break only the oxide layers built but did not show any LME/EAC cracks. In Fig. 7, the threshold stress temperature course is shown.

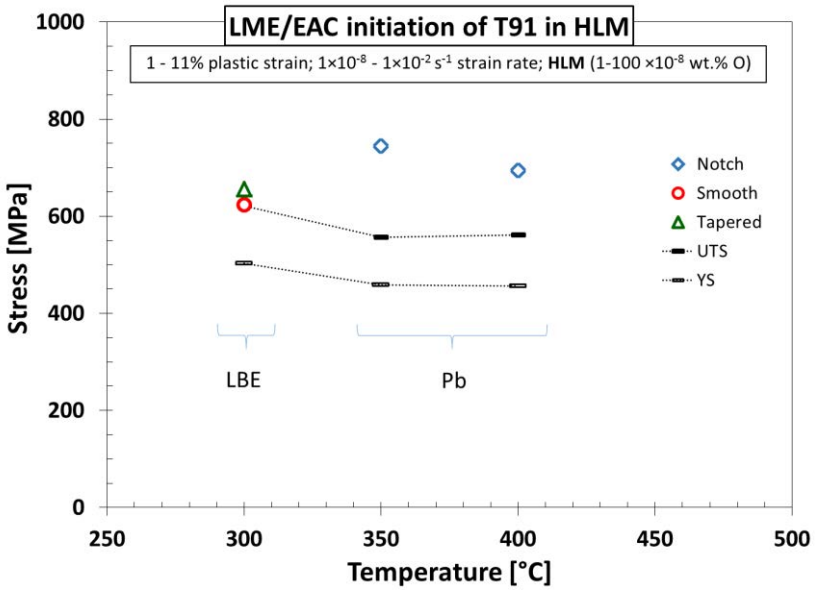

FIG. 7. Scheme of LME/EAC initiation conditions estimated from tests of several types. For the notched specimens, the stress means the maximum stress under notch, i.e. the nominal stress multiplied with the stress concentration.

4.4. **15-15Ti in liquid LBE**

CERT testing of 15-15Ti tapered specimens was performed in LBE at 300 °C and compared with test in air (Fig. 4). The three curves have very similar shape; stress oscillations occurred too. The tapered specimens did not show any typical LME/EAC cracks. After loading, slip bands and small cracks appeared on the surface (Fig. 8a). Most of the cracks initiated around and from surface and subsurface particles even in case of over–yield loading (Fig. 8b). The small difference of tests in LBE compared to air was in fine superficial cracks appeared in micro slip bands in the environment [29].

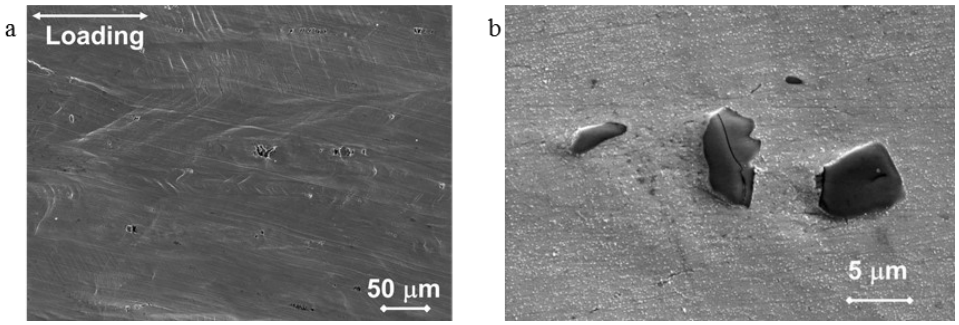

FIG. 8. Surface of 15-15Ti after CERT in LBE & 300 °C: (a) slip bands and cracks within particles; (b) broken particles after over-yield loading.

4.5. **15-15Ti in liquid Pb**

The YS pre-stressed coupons, exposed for 1000 hours in liquid Pb of 10^{-7} wt. % oxygen concentration at 400 °C, did not show any cracking. On the surface a non-continuous thin oxide layer was observed (Fig. 9a) as confirmed by EDS analysis. In cross section (Fig. 9b) the oxide layer consisted of Fe-Cr-O, with a thickness in the range of 0.6-2.4 μm. In some sites, double layer character with the inner Cr rich and the outer Fe rich layers oxide was indicated.

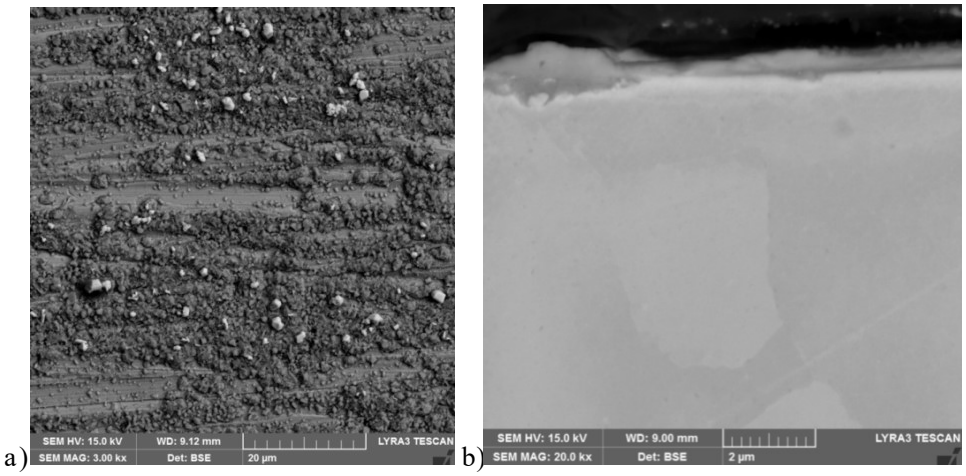

FIG. 9. Surface of 15-15Ti after test in Pb & 400 °C: (a) surface after cleaning; (b) oxide layer in cross section view.

5. RESULTS III - CONDITIONS FOR LME/EAC CRACKING IN HLM: KINETICS

To investigate further the conditions of the LME/EAC development, fracture resistance testing (J integral tests) were performed. From this kind of tests, as well as from those with RCT and SSRT with smooth and notched and CERT with tapered specimens, the kinetics of the cracking can be evaluated.

5.1. **Fracture resistance of T91 in liquid LBE**

Experimental data of fracture resistance measured with 0.5T CT specimens in LBE were obtained in the MATTER project [26, 27, 30] following single specimen test method from the ASTM 1820 standard. The data are plotted in the graph in Fig. 10. The slope of the J-R curve was changed in LBE; the lowest value was measured in case of cleavage-like fracture modes of the LBE pre-fatigued and the extended cracks. The graph shows that in case of the pre-crack and its extension in the cleavage-like mode the critical fracture resistance (fracture toughness) in LBE at the onset of the crack extension was about 50 kJ/m^2. Only stable kinetics was observed. Unstable fracture did not occur.

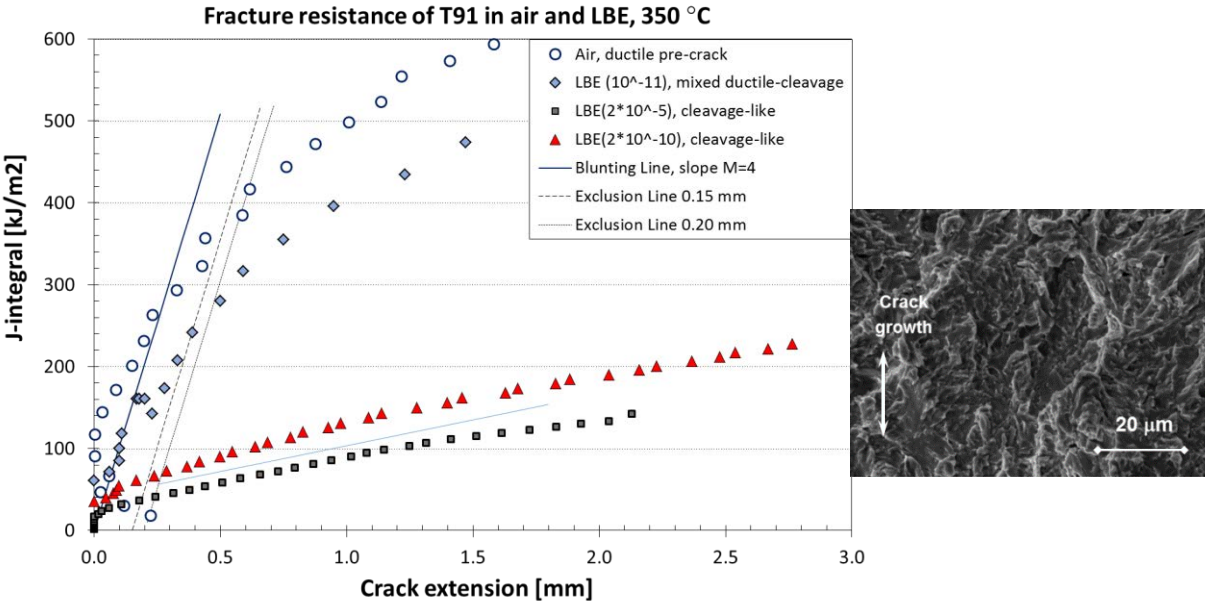

FIG. 10. Fracture resistance curves of T91 in air and LBE at 350 °C (O in bracket) in case of ductile pre-crack made in air and cleavage-like pre-cracking in LBE of low O at 450 °C. The SEM image shows the cleavage–like crack growth.

5.2. **Crack Growth Rate of T91 in HLM**

Experimental data of the average crack growth rate were evaluated from above mentioned tests [9, 13, 14, 20, 21, 23, 24, 26], these data plotted versus test rate of various test types, as shown in Fig. 11. The average crack velocity is a maximum of ten times higher in HLM than in air and its value is decreasing with test rate.

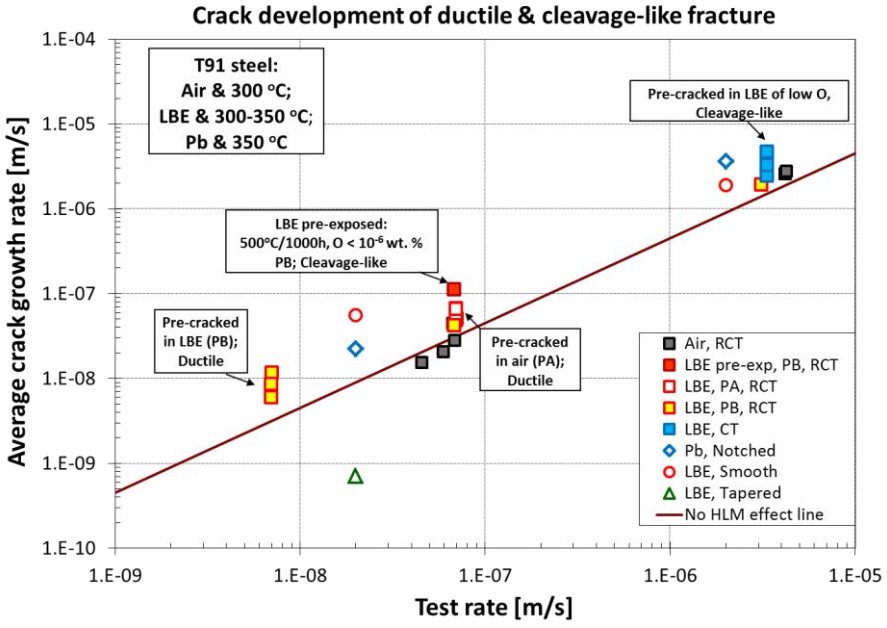

FIG. 11. Average crack growth rate evaluated from the tests.

6. DISCUSSION

Considering all findings that have been identified in the above investigations, i.e. absence of Pb atoms penetration, cleavage-like fracture appearance and the stable crack growth, the Adsorption Induced Dislocation Emission (AIDE) model proposed by Lynch in 1976 [18, 32] seems applicable to the LME/EAC. It has been verified that neither Pb nor Bi atoms penetrate into the bulk of T91 specimen loaded close to the material strength in LBE at 300 °C. In the case of the investigated open crack, LME/EAC initiated from the surface after the oxide layer broke and propagated into the depth along the martensite laths in one grain. The model explains that owing to dislocation emissions in two intersecting slip systems, the path consisting of nano-voids resulting from the dislocation motion follows crystallographic planes and although the macroscopic fracture surface is similar to cleavage, the fracture has to be considered as ductile. At the same time, the observation of the stable crack kinetics under the various test conditions is consistent with the ductile fracture.

The LME/EAC initiation was observed only in case of the ferritic-martensitic steel, but not in the austenitic one. The observation is very well in agreement with present knowledge [31] and with the AIDE model. The thin protective oxide of 15-15Ti was built in agreement with other reference, e.g. about 1 μm at 500 °C for 500 h in LBE with 10^{-6} wt. O_2 [33].

7. CONCLUSIONS

For the T91 and 15-15Ti steels the two level assessment of degradation in HLM under stress was summarized. Because the HLM atoms do not penetrate into the steels, it is proposed to requalify the degradation mode from LME to EAC.

As expected, the crack initiation tests in LBE at 300 °C and in Pb at 400 °C verified the immunity of 15-15Ti to LME/EAC. On the other hand, T91 steel showed sensitivity to LME/EAC with tendency to crack initiation in contact with liquid Pb, at 350 – 400 °C, and LBE, at 300 °C, at stresses above UTS and high plastic deformation. However, the crack initiation did not lead to unstable failure. Adsorption-induced dislocation-emission mechanism was found to be the best way to describe the observed degradation.

Based on the new and past research experience is stated that the T91 steel can be sensitive to LME/EAC in low flow HLM, but only beyond design loads of operation of Gen IV system's components.

ACKNOWLEDGEMENTS

The research leading to these results is partly funded by the EC H2020 under GA 755269 (GEMMA). This work was supported by the Czech Science Foundation (GAČR) project No. 16-15008S (KAMILE). This work has been realized within the SUSEN Project (established in the framework of the European Regional Development Fund (ERDF) in project CZ.1.05/2.1.00/03.0108 and of the European Strategy Forum on Research Infrastructures (ESFRI) in the project CZ.02.1.01/0.0/0.0/15_008/0000293, which is financially supported by the Ministry of Education, Youth and Sports - project LM2015093 Infrastructure SUSEN.

REFERENCES

[1] CINOTTI, L.; SMITH, C. F.; SEKIMOTO, H.; MANSANI, L.; REALE, M.; SIENICKI, J. J. Lead-cooled system design and challenges in the frame of Generation IV International Forum. J. Nucl. Mater. 415 (2011) 245-253.

[2] GRASSO, G.; PETROVICH, C.; MATTIOLI, D.; ARTIOLI, C.; SCIORA, P.; GUGIU, D., BANDINI, G.; BUBELIS, E.; MIKITYUK, K. The core design of ALFRED, a demonstrator for the EU lead-cooled reactors. Nucl. Eng. Des. 278 (2014) 287-301.

[3] http://sckcen.be/en/Technology_future/MYRRHA

[4] GORSE, D.; AUGER, T.; VOGT, J.-B.; SERRE, I.; WEISENBURGER, A. ET AL. Influence of liquid lead and lead-bismuth eutectic on tensile, fatigue and creep properties of ferritic/martensitic and austenitic steels for transmutation systems. J. Nucl. Mater. 415 (2011) 284–292.

[5] NICAISE, G.; LEGRIS, A.; VOGT, J.B.; FOCT, J. Embrittlement of the martensitic steel 91 tested in liquid lead. J. Nucl. Mater. 296 (2001) 256–264.

[6] LONG, B.; DAI, Y. Investigation of LBE embrittlement effects on the fracture properties of T91. J. Nucl. Mater. 376 (2008) 341–345.

[7] VAN DEN BOSCH, J.; SAPUNDJIEV, D.; ALMAZOUZI, A. Effects of temperature and strain rate on the mechanical properties of T91 material tested in liquid lead bismuth eutectic. J. Nucl. Mater. 356 (2006) 237–246.

[8] VOGT, J.-B.; VERLEENE, A.; SERRE, I.; LEGRIS, A. Mechanical behaviour of the T91martensitic steel under monotonic and cyclic stressing in liquid metals. J. Nucl. Mater. 335 (2008) 222–226.

[9] DI GABRIELE, F.; DOUBKOVA, A.; HOJNA, A. Investigation of the sensitivity to EAC of steel T91 in contact with liquid LBE, J. Nucl. Mater. 376 (2008) 307–311.

[10] COEN, G.; VAN DEN BOSCH, J.; ALMAZOUZI, A.; DEGRIECK, J. Investigation of the effect of lead–bismuth eutectic on the fracture properties of T91 and 316L. J. Nucl. Mater. 398 (2010) 122–128.

[11] AUGER, T.; GORSE, D.; HAMOUCHE-HADJEM, Z.; VAN DEN BOSCH, J.; COEN, G. ET AL. Fracture mechanics behaviour of the T91 martensitic steel in contact with liquid lead-bismuth eutectic for application in an accelerator driven system. J. Nucl. Mater. 415 (2011) 293–301.

[12] GONG, X.; MARMY, P.; VERLINDEN, B.; WEVERS, M.; SEEFELDT, M. Low cycle fatigue behavior of a modified 9Cr–1Mo ferritic–martensitic steel in lead–bismuth eutectic at 350 °C—effects of oxygen concentration in the liquid metal and strain rate. Corros. Sci. 94 (2015) 377–391.

[13] HOJNA, A.; DI GABRIELE, F.; KLECKA, J.; BURDA, J. Behaviour of the steel T91 under uniaxial and multiaxial slow loading in contact with liquid Pb. J. Nucl. Mater. 466 (2015) 292–301.

[14] DI GABRIELE, F.; HOJNÁ, A.; CHOCHOLOUSEK, M.; KLECKA, J. Behavior of the steel T91 under multi axial loading in contact with liquid and solid Pb. Metals 7 (2017) 342-356.

[15] STERGAR, E.; EREMIN, S.G.; GAVRILOV, S.; LAMBRECHT , M.; MAKAROV, O.; IAKOVLEV, V. Influence of LBE long term exposure and simultaneous fast neutron irradiation on the mechanical properties of T91 and 316L. J. Nucl. Mater. 473 (2016) 28-34.

[16] HOJNA, A., DALIKOVA, K., DI GABRIELE, F. Study of Fracture Resistance Degradation of the Steel T91 in Heavy Liquid Metals: DEMETRA Project, Report ÚJV Rez DITI 302/543 (2009). DOI: 10.13140/RG.2.2.35727.12964

[17] SERRE, I.P.; VOGT, J.-B.; NUNS, N. TOF-SIMS Investigation of Absorption of Lead and Bismuth in T91 Steel Deformed in Liquid Lead Bismuth Eutectic. Applied Surface Science 471 (2018) 36-42.

[18] LYNCH, S.P. Environmentally assisted cracking: overview of evidence for an adsorption-induced localised-slip process. Acta Metallurgica 36 (1988) 2639–2661.

[19] AUGER, T.; LORANG, G.; GUÉRIN, S.; PASTOL, J.-L.; GORSE, D. Effect of contact conditions on embrittlement of T91 steel by lead–bismuth, J. Nucl. Mater. 335 (2004) 227–231.

[20] Hojna, A.; Hadraba, H; Di Gabriele, F.; Husak, R. Behaviour of pre-stressed T91 and ODS steels exposed to liquid lead-bismuth eutectic. Corros. Sci. 131 (2018) 264–277.

[21] HOJNA, A.; DI GABRIELE, F.; CHOCHOLOUSEK, M.; HALODOVA, P.; LORINCIK, J. Initiation of LME Crack in Ferritic Martensitic Steel in Liquid Lead-Bismuth, J. Nucl. Mater. 511 (2018) 459-472.

[22] HOJNÁ, A.; DI GABRIELE, F.; CHOCHOLOUŠEK, M.; ROZUMOVÁ, L.; VÍT, J. Effect of applied stress on T91 steel performance in liquid lead at 400 °C, Materials 11 (2018) 1-17

[23] HOJNÁ, A.; ROZUMOVÁ, L.; HALODOVÁ, P.; CHOCHOLOUŠEK, M.; ŠPIRIT, Z. Environmentally Assisted Cracking of T91 in Heavy Liquid Metals, submitted to Corrosion Reviews (2019).

[24] HOJNA, A.; DI GABRIELE, F. On the kinetics of LME for the ferritic martensitic steel T91 immersed in liquid PbBi eutectic. J. Nucl. Mater. 413 (2011) 21–29.
[25] VAN DEN BOSCH, J.; COEN, G.; ALMAZOUZI, A.; DEGRIECK, J. Fracture toughness assessment of ferritic-martensitic steel in liquid lead-bismuth eutectic, J. Nucl. Mater. 385 (2009) 250-257.
[26] HOJNA, A.; DI GABRIELE, F.; KLECKA, J. Characteristics and liquid metal embrittlement of the steel T91 in contact with lead-bismuth eutectic. J. Nucl. Mater. 472 (2016) 163–170.
[27] MAGIELSEN, L.; VAN STAVEREN, T.O.; LAMBRINOU, K. DELIVERABLE 3.5: "Guidelines, results and evaluations for fracture toughness tests", MATTER (Materials Testing And Rules), in: Collaborative Project Co-funded by the EC under the Euratom Research and Training Programme on Nuclear Energy within the 7FR, GA 269706 (2015).
[28] HALODOVÁ, P.; LORINČÍK, J.; HOJNÁ, A. Microstructural Investigation of LME Crack Initiated in Ferritic/Martensitic Steel T91 Loaded in Liquid Lead-Bismuth Eutectic at 300 °C. Materials 12 (2019) 38.
[29] HOJNÁ, A., DI GABRIELE, F., CHOCHOLOUŠEK, M., ŠPIRIT, Z., ROZUMOVÁ, L. Study of crack initiation of 15-15Ti austenitic steel in liquid PbBi, Journal of Nuclear Engineering and Radiation Science 5 (2019) 1-8.
[30] ERSOY, F.; GAVRILOV, S.; VERBEKEN, K. Investigating liquid-metal embrittlement of T91 steel by fracture toughness tests. J. Nucl. Mater. 472 (2016) 171-177.
[31] SOLER, L. ET AL. Chapter 6, Compatibility of Structural Materials with LBE and Pb Standardisation of Data Corrosion Mechanism and Rate, in "Handbook on Lead-bismuth Eutectic Alloy and Lead Properties, Materials Compatibility, Thermal-hydraulics and Technologies", OECD/NEA (2015) 231-274.
[32] LYNCH, S. Mechanistic and Fractographic Aspects of Stress-Corrosion Cracking, In: Stress Corrosion Cracking: Theory and Practice, V.S. Raja and T. Shoji (Eds.), Woodhead Publishing, Cambridge (2011) 3-89.
[33] LI, H., BA, P., LIN, Z., ZHANG, J., TANG, Q., PAN, Y. Corrosion resistance in Pb-Bi alloy of 15-15Ti steel coated with Al_2O_3/SiC bilayer thin films by magnetron sputtering. Fusion Engineering and Design 125 (2017) 384-390.

RATEN ICN STATUS ON MECHANICAL PROPERTIES INVESTIGATION OF 316L GENERATION IV CANDIDATE MATERIAL

ALEXANDRU NIȚU
Institute for Nuclear Research
Pitești/Romania
Email: alexandru.nitu@nuclear.ro

VASILE RADU
Institute for Nuclear Research
Pitești/Romania
Email: vasile.radu@nuclear.ro

VIOREL IONESCU
Institute for Nuclear Research
Pitești/Romania
Email: viorel.ionescu@nuclear.ro

Abstract

The development of ALFRED Generation IV reactor requires the proper selection of the structural materials able to withstand the harsh environment of liquid lead. The compatibility of the candidate structural materials with the liquid lead is considered one of the critical issues in the development of the LFR reactors. In contact with the liquid metal, the deterioration of the mechanical properties of the structural materials can occur. Generally, when a solid metal or alloy is subjected to low stress while it is wetted by a liquid metal, it could be subjected to a phenomenon called liquid metal embrittlement. RATEN ICN is involved in several European projects aimed at Generation IV research activities; in this respect, a laboratory material tensile testing installation has been set up. The paper presents the preliminary tensile tests in the liquid lead on the 316L material (in static conditions) at 400 °C, 450 °C and 500 °C, without an oxygen monitoring system. Stress-strain curves of slow strain rate tests have been obtained in conformity with the standard ASTM, E-8.

1. INTRODUCTION

The challenges of meeting the rapidly growing demand for energy have rekindled a worldwide interest in nuclear power systems. Advanced nuclear power plants aim for improved thermal efficiency by extending the operational temperature window. Design and introduction of the future reactor systems are strongly dependent on the choice of structural materials. These materials need to withstand more demanding conditions within the international program Generation IV. In comparison to the current commercial reactors, all construction material (particularly for internal components and fuel cladding) of the Generation IV reactors will be operated at elevated temperatures, corrosive environment and has to be designed for higher radiation damage due to high fast neutron flux. Therefore, it is advised to test the structural materials to improve their mechanical properties [1, 2].

The objective of this paper is to make an overview of the first results obtained by RATEN ICN in the mechanical testing facility for the IV generation candidate materials in the liquid lead environment.

The first lead test facility completed in ICN is called LIquid LEad Testing INstallation (LILETIN). There are also some facilities at various stages of development, such as the Liquid Metal Creep Machine (LMCM) that is in the final stage and pre-testing. LILETIN testing facility allows performing the tensile tests under temperature conditions (temperature range of 400 – 500 °C) in the static liquid lead environment or air and the tested samples can have flat or cylindrical geometries [3].

The slow strain rate tensile tests have been performed in the following conditions:

— small size flat and cylindrical 316L steel tensile specimens;
— the constant strain rate of $5 \cdot 10^{-5}$ s^{-1};
— the tests are conducted by using the Instron testing machine software according to ASTM E8;
— the results consist of the stress-strain diagrams.

2. EXPERIMENTAL METHOD

The experimental facility, called LILETIN has been set up at RATEN ICN. It allows performing the experimental tensile tests in the liquid lead environment. At this early stage, the LILETIN facility can perform tensile tests in a liquid metal crucible configuration, with temperatures up to 500 °C in static lead conditions, but without any oxygen monitoring system [2].

The global view LILETIN facility, which was set-up in the Instron tensile system, is given by Fig.1. Its main parts are:

— the heating system (1);
— the crucible for molten lead (2), the sample fixing assembly (3);
— the pull rod (4),
— the Instron tensile tests system.

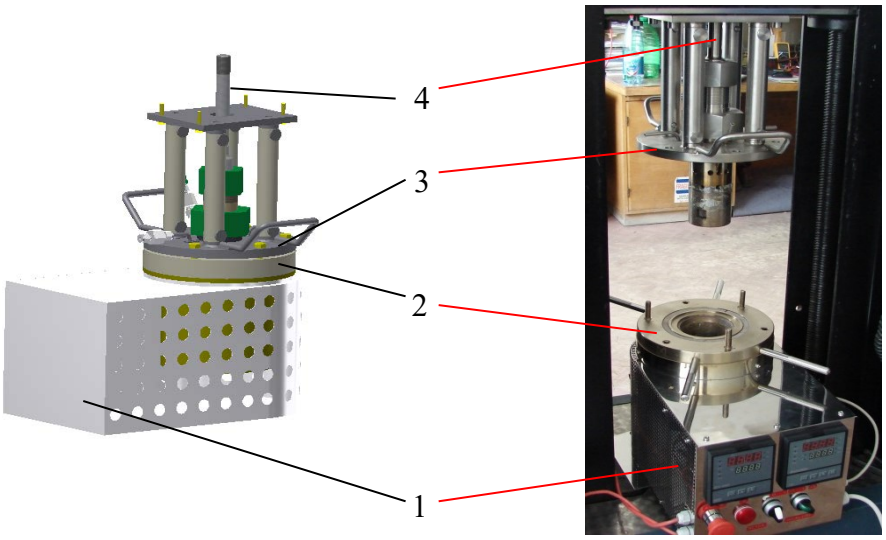

FIG. 1. Laboratory material tensile testing installation: 1-furnace, 2-liquid lead vessel, 3-sample fixing assembly, 4-pull rod.

This facility [3] is designed and built to study the effects of Pb on the mechanical properties of structural materials, in static conditions. It has the following operational parameters - maximum temperature: 500 °C, the volume of Pb: 0.9liter, strain rates controller, without Oxygen Control System (this is under development) and without extensometer. The liquid metal temperature is monitored by a thermocouple inserted in the crucible. To perform the tensile tests a constant strain rate of $5 \cdot 10^{-5}$ s^{-1} was applied. This strain rate was chosen as an optimum between practical and physical considerations. For physical reasons, it was best to have a slow strain rate to obtain wetting of fresh metal surface that appears by breaking the oxide layer on the sample surface and allowing the penetration of lead. On the other hand from a practical point of view, it is desirable to have a strain rate which results in the optimal use of the testing setup, taking into account the time needed for attaching the sample, heating, settling of temperature, testing and cooling [4].

The tensile tests were carried out on small size flat and cylindrical 316L steel tensile specimens (Fig. 2) in the liquid lead at 400 °C, 450 °C and 500 °C. The pull grips (Fig. 3) are adapted for every type of sample. The temperature is set out to the desired testing temperature and as soon as the liquid metal temperature has been stabilized, the test can be started.

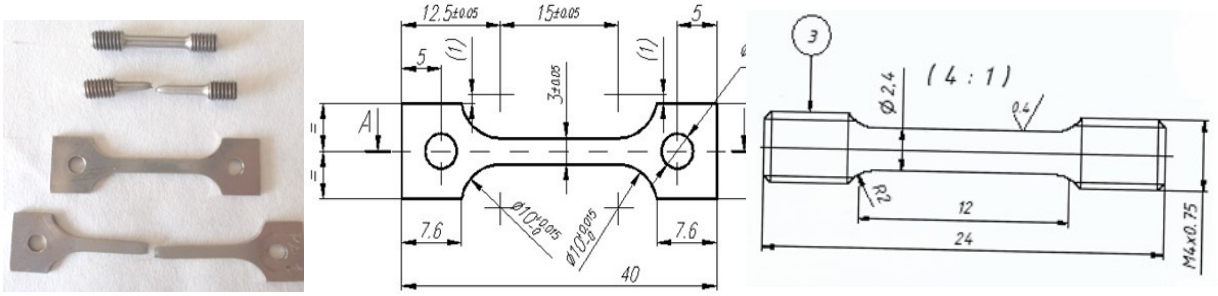

FIG. 2. Small size flat and cylindrical tensile samples (aspects and sketches)

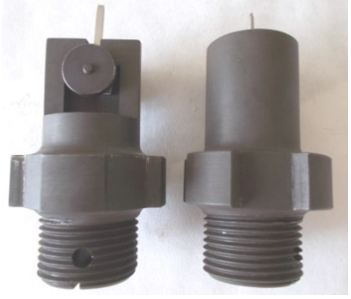

FIG. 3. Pull grips

Tensile testing in the liquid metal environment inside the crucible of this facility is following the methodology from ASTM standard E8M. However, this standard does not include any liquid metal environment and therefore does not strictly apply to the tensile testing in the liquid metal environment.

3. RESULTS AND DISCUSSION

Flat and cylindrical specimens were tested in the liquid metal environment under temperature conditions (400 °C, 450 °C and 500 °C). The test results are presented graphically in the form of test charts: mechanical stress versus relative elongation (stress-strain curves). Figures 4 to 10 show combinations of diagrams and one may see the material behavior in the test environment (air and liquid lead) at different temperatures.

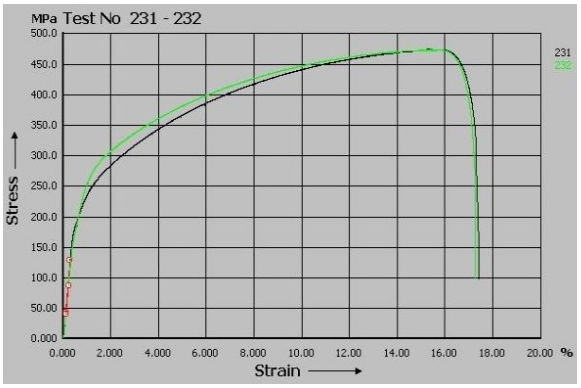

FIG. 4. Tensile test diagram on the flat specimen in the liquid lead at 400 °C

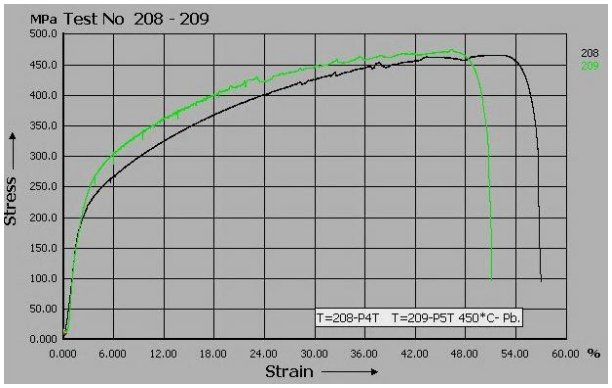

FIG. 5. Tensile test diagram on the flat specimen in the liquid lead at 450 °C

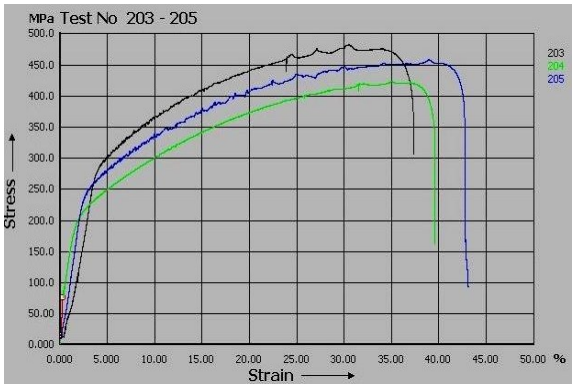

FIG. 6. Tensile test diagram on the flat specimen in the liquid lead at 500 °C

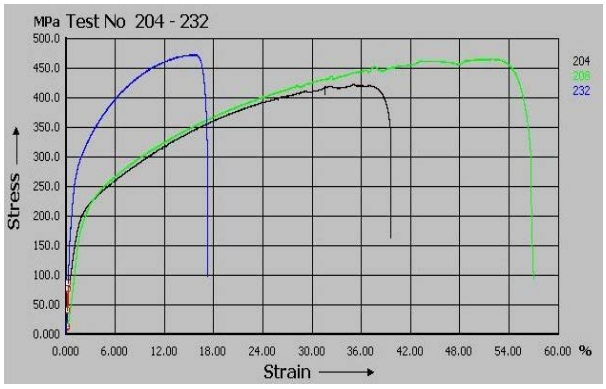

FIG. 7. Tensile test diagram on the flat specimen in the liquid lead (204 at 500 °C, 208 at 450 °C, 232 at 400 °C)

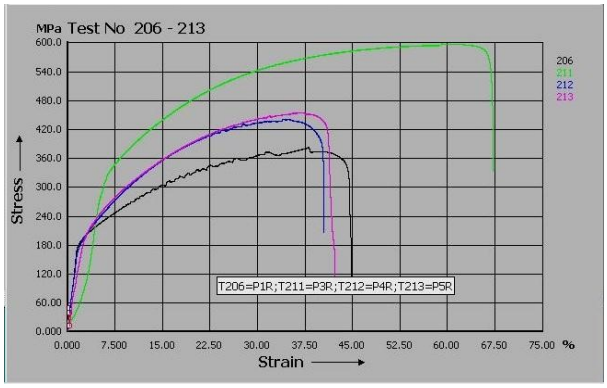

FIG. 8. Tensile test diagram on the cylindrical specimen in the liquid lead (206 at 500 °C and 212, 213 at 450 °C) and in the air (Test 211 at RT)

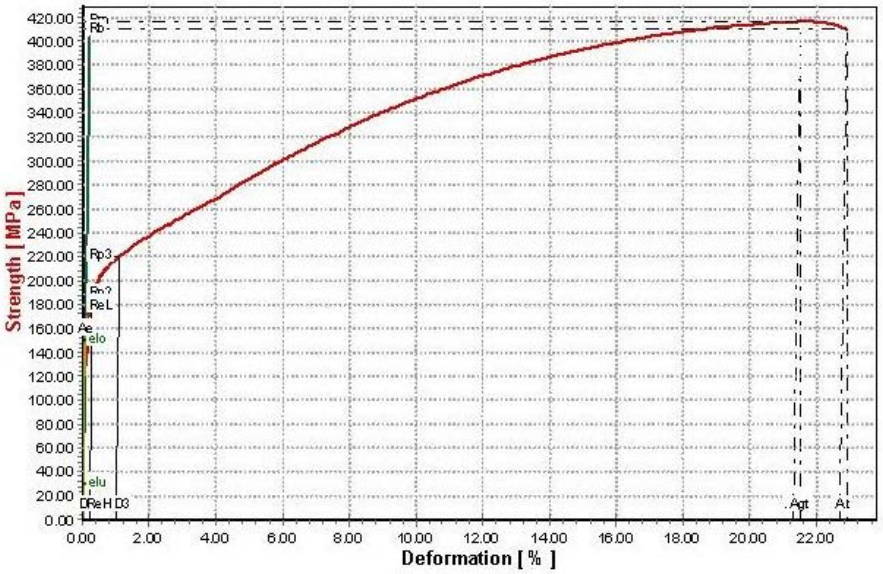

FIG. 9. Tensile test diagram on the flat specimen in the air at 500 °C (AF)

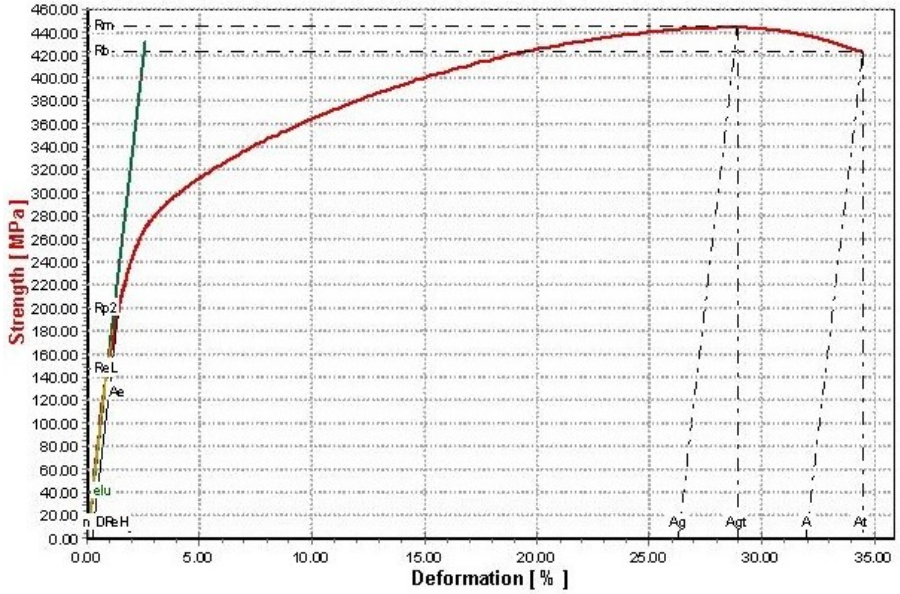

FIG. 10. Tensile test diagram on the cylindrical specimen in the air at 500 °C (AC)

Experimental data is presented in table 1 and table 2 (flat specimens – table 1 and cylindrical samples – table 2)

TABLE 1. EXPERIMENTAL DATA ON THE FLAT SPECIMENS

No. Crt.	Test no.	Material	Testing environment	Testing temperature [^{0}C]	UTS [MPa]
1.	201	316L	air	20	647
2.	210	316L	air	20	651
3.	231	316L	Liquid lead	400	474
4.	232	316L	Liquid lead	400	473
5.	208	316L	Liquid lead	450	465
6.	209	316L	Liquid lead	450	474
7	AF	316L	air	500	417
8.	204	316L	Liquid lead	500	422
9.	205	316L	Liquid lead	500	458

TABLE 2. EXPERIMENTAL DATA ON THE CYLINDRICAL SPECIMENS

No. Crt.	Test no.	Material	Testing environment	Testing temperature [^{0}C]	UTS [MPa]
1.	211	316L	air	20	597
2.	207	316L	Liquid lead	450	409
3.	212	316L	Liquid lead	450	440
4.	213	316L	Liquid lead	450	454
5	AC	316L	air	500	447
6.	206*	316L	Liquid lead	500	382
7.	202	316L	Liquid lead	500	482

** - inconclusive*

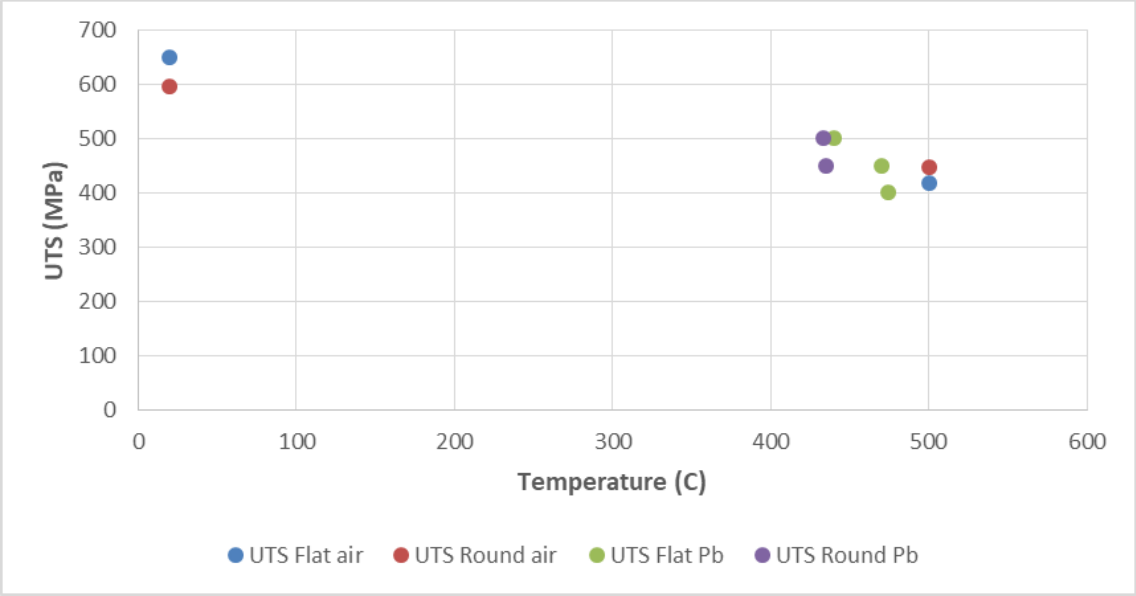

FIG. 11. Values of UTS in Liquid Lead Environment and Air

The results from Table 1, Table 2 and Figure 11, show the need to perform more tests in the liquid lead environment to establish the temperature influence on the mechanical properties, as well as by comparison with more tests in air. To perform SEM analysis (Figure 12 and Figure 13), the fracture surface was cleaned by solidified lead using a solution of acetic acid, hydrogen peroxide and ethanol in a 1: 1: 1 ratio.

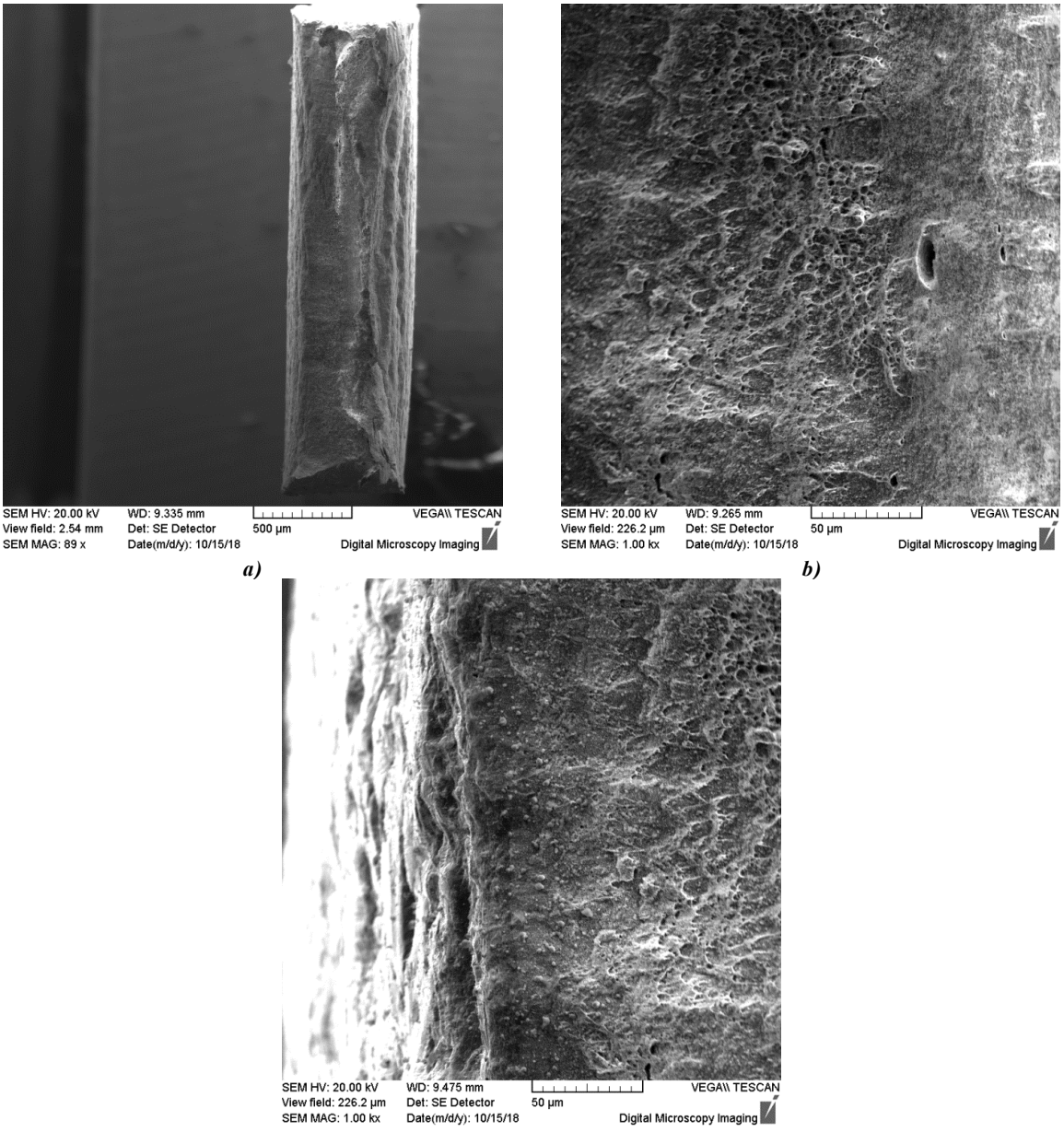

FIG. 12. SEM aspects of 316L flat specimen fracture surfaces tested at 400 °C: a) x100 magnification; b) x1000 magnification; c) x1000 magnification.

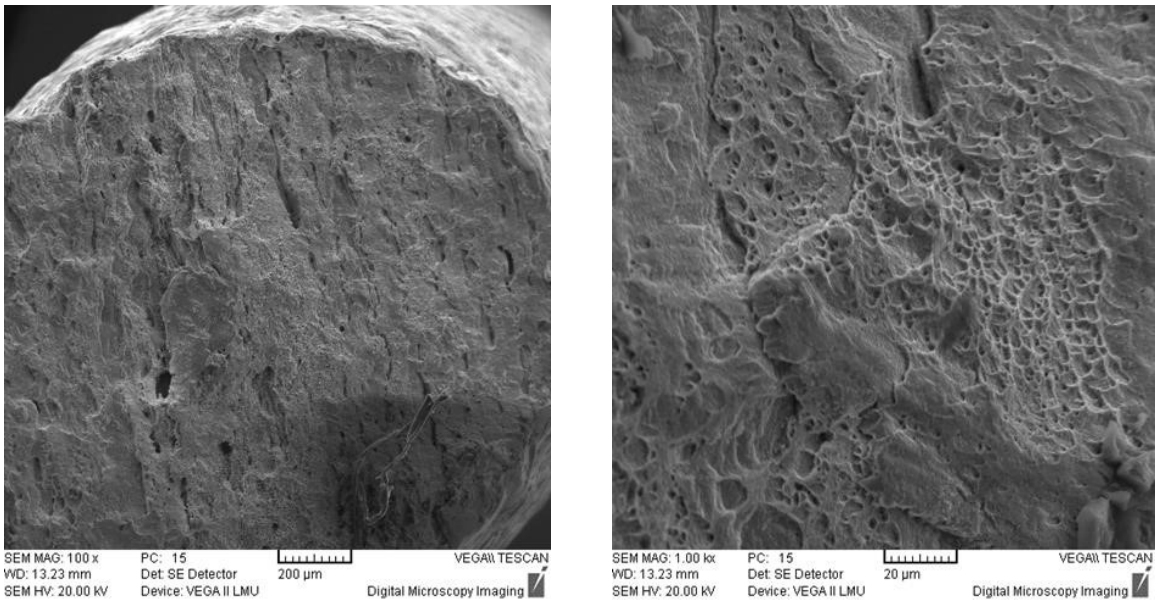

FIG. 13. SEM aspects of 316L cylindrical specimen fracture surfaces tested at 450 °C: a) x100 magnification; b) x1000 magnification.

The SEM aspects put into evidence the ductile behavior of the surface fracture. From the SEM microscopy images (Figures 12 and 13) it is also observed that the rupture begins at the surface of the sample and evolves inwards.

4. PLANNED WORKS

An important issue that has to be solved is the monitoring and controlling the dissolved oxygen concentration. For this purpose, we decided to use electrochemical oxygen pump (EOP). The working principle of electrochemical oxygen pump is based on oxygen ion migration through a solid electrolyte under an externally applied electrical potential as illustrated in Figure 14 [5]. This method allows both removal and addition of oxygen to the crucible containing liquid lead, depending on the polarity of the applied electrical potential.

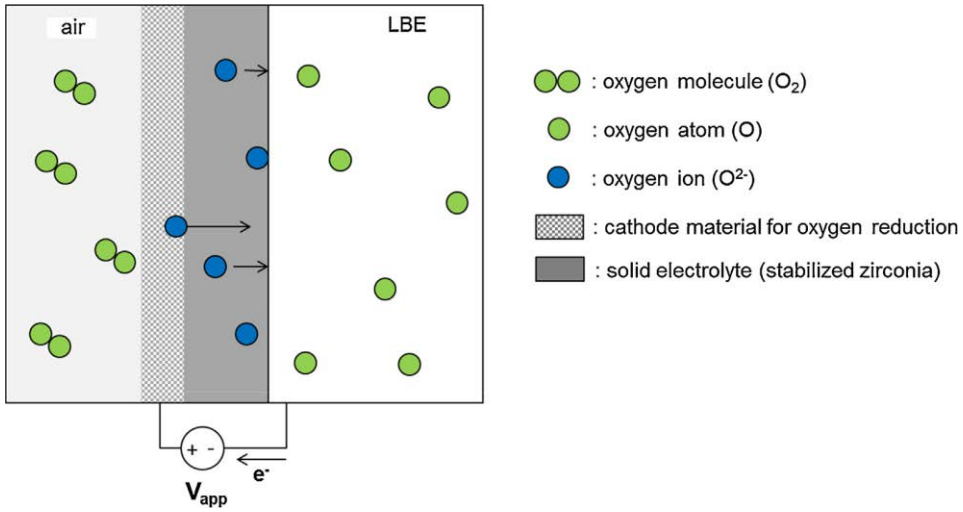

FIG. 14. Electrochemical oxygen pump working principle [5]

In order to be able to implement this method of regulating the oxygen concentration on the LILETIN installation, some modifications were needed. Thus, the installation of two oxygen sensors was performed as shown in Figure 15. One of the sensors measures the oxygen concentration and the other it is the electrochemical oxygen pump, performing the oxygen concentration adjustment. Both sensors were designed and supplied by ENEA Brasimone Research Centre. The EOP was fabricated by using yttria partially stabilized zirconia (YPSZ) as a solid electrolyte and inside a Pt leaf as a cathode. To connect the cathode, a 316 L wire it was used (Figure 16).

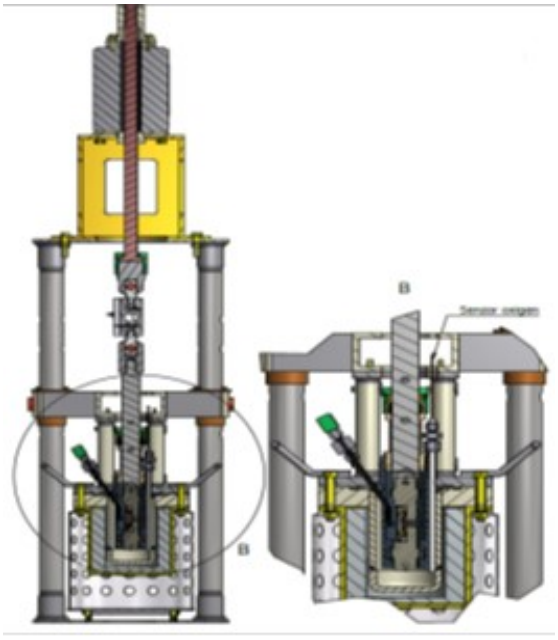

FIG. 15. Facility upgrade by including oxygen sensor

FIG. 16. Electrochemical oxygen pump aspect

5. CONCLUSIONS

The experimental facility, called LILETIN (Liquid LEad Testing INstallation), which has been set up at RATEN ICN, allows performing the experimental tensile tests in the liquid lead environment. At this early stage, the LILETIN facility can perform tensile tests in the liquid metal crucible configuration, with temperatures up to 500 °C in static lead conditions, and without any oxygen monitoring system.

Few conclusions from works performed on the 316L steel specimens tested in the liquid lead environment at 400 - 500 ºC are:

— To examine the mechanical properties of the 316L steel tested in the liquid lead environment, the specimens are tested under tensile loading at a constant strain rate of $5x10^{-5}$ s^{-1};
— SEM pictures highlight the ductile behaviour of the surface fracture for the base material and it is observed that the rupture begins at the surface of the sample and evolves inwards;
— The results show the need to perform more tests in the liquid lead environment to establish the temperature influence on the mechanical properties, as well as by comparison with more tests in the air.

It has been analyzed the operation of the LILETIN facility, a versatile system for uniaxial mechanical tests in liquid lead, designed and developed within RATEN ICN Pitesti. The good points and several issues need to be solved are underlined below:

— The use of the facility is relatively easy for the operator;
— The tensile test diagrams could be exploited to obtain the ultimate tensile strength (UTS);
— There is a request to reduce the lost heat through the device components to achieve the test temperature above 450 °C in a reasonable interval of time;
— Because is not possible to use the normal extensometers for measurements in the liquid lead, it is necessary to find a practical solution to measure the sample elongation during the tensile tests;
— The system for measuring and controlling the concentration of oxygen in the liquid lead is under development.

ACKNOWLEDGMENT

We express our gratitude to the ENEA Brasimone Research Centre partners, for providing the yttria partially stabilized zirconia oxygen sensors.

REFERENCES

[1] S. GAVRILOV, G. COEN, J. VAN DEN BOSCH, "Mechanical Properties of Structural Materials in HLM", SEARCH meeting, Pisa, 2012.
[2] D. GÓMEZ-BRICEÑO, "Guideline document for HLM technology,Deliverable N. 25 VELLA",Ciemat, Spain, 2009.
[3] V. IONESCU, V. RADU, AL.NIȚU, A ION, V. OLARU, L.STOICA," The study of mechanical properties for generation IV candidate materials by tensile tests", Internal Report,2018
[4] V. IONESCU, V. PITIGOI, AL. NIȚU, M. HORORoI, F. VOICU, V. COJOCARU," Effects of liquid lead on 316L tensile properties", Nuclear 2016 Conference, Pitești, Romania, 2016
[5] J. LIM, G. MANFREDI, S. GAVRILOV, K. ROSSEEL, A. AERTS, AND J. VAN DEN BOSCH, Sens. Actuators B, 204 (2014)

SIMULATIONS OF SOME STRUCTURAL MATERIALS BEHAVIOR UNDER NEUTRON IRRADIATION

D.GUGIU
Technologies for Nuclear Energy State Owned Company - Institute for Nuclear Research
Pitesti, Romania
Email: daniela.gugiu@nuclear.ro

Abstract

One of the most important factors in assessing the candidate materials for the new generation of the innovative nuclear systems is the material performance under neutron irradiation. In the case of structural materials the objective of the work is to provide a preliminary analysis of the impact of using molybdenum (TZM, Mo-Re5%, Mo-Re47.2%) and vanadium (V-4Cr-4Ti, V-4Cr-4Ti-0.15Y and V-4Cr-4Ti-0.5Y) based alloys on some neutronic parameters of the ALFRED reactor (Advanced Lead-cooled Fast Reactor European Demonstrator) if they are used as fuel cladding materials. The quantities investigated refer to the multiplication factors, neutron fluxes, heat deposition as well as the isotopic inventory of these alloys at various irradiation and cooling steps. Moreover, the isotope inventories could be used as starting point for further analyses regarding the radioprotection, waste characterization and disposal or for studies concerning the changes in the mechanical and physical properties induced by irradiation.

1. INTRODUCTION

Various stainless steels and other alloys have been considered and investigated during time as candidates for GEN IV and fusion nuclear reactors or for spacecraft devices and a large number of studies have been performed and reported regarding their behavior under different neutron spectra and irradiation temperatures.

Among them molybdenum alloys are investigated extensively being considered as promising materials able to withstand a harsh environment due to their characteristics: high strength and melting point, high thermal conductivity or good corrosion resistance against liquid metals [1-6]. Also, the vanadium alloys are recognized as attractive structural materials for fusion systems due to their mechanical tolerance to neutron damage, high temperature strength, low long-term activation or low decay heat as have been reported in a large number of studies [7-10].

Starting from the favorable characteristics and the potential for high performances of both Mo and V based alloys a preliminary analysis of their behavior under neutron irradiation in a Lead-cooled Fast Reactor (the ALFRED Demonstrator) have been performed. The reference active core configuration was developed in the Seventh Framework Programme (FP7) Lead-cooled European Advanced Demonstration Reactor (LEADER) project and it is presented in detail in [11].

The purpose of the present work is to investigate the impact of these alloys if used as material for fuel claddings on the reactor reactivity as well as to obtain information about the changes in their isotopic composition with irradiation.

2. REACTOR CONFIGURATION AND COMPUTATIONAL TOOLS

ALFRED is a critical reactor (300 MW_{th}) for the demonstration of Lead-cooled Fast Reactor Technology; the reference core is mixed oxide (MOX) fueled (171 fuel assemblies (FAs), hexagonal lattice) with two enrichments zones (57 FAs (out of 171) in the inner core, with fuel enriched at 21.7 at.% (Pu +241Am)/(Pu +241Am + U), and the surrounding 114 FAs with fuel enriched at 27.8 at.%) and it is provided with a control system (12 rods) used for both normal control of the reactor and for SCRAM in case of emergency and a safety system (4 rods) used only for SCRAM. The computational tools used in the present work are the following:

(1) MCNPX 2.6.0 [12] – used for criticality simulations and evaluation of the neutron flux in the fuel claddings (using JEFF 3.1 [13] neutron cross-section library). The actual, detailed geometry of the whole reactor system including the Steam Generators (SG) that are immersed in the cold collector of the primary system has been modelled using MCNPX capabilities (Fig.1);
(2) EASY-2005, the European Activation System that includes the inventory code FISPACT-2005 [14]. FISPACT is used to evaluate the activity, the isotopic inventory and the hazard factors for each alloy used as fuel cladding based on the flux-spectrum computed by MCNPX in the respective material.

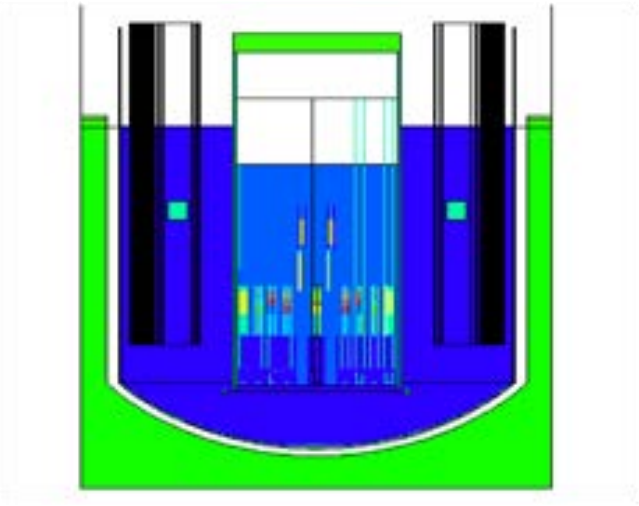

FIG.1. MCNPX model of the reactor

3. RESULTS AND DISCUSSION

3.1. Molybdenum Alloys

The alloys investigated in the present paper refer to Mo-TZM (containing 0.55% Ti, 0.12% Zr and 0.04% C (wt %)), Mo-Re5% and Mo-Re47.2%.
(a) The first step consists in the evaluation of the effect of using these alloys as fuel cladding materials on the neutron economy of the reactor (at BOL-Beginning- of- Life). Thus, criticality simulations using MCNPX code have been performed for each of them; Table 1 shows the k_{eff} values carried out for each case along with the k_{eff} obtained for the reference ALFRED core configuration where the fuel cladding material is 15-15 Ti stainless steel.

TABLE 1. K-EFFECTIVE VALUES FOR MOLYBDENUM ALLOYS

Cladding	TZM	Mo-Re 5%	Mo-Re 47%	15-15 Ti
k_{eff}	0.9953	0.9823	0.8750	1.0805

As can be observed the reactor could become strongly sub-critical when using Mo-Re alloys having a high concentration of Re. This behavior is mainly due to the large neutron absorption cross-sections of both Mo and Mo-Re47% in the energy range 1eV – 1keV as can be observed in Fig. 2.

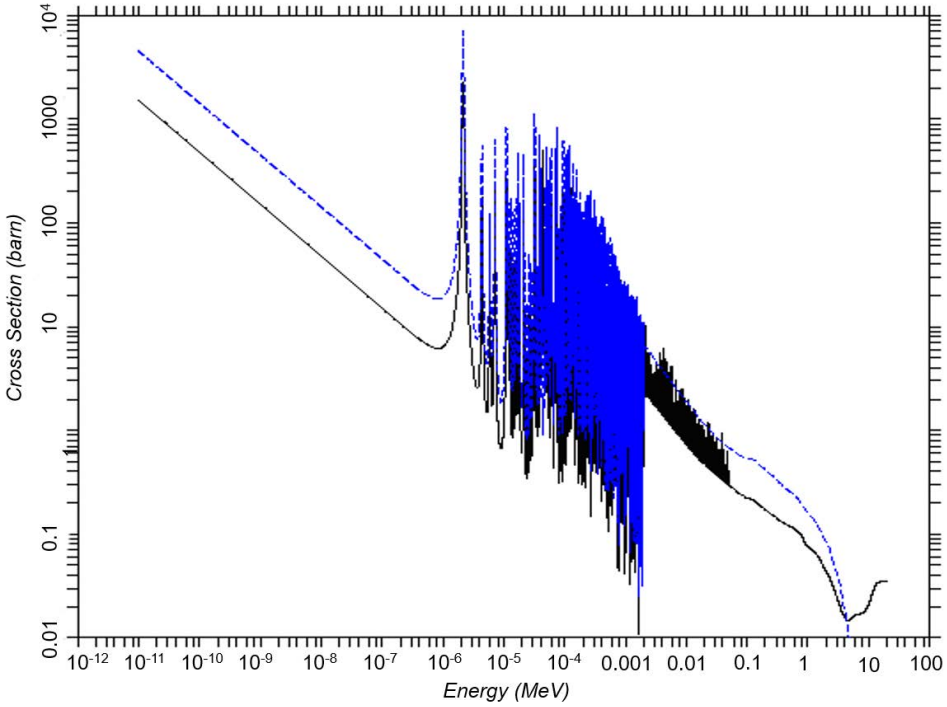

FIG. 2. Mo and Mo-Re 47% neutron absorption cross-sections

Their impact is also reflected in the average neutron flux-spectra evaluated in the fuel claddings for each Mo alloy, Fig. 3.

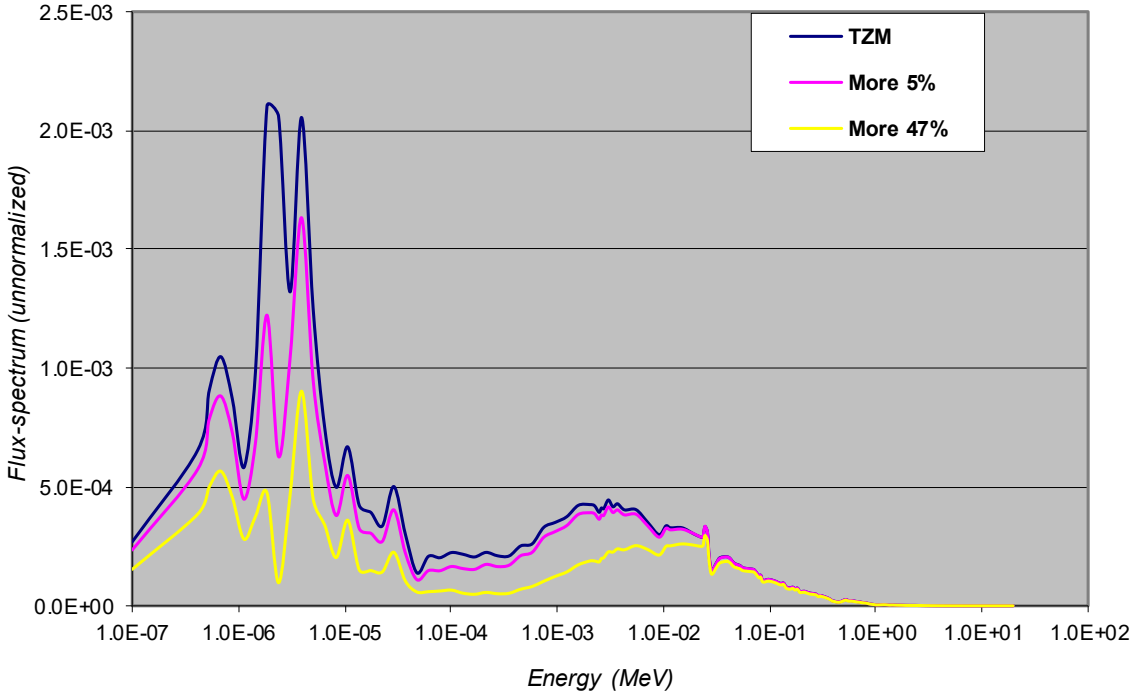

FIG. 3. Neutron -flux spectra

It should be also noticed that the high level of neutron absorption affects the evaluation of the damage produced by neutrons (DPA) in these alloys. The DPA is computed in accordance with the standard NRT model [15]; it means that MCNPX code is used to evaluate the flux and the damage reaction rates in the claddings. These tallies should be multiplied by the flux-to-power normalization factor (FP) [12] which is computed using the following formula:

$$FP = \frac{\nu P}{k_{\text{eff}} \cdot 1.602 \cdot 10^{-13} Q_{av}} \quad (1)$$

where ν is the average number of neutrons emitted per fission, P is the total reactor power, and Q_{av} represents the average value of the recoverable energy per fission. The radiation damage rate expressed in displacements/cm^3/n divided by the atomic density of the respective material and multiplied by the factor 0.8/2*E_d (accordingly to the NRT model, where E_d is the effective threshold displacement energy) leads to the accumulated DPA value.

In case of Mo-TZM alloy (which leads to a k_{eff} value of 0.99529 that could be compensated by the reactor control rod system) the computed value of the DPA after 5 years (the maximum residence time of the fuel in the reactor core) is around 80 dpa which is lower than the limit imposed by the safety requirements (100 dpa). Actually, if one takes into account that the system is subcritical and the flux should be increased, the DPA values has to be multiplied by 1./(1-k_{eff}) [12]; on the other hand, this produces an overestimation of the neutron damage value. The overestimation is much higher in case of Mo-Re5% alloy and especially for Mo-Re47% which is a strong absorber.

Moreover, the transmutation processes (mentioned in the next paragraphs) affect the DPA computed values because of the alloy composition changes with irradiation.

It should be also mentioned that the MCNPX evaluation of the damage cross sections are based on the contributions (by weight) of the individual isotopes; actually, the damage cross sections provided in MCNPX code libraries refer to the monoatomic crystalline materials and not to the composite materials such as alloys. The polyatomic DPA model results can be significantly different than the sum of monoatomic displacement terms [16].

If these alloys are intended to be used in the core of a nuclear reactor provisions needs to be taken with regards to the control rod system reactivity or the fuel enrichments during the design stage of the reactor. It seems that from neutronic point of view, the use of Mo alloys with a high concentration of Re inside the active core should be treated with caution and more detailed analyses have to be performed.

(b) With regard to the energy deposition in the claddings it could be observed that higher Re concentration leads to an increase of the neutron and gamma heating as presented in Table 2. The values have been obtained in the central fuel assembly using MCNPX code.

TABLE 2. ENERGY DEPOSITION FOR MOLYBDENUM ALLOYS

Heating (MeV/g/ting	TZM	Mo- Re5%	Mo-Re47%	15-15 Ti
n-source)	1.16E-07	1.54E-07	3.65E-07	1.47E-07

The results show that the heating value in case of MO-Re47% alloy is almost 2.5 times higher than for reference 15-15 Ti steel which means that the lead coolant should remove the supplementary heat and additional thermal-hydraulics studies has to be performed. The higher heating value will also affect the secondary stress on the cladding.

(c) Estimations of the activation and isotope inventories of the fuel claddings at various irradiations and cooling time steps are of interest as input for further analyses regarding the radioprotection and waste characterization and disposal. Moreover, the claddings activation could provide useful information about the radioactivity level of the corrosion/erosion products (slag) transported by the lead coolant to the free surface in the absence of corrosion resistance treatment [17].

The computational steps consisted in the computation of the average neutron flux (175 energy groups, normalized to the reactor power) using MCNPX in the fuel claddings which has been subsequently used in the FISPACT code in order to evaluate the activation and the isotopic compositions of the Mo alloys after 5 years (the maximum residence time of the fuel in the core).

The total activities (Bq/kg) obtained for Mo-TZM, Mo-Re5% and Mo-Re47% are of 2.92E+14, 4.20E+14 and 1.24E+15 respectively and they show an increase with Re concentration, being also higher than 15-15 Ti activity (7.03E+13). Moreover, the FISPACT code output provides information about the contribution of each type of radiation to the total activity; the beta decay is the main contributor and, together with the alpha decay should be taken into consideration (from personnel radioprotection point of view) during handling and transportation. Even after 100 cooling years, the total activities are still high (order of 10^{10} Bq/kg) and the clearance index remains also enough high due to long-lived isotopes as ^{93}Mo, ^{93m}Nb, ^{99}Tc, and ^{91}Nb.

The changes of Mo alloys isotopic composition with irradiation have been extensively studied with respect to their impact on the crystallographic structure and subsequently on the mechanical, thermal, etc. properties [1-3]. In the present study, Mo-TZM alloy shows a decrease of the Mo concentration mainly due to the (n,p) reactions leading to the formation of niobium isotopes (their concentrations increase with the irradiation time). Moreover, $^{99}_{42}Mo$ produced by ^{98}Mo (n, gamma) reaction leads through beta decay to ^{99}Tc which contribution increases significantly with irradiation. The presence of zirconium in the alloy contributes to the formation of Yttrium through $^{90}Zr\ (n,p)$ interaction and to the production of strontium as result of $^{92}Zr(n,\alpha)^{89}Sr$ reaction. On the other hand, $^{92}Mo\ (n,\alpha)$ reaction contributes to the formation of ^{89}Zr.

In the case of Mo-Re alloys, besides the changes in the Mo concentration and the formation of some elements as Zr, Nb or Tc through the reaction channels already mentioned, one could observe a significant decrease of rhenium mass, an increase of tungsten concentration as well as the formation and the increase of osmium mass with irradiation. Rhenium element consists in $^{185}_{75}\mathrm{Re}$ (37.4%) and $^{187}_{75}\mathrm{Re}$ (62.6%); as a result of neutron interaction $^{185}_{75}\mathrm{Re}$ leads to $^{186}\mathrm{Re}$ which goes through beta decay in ^{186}Os (93.1% branching ratio) and with 6.9% leads to ^{186}W. With regard to $^{187}_{75}\mathrm{Re}$ isotope, this one contributes to the formation of ^{189}Os by beta disintegration of $^{188}_{75}\mathrm{Re}$ produced previously by (n,γ) reaction. Moreover, the observed increase of W is due to both ^{182}Ta disintegration and ^{186}Os contribution.

These changes in the elemental composition with irradiation affect the alloys microstructure and consequently their physical, chemical or mechanical properties which are extensively studied [1-6]; as mentioned before the transmutation process makes more difficult the accurate evaluation of the neutron irradiation damage which value is one of the main constraints during the design phase of the reactor.

3.2. **Vanadium Alloys**

Nowadays the scientist's efforts are focused on the improvement of the vanadium alloys microstructure either starting from the reference V-4Cr-4Ti alloy or by considering new alternative compositions or fabrication routes [10].

One alternative envisaged, for better performances versus high temperatures and for irradiation damage reduction, was yttrium alloying.

Thus, in this paper three vanadium alloys (V-4Cr-4Ti, V-4Cr-4Ti-0.15Y and V-4Cr-4Ti-0.5Y) have been considered as fuel claddings material for ALFRED reactor. The same computational steps as for molybdenum alloys have been performed.

(a) Table 3 presents the multiplication factors carried out by the criticality computations performed using MCNPX code for each case.

TABLE 3. K-EFFECTIVE VALUES FOR VANADIUM ALLOYS

Alloy	V-4Cr-4Ti	V-4Cr-4Ti-0.15Y	V-4Cr-4Ti-0. 5Y	15-15 Ti
k_{eff}	1.08751	1.08754	1.08711	1.08050

As could be seen the use of vanadium alloys as cladding material leads to an increase of the reactivity (~ 700 pcm) which can be controlled/compensated either by the control rods system or by acting on the fuel enrichment values.

(b) The values of the energy deposition in the fuel claddings of the central fuel assembly (Table 4) do not show significant differences among the vanadium alloys investigated; a slight increase which could be due to a higher concentration of yttrium is observed. It should be noted that the heating values of vanadium alloys are lower than the value obtained for the reference 15-15 Ti steel used in the design of ALFRED reactor.

TABLE 4. ENERGY DEPOSITION FOR VANADIUM ALLOYS

Vanadium alloy	V-4Cr-4Ti	V-4Cr-4Ti-.15Y	V-4Cr-4Ti-.5Y	15-15 Ti
Heating (MeV/g/n-source)	1.151E-07	1.152E-07	1.155E-07	1.473E-07

(c) The changes in the elemental composition of the vanadium alloys at various irradiation time steps (1, 3, and 5 years, respectively) have been computed using the same methodology as for molybdenum alloys; the average neutron flux evaluated using MCNPX was used as input in the FISPACT inventory code.

It has been observed the formation and the increase of the gaseous elements concentrations (H, He, etc) and also a significant increase of chromium concentration after 5 years irradiation. Moreover, the burnup of vanadium with irradiation time should be noted.

The total activity after 5 years irradiation provided by FISPACT code lays between 2.91 – 2.97 E+14 Bq/kg for the vanadium alloys and has as main contributor the beta decay. The alloys containing yttrium shows higher values for the ingestion and inhalation hazard factors mainly due to the yttrium and strontium long-lived isotopes which are among the main dominants even after 100 years of cooling. Even so, vanadium alloys presents a low long-term activation, their total activities after 100 years cooling being much lower (almost two order of magnitude) than for 15-15 Ti reference material.

4. CONCLUSIONS

Mo alloys and especially Mo-Re alloys with higher content of Re affect significantly the neutron economy of the reactor when they are used as fuel pins cladding. Besides the neutron absorption and Re transmutation it has been observed [2] pronounced microstructural changes that do not reccommend the use of Mo-Re alloys with high Re concentration in neutron environments.

The use of vanadium alloys as fuel cladding material in ALFRED reactor lead to an increase of the reactivity that could be managed either by the control rods system with enough anti-reactivity to fulfill the safety requirements or by acting on the system criticality through changes on the fissile enrichment during the design stage. No significant differences have been observed for the computed energy depositions and the neutron damage values with respect to those obtained for 15-15 Ti reference cladding material. It has been observed the formation and the increase of the gaseous elements content with irradiation and also a significant increase of chromium concentration that should be futher studied because of its impact on the vanadium alloy properties.

REFERENCES

[1] SINGH, B. N., EVANS, J. H., HORSEWELL, A., TOFT, P., MULLER, G.V., Effects of neutron irradiation on microstructure and deformation behaviour of mono- and polycrystalline molybdenum and its alloys, J. Nucl. Mat. (1998) 865-872.

[2] EDWARDS, D.J., GARNER, F.A., GELLES, D.S., The influence of neutron irradiation in FFTF on the microstructural and microchemical development of Mo-41Re at 470-730 ^{0}C, J. Nucl. Mat. 375 (2008) 370-381.

[3] KITSUNAI, S.Y., KURISHITA, H., KUWABARA, T., NARUI, M., HASEGAWA, M., TAKIDA, T., TAKEBE, K., Radiation embrittlement behavior of fine-grained molybdenum alloy with 0,2 wt % TiC addition, J. Nucl. Mat. 346 (2005) 233-243.

[4] BUSBY, J. T., LEONARD, K. J., ZINKLE, S. J., Radiation-damage in molybdenum-rhenium alloys for space reactor applications, J. Nucl. Mat. 366 (2007) 388-406.

[5] MAJUMDAR, S., KAPOOR, R., RAVEENDRA, S., SINHA, H., A study of hot deformation behavior and microstructural characterization of Mo-TZM alloy, J. Nucl. Mat. 385 (2009) 545-551.

[6] MEIMEI, LI, ELDRUP, M., BYUN, T. S., HASHIMOTO, N., Low temperature neutron irradiation effects on microstructure and tensile properties of molybdenum," 376 (2008) J. Nucl. Mat. 11-28.

[7] Loomis, B.A., Hull, A.B., Smith, D.L., 1991, "Evaluation of low-activation vanadium alloys for use as structural material in fusion reactors," Journal of Nuclear Materials 179-181, pp. 148-154.

[8] HIROHATA Y., YAMADA T., YAMAUCHI Y., HINO T., NAGASAKA, T., MUROGA, T., Helium thermal desorption and retention properties of V-4Cr-4Ti alloy used for first wall of breeding blanket, 81(2006) Fusion Engineering and Design 193-198.

[9] SMITH, D.L., BILLONE M.C., NATESAN, K., Vanadium-base alloys for fusion first-wall/blanket applications, Intl. J. Refractory Metals & Hard Materials, 18 (2000) 213-224.

[10] KURTZ, R.J., ABE, K., CHERNOV, V.M., HOELZER, D.T., MATSUI, H., MUROGA, T., ODETTE, G.R., Recent progress on development of vanadium alloys for fusion, J. Nucl. Mat. 329-333 (2004) 47-55.

[11] PETROVICH, C., GRASSO, G., ARTIOLI, C., ROCCHI, F., SCIORA, P., Definition of the ETDR core and neutronic characterization, DEL007-2012, WP2, LEADER project, UTFISSM-P9SZ-002, Rev.0, ENEA-CEA (2012).
[12] PELOWITZ, D.B. ET AL., MCNPX 2.7.E Extension, LA-UR-11-01502, Los Alamos (2011).
[13] KONING, A., FORREST, R., KELLETT, M., MILLS, R., HENRIKSSON, H., RUGAMA, Y., The JEFF – 3.1 Nuclear Data Library, JEEF Report 21, OECD 2006/NEA Data Bank N° 6190, ISBN 92-64-02314-3.
[14] FORREST R. A., The European Activation System: EASY – 2005, UKEA FUS 513; FISPACT -2005 User's Manual, UKEA FUS 614 (2005).
[15] NORGETT, M. J., ROBINSON, M. T., TORRENS, I. M., A Proposed Method of Calculating Displacement Dose Rates, J. Nucl. Eng. Design, 33 (1975) 50-54.
[16] OECD-NEA, Computing Radiation Dose to Reactor Pressure Vessel and Internals, NEA/NSC/DOC (96)5 (1996).
[17] GUGIU, D., PETROVICH, C., ETDR core: DPA rates in the main components, activation, doses, Technical report TEC061, FP7 – LEADER Project (Lead-cooled European Advanced Demonstrator Reactor) (2012).

VACANCY TYPE DEFECTS BEHAVIOR IN MATERIALS FORESEEN FOR LIQUID METAL COOLED FAST REACTORS

V. SLUGEN
Institute of Nuclear and Physical Engineering, Slovak University of Technology Bratislava, Slovakia
Email: Vladimir.Slugen@stuba.sk

Abstract

Liquid metal cooled fast reactors is a promising technology but sensitive for material resistance to radiation and chemical treatment in primary coolant area. The paper summaries research activities in last 20 years focused on distinct effects of flux and temperature on the behavior of nuclear materials which could be potentially applied in lead cooled reactors. Neutron treatment was experimentally simulated via Hydrogen ions implantation into near surface region of studied materials. This contribution reviews experimental positron annihilation spectroscopy (PAS) studies of various grades of advanced nuclear structural steels. The new results are compared with those from the earlier studies in order to distinguish between various processes involved in the formation of the microstructure of irradiated materials.

REFERENCES

[1] YVON, P., Structural Materials for Generation IV Nuclear Reactors. ISBN: 9780081009123, (2016)
[2] ZINKLE, S., WAS, G. Material challenges in nuclear energy. Act. Mater. 61, 735-758 (2013)
[3] PHYTHIAN, W.J., ENGLISH, C.A., J. Nucl. Mater. 205, North-Holland, 162-177, Holland, (1993)
[4] SLUGEN, V., et al, J. Nucl. Mater. 442, 499-506 (2013)
[5] SLUGEN, V., Safety of VVER-440 Reactors – Barriers Against Fission Products Release, Springer, London (2011)
[6] PECKO, S. et al, Appl. Surf. Sci. 312, 172-175 (2014)
[7] KRSJAK, V., et al, Probl. At. Sci. Technol. 4, 109–115 (2009)
[8] SABELOVA, V., et al, J. Nucl. Mater. 458, 350-354 (2015)
[9] KOUTSKY, J. KOCIK, J., Radiation damage of structural materials, Academia, Prague (1994)
[10] SLUGEN, V., KRYUKOV, A., Nucl. Eng. Des. 261, 308 - 312 (2013)
[11] BECVAR, F., et al, Mat. Sci. Forum 105-110, 901 (1992)
[12] KOCIK, J., KEILOVA, E., J Nucl. Mater. 172, 126 (1990)
[13] DE BAKKER, P., et al, Proc. Int. Conf. Vol. 50, ICAME'95, I. Ortalli (ed.), SIF, Bologna,145 (1996)
[14] BOHMERT, J., GROSSE, M., Proc.of Jahrestagung Kerntechnik 1998, (ed. Inforum Verlag, Bonn), 741 (1998)
[15] BRAUER, G., et al, Nucl. Eng. Des. 158, 149 (1995)
[16] HAUTJARVI, P., Positrons in solids, Springer-Verlag, Berlin (1979)
[17] DUPASQUIER, A., Mills, A.P., Positron Spectroscopy of Solids, IOS Press, Amsterdam, (1995)
[18] ANDERSEN, O.K., JEPSEN, O., SOB, M., Electronic Band Structure and Its Applications, ed. M. Yussouff, Springer, Heidelberg (1987)
[19] PUSKA, M.J., NIEMINEN, R.M., J. Phys. F 13, 333 (1983)
[20] SEITOSEN, A.P., PUSKA, M.J., Nieminen, R.M., Phys. Rev. B 51, 14057 (1995)
[21] www.itereu.de
[22] ITER, Materials Assessment Report, Section 1.4 - Copper Alloys, EFDA Garching, 1-44 (1998)
[23] SLUGEN, V., et al, Fus. Eng. Des. 70/2, 141 (2004)
[24] SLUGEN, V., et al, Nuclear Fusion 44, 93 (2004)
[25] BALLO, P., SLUGEN, V., Comp. Mater. Sci. 33, 491 (2005)
[26] PUSKA, M.J., NIEMINEN, R.M., Rev. Mod. Phys. 66, 841 (1994)
[27] UENO, K., et al, Mater. Sci. Forum 255-257, 430 (1997)
[28] MIKULOWSKI, B., GROGER, V., KREXNER, G., HEWARTH, M., Archives of Metallurgy 45, 237 (2000)
[29] HAKINEN, H., MAKINEN, S., MANNINEN, M., Phys. Rev. B 41, 12441 (1990)
[30] GROGER, V., et al, Mater. Sci. Forum 210-213, 743 (1996)

[31] BAUER-KUGELMANNN, W., SPERR, P., KOGEL, G., TRIFTSHAUSER, W., Mater. Sci. Forum 363-365, 529 (2001)
[32] KOVAC, P., BORTIANSKY, A., KLOPENKOV, M., PAVLOVETS, M., Proc. Int. Conf. on Applied Charged Particle Accelerators in Medicine and Industry ACCELERATORS 2001, (October 1-4, 2001, St. Petersburg, Russia), CNIIatominform Moskva, 430 (2001)
[33] KURIPLACH, J. et al, Mater. Sci. Forum 363-365, 94 (2001)
[34] VETERNIKOVA, J. et al, Nucl. Eng. & Desg. 251, 354 (2012)
[35] SIMEG-VETERNIKOVA, J. et al, Act. Phys. Pol. 125, 741 (2014)

RESEARCH OF CORROSION BEHAVIOR OF STEAM GENERATOR TUBES FOR LEAD-COOLED POWER UNIT

K.I. Shutko
NIKIET JSC
Moscow, Russia
E-mail: correnes@nikiet.ru

D.A. Marchenkov
NIKIET
Moscow, Russia

O.P. Arkhipov
NIKIET
Moscow, Russia

Abstract

For lead-cooled power unit the direct-flow type steam generator is designed. Material of heat exchanger tubes will serve simultaneously in contact with liquid lead (the primary coolant side) and in secondary coolant – water and a superheated steam. New grade EP302M stainless steel was developed for this application. For confirmation of proper resistance to corrosion of heat exchanger tubes under service conditions research is carried on by NIKIET involving other research organizations.

The results of research describe the corrosion behavior of the structural material of heat exchanger tubes in liquid lead, water and superheated steam. As revealed, material of heat exchanger tubes demonstrates adoptable corrosion and corrosion-mechanical behavior for providing reliable SG designed service life.

1. INTRODUCTION

For the reactor unit BREST-OD-300 vertical type steam generator (SG) is designed. The SG has steam overheating zone in an upper part of lifting section of twisted heat-exchange tubes (HET). Under operation the external surface of HET is in contact with flowing liquid lead. Internal surface of HET is in contact with water-overheated steam environment. This leads to significant difference in corrosive effect on HET material from media of the secondary circuit. In this regard, HET constructive material should be highly corrosion resistance in the range of operating temperatures of 340-530 ºC at pressure 17 MPa (from secondary circuit). Based on the foregoing, one of the important tasks in the design of the innovative BREST-OD-300 reactor unit is the creation of a structural material capable of providing the necessary strength and durability of the HET under operating conditions of the steam generator.

For this purpose, the new nitrogen, molybdenum, silicon containing austenitic stainless steel (grade EP302M) was developed. Proper technology for the production of long-length (for avoiding cold-rolled) tubes was also developed. This choice is based on both experience of application of type EP302 stainless steel that is resistant to corrosion in lead coolant and previously obtained positive test results of high-strength nitrogen-containing cold-deformed steels which are highly resistant to local types of corrosion in seawater and other chloride-containing environments.

Nowadays, NIKIET in collaboration with other research centers carry out material and constructive elements testing to confirm satisfactory corrosion resistance and corrosion-mechanical behavior of grade EP302M steel that is selected for the manufacturing of SG HET.

The following works were carried out:

— assessment of the rate of general corrosion, determination of the value of increase in corrosion according to the results of HET samples tests in liquid lead, water and superheated steam for using in strength calculations;
— assessment of effect of superheated steam and water environment on corrosion behaviour of the model 'tube-tube sheet' joint of SG under static loading and low-cycle fatigue tests;
— assessment of the resistance of HET material microstructure sensitization and subsequent intergranular corrosion (IGC) susceptibility.

2. CORROSION RESISTANCE IN LIQUID LEAD

Samples of HET trial part tested in non-isothermal test loop in flowing lead (0.5 m/s) at 550 ºC. Dissolved oxygen level maintained in base range.

Figure 1 illustrates the oxide film in cross-section view of metallographic sample of heat exchange tube after 9000 h of testing. It is revealed that two-layer oxide film formed (magnetite outer layer, chromium-rich spinel internal layer and some internal oxidation). Oxidation mode has the fading character in time. Mechanical stress within designed range does not arise corrosion interaction.

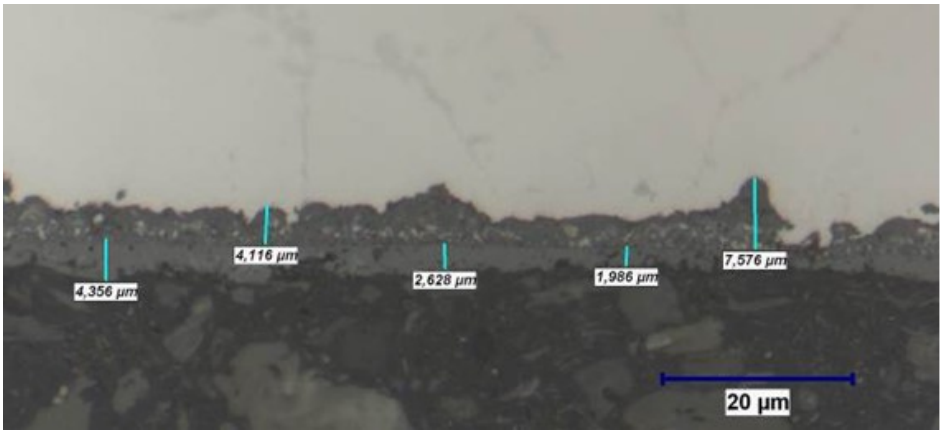

FIG. 1. Oxide film formed on the surface of sample of grade EP302M steel. Tested in flowing lead at 550 ºC for 9000 h
Numerical results

3. CORROSION RESISTANCE IN WATER AND SUPERHEATED STEAM

Corrosion tests of samples of steel grade EP302M machined from long-length heat exchange tubes were carried out in autoclave loops in NIKIET. Samples of type 321 stainless steel were also tested as the reference material. When tested the main water-chemical parameters of feedwater of the steam generator, the parameters are steadily maintained with high accuracy (temperature 350 ± 5 ºC and 525 ± 5 ºC, pressure 17 ± 1 MPa). Chemical parameters of water environment also continuously controlled: electrical conductivity (EC) of 0.10 ± 0.05 µS/cm and concentration of dissolved oxygen (DO) of 10 ± 5 µgr/dm3 (at water sample temperature of 25 ºC).

Figure 2 shows oxide film in cross-section of metallographic sample cut from heat exchanger tubes with an electrochemical polished surface after testing in water at 350 ºC for 1000 h.

According to the results of the elemental analysis, the oxide film (reference points 1-7, figure 2) consists mainly of iron oxides with a small addition of chromium and nickel oxides, with the weight fractions of iron, chromium and nickel averaging ~ 50%, ~ 15% and ~ 10%, respectively, and the thickness of the oxide film after 1000 h of testing not exceeding 4 μm.

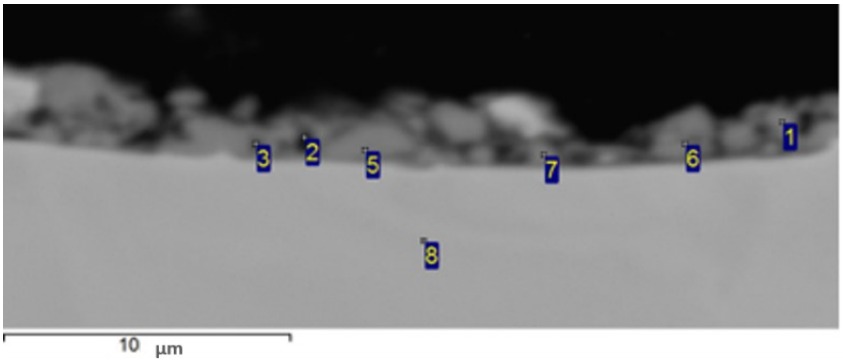

FIG. 2. Oxide film (REM image) formed on the surface of specimen of grade EP302M stainless steel. Tested in superheated steam at 350 ºC for 1000 h

The general corrosion rate of new austenitic steel EP302M calculated according to the results of tests in water at 350 ºC is 1.5 times lower than the corrosion rate for austenitic stainless-steel grade 321 that is widely used in nuclear engineering. This is due to the presence of silicon and molybdenum in the composition of EP302M steel.

In Figure 3 the structure of the oxide film on sample with an electrochemically polished surface after testing in superheated steam at temperature 525 ºC for duration 1000 h is shown.

As can be seen at Figure 3, that the two-layer oxide film is formed on specimen surface. Its outer layer is iron oxide, which in stoichiometric composition corresponds to magnetite - Fe_3O_4 (points 1-3). The inner layer is a mixed spinel of complex composition (points 4-6), in which the mass fractions of chromium (Cr), iron (Fe) and nickel (Ni) are on average 27%, 22% and 19%, respectively, and the thickness of this oxide film after 1000 hours of testing averages from 5 to 7 μm.

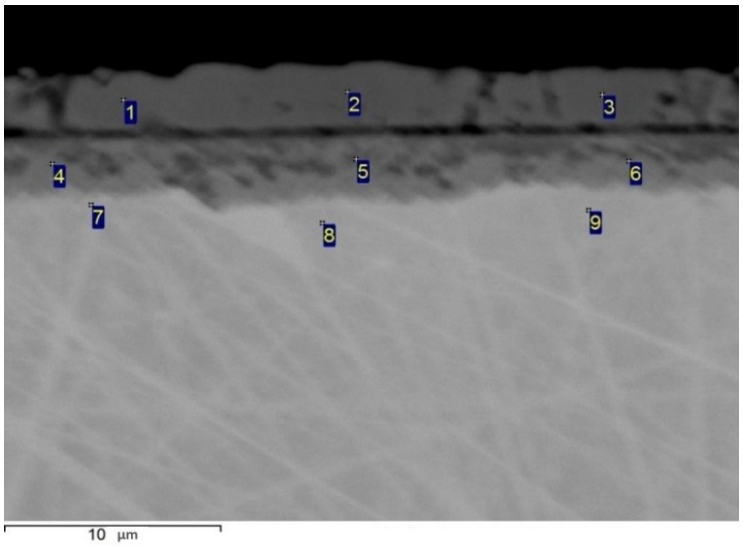

FIG. 3. Oxide film (REM image) formed on the surface of specimen of grade EP302M stainless steel. Tested in superheated steam at 525 ºC for 1000 h

Using extrapolation of the data obtained from corrosion autoclave tests it was found that the corrosion to HET wall thickness calculated for the 30-year designed service-life of the SG in contact with water at a temperature of 350 ºC increases (based on 6000 h of testing). It is estimated to 0.01 mm. The increase in corrosion to wall thickness is 0.1 mm in contact with superheated steam at temperature 525 ºC based on 8000 h of testing.

To perform weld joints of SG heat exchange tubes made of steel grade EP302M to tube sheet made of steel grade 321, 2 variants of welded joints are proposed: welding of tubes directly to tube sheet or welding of tubes through double austenitic plating over tube sheet.

Corrosion-mechanical autoclave tests under static loading and low-cycle fatigue conditions are carried out in water and superheated steam media for experimentally validated choice of type of welded joint of 'HET – tube sheet'. For this purpose, the samples of model welded joints made using different welding materials with and without double austenitic plating were tested, see figure 4.

Samples were tested 2000 h in the model water and steam SG environments in the conditions of the static loading corresponding to tension 0.8 of yield strength (relatively to material grade 321 stainless steel). After 2000 hours of tests under static loading, tests were carried out for low-cycle fatigue with stress amplitude of 200 MPa, number of cycles of 102 at frequency 0.1 Hz. Test conditions are selected based on SG operation model in transient regime.

According to the results of corrosion-mechanical tests, the metal of welded joints showed resistance to corrosion cracking in model of water and steam environments of SG after both static loading and cyclic loading.

Visual and optical inspection of the sample surface (see Figure 4) after testing has not revealed surface cracks and other defects. Oxide film formed on the samples surface that protected the metal from corrosion local corrosion damage.

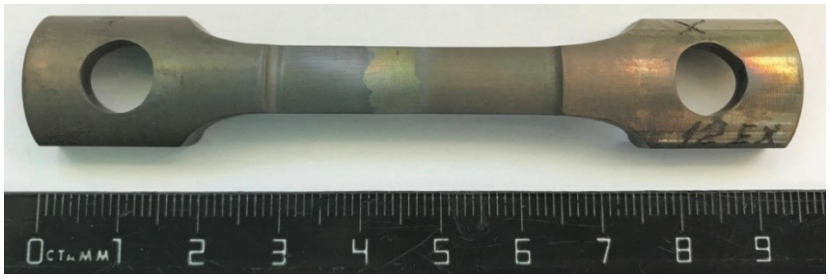

FIG. 4. Sample of welded tube segment after static loading and subsequent low cycle fatigue tests in superheated steam at 505 ºC

Selection of the type of the welded joint 'HET - tube sheet' for the SG will be made after completion of tests of model joints, including testing after additional heat treatment at temperature 550 ºC for simulating material aging (sensitization) during SG operation.

4. INTERGRANULAR CORROSION RESISTANCE

Intergranular corrosion resistance of samples cut from the trial party of heat exchanger tubes estimated by electrochemical method of potentiokinetic reactivation (DL-EPR) according ISO 12732 for quantitative measurements and by using chemical method ASTM A-262 pr. E for qualitative assessment. The effect of samples aging at temperature 650 ºC and exposures up to 100 h as well as aging at 550 ºC for 7000 h on susceptibility to intergranular corrosion (sensitization) studied.

It was experimentally proved that EP302M stainless steel is resistant to intergranular corrosion both in the initial as received conditions and after aging at a temperature of 650 ºC for 100 h and at temperature 550 ºC for 7000 h.

5. THE MAIN RESULTS AND CONCLUSIONS

In the scope of work, the following results were obtained:

— basing on the data of corrosion tests of grade EP302M stainless steel the calculated increases in corrosion to the wall thickness of heat exchange tubes are determined for the 30-year design life of the SG: in superheated steam at temperature 525 ºC - 0.1 mm; in water environment at temperature 350 C - 0.01 mm; in a liquid lead at temperature of 550 ºC - 0.1 mm (with controlled values of oxygen content ~ 10-6 mass (%));
— resistance to local corrosion damage (corrosion cracking etc.) of a model welded-joint without surface cladding under static loading and low-cycle fatigue water and steam SG environments confirmed for samples without sensitizing heat treatment;
— resistance against intergranular corrosion of heat exchanger tubes in as received condition and after aging under following regimes 650 ºC, 100 h and 550 ºC, 7000 h confirmed;

An analysis of test data allows to conclude that grade EP302M stainless steel correctly proposed as the structural material for heat exchanger tubes. Corrosion and corrosion-mechanical properties allow providing reliable operation of the steam generator of BREST-OD-300 during the 30-year design life under conditions of sustainable compliance with the quality requirements of lead coolant and working environment from the side of the secondary circuit.

In order to confirm the resource characteristics of heat exchanger tubes and reliable option of welded-joints ‘tube - tube sheet’ for steam generator, the following experimental studies are carried on:

— comparative evaluation of the corrosion behaviour of heat exchanger tubes with various finish processing of the inner surface (electrochemical polishing with different etching intensity, light annealing), issuing requirements to manufacturer;
— comparative tests under static loading and low-cycle fatigue of model ‘tube - tube sheet’ welded-joints after long sensitizing heat treatment;
— evaluation of deviation of dissolved oxygen content in liquid lead on corrosion behaviour;
— influence of stress-strain state in the region of bending on corrosion behaviour of the material.

ACKNOWLEDGEMENTS

The authors are gratefully thanking to A.V. Bashkin - leading engineer of the NIKIET Materials Science Dept. for metallographic studies; colleagues from FSUE 'I.P.Bardin TsNIIchermet' for RC 'Kurchatov Institute - CRI KM Prometey' for experimental work and collaboration

TENSILE TESTING OF SUB-SIZED T91 STEEL SPECIMENS IN LIQUID LEAD

Z. SZÁRAZ
European Commission, Joint Research Centre
Petten, the Netherlands

K. TUČEK
European Commission, Joint Research Centre
Petten, the Netherlands
Email: kamil.tucek@ec.europa.eu

R. NOVOTNÝ
European Commission, Joint Research Centre
Petten, the Netherlands

K.-F. NILSSON
European Commission, Joint Research Centre
Petten, the Netherlands

Abstract

The aim of the present work is to study the effect of controlled liquid lead environment on mechanical properties of T91 ferritic-martensitic steel. Tensile tests on sub-sized flat specimens were performed in both argon and liquid lead environment. The polished tensile specimens were pre-exposed in liquid lead at 450 °C for a period of at least 100 h prior to testing and at 500 °C for a period of 1000 h, at dissolved oxygen concentrations below 10-9 weight %. The pre-exposure improves the wetting, i.e., the contact between the tested material and heavy liquid metal. The tensile tests were performed at 400 °C and an initial strain rate of 1x10-4 s-1, with the load exerted by pneumatic bellow-based devices. The oxygen content in lead was continuously monitored during the tests and kept below 10-9 weight %. Reference tests in Ar protective atmosphere were conducted at the same test conditions (temperature and strain rate). The test conditions were selected based on results obtained on T91 tested in lead-bismuth eutectic (LBE). For LBE, it has been shown that the mechanical properties strongly depend on temperature, strain rate and dissolved oxygen content. The research work forms an in-kind contribution to the GEMMA Horizon 2020 collaborative project, which supports component design, safety assessments, and licensing of European lead-cooled fast reactor (LFR) technology demonstrators, Multi-purpose Hybrid Research Reactor for High-tech Applications (MYRRHA) (cooled by LBE) and ALFRED (cooled by lead). The testing was done in the JRC LIquid Lead LAboratory (LILLA). The LILLA experimental facility allows conducting qualification tests of candidate structural materials for Generation IV LFRs at temperatures up to 650 °C with well-controllable parameters, in particular oxygen content in lead, test temperature, load and displacement/strain. The paper presents and discusses results of the tensile test campaign conducted in actively oxygen-controlled liquid lead environment.

1. INTRODUCTION

In European and international partnerships, the Joint Research Centre (JRC) studies feasibility of advanced reactor concepts, which aim at improved safety and reliability performance, more efficient fuel use, reduction of high-level, long-lived waste, and improved economy. Research and development (R&D) in support of these innovative reactor concepts are also being performed in multilateral collaboration within the Generation IV International Forum (GIF). The GIF has fourteen members (signatories of the GIF Charter) including European Union (EURATOM) [1-2].

The Lead cooled Fast Reactor (LFR) is one of the six promising next generation reactor concepts selected in GIF. The application of liquid lead as a primary coolant brings several important inherent safety advantages vis-à-vis the current generation of reactors. LFRs can be operated at close to atmospheric pressure; there is therefore no need to maintain complex (and expensive) structures to provide pressure boundaries like in light-water reactors. Lead has a high boiling point (1749 °C), good natural convection characteristics, and high thermal inertia providing robust passive safety behavior. Finally, lead is also chemically relatively inert in contact with water and air, which leads to improved safety and economic competitiveness [3].

The paper first presents some features and capabilities of JRC's liquid lead experimental facility, LIquid Lead LAboratory (LILLA). The LILLA facility has been developed in the joint programming with EU Member States, with the aim to support the development of the European heavy liquid metal (HLM) cooled concepts, MYRRHA [4] and ALFRED [5], as well as related activities in GIF [6]. The facility allows studying the degradation of mechanical properties of structural materials under tensile and compressive stress, the load being generated by pneumatic bellow-based devices. LILLA gives the possibility to perform a variety of mechanical tests (e.g., tensile, creep, fracture toughness, and small punch tests) of candidate structural materials for LFRs at temperatures up to 650 °C with well-controllable parameters of, in particular, oxygen content in lead, test temperature, load and displacement/strain. The reliability of systems controlling lead chemistry and related components and instrumentation can be tested as well.

The paper thereafter summarizes the outcomes of the first campaign of the tensile tests on sub-sized flat T91 specimens, 30 mm in length and 1.5 x 2 mm^2 in cross-section, conducted both in Ar and liquid lead environment in oxygen-depleted conditions ($< 10^{-9}$ weight %). It has been shown that the mechanical properties in lead-bismuth eutectic (LBE) strongly depend on temperature, strain rate and dissolved oxygen content [3,7]. The performed research work contributes in-kind to the GEneration iv Materials Maturity (GEMMA) Horizon 2020 collaborative project [8]. The GEMMA project aims at bringing to maturity the structural materials for fast spectrum Generation IV concepts considered in Europe.

2. THE LILLA FACILITY AND TEST SECTIONS

2.1. **The description of the LILLA facility**

The LILLA facility features two cylindrical tanks: a dump tank and a measuring tank, both with connecting piping to transfer molten lead between the tanks. An integrated piping system also delivers and extracts gases to and from the facility, respectively. A 3D drawing and view of the facility is displayed in Figs. 1 and 2.

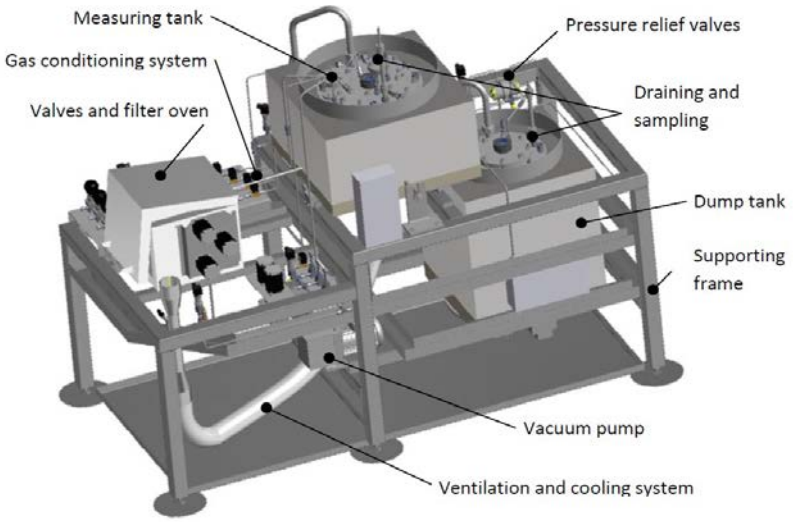

FIG.1. Drawing of the LILLA experimental facility for mechanical testing in liquid lead

The main characteristics of the LILLA facility are:

— operating temperatures in lead: up to 650 °C;
— operating range of oxygen concentrations in lead: from saturation to at least 10^{-10} weight %;
— operating pressure: 0.2 MPa;
— lead inventory: ca. 35 l;
— structural material: AISI 316 Ti;
— surfaces in contact with molten lead are protected by Al_2O_3 coating (using the pack cementation technology);
— active control of gas / oxygen injected to cover gas space and to molten lead (below surface) by an appropriate admixture and delivery of Ar, Ar-H_2, and air to the facility;
— up to four test sections (with possibility to conduct four mechanical tests independently);
— two reserve ports (diameter 35 mm) with a possibility for multiple feedthroughs;
— online sampling of lead during operation of the facility to control the content of impurities;
— gas and lead filtering capability.

FIG.2. View of the LILLA experimental facility for mechanical testing in liquid lead

Inert heavy gas (argon) is used as cover gas in the tanks and to transfer molten lead in the facility. The heaters can be operated both automatically and manually, allowing melting, heat-up, maintenance of lead temperatures, shutdown, and passive drainage of lead to the dump tank. The natural convection flow of the lead in the measuring tank can be regulated by the adjustment of the power of external heaters and heat losses to an internal cooling channel. In addition to an oxygen diffusion process from the cover gas space, this feature also facilitates a time-efficient control of oxygen content in lead. The oxygen content in molten lead is actively monitored by installed electrochemical sensors with yttria-stabilized zirconia (YSZ)/Pt(air) reference electrode.

The digital data acquisition system automatically records all experimental and measured data. These are stored on a dedicated data drive for quality assurance and further assessments and evaluations.

2.2. **The description of the test sections**

Future Generation IV reactor concepts seek to increase operating temperatures to achieve higher thermodynamic efficiency and/or end-product flexibility through the use of innovative coolants. The qualification of existing and/or new materials for advanced reactor system therefore requires the development of a new testing equipment, which can be used reliably and safely in such demanding testing conditions. Material testing in these harsh environments then also typically requires small-size (i.e., sub-size) specimens, below the minimum specimen size prescribed by material testing standards, such as ANSI, ASTM, DIN, and ISO.

To this end a new, innovative test equipment has been developed, assembled and calibrated for the use in the LILLA facility to perform mechanical tests on small specimens in liquid lead. The developed design solution is highly flexible, allowing to use a wide variety of test specimens, including the disk-shaped compact tension DC(T), flat and round bar tensile, and small punch types of the specimens.

The test section load is exerted by a new type of the pneumatically driven double2bellows (D2B) loading device, cf. Fig. 3. This apparatus can generate both tensile and compressive loads measured by a load cell in a continuous way.

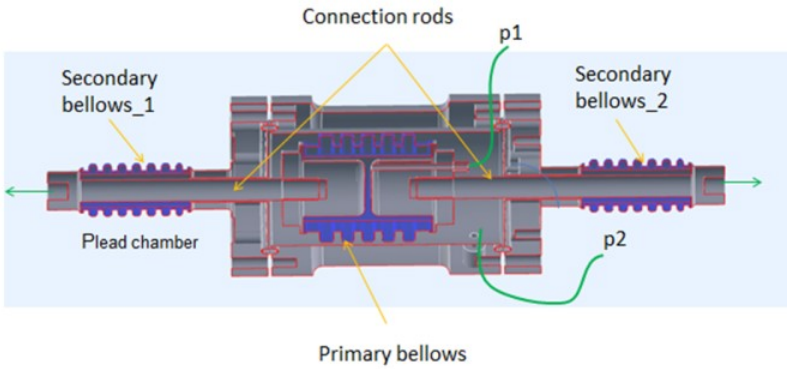

FIG.3. The double2bellows (D2B) loading device

The LILLA facility features four independent test sections integrated into the measuring tank with the following parameters:

— maximum air pressure in the test sections: 15 MPa for pneumatic bellows-based loading devices;
— maximum load: 12 kN, push/pull;
— strain rates: 10^{-7} to 10^{-2} s^{-1} (based on the specimen geometry described in Sub-section 3.1);
— fatigue frequency: maximum 0.1 Hz;
— range of amplitudes: 0.1 to 0.0005 Hz;
— test / hold times: up to 5000 h;
— each test section has its own YSZ/Pt(air) reference electrode oxygen sensor and thermocouple.

The test sections of the LILLA facility consequently allow a wide range of tests, including constant strain rate tensile tests, e.g., Slow Strain Rate Tensile (SSRT) tests, fracture toughness tests, crack growth rate tests and small punch tests.

A detachable fixing system for the various test specimen types is an integrated part of every test section, cf. Fig. 4. Each test section is also independently controlled by a servo-controlled pressure control system using the PLC (Programmable Logic Control). The required PLC programs (using the Moog Axis Control Software [MACS] software) have also been developed and thoroughly tested.

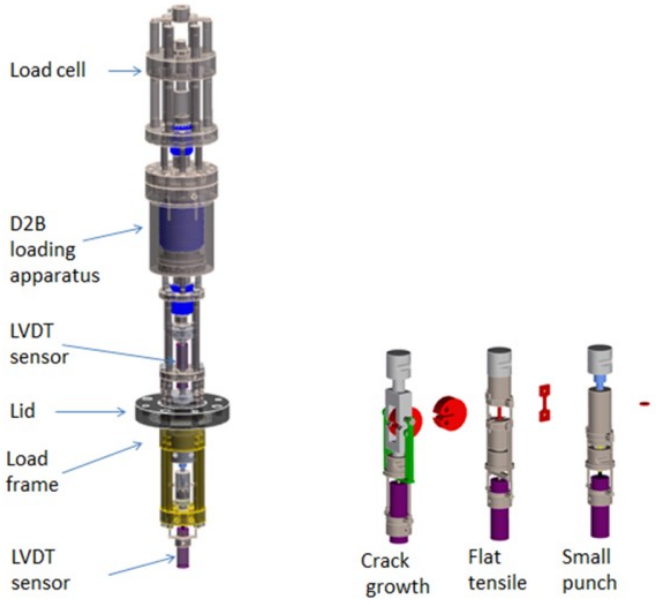

FIG.4. Main parts of the test section together with the fittings for the crack growth/fracture toughness, tensile, and small punch tests

Before its first use, the D2B loading device of each test section was calibrated and its load symmetry verified. The calibration involved the comparison of readings given by the calibration load cell and load cell installed in the test section for several different primary and secondary pressures. These readings were also compared with calculated theoretical values. Very good agreement was achieved between measured and calculated loads, typically below ± 5 N (NB. loads were calculated from measured pressures in the bellows and their effective cross-sections).

3. SSRT TESTS OF T91 IN ARGON AND LIQUID LEAD

3.1. **Material and test conditions**

The investigated material was the 9% chromium ferritic-martensitic steel T91 received from SCK•CEN and originating from the DEMETRA domain of the EUROTRANS 6th EU Framework Programme integrated collaborative project [9]. The material was hot rolled into a 15 mm thick sheet. After the rolling, normalizing treatment (15 minutes at 1050 °C) and tempering treatment (45 minutes at 770 °C) were applied.

The sub-sized un-notched flat tensile specimens were cut from the plate material by wire erosion. The total length of the dog bone shaped specimens was 30 mm, with 1.5 x 2 mm^2 in cross section and 5.6 mm in gauge length, Fig. 5. They were taken from the plate in L direction.

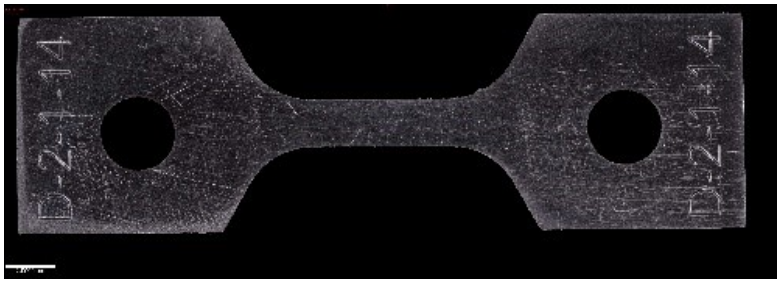

FIG.5. Sub-sized flat specimen for tensile testing

The tensile tests were performed in a displacement control mode, i.e., with a constant speed of the pulling rod. The displacement of the pulling rod was measured by a linear variable differential transformer (LVDT) position sensor placed outside of the measuring tank. The initial strain rate was $1x10^{-4}$ s^{-1}. The specimens were loaded until fracture. The measured curves were corrected for the own stiffness of the bellows; however, a frame compliance correction was not applied. All elevated temperature tests were conducted in the measuring tank, using two test sections. The reference tests were performed in inert (Ar) atmosphere and the temperature was controlled within ± 2 °C.

The polished tensile specimens were pre-exposed in liquid lead at dissolved oxygen concentration below 10^{-9} wt.% for a period from 100 h to 1100 h, at higher temperatures than the testing temperature used in the SSRT tests in lead. The pre-exposure improves the wetting, i.e., contact between the specimen surface and the heavy liquid metal. During the current test campaign, the effect of three different pre-exposure conditions was investigated:

— Pre-exposure 1: 180 h in liquid Pb prior the test, at 450 °C and oxygen concentration ~10–9 wt.%;
— Pre-exposure 2: 100 h in liquid Pb prior the test, at 500 °C and oxygen concentration ~10–9 wt.%;
— Pre-exposure 3: specimen kept 1000 h in liquid Pb, at 500 °C and oxygen concentration < 10–11 wt.%; the pre-exposure was performed by SCK•CEN.

Specimens were pre-loaded to approx. 50 N during pre-exposure 1 and pre-exposure 2. There was no pre-load applied on specimens during pre-exposure 3. Pre-exposure 3 was used in combination with pre-exposure 2 for one of the specimens. In other words, this specimen was first pre-exposed 1000 h in liquid lead at SCK•CEN in Belgium. Subsequently, the specimen was introduced into the measuring tank of the LILLA facility into liquid lead and before starting the tensile test pre-exposure 2 was performed.

Fig. 6. shows the temperature and the dissolved oxygen concentration in lead during pre-exposure 2. The lead was transferred to the measuring tank at 420 °C, the temperature was then increased to 500 °C and oxygen content in liquid lead was adjusted and maintained to perform the pre-exposure.

The tensile tests were performed at 400 °C and a strain rate of $1x10^{-4}$ s^{-1}. The dissolved oxygen content had been continuously monitored during the tests and kept below 10^{-9} wt.%. The test conditions were selected based on the results obtained on T91 tested in lead-bismuth eutectic (LBE). For LBE it has been shown that the mechanical properties strongly depend on temperature, strain rate and dissolved oxygen content. It was shown that under certain test conditions T91 exhibits liquid metal embrittlement (LME) resulting in strong decrease in tensile elongation at fracture [3,7].

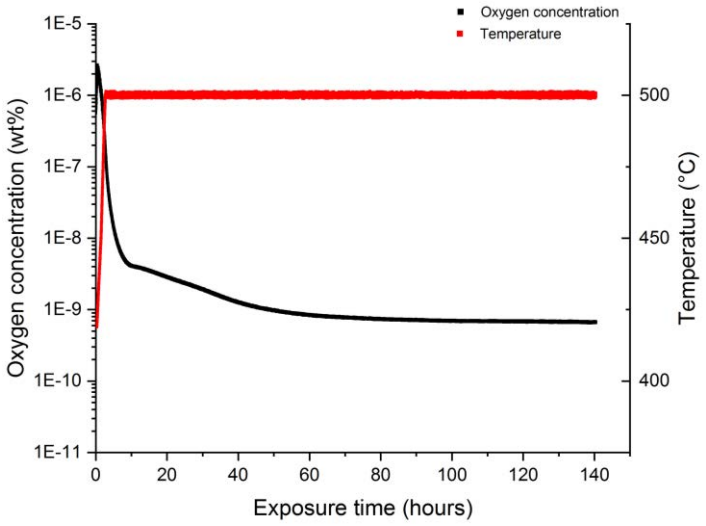

FIG.6. Temperature and the dissolved oxygen concentration in lead during pre-exposure 2

3.2. **Tests in argon and liquid lead**

Prior to starting an experimental program, the LILLA facility was commissioned and acceptance-tested according to a pre-defined programme to demonstrate that the facility functions in accordance with the technical requirements. During the commissioning tests, several tensile tests of T91 material were also conducted in air at room temperature as well as in argon at 420 °C and 450 °C. The temperature was measured in the autoclave with an accuracy of ± 2 °C. The displacement rate for all these tests was 0.001 mm/s and full tensile curves were obtained. Good repeatability of the measurements was achieved together with a very good linearity of the displacement response, see Fig. 7. Additionally, one test was performed in liquid lead at 450 °C with the oxygen content actively controlled at ~10^{-6} wt.%, cf. Fig.8. The specimen was deformed right after achieving the set test parameters (temperature and oxygen content), without a pre-exposure in liquid lead. The specimen deformed in lead shows the same mechanical properties as the specimen tested in argon. There is a slight decrease in the total elongation to failure when the specimen was tested in lead, which is within the statistical scatter.

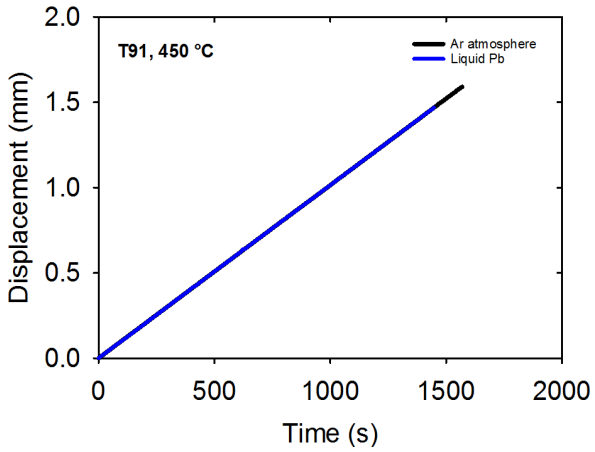

FIG.7. Displacement as a function of time during the tensile tests of T91 in argon and liquid lead at 450 °C

The results of the test campaign at 400 °C are shown in Fig. 9. The tensile curves obtained in argon are displayed on top of each other which, despite the small specimen size, shows a good repeatability of the tensile test. The measured ultimate tensile strength (UTS) is 590 MPa, which is in a good agreement with the values reported by Van den Bosch et al. on the same batch of the material [10]

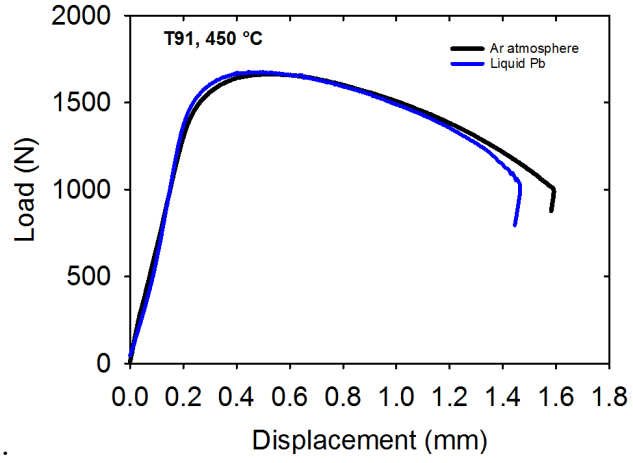

FIG.8. Displacement as a function of time during the tensile tests of T91 in argon and liquid lead at 450 °C (oxygen content actively controlled at ~10^{-6} wt.%; no pre-exposure was conducted in Pb prior to the tensile test)

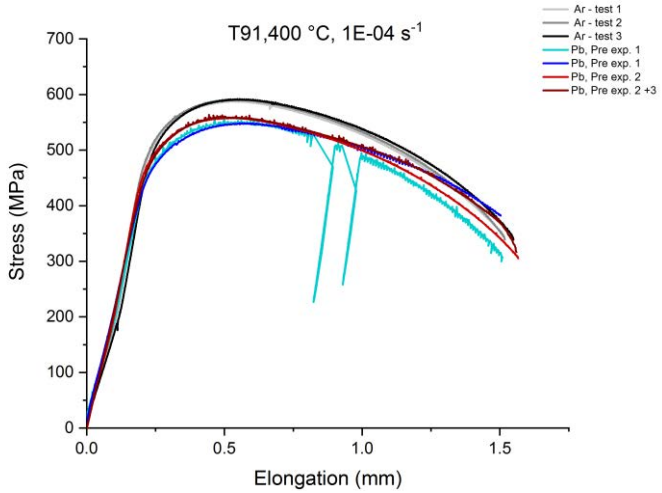

FIG.9. Tensile curves of T91 in argon and liquid lead at 400 °C (oxygen content actively controlled at <10^{-9} wt.%)

Four tests in oxygen-depleted liquid lead environment (oxygen content $<10^{-9}$ wt.%) were successfully performed. Two specimens were pre-exposed at 450 °C (pre-exposure 1) and one at 500 °C (pre-exposure 2). The fourth specimen was first pre-exposed 1000 h at 500 °C in liquid Pb (pre-exposure 3) before introducing it into the LILLA facility, where it was additionally pre-exposed 100 h at 500 °C (pre-exposure 2). Thus, in total, three pre-exposure conditions were used.

One of the measured stress-strain curves exhibit two abrupt jumps in load. The cause of the jumps is not yet fully understood. The observed behavior could be material- and/or test control-related, the former including dynamic strain ageing. Both options are under further examinations. However, the test in question was not excluded from the result comparison.

The UTS for specimens tested in liquid lead was 30 MPa lower than in argon. Furthermore, there is no remarkable change in elongation at fracture; specimens tested in argon and in liquid lead environment have the same ductility. This indicates that LME under the used test conditions did not occur.

However, to make a conclusion on susceptibility of T91 to LME in liquid lead further investigations need to be performed. It is necessary to verify that the used pre-exposures are effective to remove the protective oxide layer from the specimen surface. The fracture surfaces of specimens tested in Pb are also currently under metallographic investigations to identify fracture modes and search for any sign of LME, specifically on the edge of the fracture surfaces.

As discussed above, the previous studies in LBE showed that LME occurs in a certain range of temperatures combined with a range of strain rates [7]. Therefore, the temperature and strain rate may play an important role in lead, too. After identifying suitable pre-exposure conditions, SSRT tests will therefore be performed at different temperatures and with different (slower) strain rates in liquid lead.

4. CONCLUSIONS

Key features and design characteristics of the heavy liquid metal experimental facility for performing pre-normative and qualification tests of candidate structural materials for LFRs in realistic environmental conditions of liquid lead up to 650 °C were presented in this paper. The developed, assembled and successfully qualified test sections feature unique, pneumatic bellow-based loading devices. They also provide great flexibility with respect to the type of a mechanical test and specimen that can be used. In the facility, oxygen concentration in liquid lead can be actively monitored and controlled, from saturation down to the oxygen-depleted conditions at the levels well below 10-8 wt.%.

Tensile tests in liquid lead were performed at 400 °C and a strain rate of 1x10-4 s-1. The dissolved oxygen content in lead was continuously monitored and kept at < 10-9 wt.%. Three different pre-exposure conditions were used to remove the oxide layer from the specimen surface. Compared with reference tests performed in Ar, the ductility of T91 did not decrease, which indicates no LME effect under the used test conditions. However, further testing is necessary to make conclusions whether T91 is susceptible to LME in liquid lead.

In the frame of the GEMMA EURATOM collaborative project, the SSRT, fracture toughness, and creep tests in molten lead will be performed. The objective is to contribute to the joint European and international programs and more specifically to complement related databases and develop Design Rules and Procedures, suited also for welded components used in LFRs.

The focus is on reference structural materials for European HLM cooled reactor concepts, MYRRHA and ALFRED, and for reference GIF concepts, i.e., relatively thick-walled welded components of 316L. The primary goal is to support the development of Rules and Procedures into AFCEN's RCC-MRx Design Code, which has been chosen for the design of both MYRRHA and ALFRED. This also supports the objectives of European Energy Research Alliance (EERA) Joint Programme on Nuclear Materials (JPNM) as well as CEN/WS-64 to develop RCC-MRx into a joint European Design Code for all future European advanced nuclear installations.

The LILLA facility at JRC Petten also supports an open access to the EURATOM research infrastructures.

ACKNOWLEDGEMENTS

The authors wish to acknowledge the continuous support of the European and international collaborative partners provided to the R&D activities carried out in this field, forming also as a part of the EURATOM contribution to the Generation IV International Forum, European Sustainable Nuclear Energy Technology Platform (SNETP) and its ESNII pillar. The authors also thank S. Gavrilov from SCK•CEN for the provision of the material and long pre-exposure of the test specimen in liquid lead.

REFERENCES

[1] A TECHNOLOGY ROADMAP FOR GENERATION IV NUCLEAR ENERGY SYSTEMS, Generation IV International Forum, GIF-002-00, December 2002.

[2] TECHNOLOGY ROADMAP UPDATE FOR GENERATION IV NUCLEAR ENERGY SYSTEMS, Generation IV International Forum, January 2014.

[3] HANDBOOK ON LEAD-BISMUTH EUTECTIC ALLOY AND LEAD PROPERTIES, MATERIALS COMPATIBILITY, THERMAL-HYDRAULICS AND TECHNOLOGIES, 2015 Edition, NEA. No. 7268, OECD, 2015.

[4] AÏT ABDERRAHIM, H., et al., MYRRHA: A Multipurpose Accelerator Driven System for Research & Development, Nuclear Instruments & Methods in Physics Research, A **463** (2001).

[5] FRIGNANI, M., et al., "Advancements towards the Implementation of the ALFRED Project", Fast Reactors and Related Fuel Cycles: Next Generation Nuclear Systems for Sustainable Development (FR17) (Proc. Int. Conf. Yekaterinburg, 2017), IAEA, Vienna (2018) Paper CN245-485.

[6] ALEMBERTI, A., et al., "Status of Generation-IV Lead Fast Reactor Activities", Fast Reactors and Related Fuel Cycles: Next Generation Nuclear Systems for Sustainable Development (FR17) (Proc. Int. Conf. Yekaterinburg, 2017), IAEA, Vienna (2018) Publication CN245-65.

[7] GAVRILOV, S., Slow Strain Rate Test round robin exercise, Deliverable D2.3, MATTER Euratom FP7 collaborative project (Grant Agreement no. 269706), 2014.

[8] AGOSTINI, P., et al., GEMMA: GenIV Materials Maturity, Euratom H2020 collaborative project (Grant Agreement no. 755269), 9th European Commission Conference on EURATOM Research and Training in Safety of Reactor Systems – FISA 2019 (To be published in Proc. Int. Conf. Pitesti, 2019), European Commission, Brussels.

[9] EUROTRANS: EUROpean Research Programme for the TRANSmutation of High Level Nuclear Waste in an Accelerator Driven System, 6th EU Framework Programme, Contract number FI6W-CT-2004-516520.

[10] VAN DEN BOSCH, J., et al., Procurement and Characterisation of T91 and SS316L plates, Deliverable D4.2, EUROTRANS 6th EU Framework Programme integrated collaborative project, 2005.

SESSION II: CORROSION MITIGATION MEASURES: COATING, NEW STRUCTURAL MATERIALS, ENVIRONMENTAL CONDITIONING

CORROSION AND MECHANICAL TESTING OF A LOW ALLOYED ALUMINA FORMING AUSTENITE FOR LIQUID LEAD APPLICATIONS

Peter Dömstedt
KTH, Royal Institute of Technology
Stockholm, Sweden
Email: peterdom@kth.se

Marta Serrano Garcia
CIEMAT, Centre for Energy, Environment and Technology
Madrid, Spain

Rebeca Hernandez Pascual
CIEMAT, Centre for Energy, Environment and Technology
Madrid, Spain

Peter Szakálos
KTH, Royal Institute of Technology
Stockholm, Sweden

Abstract

The aim of this work has been to study the corrosion resistance, as well as the mechanical properties, of a new experimental AFA-alloy as a potential cladding tube material in future LFRs. The corrosion exposures were conducted in stagnant liquid lead at 550°C and 600°C, with controlled partial oxygen pressures, for up to 1272 hours. Mechanical tests were conducted in a small punch test facility at temperatures from 25°C to 500°C. The AFA alloy showed promising corrosion behavior and mechanical properties when compared with the AISI 316L reference material used in the experiments. These results indicate that AFA steels could be suitable cladding tube materials that can operate in liquid lead at elevated temperature with little to no corrosion, as well as maintaining good mechanical integrity.

1. INTRODUCTION

The next generation (Gen IV) of nuclear reactors provides several benefits to today's energy production. These benefits include increased safety features and the potential use of nuclear waste as fuel through recycling [1, 2]. One such Gen IV reactor that has established fundamental improvements in safety is the lead-cooled Fast Reactor (LFR), which use liquid lead as Heat Transfer Fluid (HTF). Lead is a natural gamma radiation shield and can retain fission products, which otherwise is a potential safety threat [3]. Lead also have the ability to naturally circulate upon heating due to its large density change, which provides cooling of the core in case station blackout [4]. One predominant topic with the LFRs is the corrosion issues that the liquid lead environment introduces. Commercial construction steels, such as AISI 316L (316L), rely on the formation of a chromia (Cr_2O_3) layer to protect against the substrate material from corroding. With lead temperatures rising to 550 °C, the chromia scale will no longer provide the protection necessary against the increasing corrosive environment. This can result in component failure and clogging issues as the structural components exhibit critical oxidation and metal dissolution [5-7].

Ferritic Alumina (Al_2O_3) Forming (FeCrAl) alloys have gained increased interest for liquid lead applications due to their superior corrosion resistance in many extreme and high-temperature environments [5, 6, 8-17]. Recent material advancements of low alloyed FeCrAl steels, specifically aimed for liquid lead applications, have shown promising oxidation properties and ductile behavior in liquid lead up to 750 °C [5, 18-22]. The work showed that it is possible to design a unique FeCrAl alloy for a specific environment by optimizing the Reactive Element (RE) mixture, with respect to the carbon content. However, the ferritic steels do not possess the mechanical properties necessary for cladding tube applications required in the LFR and are susceptible to the phenomenon known as Liquid Metal Embrittlement (LME) [23-26].

The need for a suitable Alumina Forming Austenitic (AFA) steel has, therefore, been addressed for components in the LFR. Over the past decade, the AFA steels have generated a great deal of attention due to their success of combining both excellent corrosion resistance and good mechanical properties. The promotion and success of the AFA steels have largely been due to the work of Oak Ridge National Laboratory (ORNL), United States, as they managed to produce an AFA alloy capable of forming a protective alumina scale with as low as 2.5 wt. % Al addition [27-31]. In addition, recent material advancements by Karlsruhe Institute of Technology (KIT), Germany, have generated a series of AFA alloys for liquid lead applications with success, showing promising oxidation behavior up to 600 °C [32].

Within the framework of the GEMMA project [33], part of the Horizon 2020 programme [34], parallel work has been carried by KTH, Stockholm, in a collaboration with CIEMAT, Madrid. The objective has been to develop a series of low alloyed AFA steels that facilitates formability and producibility, specifically with the intention as cladding tube material for the LFR design. By optimizing the RE additives, the concept is to minimize the alloying elements required, such as Ni, Cr and Al, without compromising the mechanical stability or the corrosion resistance. The aim of the paper has, therefore, been to study the corrosion and mechanical behavior of the best performing experimental low alloyed AFA steel, developed within the GEMMA project, to evaluate if it is a suitable candidate as cladding tube material for future LFRs.

2. MATERIALS AND EXPERIMENTS

2.1. **Materials**

The experimental AFA alloy was produced by Kanthal, part of Sandvik Group. The small heat (2 kg) of was made in a vacuum induction furnace. The solidified heats were then hot-worked at 1100 °C and annealed at 1050 °C. Based on the liquid lead corrosion exposures, the best performing experimental AFA alloy, denoted GII-3 (GEMMA series II, alloy 3), was chosen for continued mechanical testing and compared with the commercial chromia forming alloy 316L. See TABLE 5 for detailed compositions. According to ThermoCalc, database TCFE9, some precipitates can be present in the alloy at 550 and 600 °C, these include NbC and Ni_3Nb. Aging and ductility studies, including detailed metallography of this material will be published later.

TABLE 5. COMPOSITIONS OF THE EXPOSED ALLOYS

Alloy	Ni	Al	Cr	Mo	Si	Mn	C	Nb	Fe
GII-3	15.9	2.5	14.1	-	0.14	2.5	0.01	0.93	Bal.
316L	10.1	-	16.9	2.0	0.52	0.95	0.02	-	Bal.

All values are given in wt.%

2.2. **Liquid lead corrosion exposures**

The stagnant liquid lead exposures were performed at KTH in a COSTA tube furnace, developed by KIT in Germany. For more detailed information about the furnace set up, see previous work [19, 35, 36]. The samples were placed in alumina crucibles filled with lead. The crucibles were then placed on a tray and inserted into the tube furnace. An Ar-H_2 gas mixture was flushed into the tube of the furnace for 24 h before the temperature was set. After the set temperature had been reached, the Ar-H_2 gas was adjusted and combined with an Ar-H_2O gas mixture at the gas inlet, which yields an H_2/H_2O-ratio. This ratio corresponds to an oxygen partial pressure in the gas and can be equilibrated to an amount of oxygen dissolved in the liquid lead, given in wt. % [35]. The oxygen partial pressure was measured at the gas outlet using a ZIROX SGM5 oxygen sensor [37] to control the environment inside the furnace. Two exposures temperatures, relevant to LFR cladding tube applications, were set at 550 °C and 600 °C. Oxygen activities were chosen to evaluate suitable operating conditions for the alloy. For more detailed information about the experimental setups, see TABLE 2. The Experiments, including the equilibrated wt. % O dissolved in the Pb, are visually demonstrated in an Ellingham Diagram [38] in FIG. 1.

TABLE 6. TEST PARAMETERS USED AND AVERAGE MEASURED VALUES FOR THE LIQUID LEAD EXPOSURES

Temperature (°C)	Experiments	H_2/H_2O-ratio	Measured pO_2 (bar)	Dissolved O in Pb (wt. %)	Duration (h)
550	A	3×10^{-4}	3×10^{-19}	5×10^{-4}	680
	B	7	5×10^{-28}	2×10^{-8}	552
	C*	-	-	-	680 + 552
600	D	1×10^{-2}	1×10^{-22}	2×10^{-5}	1272
	E	3×10^{-1}	2×10^{-23}	1×10^{-6}	1080

** Samples in experiment C were first exposed in experiment A, followed exposure in experiment B.*

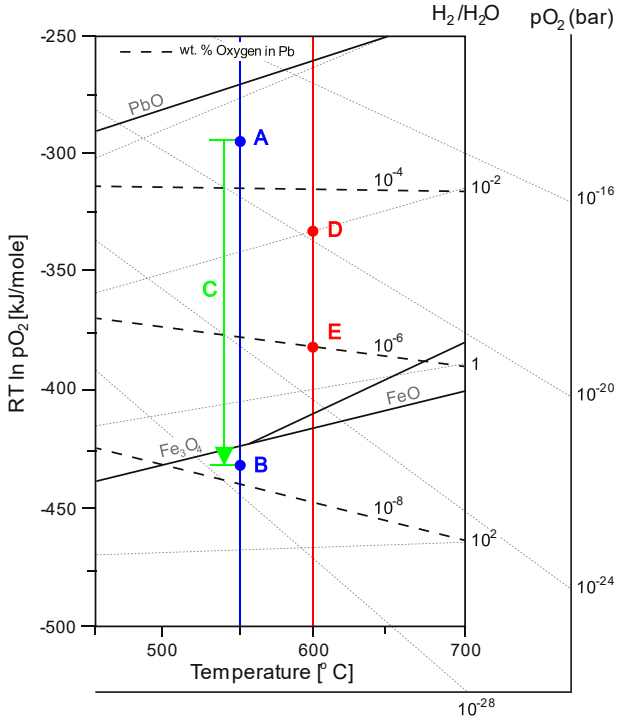

FIG. 1. Visual representation of the equilibrium systems for experiments A, B and C at 550 °C, as well as experiments D and E at 600 °C. Note that Experiment C is represented by an arrow as it was first exposed according to Experiment A, followed by Experiment B.

After the exposures, the majority of residual lead on the sample surfaces was removed in a solution of acetic acid ($C_2H_4O_2$), hydrogen peroxide (H_2O_2) and deionized water, with a ratio of 1:1:7, for 1 hour. Prepared cross-sections were sanded at an 45° angle to a 4000# paper. The preparation allows for visualization of the substrate material, metal-oxide interface and the surface in one image.

2.3. **Small punch testing**

The Small Punch (SP) test rig is used for screening procedures of materials to provide mechanical data for swift evaluation. The SP rig main components are shown in FIG. 2, which are the puncher that applies the load on the samples with a tip radius, R, of 1.25 mm and the down holder that, together with the die, holds the specimen in place. The hole in the die has a larger diameter, D, of 4 mm, than the tip radius of the puncher to minimize the influence of the deformation progress. The punch velocity was set to 0.30 mm/min for all tests. The small disc samples were prepared with a diameter, d, of 8 mm for the AFA alloys and 6 mm for the 316L sample. The thickness of each disc, h, was fixed at 0.5 mm. Two small disc samples were prepared for each material at each tested temperature. More detailed information on the SP test rig can be found in work by E. Altstadt et at. [39].

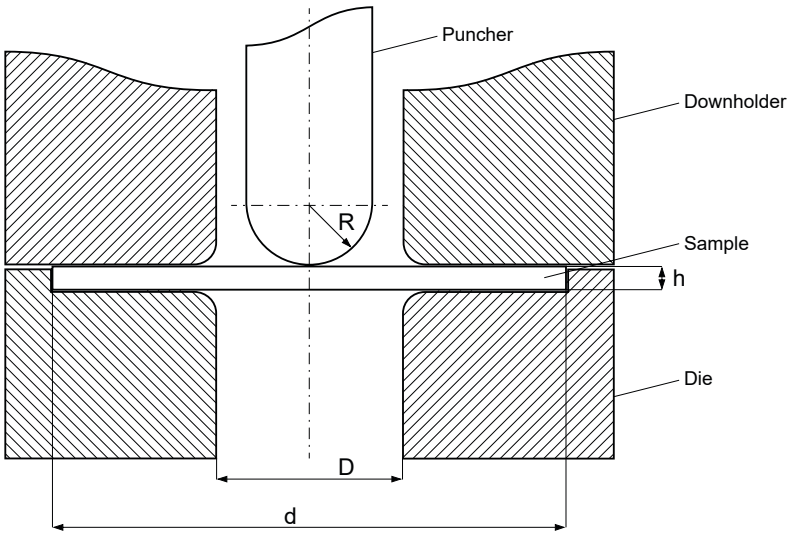

FIG. 2. The SP test rig set up. The main components are the specimen with a diameter d and thickness h, the puncher with a tip radius R, the downholder and the die that holds the specimen in place [39].

3. RESULTS

3.1. **Liquid lead corrosion exposures**

Following images show the experimental GII-3 AFA alloy to the left and the commercial 316L steel to the right. As a result of the 45° angle polishing, each SEM image shows two facades: the top surface exposed to the liquid lead on the upper half and the polished cross-section on the lower half. The facades are marked and divided with a red dashed line.

3.1.1. *550°C exposures*

Three experiments were conducted in stagnant liquid lead at 550 °C, A, B and C, see TABLE 2. SEM images using the back-scattered electron (BSE) detector of the results from experiments A, B and C can be seen in FIG. 3.

Experiment A was conducted with a relatively high oxygen activity, corresponding to 5×10^{-4} wt. % O dissolved in the Pb and was operating for 680 hours. The experimental AFA alloy, GII-3, showed promising oxidation properties. Some few minor oxidation nodules, less than 20 µm in depth, were detected. The commercial chromia forming steel, 316L, demonstrated both internal and external oxidation, both with a thickness of roughly 70 µm each, across the majority of the studied cross-section.

Experiment B, conducted with a relatively low oxygen activity equilibrated to 2×10^{-8} wt. % O dissolved in the Pb, was operating for 552 hours. The polished cross-sections demonstrated that both alloys were susceptible to liquid lead penetration. Both the area and depth of affected zones were larger on the AFA sample than on the 316L sample.

Samples in Experiment C were first exposed in liquid at 550 °C according to test conditions of A for 680 hours, followed by test conditions B for 552 hours. Some few minor oxide nodules were observed on the GII-3 sample. The 316L sample showed more severe oxidation, as well as lead penetration to an approximated depth of 45 µm.

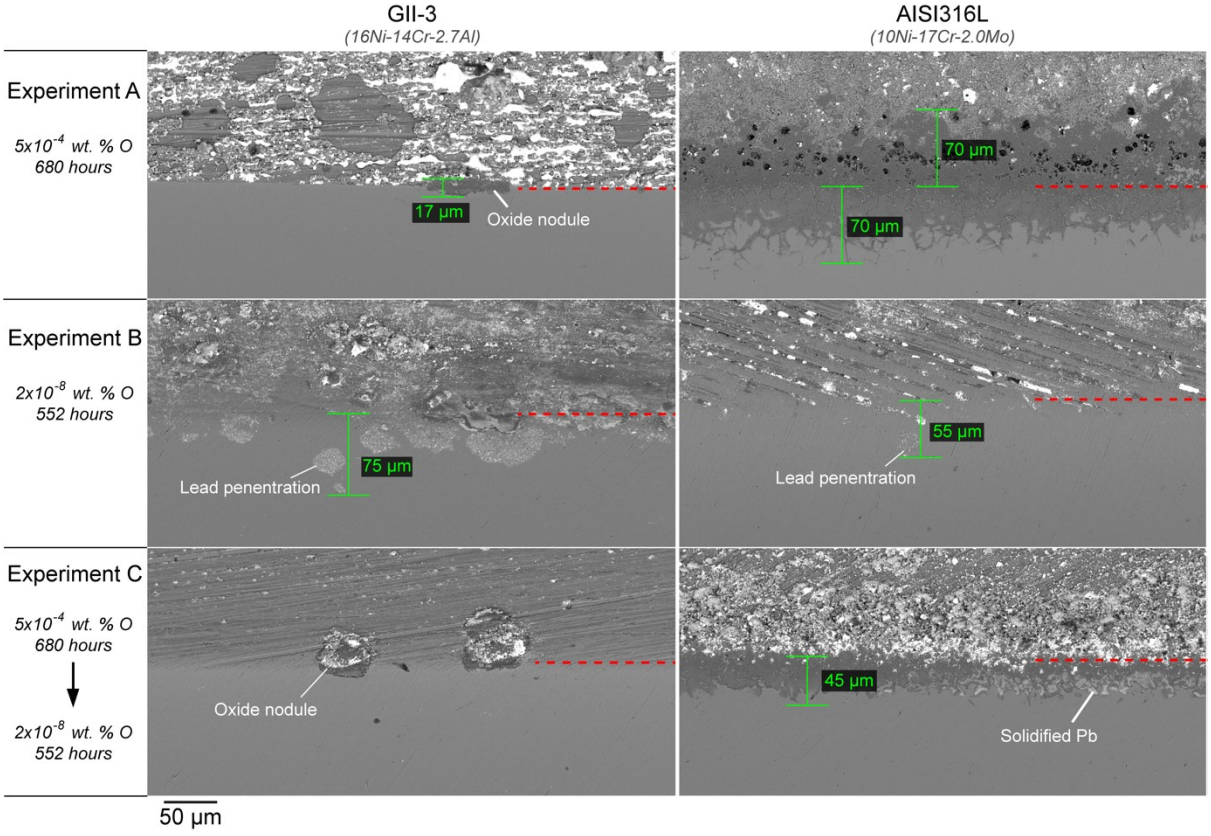

FIG. 3. 45° angled cross-sections of experimental alloy GII-3 and commercial alloy 316L, exposed in stagnant liquid lead at 550°C for experiments A, B and C. The top half, above the red dashed line, of each image represents the top surface of the samples while the bottom half shows the polished cross-section.

3.1.2. *600°C exposures*

Two experiments were conducted at 600°C, D and E, see TABLE 2. Experiment D was conducted at higher oxygen activity than experiment E, corresponding to 2×10^{-5} and 1×10^{-6} wt. % O dissolved in the Pb, respectively. Some images, using the BSE detector, of the exposed samples are shown in FIG. 4.

Cross-sections after Experiment D revealed both internal oxidation and lead penetration on the experimental alloy GII-3, reaching a depth of roughly 100 µm. Also, large areas of the top surface were covered with mixed oxides, mainly iron rich. The commercial steel 316L, demonstrated internal oxidation at a depth of 30 µm.

From experiment E, using lower oxygen activity, the GII-3 sample had formed a protective Al-rich oxide across the entire surface, with little to no sign of corrosion attacks. Mean elemental compositions from the EDS analysis of the top surface and substrate material of the GII-3 sample, after exposure E, are shown in TABLE 7. All values are given in wt. %. The 316L sample suffered from both internal and external oxidation, with thicknesses of approximately 65 µm and 35 µm, respectively.

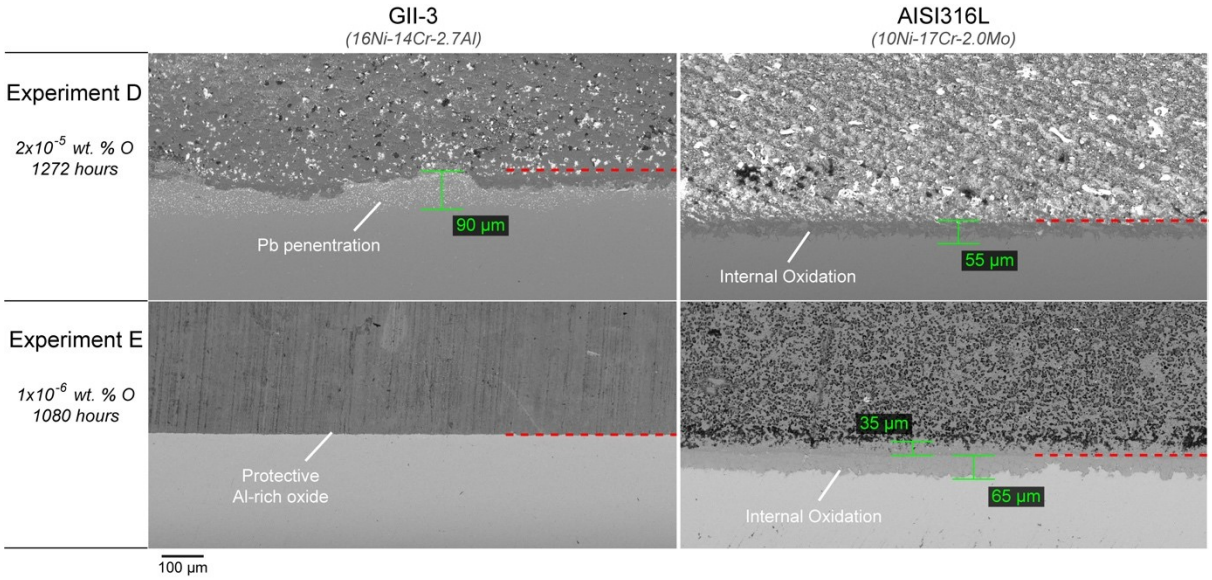

FIG. 4. 45° angled cross-sections of experimental alloy GII-3 and commercial alloy 316L, exposed in stagnant liquid lead at 600°C for experiments D and E. The top half, above the red dashed line, of each image represents the top surface of the samples while the bottom half shows the polished cross-section.

TABLE 7. AVERAGE ELEMENTAL COMPOSITIONS OF THE GII-3 SAMPLE TOP SURFACE AND SUBSTRATE MATERIAL, AFTER EXPERIMENT E

Spectrum area	O	Al	Cr	Fe	Ni
Top surface	15.42	9.76	5.57	55.12	14.13
Substrate	0.77	2.14	19.19	60.40	17.50

All values are given in wt.%

3.2. **Small punch testing and aging**

The small punch tests were conducted in air at temperatures ranging from 25 °C to 500 °C, see FIG. 5. The fracture energy, measured in Newton millimeters (Nmm), is plotted against the temperature (°C). The GII-3 alloy showed higher fracture energy than the 316L steel sample for the majority of the temperatures, except at 100°C. SEM (SE detector) fractography images from 25 °C, 300 °C and 500 °C of the GII-3 AFA steel is shown in FIG. 6.

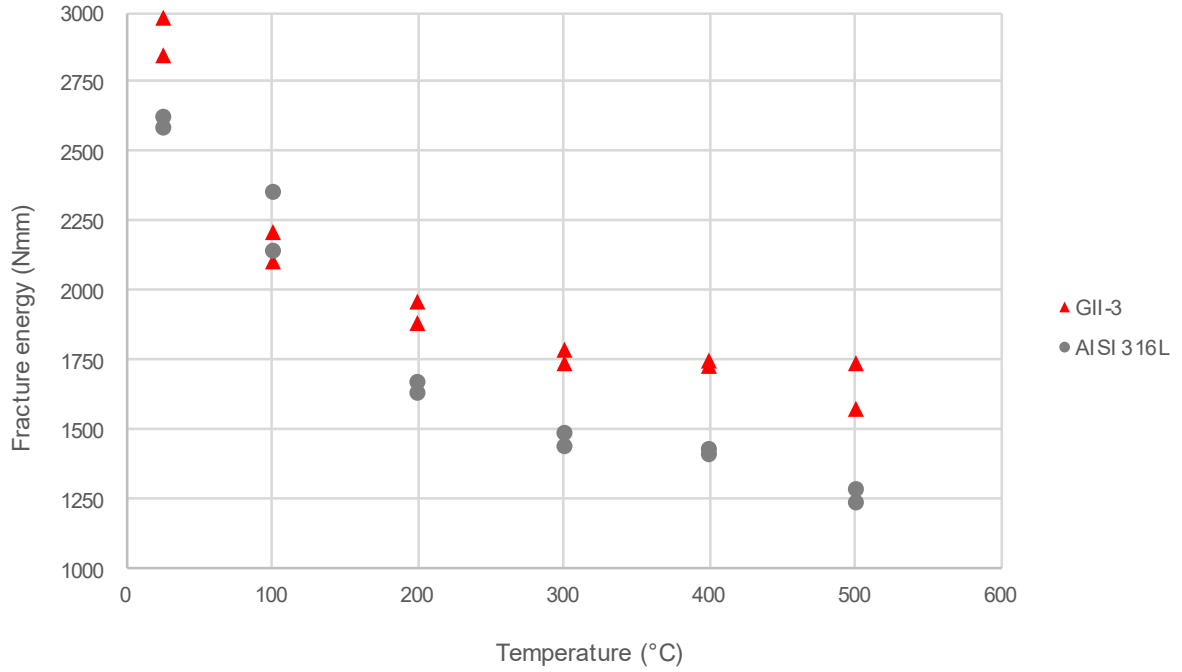

FIG. 5. Results from the small punch test. The fracture energy (Nmm) is plotted against the temperature (°C).

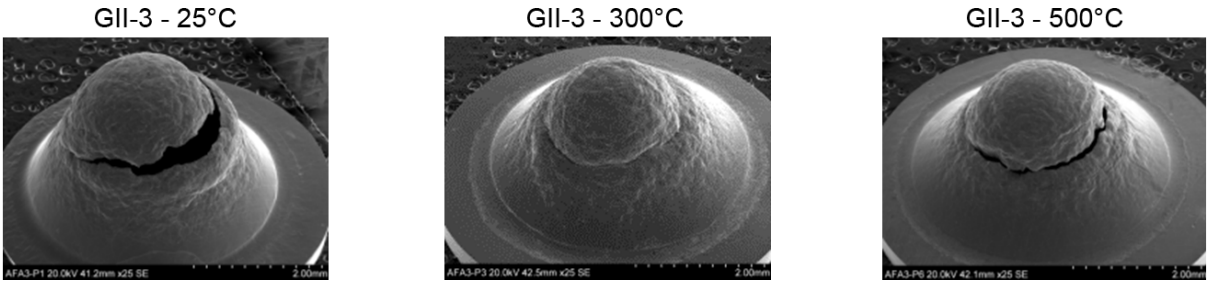

FIG. 6. Fractography SEM images (SE detector) of the GII-3 AFA steel at 25°C, 300°C and 500°C.

4. DISCUSSION

The experimental AFA alloy, GII-3, demonstrated, in general, better corrosion properties than the commercial chromia forming steel, 316L, which showed some form of corrosion attack in all conducted experiments. The GII-3 sample showed promising results in experiments, A, C and E, but exhibited different types of corrosion/oxidation attacks after exposures to test conditions B and D.

In Experiment A, the AFA steel, was indicated with EDS to have formed an Al-rich protective oxide, as is also indicated by its performance. The oxygen activity for the test was relatively high, equivalent to 5×10^{-4} wt. % O in the Pb, which seems beneficial for the AFA steel but not for the 316L sample, which suffered from both internal and external oxidation. The higher oxygen activity could cause extensive oxidation of the chromia and iron oxides of the 316L sample.

In the case of Experiment B, the oxygen activity was lower than what is required to form an iron oxide, see the Ellingham diagram in FIG. *1*. Iron oxides are believed to hinder lead dissolution of steel constituents and penetration of lead into the material to some extent, while not constrain oxygen diffusion entirely [13]. As a result, moderate oxidation of iron could be beneficial by allowing more time to form a protective alumina scale beneath. Fe-Al-rich oxides have been previously detected on-top of the alumina scale on FeCrAl alloys exposed to liquid lead [20, 21]. The inability to generate any kind of iron oxide could, therefore, result in the more severe lead penetration, as observed on the GII-3 sample after the exposure to Experiment B. The chromia forming 316L sample suffered from lead penetration as well, although, to a smaller extent. The 316L steel oxidize more rapidly than the GII-3 alloy, which, in the case of Experiment B, could have reduced the degree of lead penetration when comparing the two samples. The experimental GII-3 alloy has relatively low alloying additions of Al and Cr, 2.5 wt.% and 14 wt.% respectively. Recent work by H. Shi et. Al. [32] produced several similar Fe-Cr-Al-Ni model alloys, exposed to liquid lead at 550 °C and 600 °C. Alloys containing 14 wt. % Cr or less did not manage to form a continuous protective oxide scale at any tested temperature, even at higher oxygen activities (10^{-6} wt. % O dissolved in the liquid Pb). However, the alloys had higher Ni content (at least 20 wt. %), which increases the likelihood of dissolution in liquid lead environments [5, 40]. Earlier study by J. Ejenstam and P. Szakálos [5] produced a AFA alloy containing 14wt. % Cr and 14 wt. % Ni. The alloy used similar RE addition (0.9 wt. % Nb) and did not suffer from dissolution attacks after long term exposure in liquid lead at 550 °C and 10^{-6} wt. % dissolved O. Although, the alloy lacked the austenitic phase stability desired. Therefore, further optimization of RE additions with respect to the Al, Cr and Ni contents of the GII-3 alloy is required to promote protective oxidation scale formation for a wider range of oxygen activities.

Experiment C showed, again, promising results for the GII-3 sample while the 316L steel demonstrated internal oxidation and lead penetration. As the experiment started with higher oxygen activity, the GII-3 sample would have the ability to form a protective oxide, as observed from experiment A. The oxide seems to be stable as the O activity was decreased and, therefore, no lead penetration was observed. The 316L sample most likely stared by forming the thick non-protective oxide scale as observed in Experiment A, followed by lead penetration as indicated from Experiment B.

After exposing the samples to Experiment D, the surface of the GII-3 alloy was largely covered with iron-rich oxides. In this case, due to the higher oxygen activity, as well as temperature, the oxidation could have been too rapid, generating too much of the non-protective oxides and thus disrupting the formation of the alumina scale, allowing for liquid lead penetration. Hence, 600 °C could be close to the maximum usable temperature for this particular AFA alloy. The 316L sample also showed internal oxidation, but not to the same extent. This could, again, be due to the benefit of the chromium oxide for the specific test conditions. As chromia oxidize faster than alumina, it has a better chance to compete in extreme cases of rapid iron oxidation.

Experiment E indicated that lower oxygen activities could be beneficial for the AFA alloy at 600 °C. The sample demonstrated an ideal performance with the formation of a protective Al enriched (identified with EDS analysis) on the entire surface. Although the true composition and structure of the oxide scale could not be determined, Cr-rich oxides have often been detected on-top of the thin alumina scale on FeCrAl alloys [20, 21, 41]. The recent study by H. Shi et. Al. [32] identified (with XRD analysis) that the protective scale formed on similar Fe-Cr-Al-Ni model alloys consisted of Cr_2O_3 and Al_2O_3-Cr_2O_3 solid solution. Hence, the oxide scale formed on the GII-3 alloy is could have similar structure. The oxide thickness of the 316L steel was thicker with decreasing oxygen activities at 600 °C. This could be due to the formation of a less protective oxide layer at lower oxygen activities, which could result in a faster growing non-protective oxide scale.

Although additions of aluminium tend to reduce the mechanical properties in steel alloys, the SP test indicated that the GII-3 alloy had a comparable fracture energy with that of the 316L steel. As seen in FIG. 6, the cracks have a circumferential shape, similar to that of the puncher. For SP tested specimens, ductile failure is characterized by such circumferential shaped cracks while brittle failure is often indicated by more cleavage facets and crack edges [39, 42, 43]. Therefore, the conducted SP tests speaks for ductile fracture behavior of the GII-3 alloy at all tested temperatures. For AFA steels, the combination of Fe, Ni, Al and Nb can be beneficial due to the formation of several different precipitates, as have previously been demonstrated by Y. Yamamoto et. al. [44]. While NbC precipitates are likely already formed during the production of the steel, Ni_3Nb is promoted at intermediate temperatures, such as the 550 600 °C range. Hence, it could be assumed that these Ni_3Nb particles could precipitate at operating temperatures thus promoting the high-temperature mechanical properties of the AFA sample.

5. CONCLUSIONS

From the results presented in the work, the following conclusions can be made:

— The AFA steel alloy, GII-3, demonstrated, in general, better corrosion properties than the commercial chromia forming steel, 316L, which showed some form of corrosion attack or deteriorating oxidation behaviour in all conducted experiments.
— The GII-3 alloy exhibited metal dissolution and lead penetration when the oxygen activity was lower than what is required to form magnetite (Fe_3O_4) at 550 °C, as well as at 600 °C with higher oxygen levels at 2×10^{-5} wt. %. Liquid lead at 600 °C could be close to the maximum operating temperature for this specific AFA steel.
— It was indicated by the small punch test that the GII-3 alloy had ductile fracture behaviour at all tested temperatures and the mechanical properties was at least as good as that of the 316L steel. The presence of evenly distributed precipitates, such as NbC and Ni_3Nb, could be the cause of the high-temperature mechanical strength.
— Considering the presented results and recently published work by others [5, 32], the AFA type of steels looks promising as future construction material in Gen IV LFRs and could be possible to use for cladding tubes. However, further optimisation of RE additions and research is required, including irradiation and ageing exposures to properly evaluate their applicability in the field.

ACKNOWLEDGEMENTS

The work is financed by the GEMMA project, part of the European programme Horizon 2020. The authors would like to thank Peter Bylin at Kanthal, part of Sandvik Group, for the production of the experimental alloy used in this study.

REFERENCES

[1] WALLENIUS, J., *Maximum efficiency nuclear waste transmutation.* Annals of Nuclear Energy, 2019. **125**: p. 74-79.
[2] WALLENIUS, J. AND S. BORTOT, *A small lead-cooled reactor with improved Am-burning and non-proliferation characteristics.* Annals of Nuclear Energy, 2018. **122**: p. 193-200.
[3] WALLENIUS, J., et al., *Design of SEALER, a very small lead-cooled reactor for commercial power production in off-grid applications.* Nuclear Engineering and Design, 2018. **338**: p. 23-33.
[4] WALLENIUS, J., R. SUVDANTSETSEG, AND A. FOKAU, *ELECTRA: European lead-cooled training reactor.* Nuclear Technology, 2012. **177**: p. 303-313.
[5] EJENSTAM, J. AND P. SZAKALOS, *Long term corrosion resistance of alumina forming austenitic stainless steels in liquid lead.* Journal of Nuclear Materials, 2015. **461**: p. 164.
[6] MÜLLER, G., ET AL., *Results of steel corrosion tests in flowing liquid Pb/Bi at 420–600 °C after 2000 h.* Journal of Nuclear Materials, 2002. **301**(1): p. 40-46.
[7] LAMBRINOU, K., ET AL., *Corrosion scales on various steels after exposure to liquid lead–bismuth eutectic.* Journal of Nuclear Materials, 2014. **450**(1): p. 244-255.
[8] HEINZEL, A., M. KONDO, AND M. TAKAHASHI, *Corrosion of steels with surface treatment and Al-alloying by GESA exposed in lead–bismuth.* Journal of Nuclear Materials, 2006. **350**(3): p. 264-270.
[9] WEISENBURGER, A., ET AL., *Corrosion, Al containing corrosion barriers and mechanical properties of steels foreseen as structural materials in liquid lead alloy cooled nuclear systems.* Nuclear Engineering and Design, 2011. **241**(5): p. 1329-1334.
[10] LIM, J., I. HWANG, AND J. KIM, *Design of alumina forming FeCrAl steels for lead or lead-bismuth cooled fast reactors.* J. Nucl. Mater., 2013. **441**(1-3): p. 650-660.

[11] PINT, B., ET AL., *Development of ODS FeCrAl for Compatibility in Fusion and Fission Energy Applications.* The Journal of The Minerals, Metals & Materials Society (TMS), 2014. **66**(12): p. 2458-2466.
[12] HATTENDORF, H., ET AL., *A new austenitic alumina forming alloy: an aluminium-coated FeNi32Cr20.* Materials and Corrosion, 2008. **59**(6): p. 449-454.
[13] FETZER, R., ET AL., *Oxide scale formation of modified FeCrAl coatings exposed to liquid lead.* Corrosion Science, 2012. **55**: p. 213-218.
[14] WEISENBURGER, A., ET AL., *Oxygen for protective oxide scale formation on pins and structural material surfaces in lead-alloy cooled reactors.* Nuclear Engineering and Design, 2014. **273**: p. 584.
[15] ZHANG, J., *A review of steel corrosion by liquid lead and lead–bismuth.* Corrosion Science, 2009. **51**(6): p. 1207-1227.
[16] ASHER, R.C., D. DAVIES, AND S.A. BEETHAM, *Some observations on the compatibility ofstructural materials with molten lead.* Corrosion Science, 1977. **17**(7): p. 545-557.
[17] LIM, J., ET AL., *A study of early corrosion behaviors of FeCrAl alloys in liquid lead-bismuth eutectic environments.* J. Nucl. Mater., 2010. **407**(3): p. 205-210.
[18] DÖMSTEDT, P., M. LUNDBERG, AND P. SZAKALOS, *Corrosion Studies of Low-Alloyed FeCrAl Steels in Liquid Lead at 750 °C.* Oxidation of Metals, 2019.
[19] EJENSTAM, J., *Corrosion resistant alumina-forming alloys for lead-cooled reactors.* 2015, Kungliga Tekniska högskolan: Stockholm.
[20] EJENSTAM, J., ET AL., *Oxidation studies of Fe10CrAl–RE alloys exposed to Pb at 550 °C for 10,000 h.* Journal of Nuclear Materials, 2013. **443**(1-3): p. 161-170.
[21] EJENSTAM, J., B. JÖNSSON, AND P. SZAKALOS, *Optimizing the Oxidation Properties of FeCrAl Alloys at Low Temperatures.* Oxidation of Metals, 2017. **88**(3): p. 361-370.
[22] EJENSTAM, J., ET AL., *Microstructural stability of Fe-Cr-Al alloys at 450-550 °C.* Journal of Nuclear Materials, 2015. **457**: p. 291.
[23] YE, C., J.-B. VOGT, AND I. PRORIOL SERRE, *Liquid metal embrittlement of the T91 steel in lead bismuth eutectic: The role of loading rate and of the oxygen content in the liquid metal.* Materials Science and Engineering: A, 2014. **608**: p. 242-248.
[24] ERSOY, F., S. GAVRILOV, AND K. VERBEKEN, *Investigating liquid-metal embrittlement of T91 steel by fracture toughness tests.* Journal of Nuclear Materials, 2016. **472**: p. 171-177.
[25] GONG, X., ET AL., *Tensile fracture behavior of notched 9Cr-1Mo ferritic-martensitic steel specimens in contact with liquid lead-bismuth eutectic at 350 °C.* Materials Science & Engineering A, 2017. **692**: p. 139-145.
[26] ERSOY, F., S. GAVRILOV, AND K. VERBEKEN, *Developing Procedures for Fracture Toughness Tests in Lead-bismuth Eutectic.* Procedia Materials Science, 2014. **3**: p. 1866-1871.
[27] BEI, H., ET AL., *Aging effects on the mechanical properties of alumina-forming austenitic stainless steels.* Materials Science and Engineering: A, 2010. **527**(7): p. 2079-2086.
[28] MAZIASZ, P.J., *Development of Creep-Resistant and Oxidation-Resistant Austenitic Stainless Steels for High Temperature Applications.* JOM, 2018. **70**(1): p. 66-75.
[29] YAMAMOTO, Y., ET AL., *Creep-Resistant, Al_2O_3-Forming Austenitic Stainless Steels.* Science, 2007. **316**(5823): p. 433-436.
[30] BRADY, M.P., ET AL., *The development of alumina-forming austenitic stainless steels for high-temperature structural use.* JOM, 2008. **60**(7): p. 12.
[31] BRADY, M. P., ET AL., *Composition, Microstructure, and Water Vapor Effects on Internal/External Oxidation of Alumina-Forming Austenitic Stainless Steels.* Oxidation of Metals, 2009. **72**: p. 311-333.
[32] SHI, H., ET AL., *Corrosion resistance and microstructural stability of austenitic Fe–Cr–Al–Ni model alloys exposed to oxygen-containing molten lead.* Journal of Nuclear Materials, 2019. **524**: p. 177-190.
[33] *GEMMA*. [cited 2019 August 13]; Available from: http://www.eera-jpnm.eu/gemma/.
[34] *HORIZON 2020*. [cited 2019 August 13]; Available from: https://ec.europa.eu/programmes/horizon2020/en.
[35] MÜLLER, G., ET AL., *Control of oxygen concentration in liquid lead and lead–bismuth.* Journal of Nuclear Materials, 2003. **321**(2): p. 256-262.
[36] MÜLLER, G., G. SCHUMACHER, AND F. ZIMMERMANN, *Investigation on oxygen controlled liquid lead corrosion of surface treated steels.* Journal of Nuclear Materials, 2000. **278**(1): p. 85-95.
[37] *ZIROX SGM5*. [cited 2019 August 13]; Available from: https://www.zirox.de/en/products/analyzers/oxygen-analyzer-sgm5/.

[38] ELLINGHAM, H.J.T., *Transactions and Communications.* Journal of the Society of Chemical Industry, 1944. **63**(5): p. 125-160.

[39] ALTSTADT, E., ET AL., *Critical evaluation of the small punch test as a screening procedure for mechanical properties.* Journal of Nuclear Materials, 2016. **472**: p. 186-195.

[40] N.E.A., O.E.C.D., *Handbook on Lead-bismuth Eutectic Alloy and Lead Properties, Materials Compatibility, Thermal-hydraulics and Technologies*. 2015: Nuclear Science.

[41] LIM, J., I.S. HWANG, AND J.H. KIM, *Design of alumina forming FeCrAl steels for lead or lead–bismuth cooled fast reactors.* Journal of Nuclear Materials, 2013. **441**(1): p. 650-660.

[42] TURBA, K., R. HURST, AND P. HÄHNER, *Evaluation of the ductile–brittle transition temperature in the NESC-I material using small punch testing.* International Journal of Pressure Vessels and Piping, 2013. **111-112**: p. 155-161.

[43] GAI, X., ET AL., *Ductile—brittle transition of steel electron beam weld metal in small punch test.* Science and Technology of Welding and Joining, 2002. **7**(4): p. 204-211.

[44] YAMAMOTO, Y., ET AL., *Alloying effects on creep and oxidation resistance of austenitic stainless steel alloys employing intermetallic precipitates.* Intermetallics, 2008. **16**(3): p. 453-462.

ALUMINA NANOCERAMIC COATINGS: AN ENABLING TECHNOLOGY FOR HEAVY LIQUID METAL-COOLED FAST REACTORS

M. VANAZZI, B. PALADINO, D. IADICICCO, F.G. FERRÉ, F. DI FONZO
Center for Nano Science and Technology @PoliMi, IIT
Via Giovanni Pascoli 70/3, 20133 Milano, Italy
Email: fabio.difonzo@iit.it

S. BASSINI, M. UTILI, M. TARANTINO, P. AGOSTINI
ENEA FSN-ING
C. R. Brasimone, 40032 Camugnano (Bologna), Italy

M.G. BEGHI
Energy Department, Politecnico di Milano,
Piazza Leonardo Da Vinci 34/3, 20133 Milano, Italy

Abstract

Next generation nuclear systems will outperform the current fleet of reactors by providing innovative solutions to the long-lasting issues of non-proliferation, fuel cycle efficiency, radioactive waste management, safety and economics. However, in order for this scenario to become reality novel materials are to be developed to sustain the far more demanding operating conditions of these advanced plant concepts: higher burnup and operating temperature, intense radiation fields, liquid metal or molten salt corrosion and tritium permeation. A short-term solution to this daunting challenge is to develop coatings for qualified structural materials capable to withstand the reactor environment. In the last years, the Istituto Italiano di Tecnologia (IIT) has developed multifunctional nano-ceramic coatings, by means of Pulsed Laser Deposition (PLD), for high-temperature Heavy Liquid Metal (HLM)-cooled systems, such as Generation-IV (GIV) and fusion reactors. Optimized coatings of alumina (Al_2O_3) on the relevant substrates (i.e. AISI 316, 1515-Ti and EUROFER-97 steels) have been tested as anti-corrosion, anti-tritium-permeation radiation-resistant barriers. In particular, their compatibility in presence of Pb and Pb-alloys has been proven up to 10˙000 hours, at 550 °C and the tritium permeation reduction of these films has been found in the order of 104-105. Furthermore, Al_2O_3 coatings showed excellent behavior under heavy ions irradiation, at damage levels relevant for fission and fusion applications (up to 450 dpa), preserving integrity and barrier performance, while evolving from an amorphous to a crystalline state. In sum, Al_2O_3 coatings deposited by PLD hold promise as valuable technology for next generation, safe and economically competitive nuclear power plants.

1. INTRODUCTION

1.1. Lead Fast Reactor (LFR) technology: materials perspective

Nuclear energy from fission-based reactors is nowadays a fundamental source of electrical power worldwide. Nevertheless, the exploitable natural resources are enough to sustain the nuclear energy production for over 300 years, since only a very small amount of naturally occurring uranium can be fissioned in a conventional water-cooled reactor. In order to improve the resource utilization and get rid of the highly radiotoxic fuel waste, new-generation fast reactors have been designed. In this framework, innovative coolant options should be implemented, to increase the efficiency of the thermodynamic cycle and the safety of operations, as well [1].

Heavy Liquid Metals (HLMs) - particularly, Pb and Pb alloys - are considered to be one of the most promising candidates for this task. This is because of several advantages. First, since these materials have a low equilibrium vapour pressure at the operation temperature of the reactor, the system can be operated at ambient pressure. In addition, the high boiling point of lead (1˙750 °C) prevents voiding in the core. Hence, in principle a lead fast reactor could operate at relatively high temperature, meaning a high efficiency for electricity production. HLMs have also good heat transport characteristics and high heat capacity, allowing efficient heat removal from the core. Finally, HLMs do not react violently with water or air, they possess high density, thus being suitable for establishing natural circulation in accident situations, and, also, a reactor pool filled with these materials ensures an efficient radiation shielding [2], [3].

Despite the several advantages, the operating experience with HLMs as cooling media has underlined some drawbacks, such as the opacity of the material (inspection issues), the high mass (special seismic countermeasures), the relatively high melting point (risk of solidification) and the significant production of polonium if Pb-Bi alloy is employed as coolant [2], [3]. However, the most constraining issues arise from the interaction between the HLMs and the structural steels, leading to severe corrosion and to the loss of mechanical properties from the latter. The corrosion process by HLMs depends on the oxygen content inside the molten media. For low concentrations of oxygen, it involves the direct dissolution of the main alloying components of steel - specifically Fe, Ni and Cr - in the liquid media. This process is driven by the difference in solubility of the alloying elements between the solid phase and in the liquid phase, which causes the formation of a chemical potential gradient [4]. At the same time, the HLMs can induce embrittlement in structural materials - typically in ferritic/martensitic BCC steels, consisting in a loss of ductility and in a premature brittle failure of these materials under stress, while exposed to liquid metals [5] – [7]. Since the detrimental effects connected with the use of metals as coolant are strongly limiting the deployment of fast reactors, it is advised to implement novel mitigation strategies.

1.2. **Mitigation strategy for LFR development: state of the art**

As previously mentioned, steels corrosion rates are strongly influenced by the chemical composition of the HLMs in the system. For this reason, an effective method for protecting steels is self-passivation through oxygen injection and accurate chemistry control. Indeed, surface oxides can tackle the direct dissolution of steel components, acting as solid-state diffusion barriers. Nevertheless, self-passivation cannot be exploited above a certain temperature limit (i.e. 450 – 500 °C): beyond this level, the Fe_3O_4 and Fe-Cr oxide scales developed by traditional chromia-forming steels are no longer stable, leading to the material dissolution [8] – [11]. Since fuel cladding and other in-core components of future generation Lead-cooled Fast Reactors (LFRs) will face temperatures as high as 550 °C - or even higher, further options should be considered. These alternative solutions can be classified in three main groups: bulk alloys, surface alloying techniques and coatings.

Bulk alloys are usually highly enriched with metallic elements like Cr, Al, Si, which are capable of forming a protective scale on the surface, provided the proper oxygen concentration in the environment. Depending on the different percentages of the alloying elements and the structure they form, there are several classes of suitable bulk alloys. Among these, promising materials are the FeCrAl alloys and the Alumina Forming Austenitic (AFA) steels. These Fe-based systems show the capability of forming a thin scale of alumina onto their surface, which protects the underlying steel from the HLM corrosion [12], [13]. In particular, the newly developed Fe-10Cr-4Al has proven remarkable stability in presence of lead and Pb-alloys, in a broad range of oxygen contents, up to 750 °C [14]. Concerning the other bulk candidates, the High Entropy

Alloys (HEAs) and the so-called MAX phases represent new emerging classes of materials. Due to their peculiar atomic configurations, they possess excellent mechanical properties and chemical stability, even at high temperature [15] – [19]. Moreover, the presence of oxides-forming elements such as Al and Cr guarantees the anti-corrosion capability in presence of HLMs, as for AFA and FeCrAl alloys. Still, many of these bulk systems present significant drawbacks which needs to be faced. Among others, the detrimental presence of undesired inter-metallic phases (in the case of AFA steels or MAX phases), which interfere locally with the formation of alumina layer, and the need for further research concerning metallurgical processes and large-scale production, especially for MAX phases and HEAs.

Surface alloying, instead, enables surface functionalization while retaining the bulk properties and characteristics of well-characterized steels. This peculiarity represents a major advantage since the standard path for the characterization and licensing of structural materials in nuclear environment is rather costly, in terms of time and economical resources. Several methods are nowadays available, but the so-called GESA (Gepulste Elektronenstrahl Anlage/pulsed electron beam facility) process stands as the state-of-the-art technology [20] – [22]. Here, an Al-enriched layer is physically bonded to the surface of steels through irradiation with high energy electron beam pulses [23] – [25]. It was demonstrated that this technique guarantees the protection of steels from corrosion under a wide range of temperatures, stresses, oxygen contents, and flow conditions and for exposure times approaching the expected lifetime of fuel cladding [17], [21]. However, the complexity of the bonding process does not allow the alloying treatment on large-scale systems or components with a sophisticated geometry, since deformations could be introduced on the thinnest parts.

The last category consists in coatings. Like the surface alloying treatments, the use of coatings by means of different deposition techniques allows to obtain surface functionalization without affecting the bulk properties and requirements. Furthermore, oxides-based coatings are compatible with both oxygen-rich and oxygen-depleted environments, throughout all realistic operating conditions. This feature differs coatings from other solutions such as standard alumina-forming alloys, which require a precise control of the HLM chemistry to be operated safely. The choice of the deposition technique should be oriented towards obtaining an optimal adhesion on the substrate, coupled with an excellent compactness of the material, since the coating should behave as a protective barrier. Several works have examined the performance of different types of coatings [26] – [30], among which alumina (Al_2O_3) deposited by Pulsed Laser Deposition (PLD) technique results to be one of the most promising solutions.

2. ALUMINA COATINGS BY PULSED LASER DEPOSITION AND BASIC PROPERTIES

The Pulsed Laser Deposition (PLD) technique is a promising and flexible technology that offers valuable means for engineering material properties at the nanoscale. In PLD, a 20 nano-second pulse from an excimer laser produces a high energy jet of ionized and neutral species ($E \approx 100$ eV/particle) at the surface of a solid target, in the present work Al_2O_3, which expands supersonically inside a vacuum chamber towards a substrate [31]–[33]. Depending on the gas pressure in the latter, films of different densities can be grown [34]. When dense coatings at low macroscopic substrate temperature are of interest, it is advised that the energy of the species in the jet is preserved, hence the background gas molecular mass and pressure should be as low as possible, the lower limit being dictated solely by the need to maintain the correct stoichiometry. All the results shown in this paper have been obtained with the following experimental conditions: $F_L \approx 3$ J/cm^2, $d_{ts} = 5$ cm, $T_{substrate} = 298$ K, $P_{O_2} = 0.15$ Pa. Coated tubes and plates have been demonstrated already with a lab-scale set-up. SEM micrographs show that PLD-grown aluminium oxide is dense and compact, and the film covers homogenously the surface of the substrate. In addition, from top-view we can appreciate the low defect density and their size being smaller than 100 nm, thus guaranteeing optimal protective characteristics.

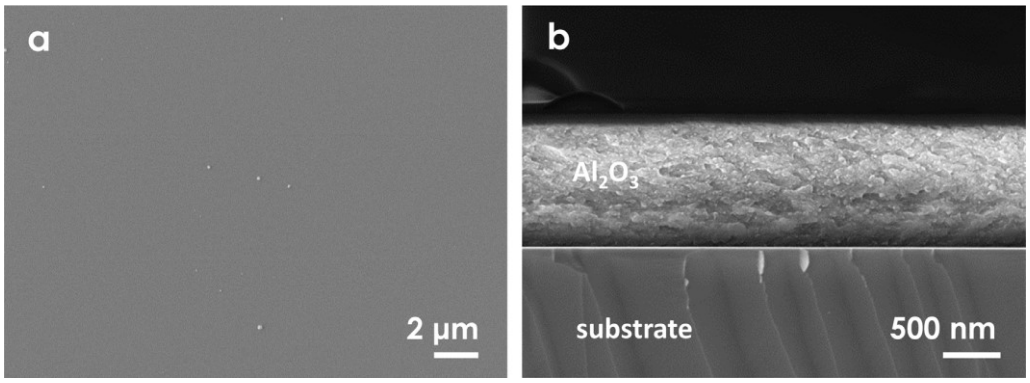

FIG. 1. Top view (a) and cross-sectional (b) SEM micrographs of the as-deposited film. Films are dense and compact, with very few nano-metric defects. Reproduced from [35] with permission courtesy of ELSEVIER.

The amorphous nature of the materials is suggested by GI-XRD diffractograms, in which no sharp peaks are present. Nevertheless, transmission electron microscopy (TEM) reveals the total absence of nanoscale porosity or other defect, as well as a low density of nano-crystalline domains with an average size of 2 – 10 nm, homogeneously dispersed in an amorphous matrix. This peculiar structure lends to the material unique mechanical properties. Differently from the typical fragile behavior of ceramics, PLD-grown aluminium oxide shows a plastic response upon stress. The quasi-metallic behavior was observed by means of nano-mechanical tests, specifically nano-indentation and nano-scratch [35], [36]. SEM analysis around the zones where the mechanical tests were performed display a plastic flow of the material, without any sign of cracks initiation and propagation.

The typical response of PLD-grown Al_2O_3 is pictured in FIG. 2:

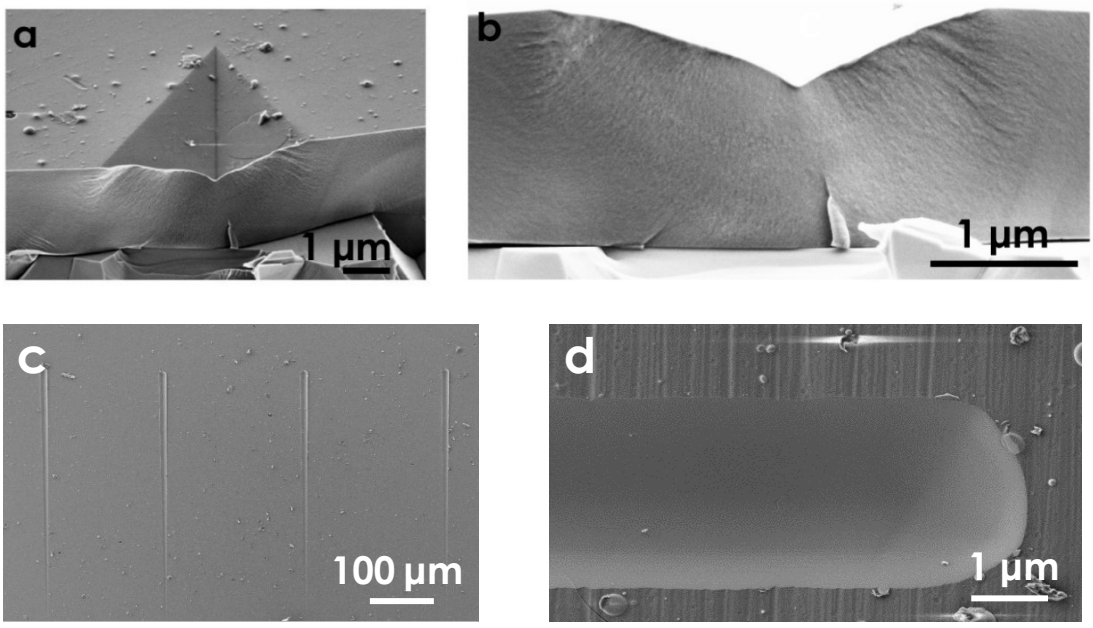

FIG. 2. (a, b) Plastic deformation in PLD-grown alumina coatings and (c, d) nano-scratch testing. Reproduced from [36] with the permission courtesy of ELSEVIER.

The outcomes of the tests showed metal-like mechanical characteristics combined with an improved hardness, resulting in high tribological properties against erosion, scratching of fretting.

More recently, encouraging evidences about the plasticity of PLD-grown alumina were collected thanks to *in situ* nano-tensile tests on free-standing Al_2O_3 layers [37]. We found a deformation to rupture around the 15% in tension with a residual plastic deformation as high as 7%, in striking contrast to conventional alumina which fails well below 1% of elongation. To support the experimental results, molecular dynamics simulations were employed. According to the models, this unusual plasticity is connected to the viscous creep of the material, which can be activated under mechanical load in a temperature range as low as the room level. Thus, the plasticity should persist as long as the system preserves its original amorphous configuration [37].

In addition, PLD-grown coatings are strongly bonded to the substrate, which is a fundamental requirement when considering coatings to be employed as protective barrier. Finally, PLD technique allows the fabrication of high quality, fully adherent and mechanically performing coatings at room temperature, without requiring any post-deposition thermal treatment, thus proposing as a promising technique for the fabrication of protective barriers to be employed in extreme environments.

3.1. **Heavy ion irradiation tests**

The first issue connected with the deployment of innovative materials in nuclear power plants is related to their radiation endurance. Typically, traditional materials undergo severe degradation when exposed to intense radiation fields, yielding to high defect density and porosity, eventually becoming amorphous. To tackle this issue, protective coatings were developed in order to operate in the amorphous state, from the begin-of-life conditions. To assess their behavior under irradiation, heavy ions have been employed, in a broad range of radiation damage levels. Specifically, heavy ions in the MeV range have been selected, in order to avoid chemical implantation inside the films and to mimic the displacement cascades proper of neutrons in matter [38], [39]. In the first experimental campaign, [40], [41] steel coated samples were exposed to a mixed flux of 12 MeV Au^{5+} and 18 MeV W^{8+} at 600 °C, up to 150 dpa. After the tests, irradiated samples were characterized, either from the structural or the mechanical point of view. FIG. 3 shows the evolution of the initially amorphous structure [41]:

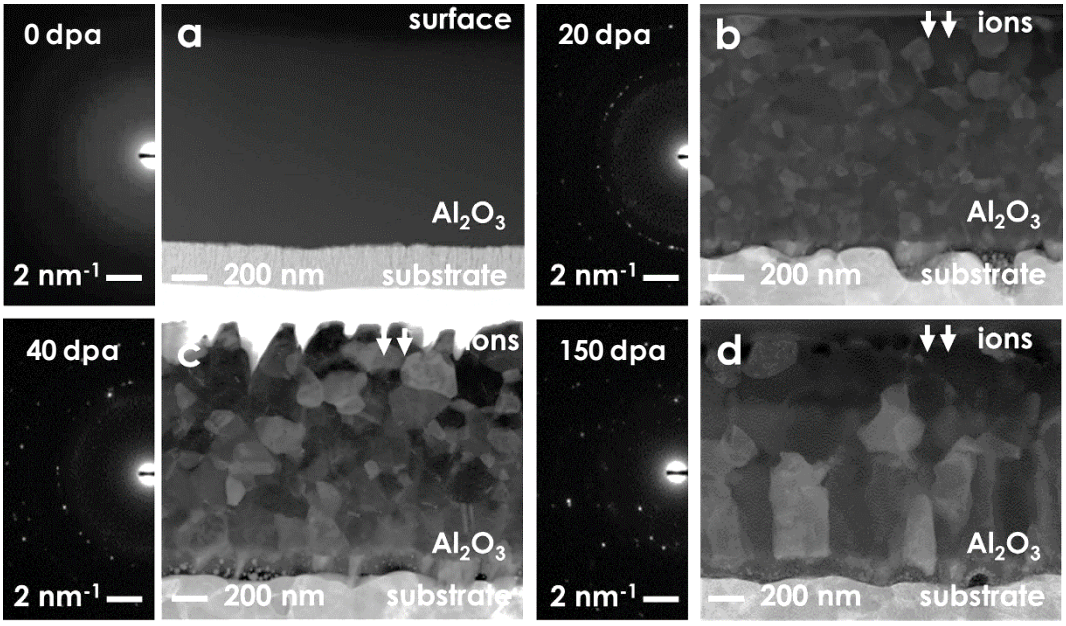

FIG. 3. TEM BF and electron diffraction patterns showing the evolution of PLD-grown Al_2O_3 under heavy ion irradiation. While the material is amorphous/nano-crystalline in the pristine condition (a), crystallization occurs under irradiation (b, c and d). Grains nucleate and grow along the dpa level. Reproduced from [41] with permission courtesy of NATURE.

According to [41], amorphous/nano-crystalline alumina underwent crystallization under ions irradiation. The results pictured in FIG. 3 are consistent with literature data for amorphous Al_2O_3 and amorphous materials in general, either under electrons or ions irradiation [42]–[47]. In particular, in [41], different crystalline phases were produced (*i.e.* metastable γ-Al_2O_3 or stable α-Al_2O_3) under irradiation, depending on the damage level. Nano-metric grains nucleated and grew according to a sub-linear growth law, reaching the maximum size at 150 dpa [41], [48]. Concerning the film mechanical properties, initial values changed in relation to the structural transformations occurring in the system. The stiffness presents a sub-linear increase, while the hardness moves up following a perfect Hall-Petch trend [41]. In this regards, by comparing the hardness and the stiffness values, it has been shown that irradiation produces an overall desirable effect, since the *H/E* parameter - the ratio between the hardness and the Young's Modulus - increases [41]. As a matter of fact, this parameter can be considered a good figure of merit to evaluate the tribological properties of the film and its resistance against

cracking initiation and other degradative phenomena such as erosion operated by the flowing media [49]–[52]. The radiation-induced crystallization mechanism was confirmed in a second campaign, when the PLD-grown alumina coatings were irradiated with 4 MeV Ni^{2+} at extreme radiation levels, up to 450 dpa [48]. However, the variations in terms of ion mass, energy and ENSP (Electronic to Nuclear Stopping Power) caused evident differences. In the second experiment, new crystalline phases were observed, while the maximum grain size value measured at 450 dpa was still lower than what observed at 150 dpa, in the case of gold and tungsten mixed irradiation [48]. To explain this lack of consistency, molecular dynamics (MD) simulations were carried out. Authors compared the effects of Ni ions to the Au ones, keeping the same energy for both the incident particles. Specifically, they evaluated their effects in terms of number and distribution of Frenkel pairs produced by the two. From the simulations, they observed how gold ions are able to form denser cascades, compared to the lighter nickel ions [48]. The higher local density of defects promotes the evolution towards the lowest energy state (*i.e.* a more stable configuration), fastening also the grain growth process.

Here, to understand the grain growth trends under irradiation, we employ simple models relating the grain size (d) with the radiation fluence or dose (φ) [53]–[58]. Indeed, grain size increases with the ion fluence according to the following power law relation:

$$d^n - d_0^n = k\varphi = k\Phi t \tag{1}$$

where n is the grain growth exponent, d_0 is the initial grain size, d is the grain size after at a certain time t, φ is the ion fluence, Φ is the ion flux and k is an experimental kinetic constant. While k is strictly related to the materials properties and the irradiation conditions, the exponent n moves in a limited range of values. The n has been found between 2 and 4 for pure metals and alloys under irradiation [53], [54], [56], [59]. As a matter of fact, a value of $n \sim 2$ generally indicates a thermally activated process, where ideal diffusion governs the grain growth. Thus, in the case of irradiated materials, n assumes higher values since irradiation plays a major role. For low temperature irradiation, Liu et al. [57] found n to be around 3 in several metallic alloys. The authors described this mechanism as a saturation trend on the grain growth, indicating that the saturation could be related to the size of the defect cascade generated by single ions in the evolving system [57]. Nevertheless, Kaoumi et al. [53] derived mathematically the $n = 3$ relation by considering the athermal process of radiation-induced growth in pure metals. The authors claimed that the process of grain growth under irradiation is governed by the interactions between the thermal spike region and the grain boundaries [53]. While statistics lacks in the case of ceramic materials, similar values have been calculated. For example, Chen et al. [45] reported a value of n equal to 2.63 for PLD-grown amorphous Y_2O_3. In this framework, the experimental data collected by Ferré et al. [41], [48] have been used to fit the present model. Calculations have been re-performed starting from the TEM Bright Fields micrographs, for the Au and W mixed ions tests.

By employing imaging correlation process software, new results have been calculated as shown in FIG. 4:

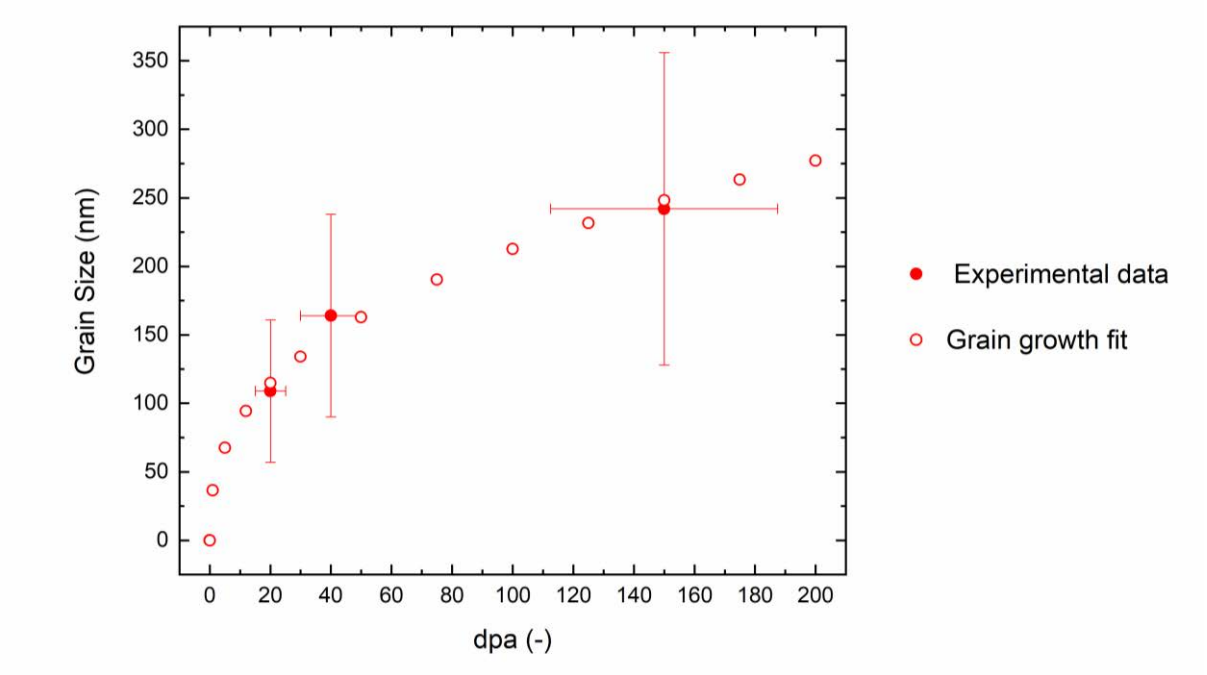

FIG. 4. Grain size values re-calculated according to the most recent analyses. New data have been used to fit the physical model presented in Eq. 1, in order to obtain the relevant parameters.

The fit matches well with the re-calculated grain size data, yielding to a value of n around 2.61. This value is in a good accordance with experimental and theoretical studies (*i.e.* $2 < n < 4$) for the grain growth process under irradiation. Moreover, 2.61 is very similar to the exponent reported in [45] for an amorphous oxide film exposed to heavy ion irradiation. These indications confirm the robustness and the validity of the physical model to describe the radiation-enhanced grain growth. Finally, yet importantly, the combined use of the Hall-Petch equation together with the present model allows the prediction of the main material features - the grain size as well as the mechanical behavior - in the PLD-grown alumina film under irradiation.

3.2. **Gas permeation tests for tritium confinement**

Albeit the production of tritium (T_2) in LFRs should remain well below the calculated values for lithium-based systems like Molten Salt Reactor (MSR) and fusion reactor breeding blankets, the amount of radioactive gas formed in fast fission systems is generally much higher than in the traditional thermal counterpart [60], [61]. Neutron captures by ^{10}B and ternary fissions - the main sources of T_2 in LFRs - increase with the neutron energy. Moreover, the fissile ^{239}Pu contained in the fuel presents a higher tritium yield compared to ^{235}U [61].

Since the production of tritium occurs mainly inside the rods - either fuel or control rods, a suitable barrier would be useful to avoid simultaneously the corrosion of the steel claddings (see next section) and the contamination of the primary circuit by the radioactive gas. Indeed, the employment of anti-permeation coatings could guarantee the retention of tritium inside the pins and its storage in the gas plenum region, in order to be collected at the end of the component lifetime [60]–[62].

In this framework, PLD-grown alumina films have been extensively characterized, to assure the T_2 confinement capability. The experiments have been accomplished in collaboration with different international partners - mainly ENEA and CIEMAT, under the framework of the EUROFUSION. Firstly, tests have been carried out with hydrogen as tritium surrogate, showing a remarkable decrease of the permeating gas in the case of PLD-coated substrates [63], [64]. Here, coated and uncoated EUROFER-97 steel substrates have been exposed to pure H_2 gas, from 350 to 650 °C. The typical figure of merit - the Permeation Reduction Factor (PRF) - has been calculated comparing the permeating gas flux between the coated and the uncoated steel. A significant PRF value in the order of 10^3 has been obtained at 450 °C, while at 550 °C the value is ~ 10^4 [63], [64]. The maximum PRF - almost 10^5 - has been registered for the highest temperature test, specifically at 650 °C [64]. It is worth mentioning that this result represents the state of the art for single side-coated steel substrates, suggesting promising anti-permeation properties for the PLD-grown films in tritium-enriched environment. PRF results are summarized in TABLE 8:

TABLE 8: PRF VALUES IN ALUMINA-COATED EUROFER-97, FOR DIFFERENT TEMPERATURE LEVELS [64].

Temperature [°C]	350	450	550	650
PRF [-]	550 ± 50	3 800 ± 300	12 600 ± 1 000	85 400 ± 2 700

In a parallel campaign, deuterium (D_2) permeation was tested under relevant radiation fields [63], [65]. Initially, pristine samples have been subjected to intense electron fields, to simulate the β^- decay emissions of tritium. Coated and uncoated specimens have been exposed to D_2 and, at the same time, irradiated with 1.8 MeV electrons at a dose rate up to 700 Gy/s, by means of a Van de Graaff electron accelerator. Without irradiation, the calculated PRF value has been confirmed around 10^3 at 450 °C. On the other hand, it has been observed that under electron irradiation the measured deuterium current is even lower than the not-irradiated case. In addition, once the electron beam is stopped, the permeability increases again, to return to not-irradiated values [63]. A summary of the permeation tests results is presented in FIG. 5 [63]:

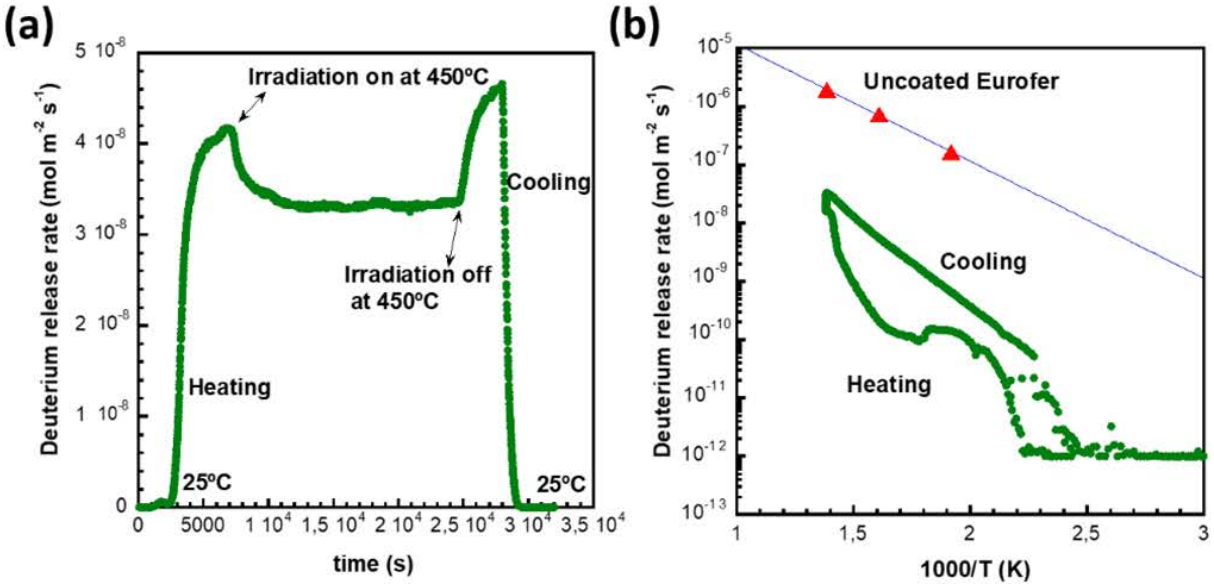

FIG. 5. Summary of the deuterium permeation results under electron irradiation. Reproduced from [63] with permission courtesy of IOP Publishing.

Thermo-stimulated desorption (TSD) experiments support these evidences, confirming that the deuterium release rate is generally lower for the samples tested under e^- irradiation [65]. Particularly, the TSD results have been obtained on deuterium pre-implanted samples, employing an ion accelerator to implant in the alumina layer deuterium ions (10 keV) up to a dose of 2.5×10^{16} ions/cm^2 [65]. The increase of the anti-permeation performance (*i.e.* the decrease of the deuterium release rate) could be due to a less-favorite deuterium uptake under electron irradiation, since the charge accumulation could interfere with the deuterium adsorption at the alumina surface.

Lastly, additional damage has been caused to the substrate/film tandem, by pre-irradiating the coated specimens. Samples have been previously irradiated with 22 MeV F^+ at 450 °C (up to a fluence of 10^{15} ions/cm^2), then exposed to deuterium gas and electrons flus, as described before [65].

Nevertheless, the anti-permeation capability has been maintained, independently from the pre-damaging (FIG. 6):

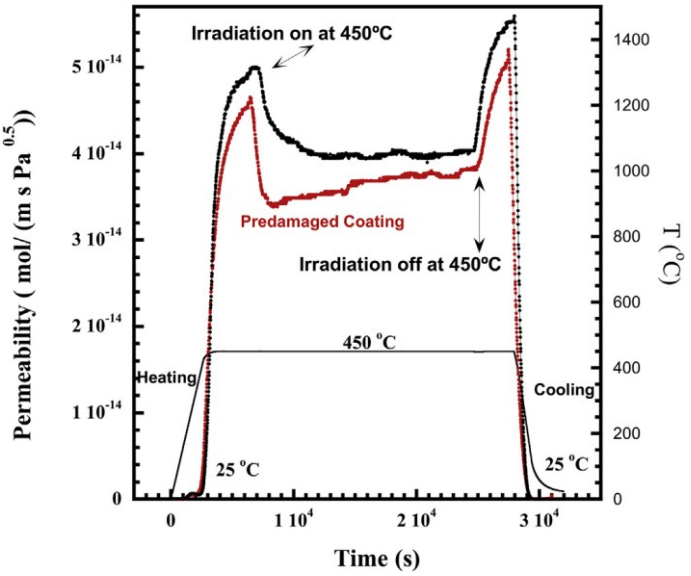

FIG. 6. Deuterium permeability in pre-damaged alumina-coated samples. The pre-irradiation with F ions does not cause any significant degradation in terms of performance. Reprinted from [65] with permission courtesy ELSEVIER.

3.3. **Corrosion tests**

HLM corrosion and HLM embrittlement of structural steels are the most concerning material-related issues for the development of the LFR technology. The deposition of a dense and compact ceramic barrier proved to be optimal in insulating the metallic substrate from the harsh environment. Initially, steel plates (ferritic/martensitic T91 steel) were coated with a few microns-thick PLD-grown Al_2O_3 and exposed to static lead at 550 °C for 500 hours, with an oxygen concentration in the order of $10^{-6} – 10^{-7}$ wt.% [66]. After the experiment, no degradation of the oxide film, nor interaction with the steel substrate was found, proving that the deposited layer had been capable of protecting efficiently the underlying substrate. A similar outcome was obtained in the subsequent experiments, when the tests were performed in the most severe chemical conditions for the structural steels (*i.e.* dissolutive regime), considering the foreseen materials for LFRs. Alumina-coated 1515-Ti steel plates and tubes were exposed to stagnant lead with a C_O around $10^{-8} – 10^{-9}$ wt.%, at 550 °C, up to 4˙000 h [35]. Again, the ceramic film avoided any kind of interaction between the molten media and the steel, independently from the exposure time.

A comprehensive analysis of the corroded specimens is reported in FIG. 7:

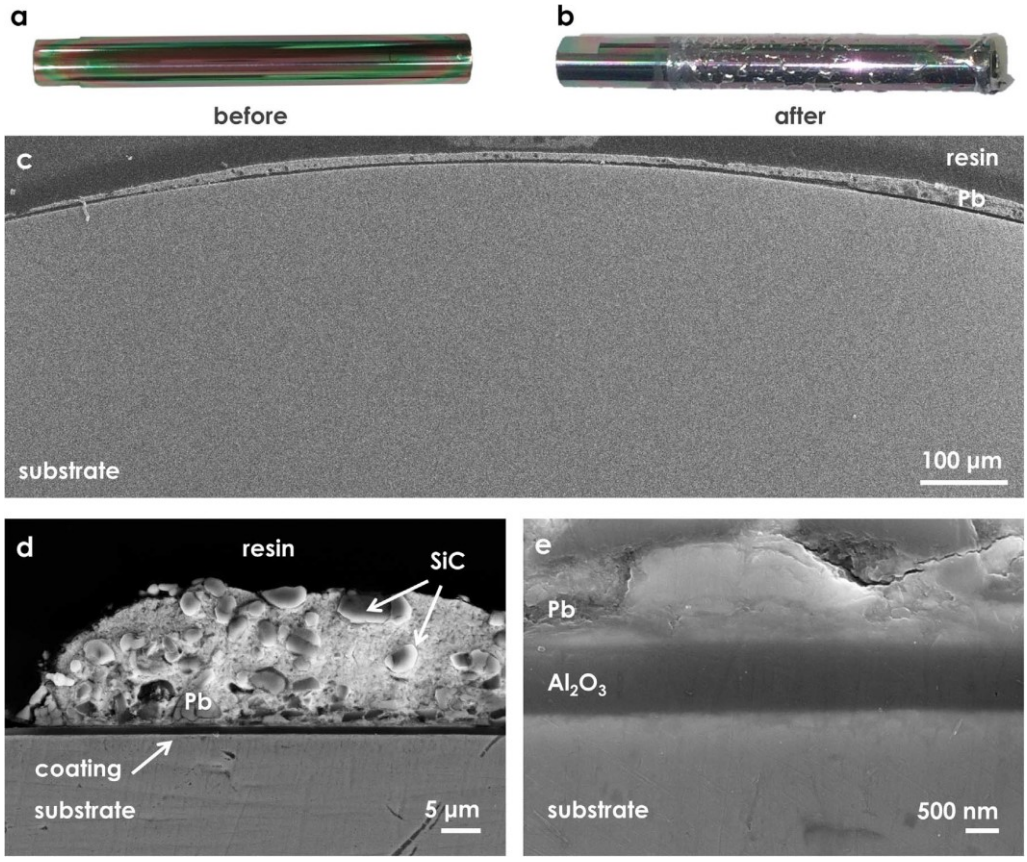

FIG. 7. Coated 1515-Ti cylinders before (a) and after (b) the corrosion tests (static lead, 550 °C, 4˙000 h, 10^{-8} wt.% O). The liquid metal does not corrode the steel cylinders, neither at the macroscopic scale (c) nor at the microscopic scale (d and e). Reproduced from [35] with permission courtesy of ELSEVIER.

Films as thin as 250 nm were tested, showing no difference in respect to their protectiveness. Then, pre-irradiated samples were evaluated in the same dissolutive conditions. To couple the radiation- and corrosion-induced degradation modes, specimens subjected to heavy ion irradiation at 150 dpa (see [41]) were exposed to molten Pb in short-term (1˙000 hours) corrosion tests. After the test, samples have been characterized according to FIG. 8 [35]:

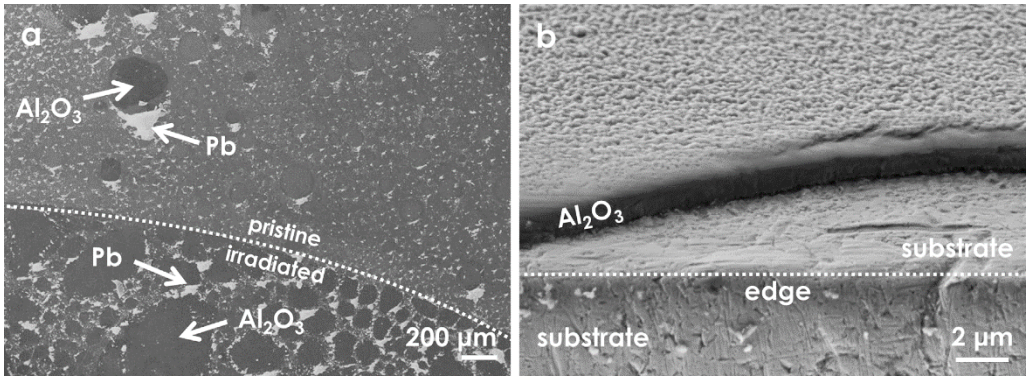

FIG. 8. Surface (a) and tilted cross-sectional (b) SEM micrographs of a coated steel sample after irradiation and exposure to stagnant lead (550 °C, 1˙000 h, 10^{-8} wt.% O). The film is still capable of protecting the underlying substrate, even if surface modifications occurred. Reproduced from [35] with permission courtesy of ELSEVIER.

Despite the extreme dpa level previously reached, the protective capability of the pristine film were maintained (FIG. 8,b) [35].

More recently, new chemical compatibility tests have been performed on the PLD-grown Al_2O_3 films developed by IIT. New results have been collected and included in the present work. In a first campaign, the behavior of amorphous/nano-crystalline alumina in oxygen-rich lead has been investigated. As reported in [67], [68], high content of oxygen inside the melt could be detrimental since alumina reacts with lead oxide (PbO) at elevated temperature. The authors of [67] also found that amorphous alumina could be even more sensitive to PbO, since the absence of a stable crystalline structure enhances the material chemical reactivity. To verify these evidences, coated 1515-Ti steel cylinders - the same type of sample used in the previous experiment - have been exposed to stagnant lead, with C_O in the order of 10^{-3} wt.%, at 550 °C, for 1˙000 h. Here, the level of oxygen has been selected to perform the test near the region of formation of PbO at 550 °C, according to the Ellingham diagram. The results of these tests resemble the ones observed in dissolutive regime: at the relevant temperature conditions for LFRs, the alumina layer is stable in a broad range of conditions, from 10^{-3} wt.% to 10^{-9} wt.% of oxygen concentration. According to the present results, these experiments prove the unique advantage of the dense oxide coatings deposited by PLD technique in a wide range of oxygen contents, thanks to the superior inertness of the material itself. This evidence represents a major achievement, since coatings could avoid any technological issue connected with the strict oxygen control inside the reactor.

Lastly, preliminary corrosion tests in flowing media have been designed and implemented. Inside the core of LFR systems, coolant will circulate at not-negligible speed, around 1 – 1.5 m/s [62], [69], [70]. For this reason, the combined action of corrosion and erosion phenomena of traditional steels should be considered. In this framework, dedicated 1515-Ti samples have been exposed to flowing lead (flow speed of 1.3 m/s) at 520 °C for 200 h, with an oxygen content in the order of 10^{-4} wt.%. Results are shown in FIG. 9:

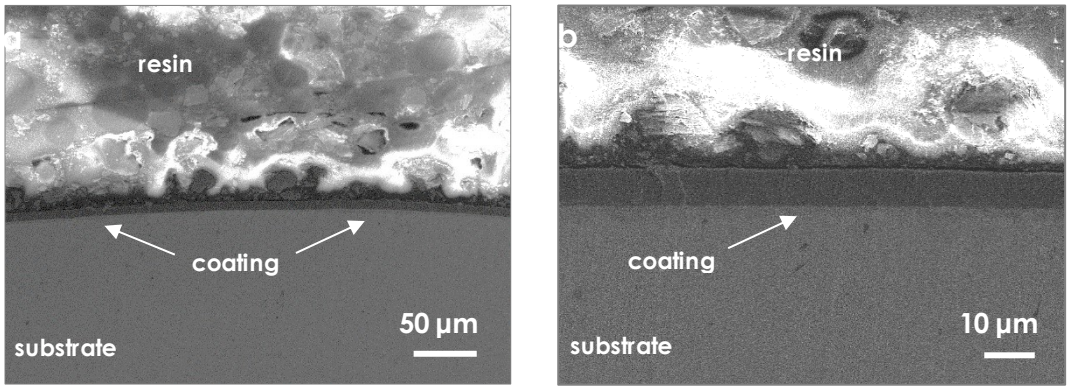

FIG. 9. Alumina-coated 1515-Ti cylinders exposed to flowing corrosion test (1.3 m/s, 520 °C, 200 h, 10^{-4} wt.% O). Cross-sectional SEM images at different magnifications (a, b) show to effectiveness of PLD-grown films in protecting the underlying substrate under to flowing media.

Despite the short duration of the present experiment, preliminary considerations can be raised. After the flowing corrosion tests, the underlying substrate is still continuously covered by the oxide layer, which shows the characteristic low wettability reported in [35], [66]. No sign of failure appears from the SEM micrographs: the cross-sectional image confirms the lack of substantial modifications in the tandem system and the absence of degradative attacks on the steel substrate. Furthermore, no variation in the coating's thickness has been found. The ceramic layer has withstood the erosive action of molten lead without losing structural integrity.

Having assessed the chemical compatibility of PLD-grown alumina coatings with molten lead in a broad range of conditions, a few words should be spent on the material performance in presence of the Pb-Li alloy. Indeed, the same material issues discussed in this work (*i.e.* radiation-induced degradation, tritium permeation and HLM corrosion) are shared between LFRs and nuclear fusion systems, particularly for what regards the breeding blanket moduli of fusion reactors. In breeding blankets, the lead lithium eutectic (Pb-16Li at.%) will be used to guarantee at the same time cooling, neutron moderation and tritium breeding [71], [72]. Here, the chemistry of the melt introduces a further degradation mechanism, since Li interacts with metal oxides such as Al_2O_3, Y_2O_3 or Er_2O_3 by forming the ternary compound $LiMeO_2$, where Me is Al, Y and Er, respectively [73]–[76]. To check the behavior of Al_2O_3 coatings while exposed to Pb-16Li, parallel corrosion tests have been performed at 550 °C, at low C_O (around 10^{-8} – 10^{-9} wt.%), up to 8˙000 h. Results have confirmed the protective capability of alumina films under Pb-16Li, despite the presence of metallic lithium (FIG. 10) [63], [64]:

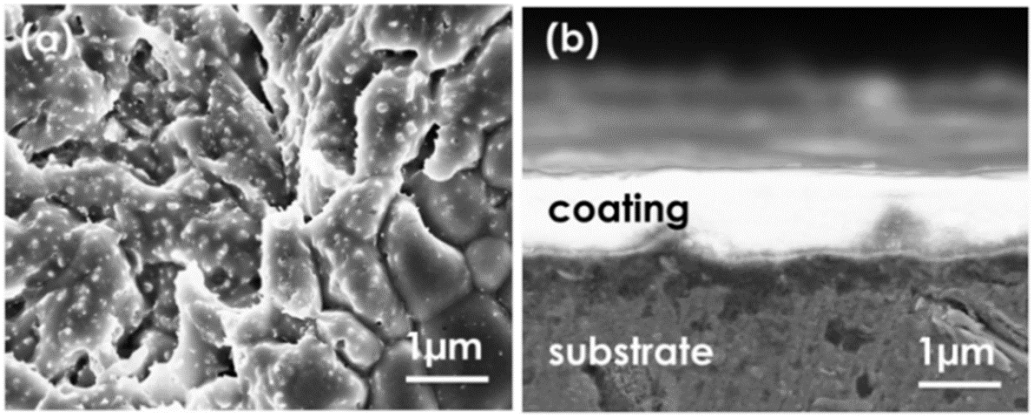

FIG. 10. Uncoated (a) and coated (b) samples exposed to corrosion tests. The uncoated samples suffer dissolution- corrosion driven by grain boundary attacks, while LLE does not interact with the substrate in the coated samples. Reproduced from [63] with permission courtesy of IOP Publishing.

According to the present studies and previous literature data, the $LiAlO_2$ layer developed during the corrosion test is stable in a set of thermodynamic conditions compatible with breeding blankets operation conditions. The formation of this layer avoids the chemical interaction between the molten media and the steel substrate, guarantying an effective protection. Detailed studies are still ongoing, in order to understand the kinetic of transformation and the thickness of the $LiAlO_2$ depending on the exposure time.

4. SUMMARY AND CONCLUSIONS

PLD-grown aluminium oxide coatings hold great promise to enable the development of structural materials for LFRs. Basic characterization of the material showed high compactness and optimal adhesion to the substrate, combined with exceptional metal-like mechanical properties and high hardness. The coatings underwent several tests in order to be qualified for their application in the nuclear field. Different heavy ions irradiation campaigns were undertaken to simulate the effect of neutrons, showing a high tolerance towards radiation-induced damages of the films. In addition, the ability of the coatings to act as an anti-permeation barrier was evaluated. The calculated PRF value was in the order of 104 at 550 °C, which was also confirmed irradiating the samples with high energy electrons during the permeation tests, and after several days of thermal cycling. These values will guarantee the suppression of the permeation of tritium through the structural steel. Finally, the chemical stability of the coatings against liquid lead were evaluated by designing corrosion tests with

different concentration of oxygen. No delamination and no reduction of the thickness of the coating were observed, meaning an optimal corrosion resistance of the material. Thanks to these peculiar and promising properties, PLD-grown coatings could ensure the mitigation of the material related criticalities for the LFRs, proving to be a viable solution to decouple the protective and the structural means of materials. In principle, without requiring any strict control on the oxygen content in the cooling medium, coatings could translate in the opportunity of increasing the operation temperature of the reactor, hence improving the efficiency of the system.

ACKNOWLEDGEMENTS

We are grateful to Konstantza Lambrinou (SCK·CEN, Belgium) and Teresa Hernandez (CIEMAT, Spain) for the scientific discussions and the technical support. The authors acknowledge financial aid by ENEA through the AdP MiSE-ENEA projects (PAR 2014 – 2018), and the European Commission for having funded the H2020 projects "GEMMA" (grant agreement N° 755269), "TRANSAT" (N° 754586) and "IL TROVATORE" (N° 740415). This work has been carried out within the framework of the EURO-fusion Consortium and has received funding from the Euratom research and training program 2014 – 2018, under grant agreement N° 633053. The French network EMIR is acknowledged for supporting financially the ion irradiation experiments at the JANNUS (Joint Accelerators for Nanoscience and Nuclear Simulation) platforms of CEA-Saclay. This work contributes also to Sub-Program 3 (SP3) of the Joint Program on Nuclear Materials (JPNM) of the European Energy Research Alliance (EERA).

REFERENCES

[1] F. ROELOFS, *Thermal Hydraulics Aspects of Liquid Metal Cooled Nuclear Reactors*. 2019.

[2] U.S. DOE, "A technology roadmap for generation IV nuclear energy systems," pp. 1–97, 2002.

[3] GIF (Generation IV International Forum), "GIF R&D Outlook for Generation IV Nuclear Energy Systems: 2018 Update," 2018.

[4] OECD NEA, "Handbook on Lead-bismuth Eutectic Alloy and Lead Properties , Materials Compatibility , Thermal-hydraulics and Technologies," 2015.

[5] I. SERRE AND J. B. VOGT, "Liquid metal embrittlement of T91 martensitic steel evidenced by small punch test," *Nucl. Eng. Des.*, vol. 237, no. 7, pp. 677–685, 2007.

[6] J. VAN DEN BOSCH, R. W. BOSCH, D. SAPUNDJIEV, AND A. ALMAZOUZI, "Liquid metal embrittlement susceptibility of ferritic-martensitic steel in liquid lead alloys," *J. Nucl. Mater.*, vol. 376, no. 3, pp. 322–329, 2008.

[7] D. GORSE *ET AL.*, "Influence of liquid lead and lead-bismuth eutectic on tensile, fatigue and creep properties of ferritic/martensitic and austenitic steels for transmutation systems," *J. Nucl. Mater.*, vol. 415, no. 3, pp. 284–292, 2011.

[8] C. SCHROER, A. SKRYPNIK, O. WEDEMEYER, AND J. KONYS, "Oxidation and dissolution of iron in flowing lead-bismuth eutectic at 450°C," *Corros. Sci.*, vol. 61, pp. 63–71, 2012.

[9] K. LAMBRINOU, E. CHARALAMPOPOULOU, T. VAN DER DONCK, R. DELVILLE, AND D. SCHRYVERS, "Dissolution corrosion of 316L austenitic stainless steels in contact with static liquid lead-bismuth eutectic (LBE) at 500 °C," *J. Nucl. Mater.*, vol. 490, no. 2017, pp. 9–27, 2017.

[10] M. ROY, L. MARTINELLI, K. GINESTAR, J. FAVERGEON, AND G. MOULIN, "Dissolution and oxidation behaviour of various austenitic steels and Ni rich alloys in lead-bismuth eutectic at 520 °c," *J. Nucl. Mater.*, vol. 468, pp. 153–163, 2016.

[11] C. SCHROER, O. WEDEMEYER, J. NOVOTNY, A. SKRYPNIK, AND J. KONYS, "Selective leaching of nickel and chromium from Type 316 austenitic steel in oxygen-containing lead–bismuth eutectic (LBE)," *Corros. Sci.*, vol. 84, pp. 113–124, Jul. 2014.

[12] M. DEL GIACCO, A. WEISENBURGER, A. JIANU, F. LANG, AND G. MUELLER, "Influence of composition and microstructure on the corrosion behavior of different Fe – Cr – Al alloys in molten LBE," *J. Nucl. Mater.*, vol. 421, no. 1–3, pp. 39–46, 2012.
[13] J. EJENSTAM, M. HALVARSSON, J. WEIDOW, B. JÖNSSON, AND P. SZAKALOS, "Oxidation studies of Fe10CrAl-RE alloys exposed to Pb at 550 C for 10,000 h," *J. Nucl. Mater.*, vol. 443, no. 1–3, pp. 161–170, 2013.
[14] P. DÖMSTEDT, M. LUNDBERG, AND P. SZAKALOS, "Corrosion Studies of Low - Alloyed FeCrAl Steels in Liquid Lead at 750 °C," *Oxid. Met.*, vol. 91, no. 3, pp. 511–524, 2019.
[15] P. EKLUND, M. BECKERS, U. JANSSON, H. HÖGBERG, AND L. HULTMAN, "The Mn + 1AXn phases: Materials science and thin-film processing," *Thin Solid Films*, vol. 518, no. 8, pp. 1851–1878, 2010.
[16] L. A. BARNES, N. L. D. RAGO, AND L. LEIBOWITZ, "Corrosion of ternary carbides by molten lead," vol. 373, pp. 424–428, 2008.
[17] A. HEINZEL, A. WEISENBURGER, AND G. MÜLLER, "Long-term corrosion tests of Ti 3 SiC 2 and Ti 2 AlC in oxygen containing LBE at temperatures up to 700 C," vol. 482, pp. 114–123, 2016.
[18] Y. ZHANG *ET AL.*, "Microstructures and properties of high-entropy alloys," *Prog. Mater. Sci.*, vol. 61, no. October 2013, pp. 1–93, 2014.
[19] D. B. MIRACLE AND O. N. SENKOV, "A critical review of high entropy alloys and related concepts," *Acta Mater.*, vol. 122, pp. 448–511, 2017.
[20] A. HEINZEL, M. KONDO, AND M. TAKAHASHI, "Corrosion of steels with surface treatment and Al-alloying by GESA exposed in lead-bismuth," *J. Nucl. Mater.*, vol. 350, no. 3, pp. 264–270, 2006.
[21] A. WEISENBURGER, G. MÜLLER, A. HEINZEL, A. JIANU, H. MUSCHER, AND M. KIESER, "Corrosion, Al containing corrosion barriers and mechanical properties of steels foreseen as structural materials in liquid lead alloy cooled nuclear systems," *Nucl. Eng. Des.*, vol. 241, no. 5, pp. 1329–1334, 2011.
[22] W. KRAUSS, J. KONYS, AND S. E. WULF, "Corrosion barriers processed by Al electroplating and their resistance against flowing Pb-15.7Li," *J. Nucl. Mater.*, vol. 455, no. 1, pp. 522–526, 2014.
[23] A. WEISENBURGER *ET AL.*, "Long term corrosion on T91 and AISI1 316L steel in flowing lead alloy and corrosion protection barrier development: Experiments and models," *J. Nucl. Mater.*, vol. 415, no. 3, pp. 260–269, 2011.
[24] G. MÜLLER, G. SCHUMACHER, AND F. ZIMMERMANN, "Investigation on oxygen controlled liquid lead corrosion of surface treated steels," *J. Nucl. Mater.*, vol. 278, no. 1, pp. 85–95, 2000.
[25] R. FETZER, A. WEISENBURGER, A. JIANU, AND G. MÜLLER, "Oxide scale formation of modified FeCrAl coatings exposed to liquid lead," *Corros. Sci.*, vol. 55, pp. 213–218, 2012.
[26] A. K. RIVAI AND M. TAKAHASHI, "Compatibility of surface-coated steels, refractory metals and ceramics to high temperature lead-bismuth eutectic," *Prog. Nucl. Energy*, vol. 50, no. 2–6, pp. 560–566, 2008.
[27] A. K. RIVAI AND M. TAKAHASHI, "Corrosion investigations of Al-Fe-coated steels, high Cr steels, refractory metals and ceramics in lead alloys at 700 °C," *J. Nucl. Mater.*, vol. 398, no. 1–3, pp. 146–152, 2010.
[28] Y. DAI, V. BOUTELLIER, D. GAVILLET, H. GLASBRENNER, A. WEISENBURGER, AND W. WAGNER, "FeCrAlY and TiN coatings on T91 steel after irradiation with 72 MeV protons in flowing LBE," *J. Nucl. Mater.*, vol. 431, no. 1–3, pp. 66–76, 2012.
[29] H. GLASBRENNER AND F. GRÖSCHEL, "Exposure of pre-stressed T91 coated with TiN, CrN and DLC to Pb-55.5Bi," *J. Nucl. Mater.*, vol. 356, no. 1–3, pp. 213–221, 2006.
[30] P. DOU AND R. KASADA, "Preliminary study on nano- and micro-composite sol-gel based alumina coatings on structural components of lead-bismuth eutectic cooled fast breeder reactors," *J. Nucl. Mater.*, vol. 409, no. 3, pp. 177–182, 2011.
[31] J. SCHOU, "Physical aspects of the pulsed laser deposition technique: The stoichiometric transfer of material from target to film," *Appl. Surf. Sci.*, vol. 255, no. 10, pp. 5191–5198, 2009.
[32] D. H. LOWNDES, D. B. GEOHEGAN, A A PURETZKY, AND D. P. NORTON, "Synthesis Thin-Film Materials by Pulsed Deposition Laser," vol. 273, no. 5277, pp. 898–903, 2012.
[33] S. WICKLEIN *ET AL.*, "Pulsed laser ablation of complex oxides: The role of congruent ablation and preferential scattering for the film stoichiometry," *Appl. Phys. Lett.*, vol. 101, no. 13, 2012.
[34] F. DI FONZO *ET AL.*, "Growth regimes in pulsed laser deposition of aluminum oxide films," *Appl. Phys. A*, vol. 93, no. 3, pp. 765–769, 2008.
[35] F. G. FERRÉ *ET AL.*, "Corrosion and radiation resistant nanoceramic coatings for lead fast reactors," *Corros. Sci.*, vol. 124, no. May, pp. 80–92, 2017.

[36] F. GARCÍA FERRÉ *ET AL.*, "The mechanical properties of a nanocrystalline Al2O3/a-Al2O3 composite coating measured by nanoindentation and Brillouin spectroscopy," *Acta Mater.*, vol. 61, no. 7, pp. 2662–2670, 2013.
[37] E. J. FRANKBERG *ET AL.*, "Highly ductile amorphous oxide at room temperature and high strain rate," *Sci. Rep.*, 2019.
[38] G. S. WAS, *Fundamentals of radiation materials science: Metals and alloys, second edition*. 2016.
[39] G. S. WAS, *Fundamentals of radiation materials science*. New York: Springer US, 2007.
[40] F. GARCÍA FERRÉ, "Radiation tolerant nanoceramic coatings for lead fast reactor nuclear fuel cladding," 2014.
[41] F. G. FERRÉ, A. MAIROV, L. CESERACCIU, Y. SERRUYS, P. TROCELLIER, AND C. BAUMIER, "Radiation endurance in Al2O3 nanoceramics," *Nat. Publ. Gr.*, no. August, pp. 1–9, 2016.
[42] M. DHANUNJAYA, S. A. KHAN, A. P. PATHAK, D. K. AVASTHI, AND S. V. S. NAGESWARA RAO, "Ion induced crystallization and grain growth of hafnium oxide nano-particles in thin-films deposited by radio frequency magnetron sputtering," *J. Phys. D. Appl. Phys.*, vol. 50, no. 50, p. aa9723, 2017.
[43] L.-U. AAEN ANDERSEN, "Crystallization of amorphous thin films during heavy-ion irradiation," *Mater. Sci. Eng. A*, vol. 134, no. C, pp. 1255–1259, 1991.
[44] J. CARTER *ET AL.*, "Effects of ion irradiation in metallic glasses," *Nucl. Instruments Methods Phys. Res. Sect. B Beam Interact. with Mater. Atoms*, vol. 267, no. 8–9, pp. 1518–1521, 2009.
[45] Y. CHEN *ET AL.*, "In situ studies of radiation induced crystallization in Fe / a-Y 2 O 3 nanolayers," vol. 452, pp. 321–327, 2014.
[46] L. U. AAEN ANDERSEN, J. BØTTIGER, J. JANTING, AND N. KARPE, "Crystallization of amorphous thin films during heavy-ion irradiation," *Mater. Sci. Eng. A*, vol. 134, no. C, pp. 1255–1259, 1991.
[47] T. NAGASE *ET AL.*, "MeV electron irradiation induced crystallization in metallic glasses: Atomic structure, crystallization mechanism and stability of an amorphous phase under the irradiation," *J. Non. Cryst. Solids*, vol. 358, no. 3, pp. 502–518, 2012.
[48] F. GARCÍA FERRÉ *ET AL.*, "Extreme ion irradiation of oxide nanoceramics: Influence of the irradiation spectrum," *Acta Mater.*, vol. 143, pp. 156–165, 2018.
[49] S. CHOWDHURY *ET AL.*, "Improvement of wear performance of nano-multilayer PVD coatings under dry hard end milling conditions based on their architectural development," *Coatings*, vol. 8, no. 2, pp. 1–14, 2018.
[50] J. MUSIL, "Hard nanocomposite coatings: Thermal stability, oxidation resistance and toughness," *Surf. Coatings Technol.*, vol. 207, pp. 50–65, 2012.
[51] B. D. BEAKE AND G. S. FOX-RABINOVICH, "Progress in high temperature nanomechanical testing of coatings for optimising their performance in high speed machining," *Surf. Coatings Technol.*, vol. 255, pp. 102–111, 2014.
[52] S. VEPREK, R. F. ZHANG, M. G. J. VEPREK-HEIJMAN, S. H. SHENG, AND A. S. ARGON, "Superhard nanocomposites: Origin of hardness enhancement, properties and applications," *Surf. Coatings Technol.*, vol. 204, no. 12–13, pp. 1898–1906, 2010.
[53] D. KAOUMI, A. T. MOTTA, AND R. C. BIRTCHER, "A thermal spike model of grain growth under irradiation," *J. Appl. Phys.*, vol. 104, no. 7, 2008.
[54] H. A. ATWATER, C. V. THOMPSON, AND H. I. SMITH, "Ion-bombardment-enhanced grain growth in germanium, silicon, and gold thin films," *J. Appl. Phys.*, vol. 64, no. 5, pp. 2337–2353, 1988.
[55] Y. ZHANG *ET AL.*, "Grain growth and phase stability of nanocrystalline cubic zirconia under ion irradiation," *Phys. Rev. B - Condens. Matter Mater. Phys.*, vol. 82, no. 18, pp. 1–7, 2010.
[56] D. KAOUMI, A. T. MOTTA, AND R. C. BIRTCHER, "Grain Growth in Nanocrystalline Metal Thin Films under In Situ Ion-Beam Irradiation," vol. 4, no. 8, pp. 1–13, 2007.
[57] J. C. LIU, J. LI, AND J. W. MAYER, "Temperature effect on ion-irradiation-induced grain growth in Cu thin films," *J. Appl. Phys.*, vol. 67, no. 5, pp. 2354–2358, 1990.
[58] J. S. IM AND H. A. ATWATER, "Kinetic and thermodynamic enhancement of crystal nucleation and growth rates in amorphous Si film during ion irradiation," *Nucl. Inst. Methods Phys. Res. B*, vol. 59–60, no. PART 1, pp. 422–426, 1991.
[59] D. E. ALEXANDER, G. S. WAS, AND L. E. REHN, "The heat-of-mixing effect on ion-induced grain growth," *J. Appl. Phys.*, vol. 70, no. 3, pp. 1252–1260, 1991.
[60] K. LIGER *ET AL.*, "Overview of the TRANSAT (TRANSversal Actions for Tritium) project," *Fusion Eng. Des.*, vol. 136, no. January, pp. 168–172, 2018.
[61] J. E. PHILLIPS AND C. E. EASTERLY, "Sources of tritium," *Nucl. Saf.*, vol. 22, no. 5, pp. 612–626, 1981.

[62] M. FROGHERI, A. ALEMBERTI, AND L. MANSANI, "The lead fast reactor: demonstrator (Alfred) and ELFR design," *Fast React. Relat. Fuel Cycles Safe Technol. Sustain. Scenar. (FR13). V. 1. Proc. an Int. Conf.*, no. March 2013, 2015.
[63] D. IADICICCO *ET AL.*, "Efficient hydrogen and deuterium permeation reduction in Al2O3 coatings with enhanced radiation tolerance and corrosion resistance," *Nucl. Fusion*, vol. 58, no. 12, 2018.
[64] D. IADICICCO *ET AL.*, "Multifunctional nanoceramic coatings for future generation nuclear systems," *Fusion Eng. Des.*, no. October 2018, pp. 0–1, 2019.
[65] P. MUÑOZ *ET AL.*, "Radiation effects on deuterium permeation for PLD alumina coated Eurofer steel measured during 1.8 MeV electron irradiation," *J. Nucl. Mater.*, vol. 512, pp. 118–125, 2018.
[66] F. GARCÍA FERRÉ, M. ORMELLESE, F. DI FONZO, AND M. G. BEGHI, "Advanced Al2O3 coatings for high temperature operation of steels in heavy liquid metals: A preliminary study," *Corros. Sci.*, vol. 77, pp. 375–378, 2013.
[67] F. OUDICH, N. DAVID, AND M. VILASI, "Phase equilibria investigations and thermodynamic modeling of the PbO-Al2O3 system," *Int. J. Mater. Res.*, vol. 106, no. 8, pp. 832–840, 2015.
[68] B. R. POWELL, "Phase equilibria in the PbO-Al2O3 system," Lawrence Berkeley National Laboratory, 1978.
[69] L. CINOTTI AND C. L. SMITH, *Handbook of Generation IV Nuclear Reactors*. Duxford: Woodhead Publishing, 2016.
[70] G. GRASSO, G. BANDINI, F. LODI, AND L. CINOTTI, "The Core of the LFR-AS-200 : Robustness for Safety," pp. 1–8, 2017.
[71] A. R. RAFFRAY, M. AKIBA, V. CHUYANOV, L. GIANCARLI, AND S. MALANG, "Breeding blanket concepts for fusion and materials requirements," *J. Nucl. Mater.*, vol. 307–311, no. 1 SUPPL., pp. 21–30, 2002.
[72] T. IHLI *ET AL.*, "Review of blanket designs for advanced fusion reactors," *Fusion Eng. Des.*, vol. 83, no. 7–9, pp. 912–919, 2008.
[73] U. JAIN, A. MUKHERJEE, S. SONAK, S. KUMAR, R. MISHRA, AND N. KRISHNAMURTHY, "Interaction of alumina with liquid Pb 83 Li 17 alloy," *Fusion Eng. Des.*, vol. 89, no. 11, pp. 2554–2558, 2014.
[74] T. TERAI *ET AL.*, "Compatibility of yttria (Y203) with liquid lithium," *J. Nucl. Mater.*, vol. 237, pp. 1421–1426, 1996.
[75] M. NAGURA, A. SUZUKI, T. MUROGA, AND T. TERAI, "LiErO2 formation on Er2O3 in static and natural convection lithium," *Fusion Eng. Des.*, vol. 84, no. 7–11, pp. 1384–1387, 2009.
[76] P. HUBBERSTEY, "The stability of tritium permeation barriers and the self-healing capability of aluminade coatings in Liquid Pb-17Li," *Fusion Technol.*, vol. 28, no. 3, pp. 1194–1199, 1995.

EVALUATION OF THE HIGH-ENTROPY CR-FE-MN-NI ALLOYS COMPATIBILITY WITH A LIQUID LEAD COOLANT

V.M. VOYEVODIN
National Science Center "Kharkiv Institute of Physics and Technology"
NAS of Ukraine, Kharkiv, Ukraine
E-mail: voyev@kipt.kharkov.ua

V.M. FEDIRKO
Karpenko Physico-Mechanical Institute of the NAS of Ukraine
Lviv, Ukraine

O.M. VELIKODNYI
National Science Center "Kharkiv Institute of Physics and Technology"
NAS of Ukraine, Kharkiv, Ukraine

I.S. KUKHAR
Karpenko Physico-Mechanical Institute of the NAS of Ukraine
Lviv, Ukraine

Kh.R. MELNYK
Karpenko Physico-Mechanical Institute of the NAS of Ukraine
Lviv, Ukraine

I.V. KOLODIY
National Science Center "Kharkiv Institute of Physics and Technology"
NAS of Ukraine, Kharkiv, Ukraine

M.A. TIKHONOVSKY
National Science Center "Kharkiv Institute of Physics and Technology"
NAS of Ukraine, Kharkiv, Ukraine

Abstract

The corrosion compatibility of the three newly developed high-entropy alloys of the Cr-Fe-Mn-Ni system with liquid lead coolant has been evaluated at temperatures of 480 °C and 580 °C up to 1000 h exposure. It was established that for all alloys at temperatures up to 480 °C, the main mechanism of the surface layers damage is intergranular corrosion, which consists in etching of the grain boundaries, lead penetration into the matrix and dissolving such elements as Ni, Cr and Mn. When the temperature rises to 580 °C, a combined mechanism of corrosion damage is realized. This mechanism consists in the combination of intergranular corrosion and diffusion of oxygen from the melt into the matrix, which results in internal oxidation of Cr and Mn. The composition of the alloy, which has a minimal corrosion tendency and can be recommended for a usage in contact with a liquid lead up to 500 °C, was established.

1. INTRODUCTION

Currently, oxide dispersion-strengthened ferrite-martensitic and austenitic steels (so called ODS steels) are considered as promising materials for the new generation nuclear reactors [1-6]. These steels have high mechanical properties and can be capable up to damaging doses of 180 dpa (displacement per atom). But the technology of ODS steel production is complicated and expensive. Therefore, the actual problem is the development of a new class of materials with much higher radiation resistance and improved values of mechanical and corrosion characteristics, which can be produced by conventional processing route. Existing theoretical studies and preliminary experimental results [7-10] show that so-called high-entropy alloys (HEAs) are promising candidates for a new generation of radiation-resistant materials due to its peculiarities of the crystalline structure.

Usually HEAs contain four or five elements with equal or close concentrations [11-13]. The entropy of mixing increases significantly with a large number of elements in the alloys and their high concentration, which contributes to the formation of the disordered substitutional solid solutions [11]. HEAs are characterized by a strong lattice distortion caused by the difference in atomic radii of the dissolved elements, which affects the solid solution hardening, and also slow diffusion [13]. Therefore, these factors determine attractive mechanical properties, which are demonstrated by some HEA compositions [13-17].

Liquid heavy metals (Pb, Pb-Bi) are considered as a coolant in the next generation nuclear power plants (NPP) [18-20]. At the same time, in the “Accelerator Driven Systems” (ADS) hybrid systems liquid lead is an environment for nuclear reactions and adiabatic deceleration of neutrons [21]. In this regard, the specific requirement for structural materials of modern nuclear power plants is their compatibility with liquid metals [22-23]. As a rule, upon the contact of a compositionally complex alloy with a liquid metal a selective dissolution of its components is observed. The thermodynamic activity of the alloying component is determined by its propensity to selective dissolution in the liquid metal [24]. Due to the selective dissolution of some of the alloying components a layer, depleted on these elements, is forming on the surface of a solid metal that facilitates phase transformation. For example, austenite in chromium-nickel steels can transform into ferrite upon the contact with Pb, Pb-Bi melts [24].

In this regard, the purpose of the work is to estimate the compatibility of the developed new class of HEAs austenitic matrix with coolant, based on lead melts.

2. MATERIALS AND METHODS

The research was carried out on newly developed high-entropy alloys (Table 1), which do not contain cobalt [10] and can be used as matrices of promising materials for new generation nuclear reactors. High-entropy alloys based on chromium, iron, manganese, and nickel (Cr-Fe-Mn-Ni) with different elements content were obtained by arc melting in pure argon [14]. The purity of initial components was not less than 99.9%. Ingots (size of 6 x 15 x 60mm) were re-melted at least 5 times and then annealed at 1100 °C for 3 hours to ensure homogeneity. Ingots of HEAs were rolled at room temperature to a thickness of 0.5 mm with intermediate annealing at 1100 °C for 3 hours (to homogenize the initial as-cast structure and to remove hardening). After that rolled HEAs stripes were finally annealed in vacuum at 850 °C and 1050 °C for 1 h.

TABLE 1. CHEMICAL COMPOSITION OF ALLOYS, % AT

Alloy	Fe	Mn	Cr	Ni
E30-2	40	28	18	14
E31-2	27	27	18	28
E32-2	40	20	20	20

Structure of alloys was characterized by XRD using DRON-4-07 diffractometer with Cu-Kα radiation and Ni filter. Metallography studies of samples were made by optical microscope Neophot-2. Microstructure analysis was conducted using TEM (JEM-100CX and JEOL-2100F microscopes). Total chemical analysis, elemental composition of oxide layers and their distribution near the primary boundary were studied by X-Ray microspectral analysis using JEOL Superprobe 733 (electron probe microanalysis - EPMA) and Philips XL (energy dispersive X-ray spectroscopy - EDX) microanalyzers. Microhardness studies were carried out by the Vickers method using PMT-3 device with an applied load of 0.196 N.

Corrosion tests were carried out by the ampoule method in static isothermal conditions. Samples were fixed in separate alundum ampoules. Ampoules were filled with the lead melt in a pressure chamber in an argon atmosphere. The filling was carried out at 350 °C followed by cooling of the ampoules in a pressure chamber. Filling in this way prevents the ingress of oxygen into the lead. Ampoules, filled with lead, were installed in protective steel crucibles and placed into the heating zone of the vacuum chamber. In order to maintain the necessary oxygen concentration in the liquid lead during the exposures a gaseous medium was created with the indicated partial oxygen pressure above the melt mirror. Exposures were performed at 480 °C and 580 °C for 100, 250, 500 and 1000 hours. After corrosion tests samples were heated at 350 °C in air to remove lead, residual lead was etched by lithium in an argon atmosphere.

Oxygen concentration in liquid lead was $C_{O[Pb]} = 5 \cdot 10^{-7}$ %wt. Oxygen concentration was calculated from the partial pressure of oxygen in the gas medium for certain temperatures. Formulae with correction for partial oxygen pressure are:

$$\log C_{max} = 1/2 \log p_{O_2} + 4.67 - 5350/T \quad (327 - 540°C) \quad (1)$$

$$\log C_{max} = 1/2 \log p_{O_2} + 4.57 - 5260/T \quad (540 - 850°C) \quad (2)$$

Subsequently, the influence of the melt on the structure and the nature of corrosion damage, microhardness changes and the elements distribution in the surface layers of both the matrix and the lead melt were evaluated.

3. RESULTS AND DISCUSSION

According to X-Ray Diffraction (XRD) analysis in the initial (as-cast) state all samples were single-phase solid solutions with FCC lattice. Lattice parameters of alloys are: $3.6152\pm3\cdot10^{-4}$ Å (E30-2), $3.6165\pm3\cdot10^{-4}$ Å (E31-2) and $3.6058\pm3\cdot10^{-4}$ Å (E32-2). TEM study shows (Fig.1a-c) that after rolling and final annealing at 850 °C alloys had fine-grained microstructure with an average grain size of 2.5 μm, 7 μm and 3 μm for E30-2, E31-2 and E32-2 alloys, respectively. At the grain boundaries of the matrix phase the σ-phase precipitations several micrometers in size were observed. The volume fraction of these precipitates was highest in E30-2 alloy (fig.1a). In E31-2 and E32-2 alloys there was only a small amount of σ-phase. Also, smaller precipitations (0.1-0.5 μm) were observed in all alloys, which were, probably, chromium and manganese-based oxides [14]; minimum amount of those precipitations was in E32-2 alloy, which had minimal manganese concentration. It should be noted that annealing at 1050 °C for 1h leads to the oxide's dissolution and significant growth of grain size (Fig.1d-f, OM). In this regard, corrosion studies were carried out on samples annealed at 1050 °C.

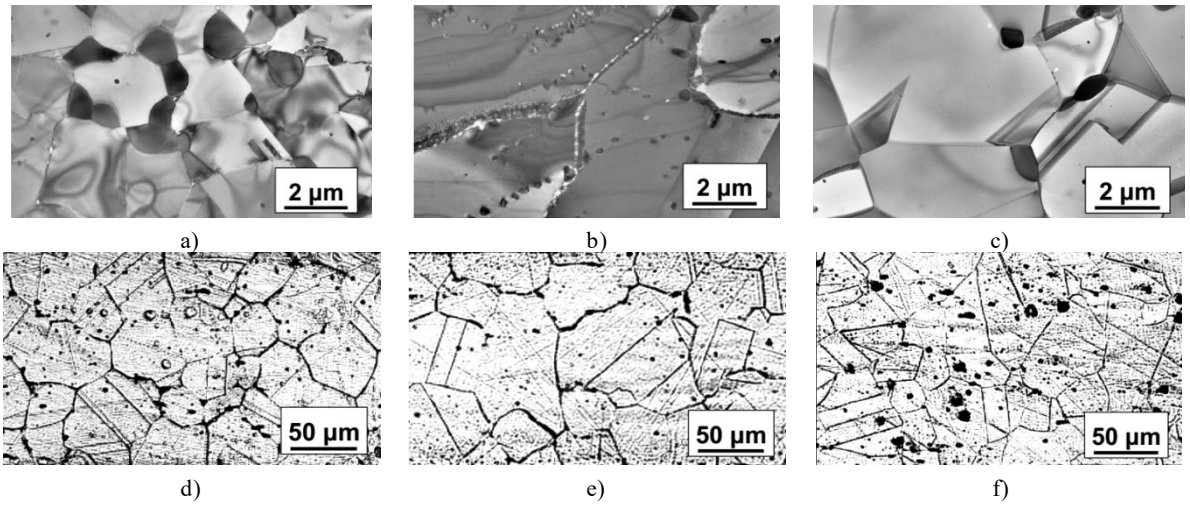

FIG. 1. Microstructure of alloys E30-2 (a, d), E31-2 (b, e) and E32-2 (c, f) after final annealing at 850 °C (a, b, c; TEM images) and 1050 °C(d, e, f; OM images) for 1 h

Microstructure of samples after corrosion tests is shown in Fig. 2. Corrosion damage is observed at the grain boundaries due to the etching and lead penetration into the matrix.

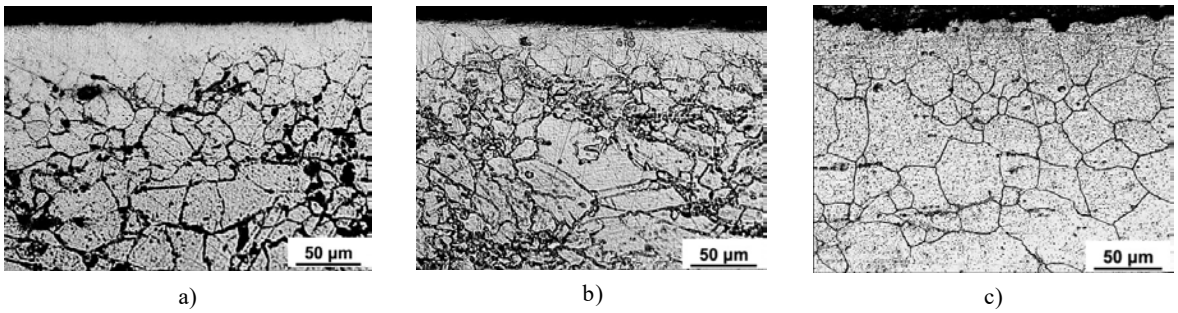

FIG. 2. Structure of the matrix and the surface layer after 1000 h exposure at 480 °C: a) E30-2; b) E31-2; c) E32-2

In the initial state the hardness of the alloys is almost at the same level $H_{0.196} \approx 220 \div 250$, but it should be noted the decrease in hardness in the surface layers of alloys E30-2 and E31-2 to a depth of about 10...20 μm, which can be explained by sublimation of manganese during the final vacuum treatment and performed by electron probe microanalyzers (EPMA). Increasing the exposure time in liquid lead at 480 °C mainly affects the decrease in the hardness of the surface layers to a depth of 10 μm in all alloys. At the same time the matrix hardness (i.e. hardness of the samples at distances more than 10 μm from the surface) tends to increase with exposure time increasing, moreover, the maximum value of hardness is observed at exposure time of 250 h (Fig. 3).

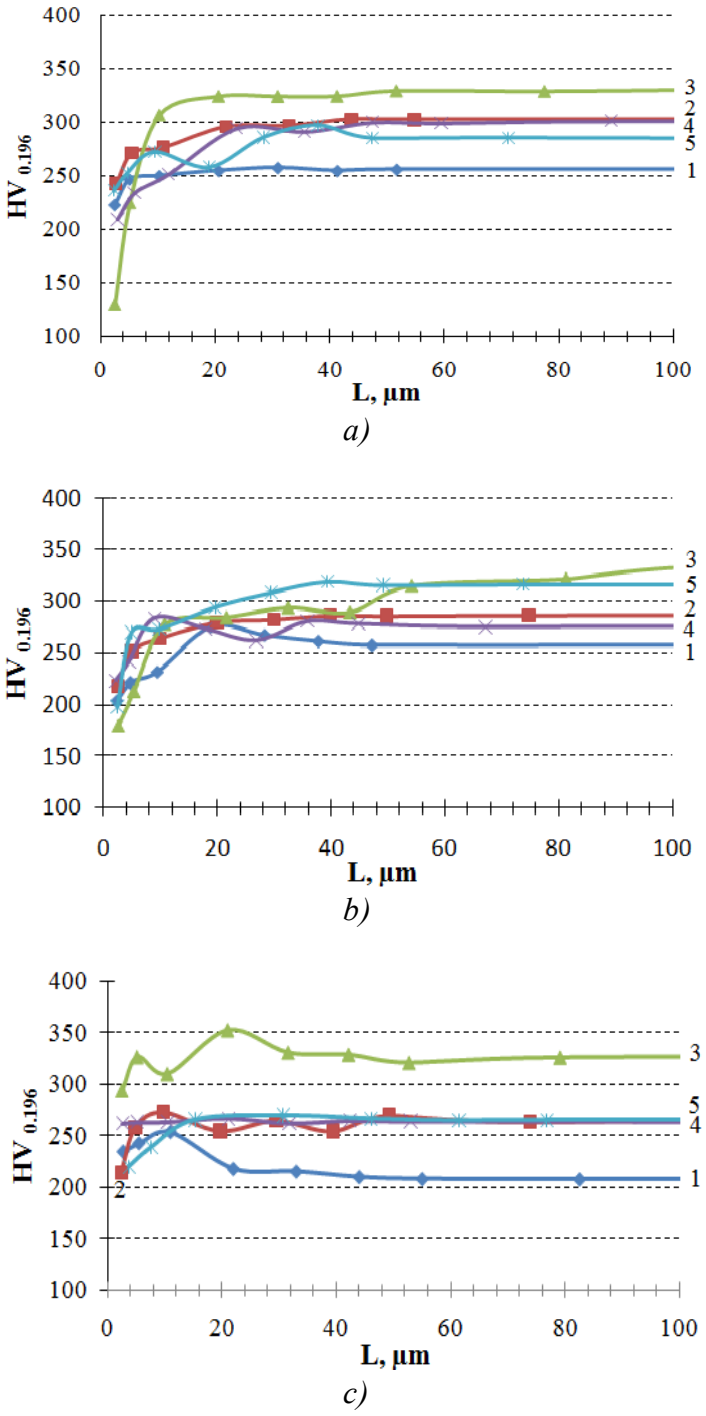

FIG. 3. Changes in hardness of the surface layers and matrix depending on the exposure time at 480 °C: a) E30-2; b) E31-2; c) E32-2; (1- initial, 2 – 100 h, 3 – 250 h, 4 – 500 h, 5 – 1000 h)

Observed changes in the hardness can be associated with the composition changes of matrix near-surface layers (Fig. 4-5).

As follows from the data above with a change of structural-phase state after 1000 h exposure the decrease in the number of dispersed precipitations in the surface layer to a depth of 50…60 μm is observed in all samples. At the same time, there are no significant changes in the structural-phase state of the matrix. But it is known, that for some HEAs compositions of this class the ordering process is carried out after the exposure at 500 °C, which leads to the significant hardness increasing [25]. Another process, which can increase the hardness, is the fine-grained σ-phase particles precipitation [26].

According to the thermodynamic calculations and literature data liquid lead actively dissolves such alloying elements as Cr, Ni and Mn. In this regard, we study changes in the concentration of Cr, Ni, Mn, Fe and Pb in surface layers after 250, 500 and 1000 h exposures. The nature of such changes is illustrated on the example of E30-2 alloy after 500 h exposition at 480 °C (Fig. 4).

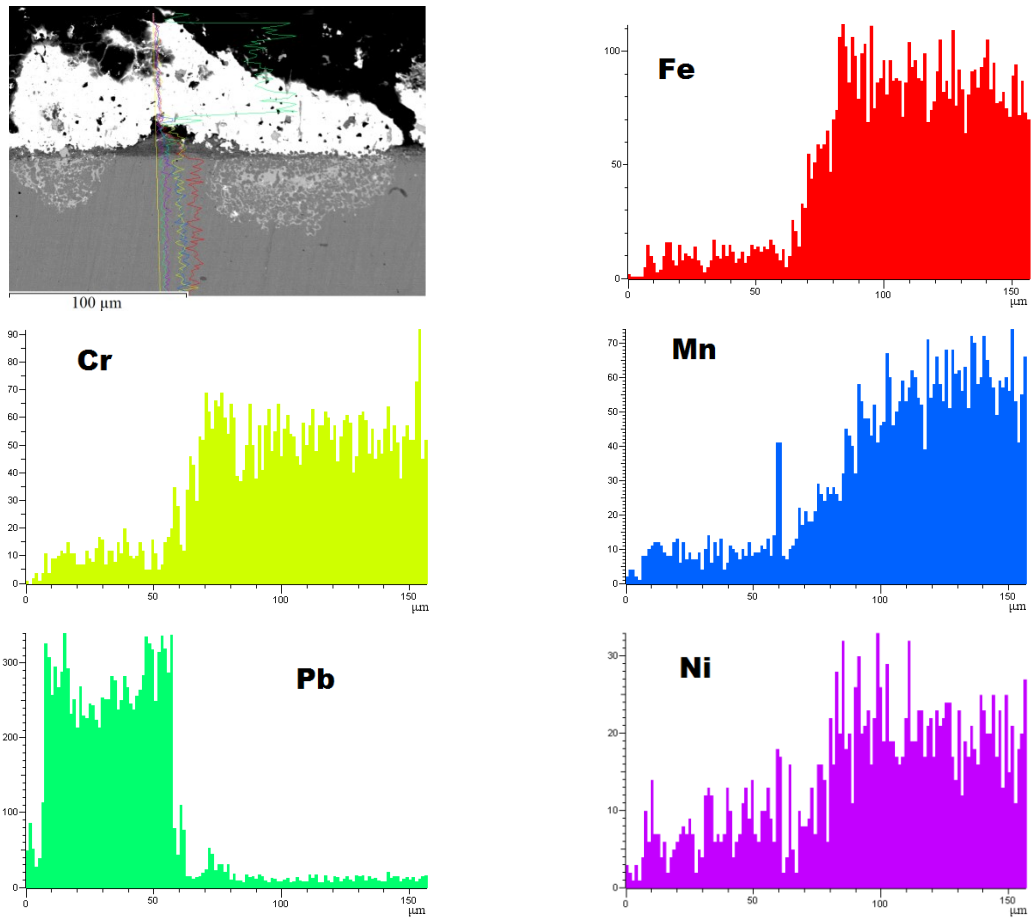

FIG. 4. Element distribution in the surface layer of the E30-2 alloy after 500 h exposition at 480 °C

Analysis of the data confirms the dissolution process of Cr, Ni, Mn and Fe in a liquid lead and their concentration changes in the surface layer of the matrix. A similar data is observed for E32-2 (Fig. 5) and other alloys.

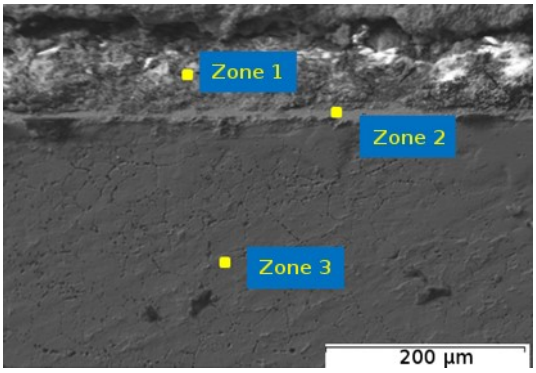

Zone 1

Element	%wt	%at
Cr K	0.98	3.38
Mn K	0.79	2.57
Fe K	3.07	9.85
Ni K	0.86	2.61
Pb M	94.31	81.59
Total	100.00	

Zone 2

Element	%wt	%at
Cr K	30.91	33.78
Mn K	9.78	10.12
Fe K	38.10	38.77
Ni K	16.61	16.07
Pb M	4.60	1.26
Total	100.00	

Zone 3

Element	%wt	%at
Cr K	17.45	18.64
Mn K	19.59	19.81
Fe K	41.28	41.05
Ni K	21.68	20.51
Total	100.00	

FIG. 5. Elements concentration in the surface layer of the lead and matrix after 1000 h exposure at 480 °C for E32-2 alloy

Thus, all studied alloys in contact with a liquid lead at 480 °C are characterized by the dissolution of elements in the melt and reducing their concentration in the matrix surface layer of the alloys. Alloys have different process of elements dissolution and penetration into the lead depending on exposure time (Fig. 4, Fig. 6). The content of dissolved elements depends on the chemical composition of these elements in the alloys. According to the thermodynamic calculations and literature data, the dissolution of the elements decreases in order Ni-Mn-Cr-Fe. But the Mn content in E30-2 alloy is much higher than Ni and Cr, and it is more intensively dissolve at the initial stages. Also, it should be noted that the E32-2 alloy has minimal penetration depth of alloying elements into the lead surface layer (see Fig. 5 Zone 1, Fig. 6).

Increasing the exposure temperature to 580 °C significantly affects the nature of the alloy's interaction with a liquid lead. Figure 7 presents the results of changes in the hardness of alloys after the exposure in the melt for 100, 250, 500, and 1000 h.

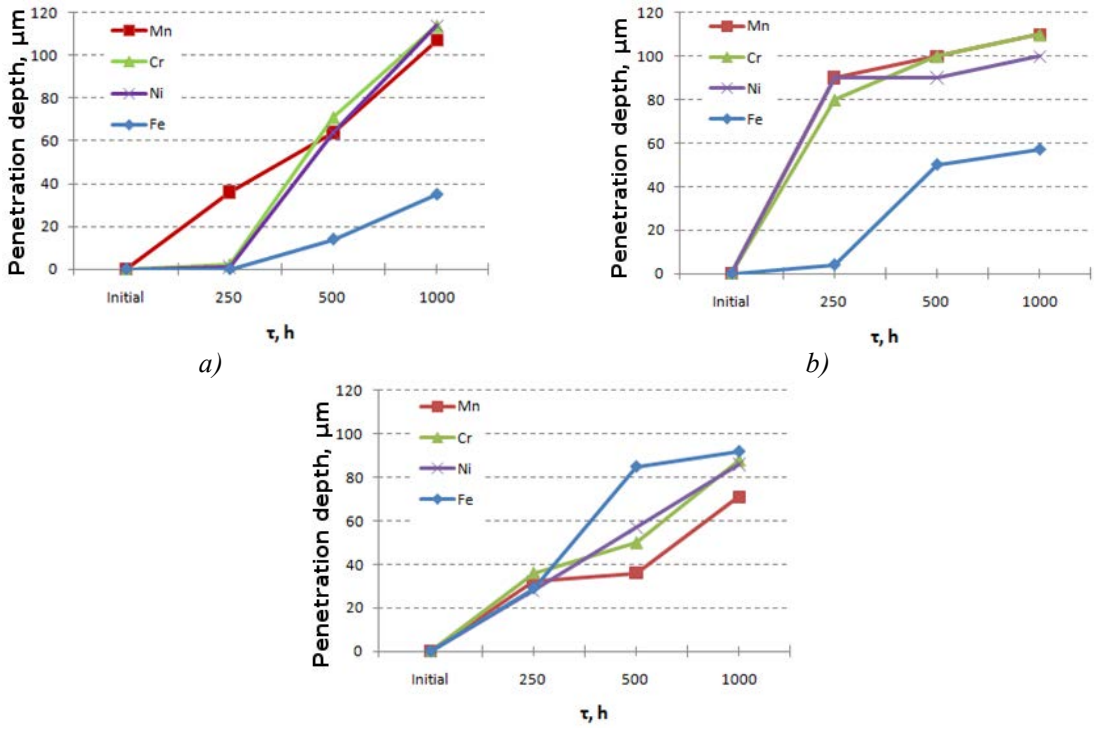

FIG. 6. Penetration depth of alloying elements into the lead surface layer depending on exposure time: a) E30-2; b) E31-2; c) E32-2

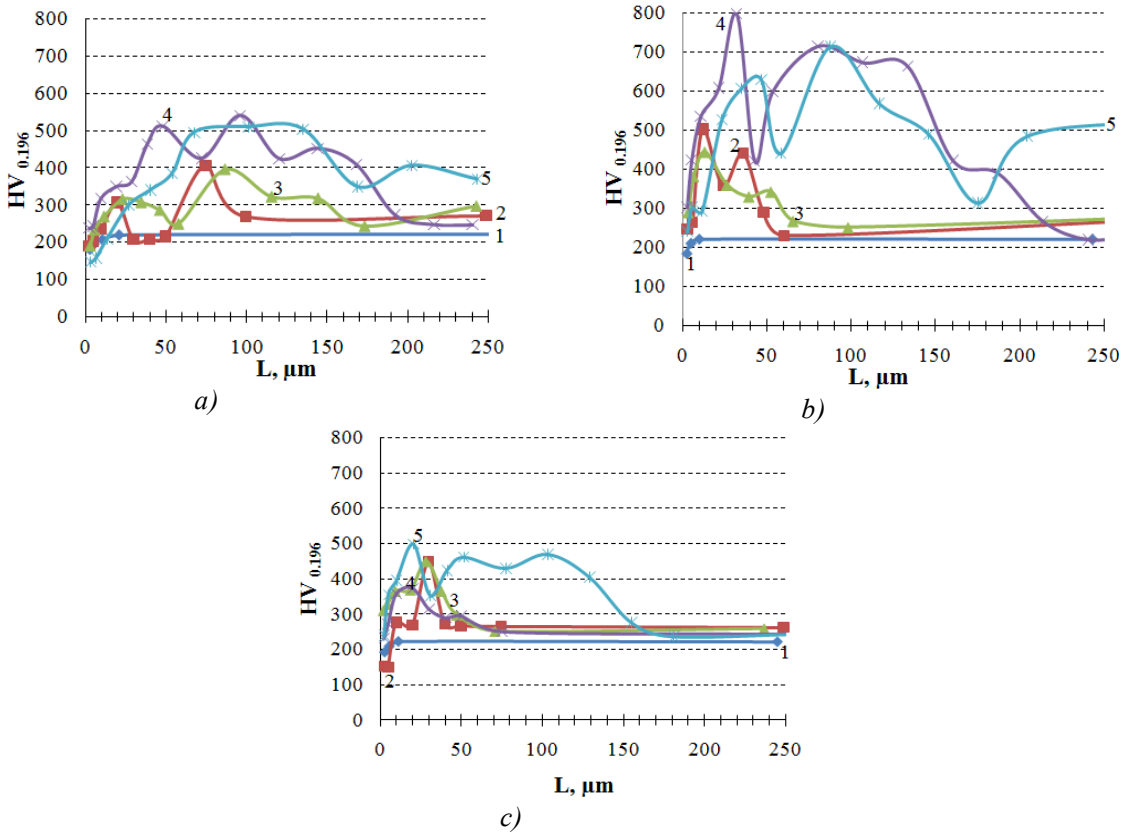

FIG. 7. The nature of changes in the microhardness of the matrix surface layers after exposures at 580 °C: a) E30-2; b) E31-2; c) E32-2 (1 – initial, 2 – 100 h, 3 – 250 h, 4 – 500 h, 5 – 1000 h)

From the analysis of the obtained results, it follows that for all alloys such regularities are observed. There is a zone with reduced hardness in the surface layer up to a depth of 20 μm. With the increasing of exposure time up to 500 h an increase in the hardness to a depth of up to 150 μm was observed for E30-2 and E31-2 alloys, and for E32-2 alloys – up to depth of 50 μm. Moreover, it should be noted that a characteristic feature for all alloys is a nonmonotonic change in the microhardness, which suggests the heterogeneity of the structural-phase composition of the surface layers. Increasing the exposure time up to 1000 h leads to an increase in the matrix hardness all over the entire samples cross-section for E30-2 and E31-2 alloys. For E32-2 alloy the increase in the hardness is observed at a much smaller depth (up to 150 μm). Maximum hardness values in the surface layer are observed in E31-2 alloy.

Analysis of the surface layers structure indicates significant changes depending on the exposure time. The nature of such changes and the concentration of elements in different zones are illustrated on the example of the E30-2 alloy (Fig. 8).

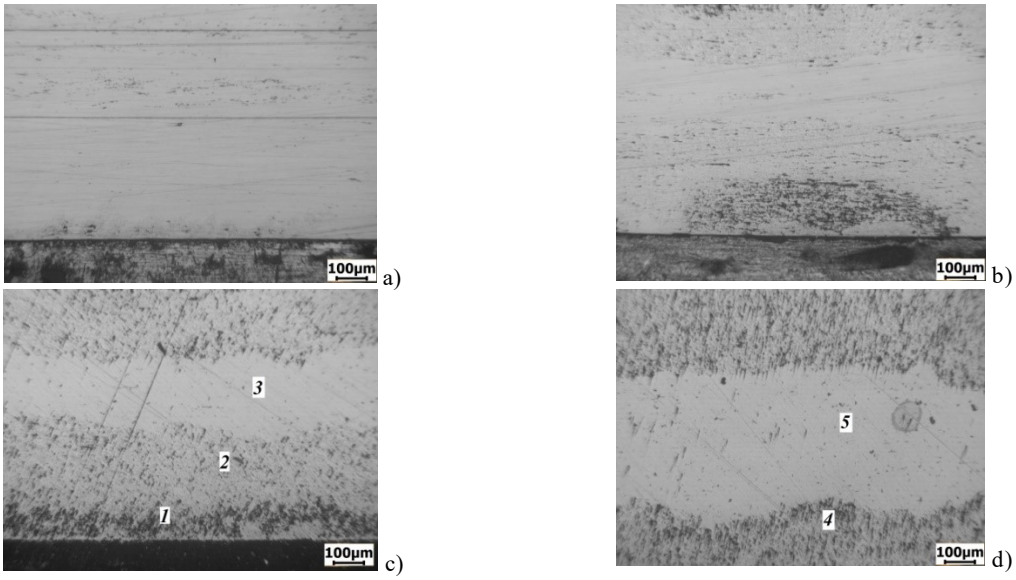

Zone 1

Element	%wt	%at
O K	2.28	7.74
Cr K	12.44	13.01
Mn K	7.19	7.11
Fe K	66.10	64.35
Ni K	6.99	6.47
Pb M	5.00	1.31
Total	100.00	

Zone 2

Element	%wt	%at
O K	1.62	5.84
Cr K	10.23	11.34
Mn K	14.93	15.67
Fe K	48.61	50.19
Ni K	14.37	14.11
Pb M	10.24	2.85
Total	100.00	

Zone 3

Element	%wt	%at
Cr K	19.83	21.03
Mn K	25.73	25.82
Fe K	41.97	41.44
Ni K	12.48	11.72
Total	100.00	

Zone 4

Element	%wt	%at
O K	0.47	1.61
Cr K	10.83	11.53
Mn K	21.61	21.78
Fe K	44.14	43.76
Ni K	22.49	21.21
Pb M	0.46	0.12
Total	100.00	

Zone 5

Element	%wt	%at
Cr K	17.92	19.04
Mn K	26.15	26.30
Fe K	42.03	41.58
Ni K	13.90	13.08
Total	100.00	

Fig. 8. Structure of the surface layer of non-etched samples of E30-2 alloy at exposure time of: a) 100 h; b) 250 h; c) 500 h; d) 1000 h

It is necessary to note the presence of two distinct zones. There is a light zone with reduced hardness on the surface of all alloys (Fig. 7-8). In the surface layer of the E30-2 and E31-2 alloys there are precipitations zones, which at small exposure time (100 and 250 hours) have island character (Fig. 8b). Increasing the exposure up to 500 and 1000 hours leads to the formation of a solid front of these precipitations in the E30-2 alloy (Fig. 8c, d). At the exposure time of 1000 h such zone extends over the entire cross section of the sample in the E31-2 alloy. With the least intensity this process occurs for E32-2 alloy, in which the first island precipitates are observed only after 500 h exposure.

It was assumed that increasing the temperature from 480 °C to 580 °C contributes, besides the acceleration of the dissolution process of the matrix elements in a lead, to the additional oxygen diffusion from the liquid lead into the matrix and, as a consequence, to the formation of the internal oxidation zone. To test this hypothesis an X-ray microspectral analysis of the changes in the elements concentration in different zones of the surface layers was carried out. The results of the X-ray microspectral analysis for E30-2 alloy are presented in Fig. 8. It is established that in zone 1, where the segregation process of precipitates begins, a change in the ratio of the matrix components is observed, namely a decrease in the concentration of Ni, Mn and Cr and a significant increase in the concentration of Fe. A similar dependence is observed in zone 2 for Fe, Mn, Cr, but the Ni concentration corresponds to the initial state. The alloy composition in zone 3 corresponds to the initial state, as well as in zone 5.

However, the main thing is the presence of significant oxygen concentration in two-phase zones 1, 2, 4.

Thus, based on the analysis of the presented results, it can be argued that two processes are implemented at 580 °C, which take place simultaneously.

The first one, like at a temperature of 480 °C, is a dissolution of the matrix elements in the surface layer of the lead, dissociation and dissolution of chromium and manganese oxides, presented in matrix, and, as a consequence, decreasing in the hardness in this surface zone. The second process, activated simultaneously, is the oxygen counter-diffusion from the liquid lead into the alloy matrix, which causes intragranular oxidation (Fig. 9).

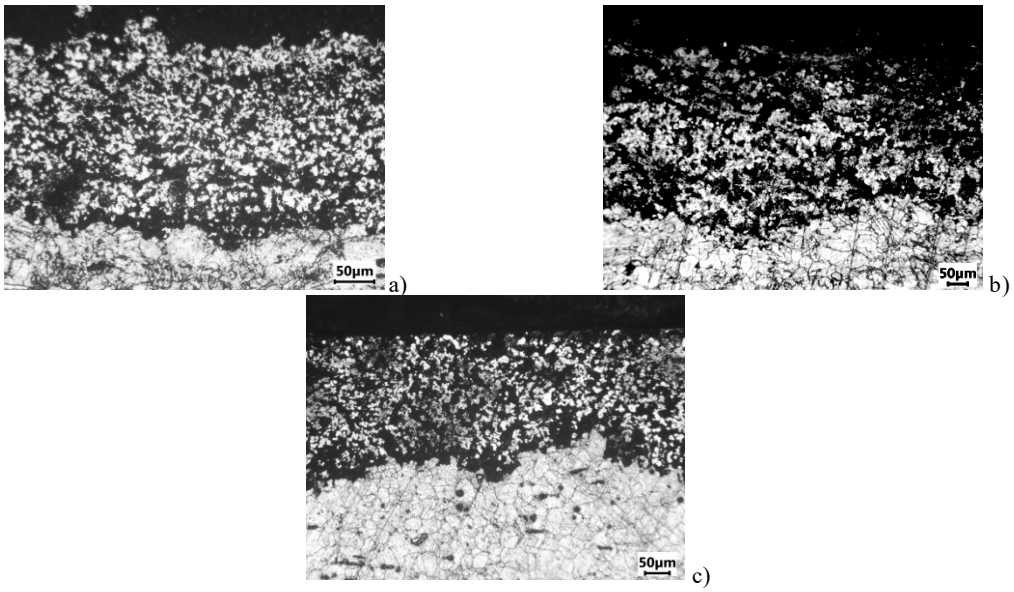

FIG. 9. Structure of the surface layer of alloys after exposure at 580 °C: a) E30-2, 500 h; b) E31-2, 500 h; c) E32-2, 1000 h

This process takes place at some distance from the surface and extends into the depth of the matrix with the increasing of exposure time. It can be assumed that the cause of this process, which starts at a certain distance from the surface, is a decrease in the concentration of Mn and Cr due to their dissolution in lead. From the X-ray microspectral analysis data it can be assumed that the process of internal oxidation consists in the formation of Mn and Cr oxides.

4. CONCLUSIONS

Based on the research results of the Cr-Fe-Mn-Ni high-entropy alloys after exposure into the liquid lead at temperatures of 480 °C and 580 °C up to 1000 h the following conclusions can be drawn. It was established that for all studied alloys compositions at 480 °C the main mechanism of corrosion damage of the surface layers is intergranular corrosion, which consists in the etching of grain boundaries, lead penetration into the matrix and dissolution of chromium, nickel and manganese in liquid lead. Increasing the temperature to 580 °C contributes to the implementation of the combined mechanism of corrosion damage, which is realized by the combination of intergranular corrosion, as well as at a temperature of 480 °C, and the diffusion of oxygen from the melt into the matrix and, as the result, implementation of the internal oxidation of chromium and manganese process. Using these alloys in contact with the lead melts can be recommended to a temperature of 500 °C, moreover, E32-2 alloy (composition 20Cr-40Fe-20Mn-20Ni %at) has an advantage among the investigated alloys. Possible options for increasing the operating temperature are optimization of the HEAs composition and additional alloying.

REFERENCES

[1] HOELZER, D., PINT B., WRIGHT I., A microstructural study of the oxide scale formation on ODS Fe-13Cr steel, J. Nucl. Mater. 283-287 (2000) 1306–1310.

[2] UKAI, S., MIZUTA, S., FUJIWARA, M., OKUDA, T., KOBAYASHI, T., Consolidation Process Study of 9Cr-ODS Martensitic Steel Tubes, J. Nucl. Mater. 307–311 (2002b) 758–76.

[3] UKAI, S., FUJIWARA, M., Perspective of ODS alloys application in nuclear environments, J. Nucl. Mater. 307-311 (2002) 749-757.

[4] TAE KYU KIM, CHANG SOO BAE, DO HYANG KIM, JINSUNG JANG, SUNG HO KIM, CHAN BOCK LEE and DOHEE HAHN, Microstructural observation and tensile isotropy of an austenitic ODS steel, Nuclear Engineering and Technology 40 №4 (2008) 305-310.

[5] VELIKODNYI A., VOYEVODIN V., TIKHONOVSKY M., BRYK V., KALCHENKO A., STAROSTENKO S., KOLODIY I., OKOVIT V., BOVDA A., ONISCHENKO L., STOROGILOV G., Structure and properties of austenitic ODS steel 08Cr18Ni10Ti, Problems of Atomic Science and Technologies (PAST). Series “Physics of radiation defects and radiation materials science” 92 №4 (2014) 94-102.

[6] LIU T., WANG L., WANG C., ZHANG H., Feasibility of using Y2Ti2O7 nanoparticles to fabricate high strength oxide dispersion strengthened Fe-Cr-Al steels, Materials & Design 88 (2015) 862-870.

[7] ZHANG Y., “Irradiation Behavior in Entropic Materials”, High-Entropy Materials, Springer, Singapore (2019).

[8] XIA, S., YANG, X., YANG, T., LIU, S., ZHANG, Y., Irradiation Resistance in AlxCoCrFeNi High Entropy Alloys, JOM 67 10 (2015) 2340–2344.

[9] YANG, T., XIA, S., GUO, W., et al., Effects of temperature on the irradiation responses of Al0.1CoCrFeNi high entropy alloy, Scripta Materialia 144 (2018) 31–35.

[10] TOLSTOLUTSKAYA, G., ROSTOVA, G., VOYEVODIN, V., VELIKODNYI, A., TIKHONOVSKY, M., TOLMACHOVA, G., KALCHENKO, A., VASILENKO, R., KOPANETS, I., Hardening of Cr-Fe-Ni-Mn high entropy alloys caused by the irradiation with argon ions, Problems of Atomic Science and Technologies (PAST). Series “Physics of radiation defects and radiation materials science” 111 №5 (2017) 40-47.

[11] YEH, J-W., CHEN, S-K., GAN, J-W., LIN, S-J., CHIN, T-S., SHUN, T-T., TSAU, C-H., CHANG, S-Y., Formation of simple crystal structures in Cu-Co-Ni-Cr-Al-Fe-Ti-V alloys with multiprincipal metallic elements, Metall. Mater. Trans. A 35 (2004) 2533.

[12] CANTOR, B., CHANG, I., KNIGHT, P., VINCENT, A., Microstructural development in equiatomic multicomponent alloys, Materials science and engineering A 375-377 (2004) 213-218.
[13] MIRACLE, D., SENKOV, O., A critical review of high entropy alloys and related concepts, Acta Mater. 122 (2017) 448.
[14] SALISHCHEV, G., TIKHONOVSKY, M., SHAISULTANOV, D., STEPANOV, N., KUZNETSOV, A., KOLODIY, I., TORTIKA, A., SENKOV, O., Effect of Mn and V on structure and mechanical properties of high-entropy alloys based on FeCrCoNi system, Journal of Alloys and Compounds 591 (2014) 11-21.
[15] STEPANOV, N., TIKHONOVSKY, M., YURCHENKO, N., ZYABKIN, D., KLIMOVA, M., ZHEREBTSOV, S., SALISHCHEV, G., EFIMOV, A., Effect of cryo-deformation on structure and properties of CoCrFeNiMn high-entropy alloy, Intermetallics 59 #4 (2015) 8-17.
[16] LI, Z., ZHAO, S., RITCHIE, R., MEYERS, M., Mechanical properties of high-entropy alloys with emphasis on face-centered cubic alloys, Progress in Materials Science 102 (2019) 296-345.
[17] MANZONIA, A., GLATZEL, U., New multiphase compositionally complex alloys driven by the high entropy alloy approach, Materials Characterization 147 (2019) 512-532.
[18] MINASHIN, V., et al., Thermophysics of liquid metal cooled nuclear reactors and electro-modeling methods, M.: Atomisdat (1971).
[19] Comparative assessment of thermophysical and thermohydraulic characteristics of lead, lead-bismuth and sodium coolants for fast reactors, IAEA-PUBLICATION-1289, IAEA, Vienna (2002).
[20] PARK, J., BUTT, D., BEARD, C., Review of liquid metal corrosion issues for potential containment materials for liquid lead and lead-bismuth eutectic spallation targets as a neutron source, Nuclear Engineering and Design 196 № 3 (2000) 315-325.
[21] KNEBEL J., CHENG X., MULLER G., et al., “Thermalhydraulic and corrosion challenges for the target module of an accelerator-driven system (ADS)”, Third International Topical Meeting on Nuclear Application of Accelerator Technology (AccApp ‘99, Long Beach CA, 1999).
[22] BESKOROVAINIY, N., IOLTUHOVSKY, A., Structural materials and liquid metal coolants, M.: Energoatomisdat (1983).
[23] GRJAZNOV, G., EVTIHIN, V., ZAVJALSKY, L., et al., Materials Science of Liquid-Metal Systems of Thermonuclear Reactors, M.: Energoatomisdat (1989).
[24] MULLER, G., HEINZEL, A., KONYS, J., et al., Results of steel corrosion tests in Flowing liquid Pb/Bi at 420-600 ºC after 2000 h, J. Nucl. Mater. 301 (2002) 40-46.
[25] GU, J., SONG, M., Annealing-induced abnormal hardening in cold rolled CrMnFeCoNi high entropy alloy, Scripta Materialia, 162 (2019) 343-369.
[26] GU, J., SONG, N., LIU, Y., SONG, M., Regulating the strength and ductility of a cold rolled FeCrCoMnNi high entropy alloy via annealing treatment, Materials Science and Engineering: A 755 (2019) 289-294.

DESIGN AND MATERIAL SELECTION FOR LEAK-BEFORE BREAK NATURE OF DOUBLE WALLED ONCE THROUGH STEAM GENERATORS IN LEAD-BISMUTH COOLED FAST REACTORS

Jung Hwan Lee
Presenting Author
Ulsan National Institute of Science and Technology (UNIST), Republic of Korea
Email: leejh96@unist.ac.kr

Jeonghyeon Lee
Author
Ulsan National Institute of Science and Technology (UNIST), Republic of Korea
Email: leejh@unist.ac.kr

Il Soon Hwang
Author
Ulsan National Institute of Science and Technology (UNIST), Republic of Korea
Email: hisline@unist.ac.kr

Ji Hyun Kim
Corresponding author
Ulsan National Institute of Science and Technology (UNIST), Republic of Korea
Email: kimjh@unist.ac.kr

Abstract

Among various types of Gen-IV reactors, lead cooled fast reactors (LFRs) can support a closed fuel cycle to minimize waste burden by managing both fertile elements and transuranic actinides efficiently. LFRs often adapt an External Boiling Bayonet Steam Generator (EBSSG) system instead of conventional once-through high-pressure steam generator. LFR with the EBSSG designs have advantages in terms of thermal efficiency and maintainability during operation. While EBSSG designs have been proven through extensive operating experiences in submarine reactors of the Former Soviet Union, their complex tube geometries invite life-limiting disadvantages ranging from vibration-led fatigue, oxide particles sedimentation and increased resistance to natural circulation under accident conditions. To assure reliable performance of steam generator over long design lives, both structural design and material degradation issues should be solved.

In the paper, we present an innovative LFR steam generator design concepts for a non-refueling and hermetically sealed 40-year life micro-modular LFR designated as Micro-Uranus. The requirements on durability, maintainability and accident-tolerance can be met with the new double-walled once-through steam generators (DWOTSG) design. In order to assure Leak-Before-Break (LBB) of steam generator in Micro-Uranus, the inter-tubular gap of double walled heat transfer tubes is filled with engineered materials for both leak detection and conductivity enhancement. Tube materials are also selected to assure adequate resistance to corrosion and liquid metal embrittlement on heavy-liquid metal side by selecting proven austenitic stainless steels and lowering operating temperatures. Additional corrosion resistance over 40 year-life can be delivered by Functionally Graded Composite (FGC) tubes with substrate made of internationally certified materials. Oxide deposition and thermal degradation can be controlled by advanced flow channel structure and maintenance designs. The LBB characteristics, corrosion resistance, thermal-hydraulic performance of the innovative DWOTSG design have been analyzed by using linear elastic fracture mechanics models. Leak detection sensitivities required in LBB qualifications for preventing excessive defect growth to unstable rupture conditions has been computed conservatively.

1. INTRODUCTION

The Gen-IV fast reactors are expected to reduce the burden of spent fuel disposal and to expand uranium resources by more than 100 times. Economic viability and safety of Gen-IV reactors can be enhanced by taking advantages of small modular designs. A small modular reactor (SMR) can be suitable where a large-scale commercial reactor is unfavorable from economy and/or safety aspects. The economy can be improved through simplified modular designs that can be fabricated in factories, transported and constructed in expedited manners. The safety improvement of SMR's can be derived from its natural cooling capabilities and can be measured by the reduction in emergence planning zone sizes. Among various types of liquid metal cooled fast reactor, lead cooled fast reactor (LFR) has particularly salient safety features with heavy liquid metal coolant with high boiling point and good natural circulation characteristics.[1-6 = ENHS, URANUS, PEACE, ALFRED, BREST, SSTAR] Due to the low Prandtl number, the heat transfer by conduction become dominant compared with convective heat transfer effects. Since both pure lead and lead-bismuth eutectic coolant have very high neutron transparency, they are suitable as coolants for fast reactors.

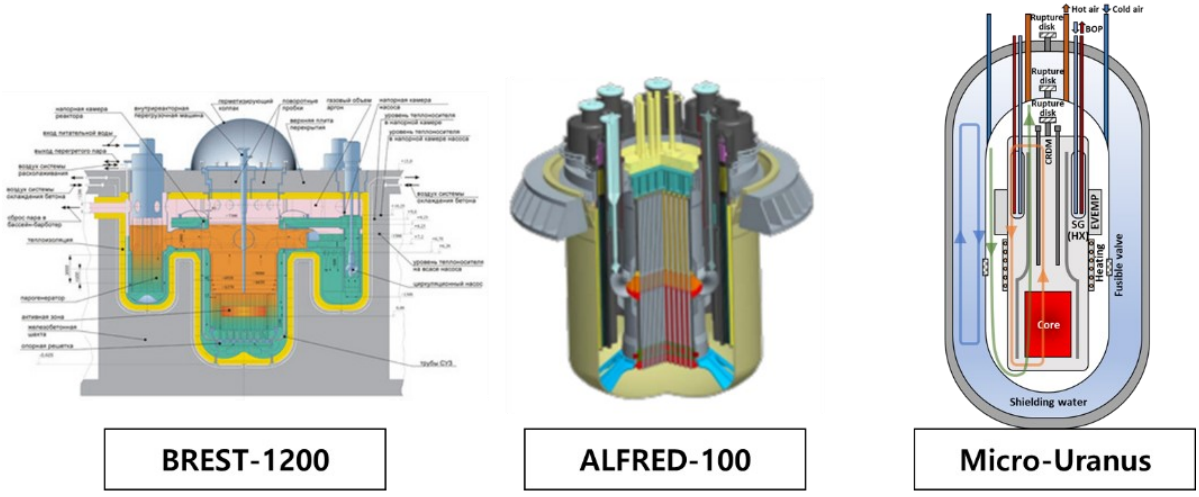

FIG.1. Schematic diagram of large, small and micro modular designs of Gen-IV lead fast reactors [2,4,5]

Under long-term nuclear phase-out scenarios, the government of Republic of Korea is redirecting nuclear power R&D activities from traditional focus on large-scale advanced light water reactors to SMRs and micro modular reactors (MMRs) for deployments at locations away from population centers. [7] The new focus includes applications of SMR's and MMR's to commercial marine propulsions such as icebreakers and floating nuclear power plants. This paper presents a steam generator (SG) design for a lead-bismuth cooled Gen-IV MMR for marine applications. [7]

Micro-Uranus design utilizes lead-bismuth eutectic (LBE) as cooling fluid for its fast neutron transparency, good thermal-hydraulic characteristics, chemical inertness, high boiling point and low-melting point. Potential release of radiotoxic Polonium-210 from LBE coolant, however, present enormous challenge in operation, inspection and maintenance operations. For Micro-Uranus that does not require refueling, the Po-210 risk can be sufficiently alleviated by assuring the Leak-Before Break (LBB) nature of high-pressure tube in steam generators. To this end, Double-Wall Once-Through Steam Generator (DWOTSG) designs have been developed for Micro-Uranus. Leak detection sensitivities of an On-line Monitoring system required in LBB qualifications for preventing excessive defect growth to unstable rupture conditions has been computed conservatively by linear elastic fracture mechanics (LEFM).

Traditional marine reactors of pressurized water reactor (PWR) type using low enriched uranium (LEU) requires extended refueling outage at an interval of every ten years or less. However, LFR design with breed-and-burn core can facilitate nuclear fuel lasting entire operation period of icebreaker at enormous economic and regulatory advantages. To assure that a non-refueling design is feasible for the 40-year design life of an icebreaker, a breed-and-burn type fast reactor core design has been made by using Monte Carlo computer model. However, such a through-life system design mandates a set of robust materials. Materials for fuel cladding, steam generator tubes and reactor structures should be judiciously chosen, and damage-tolerant design should be developed and demonstrated for licensing. In this paper, we focus our study on conceptual designs of durable steam generator tubes and lead-bismuth side materials selection for the non-refueling micro modular LFR, Micro-Uranus.

2. STEAM GENERATOR DESIGN AND MATERIALS SELECTION

2.1. **Double-walled Once-through Steam Generator Design**

Several steam generator units for heavy liquid metal reactors have been built which employed a double-wall tube. For sodium-cooled reactor, it is a double-wall tube as a barrier between the sodium and water. There is the most important application to separate reactive metals from water/steam for submarine reactor steam generators. Such a double tube naturally creates an empty space that can compromise LBE to steam heat transfer. The gap is filled with conductive packing materials. [18]

Once-through steam generator design allows easier installation of the double-wall tubes. Design schematic of DWOTSG for Micro-Uranus is shown in Figure 2. LBE hot-leg flow emerges into DWOTSG from the reactor upper plenum. LBE flows downward on tube-side while water and steam flow upward on shell-side. The design is expected to better facilitate on-line monitoring, inspection and maintenance of DWOTSG compared with other designs.

By taking advantage of the double wall tube geometry, on-line leak sensors can be introduced to qualify LBB design. Various options are under the considerations including sensors measuring temperature, pressure, humidity, electromagnetic properties and radioactivity. Adaptation of leak sensors for installation in tight annulus requires innovative designs. In addition, sensor lead wires pathway should be designed.

As R&D is still in progress to employ Leak Before Break approach for DWOTSG, results will be presented in the future. [7,8]

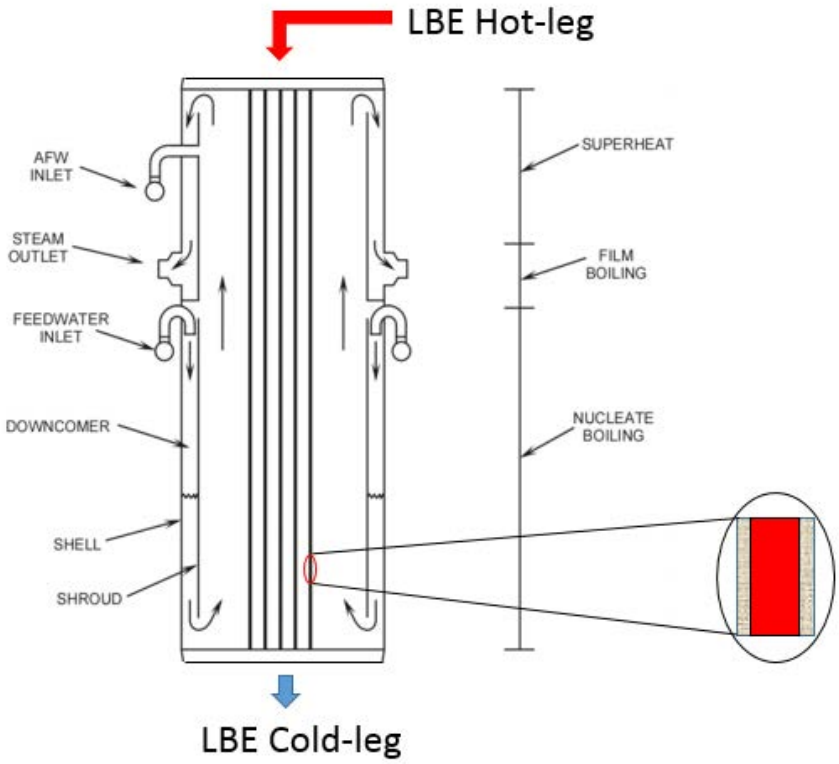

FIG. 2. Double-walled once-through steam generator design [8]

2.2. **Lead-bismuth side Materials Selection for Double Wall Tubes**

Heavy liquid metal such as lead and lead-bismuth eutectic is robust and economical coolant material for fast reactor, as demonstrated by about 80 reactor-year of submarine operation during former soviet union (FSU). However, at temperature above 400 °C corrosion issues have persisted to cause fuel failures and penetration of primary coolant boundaries.

Ferritic steels have been preferred to austenitic steels at high temperature considering high solubility of Ni in lead and lead-bismuth. SG Lee has shown that austenitic stainless steels can have higher corrosion resistance at temperature below 400 °C. [9] In addition, ferritic stainless steels can be susceptible to liquid metal embrittlement while austenitic stainless steels are immune to the degradation mode. Therefore, it is decided to select Type 316L austenitic stainless steel for lead-bismuth side materials. [11]

2.3. **Advanced Corrosion Control**

2.3.1. *Operation Temperature Reduction*

Fig. 3 shows time to grow 25 μm thick oxide layer on Type 316 stainless steel in LBE with information on standard deviation. [9] By static corrosion testing, he observed the oxide growth become unstable beyond the thickness. Although the data base has limited test temperature range, an estimation has been made on allowable operating temperature range for the design life with the oxide thickness limit. Micro-Uranus has a design life of 40 calendar years with 75% capacity factor, making the life 30 effective full power years (EFPY). Considering data uncertainty, a six sigma lower bound has been estimated to be 350 °C as the maximum operating temperature of steam generator tubes on LBE side.

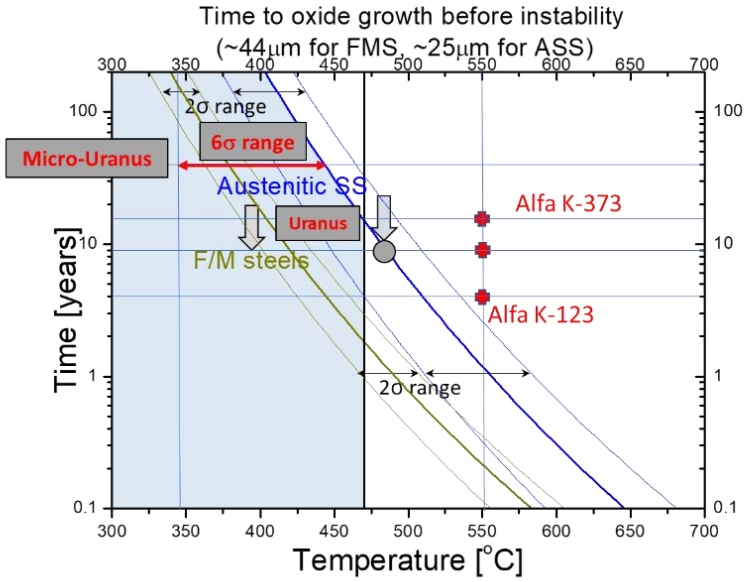

FIG. 3. Temperature of 6σ range for time to oxide growth before instability [9]

2.3.2. *Oxygen Control*

To operate DWOTSG during the operational period, about 40 years, without allowing unstable corrosion, dissolved oxygen level in the liquid metal coolant should be controlled. There are three levels of dissolved oxygen; very low, low, and high for typical austenitic stainless steel. [13,14] At very low concentrations of oxygen, protective oxide layers fail to establish on metal substrate and soluble alloying such as Ni can be leached continually with time. As shown in Fig 4., there is a threshold in dissolved oxygen concentration in the bulk LBE at which the corrosion phenomenon exhibits a peak dissolution rate. At the low level of dissolved oxygen concentration, the dissolution rate undergoes a transition section from continuous leaching to passivity-based retardation of corrosion. Furthermore, the oxygen concentration high level, stable passivation behavior is attained. Further increase in dissolved oxygen is not needed or desired considering that the increase in oxide particle releases can accelerate sedimentation and flow restrictions.

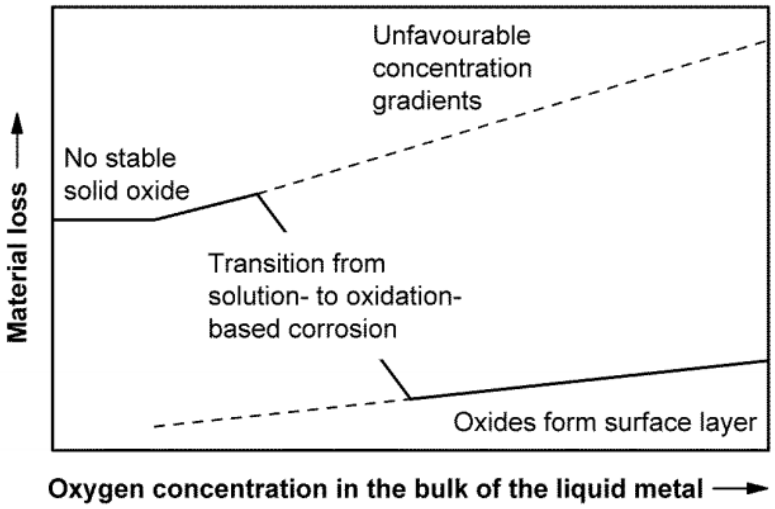

FIG. 4. Oxygen concentration in the bulk of the liquid metal with material loss [13,14]

2.4. **Alumina Forming Austenitic Steel Development**

Although Type 316L stainless steel tubes can be used for LBE side with the operating temperature and oxygen limits, it is desirable to have alternative options by developing advanced materials. Considering the liquid metal embrittlement issue, austenitic stainless steels are assumed within the near-term development scope. Alumina-forming stainless steels are shown to possess excellent corrosion resistance in LBE. V. Tsisar et al. developed alumina-form austenite stainless steel for high corrosion resistance. Therefore, the class of materials has been studied to seek further corrosion control for SG tubes on LBE side. [10,13,14]

Definition of alumina forming austenitic steel is that aluminium is added 2 wt.% or more to the existing austenitic alloy to form an Al_2O_3 oxide film having higher oxidation stability than the Cr_2O_3. Also, the aluminium contributes to the formation of a protective oxide layer that impedes the solution of the material in the heavy liquid metal. Oxygen addition to the liquid metal required in order to prevent critical oxygen depletion at the oxide/liquid metal interface.

Table 1 shows the chemical composition of specimen used in the study. An ingot of specimen based AFAS by vacuum induction melting. The measured chemical composition is given in Table 1. And then, these specimens have forged at 1230 °C. and then hot rolled from 37 to 13 mm in thickness with final rolling temperature of around 1000 °C. The specimens were solution treated at 1200 °C for 30 min followed by water quenching.

TABLE 1. CHEMICAL COMPOSITION ALUMINA FORMING AUSTENITIC STEEL (AFAS) USED IN THE STUDY [13,14]

	Fe	Cr	Ni	Mo	Mn	Si	Al	Nb	C
AFAS#1	Bal.	11.7	18.0	1.99	0.0887	0.401	2.32	0.577	0.0086
AFAS#3	Bal.	11.7	18.0	2.00	0.118	0.377	2.90	<0.01	0.0300

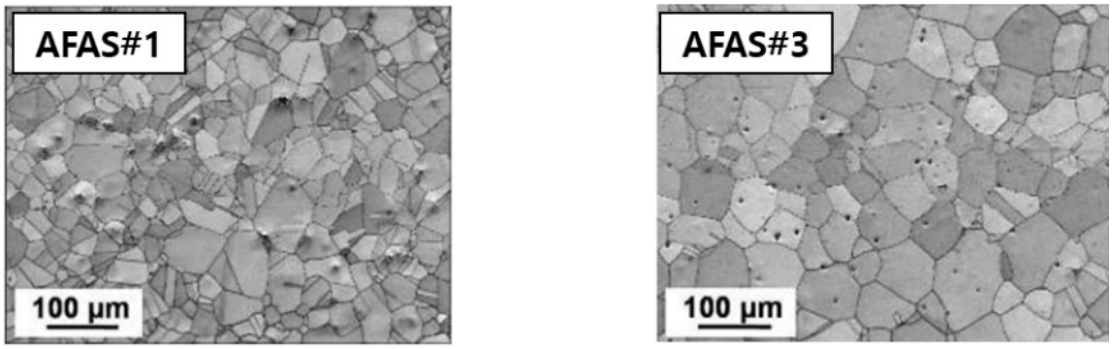

FIG. 5. Scanning electron micrographs of AFAS#1 and AFAS#3 [13,14]

As shown in Fig. 5, SEM photomicrographs after polishing are compared for AFAS#1 and AFAS#3. #1 material has smaller grain size with average diameter of 150 µm while it was 200 µm for AFAS#3. When examined at a higher magnification as shown in Figure 6., many intergranular and intragranular precipitates are observed in AFAS#1. The laves phases distributed along grain boundaries and grain interior. These precipitates indicated by yellow circles in Figure 6. (c). And based on the selected arera electron diffraction (SAED) result, it was characterized to be $(Fe,Cr)_2(Nb,Mo)$ laves phases. [21]

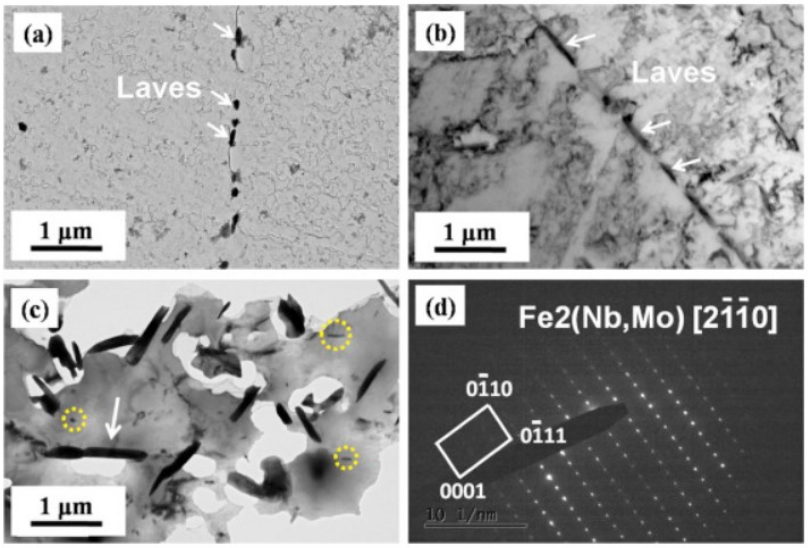

FIG. 6. TEM images of AFAS#1 (a) after aging for 10h; (b) 100h; (c) 1000h; (d) SAEF pattern corresponding to precipitate indicated by arrow in (c) [21]

Several characteristics such as oxidation behavior at high temperature. Carbide tends to coarse and dissolve at high temperature. In particular, intermetallic phases such as laves (Fe_2Nb) have been used to maintain the strength of austenitic steels at high temperatures. [22,23] During the heat treatment at 700 °C, coarse precipitates (~100-1000 μm) were formed at intergranular and intragranular sites and those were revealed as $(Fe, Cr)_2(Nb, Mo)$ laves phases and NiAl. Also, small precipitates (~10-100 nm) were exist inside the grain and those were NbC. These materials were then corrosion tested in the static liquid metal cell with controlled oxygen content. Tests were conducted in 550 °C Pb-Bi for 1000 h. oxygen concentration were varied to understand the effect of dissolved oxygen in Pb-Bi to compatibility of modified stainless steels. By varying the dissolved oxygen concentration, Gibbs free energy was changed and expected corrosion behavior is also changed for each dissolved oxygen concentration. Detailed Ellingham diagram is presented in Fig. 7. By decreasing the oxygen concentrations following compounds could be formed: PbO, NiO, $NiCr_2O_4$, $NiAl_2O_4$, Fe_3O_4, $FeAl_2O_4$, $FeCr_2O_4$, Cr_2O_3, Al_2O_3. Also, dissolution attacks could be occurred in low oxygen environment. As shown in Table 2., test was conducted in the various dissolved oxygen environment such as from 10^{-12} wt.% to 10^{-6} wt.% of dissolved oxygen concentration.

TABLE 2. ENVIRONMENT OF DISSOLVED OXYGEN CONCENTRATION

(wt.%)	Test A	Test B	Test C	Test D	Test E
Oxygen concentration	$10^{-11} \sim 10^{-12}$	10^{-10}	10^{-9}	10^{-8}	10^{-6}

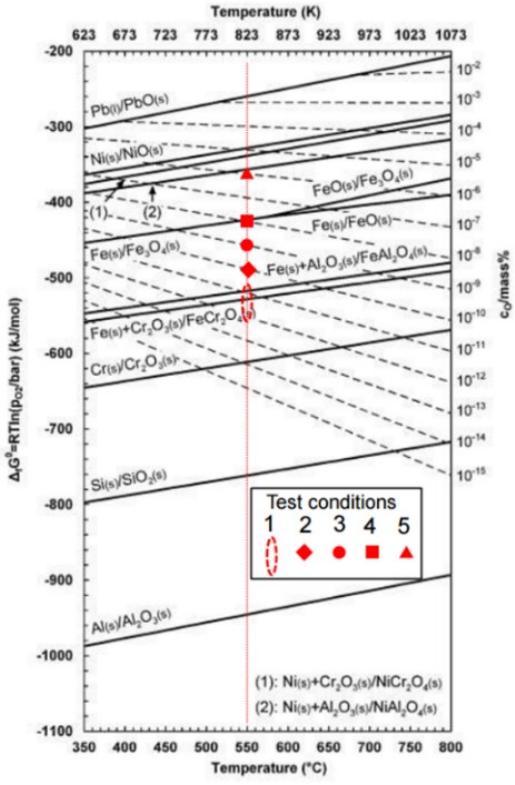

FIG. 7. Gibbs free energy following dissolved oxygen concentration [13,14,15]

Fig. 8 shows the results after corrosion test in liquid Pb-Bi. (a) and (c) are the results of #3 material, and (b) and (d) are those of #1. And (a) and (b) are the results conducted at high dissolved oxygen concentration (10^{-8} %) and (c) and (d) are those conducted at low dissolved oxygen concentration (10^{-11} %). As shown in the figure, dissolution attack was occurred in

every specimen. Spongy corrosion zone was observed in attacked region on the surface of specimen. Corrosion zone has ferrite formed along with substantial depletion of Ni and Cr, penetration of Pb and Bi. Also, as shown in Fig. 8, thin aluminium oxide layer was observed at #3 material, while it was not at #1 material. It seems that the added aluminium and NbC contributes to the formation of proactive oxide layer that impedes the oxidation and dissolution of metal ions into liquid metal. Also, oxygen addition to the liquid metal could cause formation of aluminium oxide in the surface of alloy which could prevent critical oxygen depletion or dissolution attack. Therefore, during design the material, several alloying elements should be considered carefully including common elements like aluminium and other elements which could enhance the formation of oxide layer such as NbC.

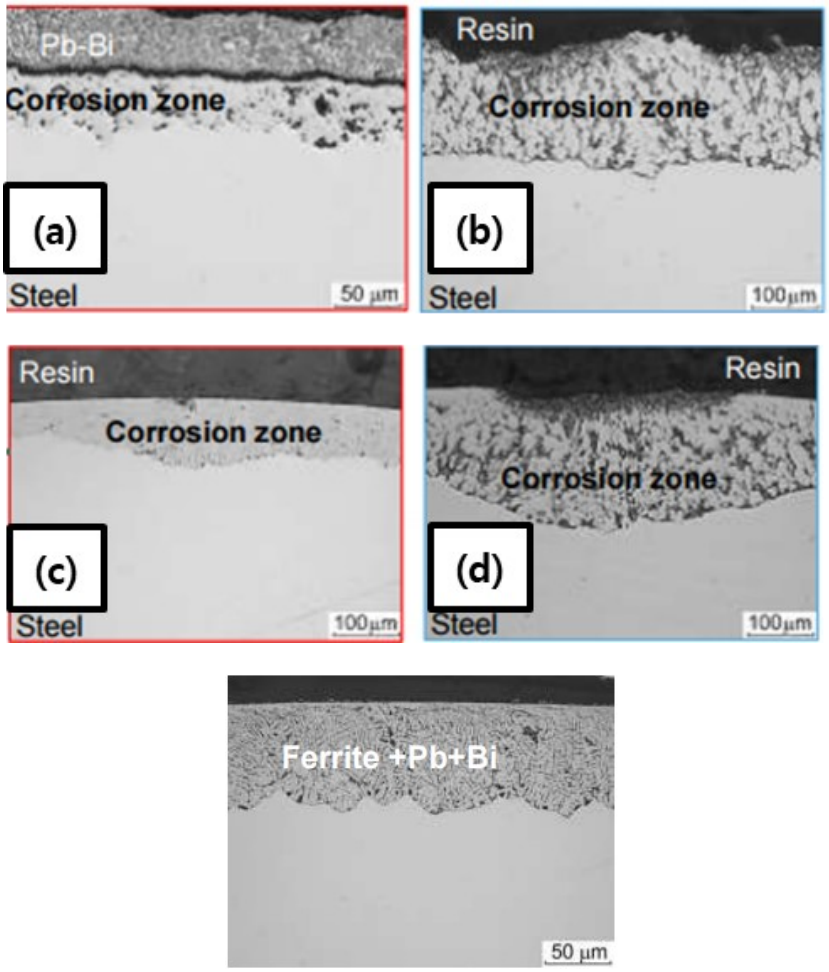

FIG. 8. Corrosion test results of each specimen; (a, c) results of #3 material, (b, d) results of #1 material, (a, b) results from 10^{-6} wt. % of dissolved oxygen concentration, (c,d) results from 10^{-12} wt.% of dissolved oxygen concentration. [13,14]

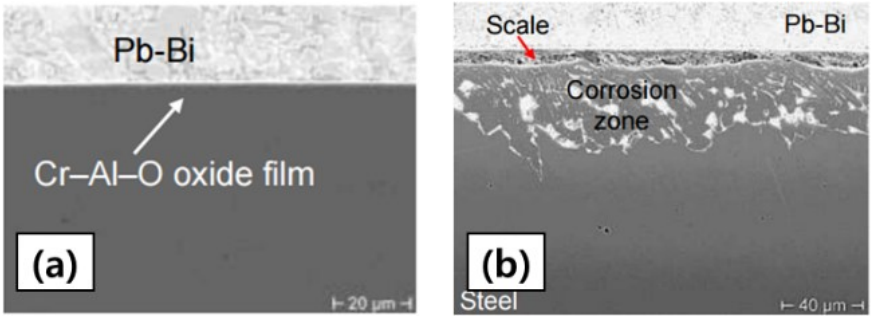

FIG. 9. (a) Oxidation at high dissolved oxygen concentration of #1 material (b) dissolution at thick oxide scale [13,14]

3. LEAK BEFORE BREAK APPROACH

Steam generator tube leakage is one of the safety issues for liquid metal cooled fast reactors such as LBE fast reactors. Steam generator failure and leakage could cause injection of highly pressurized secondary water into primary circuit. The injected waters could make voids in reactor core, which in turns decreasing heat transfer coefficient and insert reactivity. This phenomenon could be enhanced if large break happens in steam generator material. To prevent this, leak before break (LBB) concept should be adopted to steam generator in LBE fast reactors. LBB is widely known safety concept; it means the design concept which support operator to find out small leakage before large break so that large catastrophe could be prevented.

Steam generator tube of LBE fast reactors are subjected to corrosive environment; high temperature, corrosive media, high vibration and residual stress. This environment could cause stress corrosion cracking which is one of the major degradation mechanisms of most metals including stainless steels and nickel-based alloys. Also, secondary side could be suffered by similar degradations. [19,20]

LBB could be analyzed in two steps according to IAEA-PUBLICATION-710. [16] First step is screening. Screening is performed to select vulnerable part in whole system and find out the parts which have high possibility of degradation and should be observed more carefully. For that, every degradation mechanism should review thoroughly. Also, every part should be screened carefully based on that data. Second step is fracture mechanics. After the LBB candidate piping has been selected, it should be evaluated based on fracture mechanics or finite element methods. This should evaluate the system by considering that how the leak is detected, if there exist any defect stability and there is little chance of a defect occurring. Figure 9 shows basic concept of LBB, the detection and break of tube. [16,17,20]

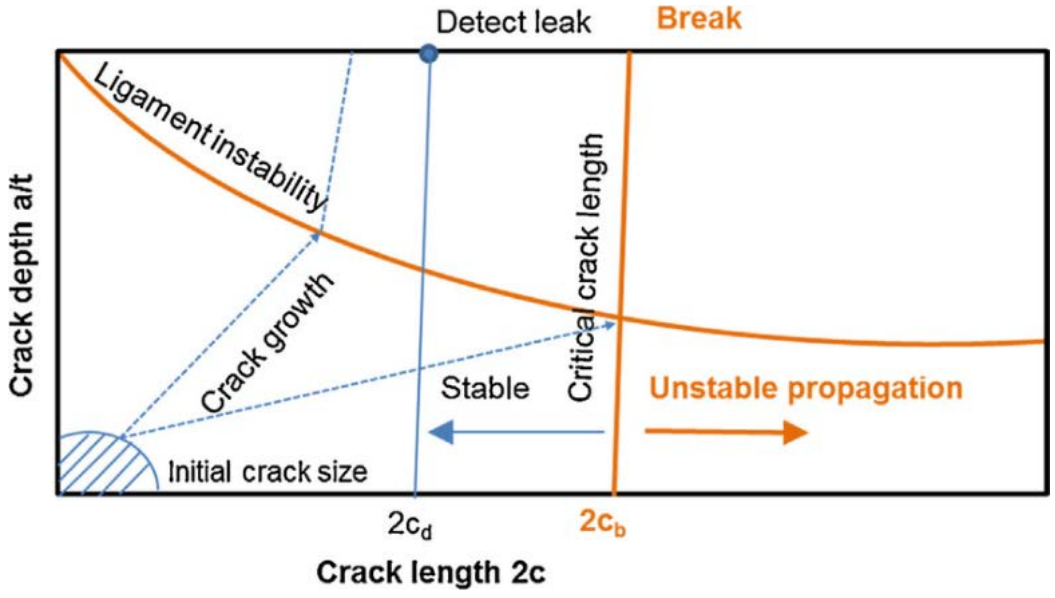

FIG. 10. Leak Before Break Concept [16,17]

Meanwhile, proper design of steam generator is not proposed for LBE cooled fast reactor which could be operated for long-term over 40 years. For that, newly designed tube for steam generator is consisted and suggested as shown in Fig. 11 which is designed to double walled layers. Tube materials are also considered to assure prolonged corrosion resistance and oxide

deposition control in heavy-liquid metal environment. Exceptional corrosion resistance over 40 year-life can be delivered by functionally graded composite (FGC) tubes; FeCrSi layer. FeCrSi has excessive corrosion resistance in liquid metal environment. Additionally, advanced flow channel structure and maintenance design will be conducted with proposed material for enhanced characteristics in oxide deposition and maintenance.

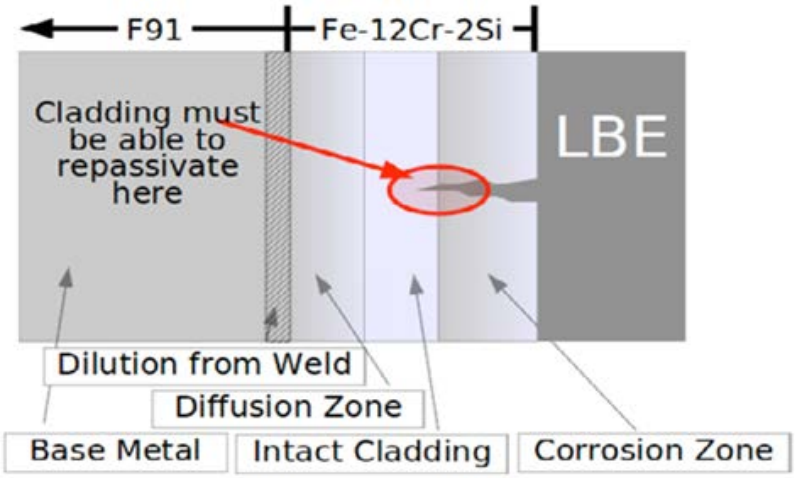

FIG. 11. Schematic diagram of FGC tube that reduces corrosion from liquid metal

Furthermore, in order to assure LBB, the inter-tubular gap will be designed which is filled with engineered materials for leak detection and thermal conductivity enhancement. The LBB characteristics, corrosion resistance, thermal-hydraulic performance will be pursued by innovative material, thermal-hydraulic design will be presented using fracture mechanics, oxidation and heat transfer models.

4. SUMMARY AND FUTURE WORK

In this paper, an innovative steam generator design concept is presented for Micro-Uranus, a non-refueling and hermetically sealed 40-year life micro-modular LFR. Schematic design of DWOTSG has been proposed to fulfill the leak-before-break requirements. For that, several corrosion issues in liquid metal cooled fast reactors were reviewed to predict expected design requirements for several structures including heat exchanger tubes. It has been determined that Type 316L austenitic stainless steel is suitable for lead-bismuth side, considering corrosion, liquid metal embrittlement at operating temperature not exceeding 350 °C for operation of 40 years. The newly designed tube for steam generator is consisted of double walled layers (FGC) and will be evaluated and expected to have enough durability to be operated over 40 years. In order to detect leak and assure LBB, the inter-tubular gap design was proposed which is filled with sensor for leak detection. Further studies are in progress to demonstrate the long-term corrosion resistance, liquid metal embrittlement and leak detection capabilities for the operating temperature regime.

ACKNOWLEDGEMENTS

This work was supported by the National Nuclear R&D program funded by Ministry of Science and ICT and by the National Nuclear R&D program (NRF-2019M2D1A1067205) organized by the National Research Foundation (NRF) of South Korea in support of the Ministry of Science and ICT and by This work was partially supported by the Human Resources Program in Energy Technology (No. 20194030202400) of the Korea Institute of Energy Technology Evaluation and Planning (KETEP), which is funded by the Ministry of Trade Industry and Energy (MOTIE), Republic of Korea.

REFERENCES

[1] JASMINA ET AL. NEW REACTOR CONCEPTS FOR NEW GENERATION OF NUCLEAR POWER PLANTS: AN OVERVIEW, Proc. 50th ETRAN Conference, Belgrade, June 6-8 (2006)

[2] Y. -H. SHIN, ET AL., Advanced Passive Design of Small Modular Reactor Cooled by Heavy Liquid Metal Natural Circulation, in *Progress in Nuclear Energy*

[3] SHEA, T. ET AL., The atoms for peace reactor concept, Symposium on international safeguards: Addressing verification challenges, Vienna (Austria), 16-20 Oct (2006)

[4] ALESSANDRO ALEMBERTI, ADVANCED LEAD FAST REACTOR EUROPEAN DEMONSTRATOR – ALFRED PROJECT, GEN IV International Forum, September 26, 2018

[5] "Russia to build fast reactor fuel plant in 2018", World Nuclear News(WNN), 29, December, 2017, http://www.world-nuclear-news.org/NN-Russia-to-build-fast-reactor-fuel-plant-in-2018-29121701.html,

[6] ARGONNE NATIONAL LABORATORY (ANL), Status Report on the Small Secure Transportable Autonomous Reactor (SSTAR)/Lead-Cooled Fast Reactor (LFR) and Supporting Research and Development, ANL-GenIV-089

[7] "Korea government that shouts the nuclear power plant develop the nuclear icebreaker", Joong-Ang Il Bo, https://news.joins.com/article/23352554

[8] US NRC, Pressurized Water Reactor B&W Technology Cross Training Course Manual, Chapter 2.4, Once-Through Steam Generator, https://www.nrc.gov/docs/ML1122/ML11221A117.pdf

[9] SG LEE, (2013), A Study on Corrosion Behaviors for Life-Prediction of Structural Materials in Lead Fast Reactors (Ph.D Thesis), Seoul National University, Seoul

[10] ESPEDITO VASSALLO, ET AL., Effect of alumina coatings on corrosion protection of steels in molten lead, Journal of Vacuum Science & Technology B, 36, 01A105 (2018)

[11] S.HÉMERY, ET AL., Liquid metal embrittlement of an austenitic stainless steel in liquid sodium, Corrosion Science, Vol 83, 1-5 (2014)I.V. Gorynin et al. Mat. Sci. Heat. Treat, 41 (1999)

[12] GENERAL ELECTRIC, DOUBLE-WALL STEAM-GENERATOR TUBE AND WELD-DEVELOPMENT STUDY

[13] VALENTYN TSISAR, ET AL., CORROSION ISSUES IN STEELS CONTACTING Pb-Bi Eutectic AT HIGH TEMPERATURES – OVERVIEW OF KIT ACTIVITY, European Commission funded international workshop 12-14 June (2017)

[14] VALENTYN TSISAR, ET AL., Corrosion in aluminium-alloyed austenitic steel caused by static lead-bismuth eutectic: Effect of dissolved oxygen concentration after exposure for 1000 h at 550 ºC, GEMMA – Generation IV Materials Maturity Workshop on AFA Steels Karlsruhe, November 28th (2018)

[15] EJENSTAN ET AL, Journal of Nuclear Materials, Vol 461 (2015)

[16] IAEA-PUBLICATION-710, Applicability of the leak before break concept.

[17] B. FLESCH, Leak-Before-Break in Steam Generator Tubes, Int. J. Pres. Ves. & Piping Vol 32, 165-179 (1990)

[18] LORENZO DAMIANI, New steam generation system for lead-cooled fast reactors, based on steam recirculation through ejector, Applied Energy, Vol 137, 292-300 (2018)

[19] MINGYA CHEN, Fracture mechanics assessment of thermal aged nuclear piping based on the Leak-Before-Break concept, Nuclear Engineering and Design, Vol 301, 333-340 (2016)

[20] MARTI JELTSOV, WALTER VILLANUEVA, PAVEL KUDINOV., Steam Generator leakage in lead cooled fast reactors: Modeling of void transport to the core, Nuclear Engineering and Design, Vol 328, 255 – 265 (2018)

[21] MAN WANG, ET AL., Evolution of microstructure and tensile properties of Fe-18Ni-12Cr based AFA steel during aging at 700 ºC, Materials Science and Engineering: A, Vol 672, 21-31 (2016)

[22] D.V.V. SATYANARAYANA, ET AL., Steady state creep behaviour of NiAl hardened austenitic steel, Material Science and Engineering A, 323 (2002)
[23] Y. YAMAMOTO, ET AL., Alloying effects on creep and oxidation resistance of austenitic stainless steel alloys employing intermetallic precipitates, Intermetallics, 16 (2008)

COMPATIBILITY EVALUATION ON STRUCTURAL MATERIALS FOR CLEAR IN OXYGEN CONTROLLED LEAD-BISMUTH EUTECTIC AT 500 °C AND 550 °C

L. LUO, Z.Q. XIAO, Z.Z. JIANG *, J.W. CHEN, L.L. SONG, S. GAO, C. J. LI, S.J. LIU, Q.Y HUANG, FDS TEAM
Institute of Nuclear Energy Safety Technology, Chinese Academy of Science
Hefei, Anhui, China
Email: zhizhong.jiang@fds.org.cn

Abstract

Material corrosion in lead or Lead-Bismuth Eutectic (LBE) is the important limiting factor to keep integrity of internal components of lead-based reactor. In order to verify engineering feasibility and screen corrosion-resistant material in LBE environment, the compatibility of structural materials with LBE at 500 °C and 550 °C was evaluated. First, T91 and 15-15Ti steels were selected to be tested in stagnant LBE with different oxygen concentrations to investigate the influence of oxygen concentrations on corrosion behaviour of typical martensitic and austenitic steels. For the two types of steels, the formation of protective oxide layer is sensitive to the oxygen concentration. Second, long-term corrosion tests were carried out in large-scaled KYLIN-II material corrosion loop to evaluate the corrosion performance of the candidate structure materials under service condition of CLEAR-I. It is found that the growth kinetics curves of oxide layers for T91, 15-15Ti, CLAM and 316L steels follow a parabolic rule ($\Delta x^2=K_p t$), and the rate constant for 15-15Ti steel is lowest. Thirdly, new Si-contained stainless steel and ODS-9Cr steel have been developed in INEST and compatibility evaluation revealed that the corrosion resistances of the above steels have attained considerable improvement.

1. INTRODUCTION

Design and key technologies development for lead-based reactor have been carried out in the Institute of Nuclear Energy Safety Technology, Chinese Academy of Sciences (INEST) • FDS Team for more than 30 years. China LEAd-based Reactor (CLEAR) series was proposed, such as China LEAd-based Research Reactor (CLEAR-I) for nuclear waste transmutation research, China LEAd-based Mini-Reactor (CLEAR-M) for independent power supply and CLEAR-A for multi-purpose [1-3].

Compatibility of materials with lead-bismuth eutectic (LBE) is the important limiting factor to keep the integrity of internal thin-walled components such as fuel cladding during the period of service, which is one of the key engineering problems to be resolved in the development of lead-based reactors [4-6]. Many compatibility tests have shown the corrosion resistances and the basic corrosion mechanisms of structural materials in LBE.

Many corrosion tests show that a protect oxide scale is formed in-situ on the surface of martensitic steel and austenite steel with the oxygen concentration of 10^{-6} wt%, which can prevent steel matrix from dissolution attack. Dissolution is the major interaction mechanism under low oxygen concentrations (10^{-8}～10^{-10} wt%) [7,8]. Therefore, the oxygen concentration in LBE is a key factor that affects the corrosion behaviors of structure materials. However, corrosion tests in LBE were mostly carried out with the oxygen concentration of 10^{-6} wt% or saturation [8-10] and the effect of oxygen concentrations on the corrosion behaviors in LBE has been still scarce.

Long term corrosion data is very important for safety assessment during reactor design. A series of long-term corrosion test in flowing LBE have been done at 300, 450, 470 and 550 °C [11-12]. However, there was no long-term corrosion test in flowing LBE at the maximum design temperature for the cladding tube of CLEAR-I. In addition, the corrosion data of CLAM steel, which is a candidate cladding material for CLEAR-I, is also missing.

In the study, typical material compatibility tests performed by INEST • FDS Team were presented. The tests are divided in three parts. First, corrosion tests of T91 and 15-15Ti in LBE were carried out in static LBE with different dissolved oxygen concentrations at 500 ºC to investigate the dependence of the type and growth behaviors of corrosion products on oxygen concentrations. Second, long term corrosion experiments for T91, 15-15Ti, CLAM and 316L steels in flowing LBE at 500 ºC to evaluate the corrosion performance of the candidate structure materials under service condition of CLEAR-I. Finally, typical tests of new Si-contained stainless steel and ODS-9Cr steel have been performed in LBE at 500 ºC or 550 ºC

2. EXPERIMENTAL

2.1. **Specimen preparation**

The investigated specimens for corrosion test in static LBE were machined from hot-rolled plates. The specimens were fabricated into thin-plate shape with a corrosion surface area of 10 mm ×10 mm, as shown in Fig. 1. All the specimen surfaces were mechanically ground using a series of silicon carbide papers up to 2000 grit, and then polished with a 2.5 μm diamond paste. After grinding and polishing, all the specimens were cleaned by acetone in an ultrasonic bath before exposing to LBE.

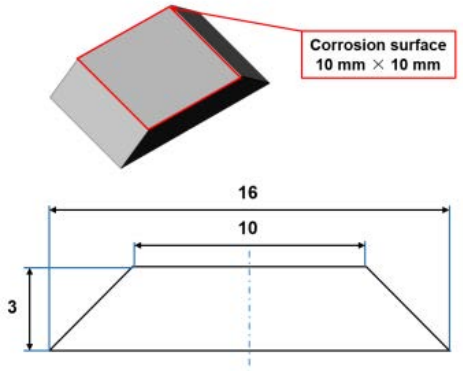

FIG. 1. The specimens for corrosion test in static LBE.

The investigated specimens for corrosion test in flowing LBE were fabricated into cylinders, as shown in FIG. 2. The diameter and height of the specimens are 12 and 35 mm, respectively. The schematic illustration and preparation process of the cylindrical specimen were described in detail elsewhere [14].

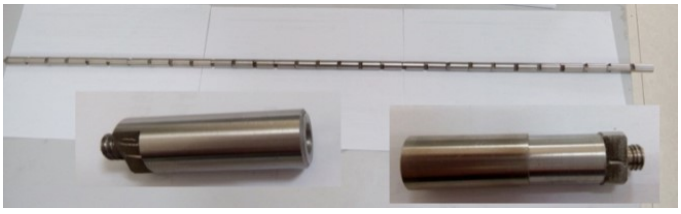

FIG. 2. The specimens for corrosion test in flowing LBE

2.2. **Post-test analysis**

For each exposure time, two specimens were prepared. One was used for the examination of cross-sections with adherent LBE. The other was used for surface analysis, which was repeatedly immersed in a mixture solution of $CH_3COOH + H_2O_2 + C_2H_5OH$ with a volume ratio of 1:1:1 at room temperature to remove the surface adherent LBE. The cross-sections were investigated to reveal the morphologies, compositions and dimensional parameters of oxide layers with scanning electron microscope (SEM) supplemented by qualitative energy-dispersive X-ray microanalysis (EDX). The surfaces of the specimens without adherent LBE were analyzed by means of SEM and X-ray diffraction (XRD) to determine the surface morphologies and phases of the oxide layers formed during the exposure, respectively.

3. EFFECT OF OXYGEN CONCENTRATIONS IN STATIC LBE ON CORROSION BEHAVIOR

The typical cross-section morphologies of T91 and 15-15Ti steel after exposure in LBE containing 10^{-6} wt%, 10^{-7} wt% and 10^{-8} wt% oxygen at 500 ºC for up to 2000 h as shown in Fig. 3 and Fig. 4, respectively.

At 10^{-6} wt% oxygen concentration, an oxide scale with a three-layer structure was formed on the surface of T91. The outermost layer was Fe_3O_4, where severe LBE penetration occurred as a result of loose structure. The middle layer was composed of $(Fe, Cr)_3O_4$ with spinel structure, and the structure was relatively dense, which could effectively block LBE continue to penetrate. The innermost layer was an internal oxidation zone (IOZ), which was structured like a needle-shaped or elongated channel and extended into the interior of the T91 substrate. For 15-15Ti, however, an oxide scale with a two-layer structure was formed on the surface, which is different from T91. The outer layer is Fe_3O_4, and the inner layer is $(Fe, Cr)_3O_4$. And LBE permeation into the oxide film could also be observed.

At 10^{-7} wt% and 10^{-8} wt% oxygen concentration, T91 underwent oxidation corrosion, but the oxide scale has changed from a three-layer structure to a two-layer structure, and no Fe_3O_4 layer existed. This is because the formed Fe_3O_4 is unstable at low oxygen content in LBE, easily decomposed, and dissolved in LBE, resulting in the disappearance of Fe_3O_4. For 15-15Ti, however, dissolution corrosion occurred under the conditions of 10^{-7} wt% and 10^{-8} wt% oxygen concentration, and LBE clearly penetrated the 15-15Ti matrix.

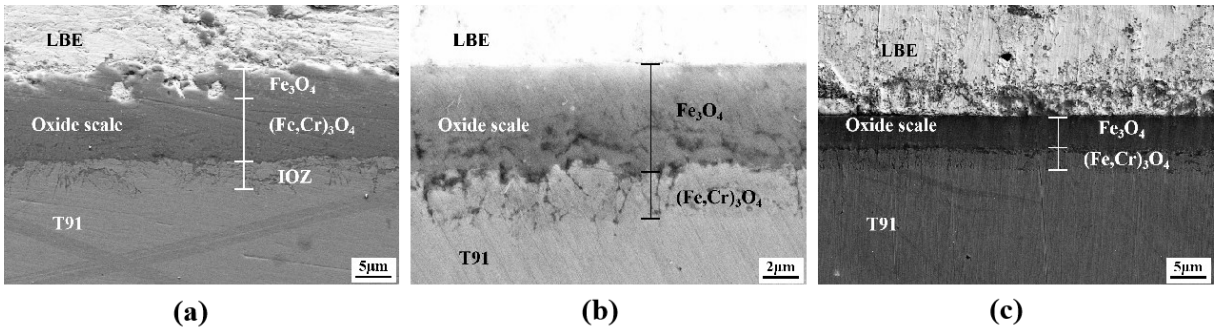

FIG. 3. Cross-section morphology of T91 steel after exposure in LBE containing 10^{-6}, 10^{-7} and 10^{-8} wt% oxygen at 500 ºC for up to 2000 h (a) 10^{-6} wt% oxygen; (b) 10^{-7} wt% oxygen; (c) 10^{-8} wt% oxygen [17]

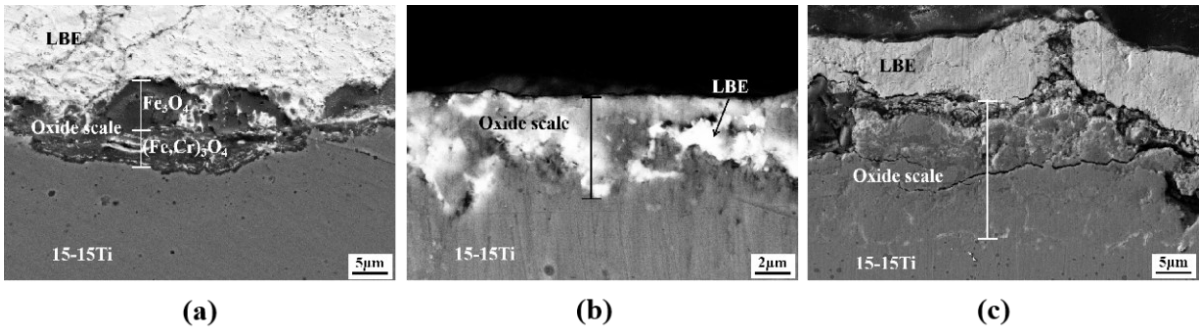

FIG. 4. Cross-section morphology of 15-15Ti steel after exposure in LBE containing 10^{-6}, 10^{-7} and 10^{-8} wt% oxygen at 500 ℃ for up to 2000 h (a) 10^{-6} wt% oxygen; (b) 10^{-7} wt% oxygen; (c) 10^{-8} wt% oxygen [17]

The above results show that ferritic/martensitic steel T91 and austenitic steel 15-15Ti exhibit different corrosion behaviors in liquid LBE. The main reason for this is high content of Ni in 15-15Ti. Because the solubility of Ni element in LBE is much larger than that of Fe and Cr, when 15-15Ti is in contact with LBE, the Ni element in the steel preferentially dissolves, and when the oxygen concentration is low, preferential dissolution corrosion will occur.

The elemental diffusion model suggested by Müller and Martinelli [11,12] could explain the formation mechanism of the three-layer oxide scale on the surface of T91 steel at 10^{-6} wt% oxygen concentration. As shown in Fig. 5, first, Fe cations diffuse outward and combine with O anions in LBE to form Fe_3O_4, which resulting in a large amount of Fe vacancies in the region near the surface of T91. These vacancies then aggregate at the steel/oxide interface to form micro-voids. In these micro-voids, Fe and Cr cations react with the diffused O anions to form Fe-Cr spinel ($Fe^{2+}O[Fe^{3+}, Cr^{3+}]_2O_3$), filling the micro-voids. Once this thin spinel layer is formed, Fe cations will pass through it to diffuse from the substrate to the surface and combine with the O anions to form Fe_3O_4 on the surface; at the same time, the O anions will pass through Fe_3O_4 and Fe-Cr spinel layer to diffuse into the substrate. As a result, Fe-Cr spinel will form in the micro-voids of the Fe-Cr spinel/IOZ interface. And O anions will continue to diffuse at the grain boundary of the surface region of the substrate to react with Fe and Cr cations, forming Cr-rich oxides. And finally an IOZ layer will form. Therefore, according to this model, Fe_3O_4 grows outward on the steel surface, while Fe-Cr spinel grows inward, and the inter-diffusion of Fe and O plays an important role in the growth of the oxide film.

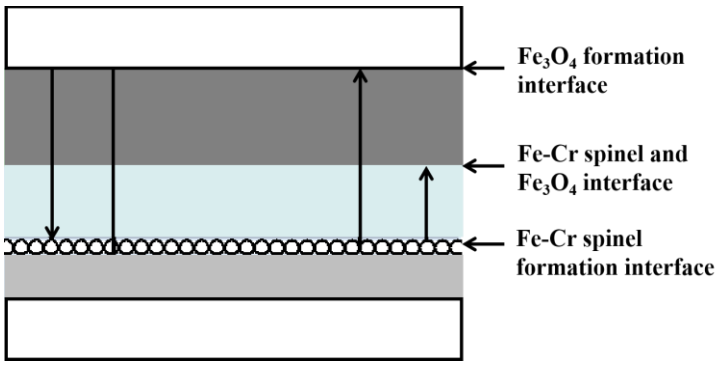

FIG. 5. Schematic diagram of the formation mechanism of three-layer oxide film on T91 steel

Fig. 6 shows the evolution of the oxide scale thickness of T91 steel with time under different oxygen concentration conditions. It can be seen from Fig. 6a that the thickness of $(Fe, Cr)_3O_4$ increased with increasing exposure time. In addition, at the same time point, the thickness of $(Fe, Cr)_3O_4$ is different under different oxygen concentration conditions. After exposure for

500 h, the thickness of $(Fe, Cr)_3O_4$ is the smallest when the oxygen concentration of LBE is 10^{-8} wt%. However, the thickness of $(Fe, Cr)_3O_4$ at 10^{-7} wt% oxygen concentration is slightly greater than that at 10^{-6} wt% oxygen concentration. The possible reason is that the outer surface oxide film of Fe_3O_4 on T91 temporarily hinders the growth of $(Fe, Cr)_3O_4$ at 10^{-6} wt% oxygen concentration. At 1000 h and 2000 h, the thickness of $(Fe, Cr)_3O_4$ increased with increasing oxygen concentrations. It can also be seen from Fig. 6b that the total thickness of the oxide scale increased with increasing exposure time and oxygen concentrations. The above data indicates that oxygen content in LBE is a key factor in determining the corrosion behavior of steel materials, and the dominant factor affecting the types and properties of corrosion interface products.

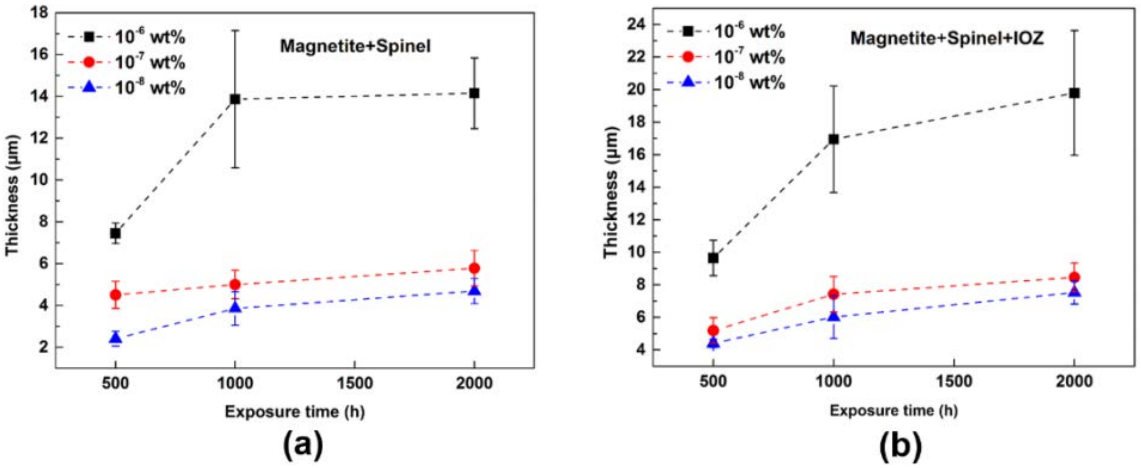

FIG. 6. Comparison results for the thicknesses of the oxide layers formed in LBE with different oxygen concentrations: (a) the thickness of the magnetite + spinel layers; (b) the total thickness [17]

Since dissolution corrosion occurred for 15-15Ti under the conditions of 10^{-7} wt% and 10^{-8} wt% oxygen concentration, the evolution relationship of corrosion depth with time under these two oxygen concentration conditions was compared. As shown in Fig. 7, the penetration depth of LBE increased with increasing exposure time under the same oxygen concentration, which basically conformed to the straight-line law. It can also be found that the penetration depth of LBE at 10^{-8} wt% oxygen concentration was slightly larger than that at 10^{-7} wt% oxygen concentration. So, the oxygen concentration is the dominant factor affecting the type and properties of the corrosion interface products.

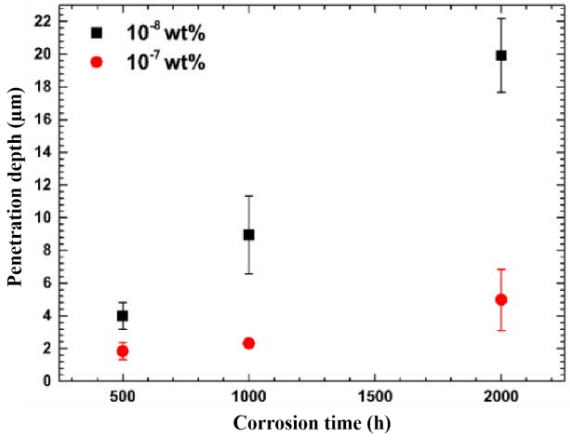

FIG. 7. Evolution of LBE penetration depth with time in 15-15Ti steel at 10^{-7} wt% and 10^{-8} wt% oxygen concentration [17]

4. LONG-TERM CORROSION BEHAVIOR

For evaluating the corrosion performance of the candidate structure materials under service condition of CLEAR-I, a long-term corrosion test was carried out in large-scaled KYLIN-II material corrosion loop. T91, 15-15Ti, CLAM and 316L steels were exposed to oxygen-controlled LBE ($1\sim3\times10^{-6}$ wt%) with 1 m/s flow velocity at 500 °C for 8000 h. Figure 2 and Fig. 8 depict the photos of the above samples before the corrosion tests and after exposed in LBE for 8000 h, respectively.

FIG. 8. The photo of the samples exposed in LBE for 8,000 hours.

After exposure, the growth thickness of the oxide layer and each sub-layer for different materials at different times were obtained by direct measurement, as shown in Fig. 9. It can be seen that oxide scale of T91 steel includes three sub-layers, i.e., Fe_3O_4, $(Fe, Cr)_3O_4$ and IOZ; the structure of oxide scale on the surface of CLAM is similar to that of T91. Moreover, the oxide scale of 15-15Ti and 316L steels are similar, which contain only a thin layer of (Fe, Cr)3O4 and are obvious different from that of T91 and CLAM. The growth kinetics curves of oxide layers in Fig. 10 follow a parabolic rule ($\Delta x^2=K_p t$), and the rate constants (K_p) were shown in Table 1. Table 1 shows that the rate constant for 15-15Ti steel is lowest.

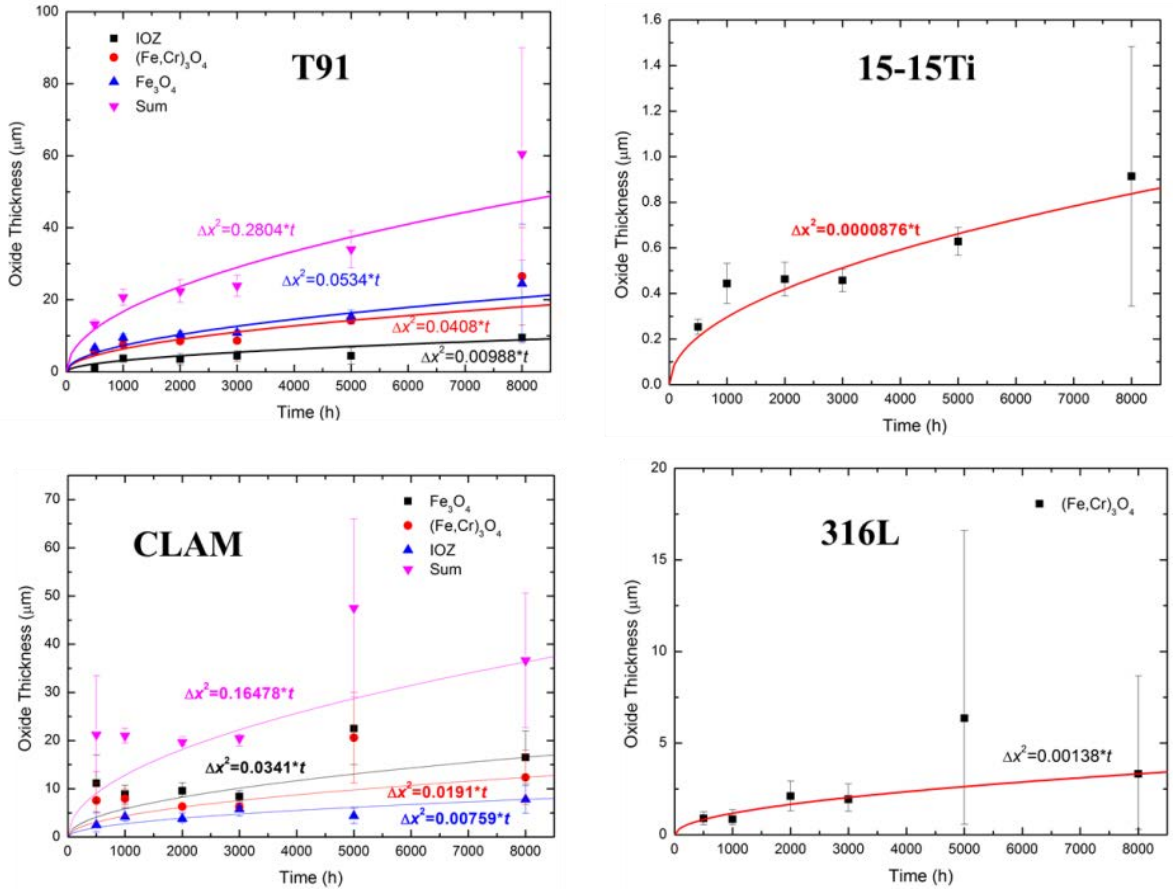

FIG. 9. The thickness of the oxide layer and each sub-layer for different materials at different times

Typical cross-section morphologies for T91 steel with different exposure times were shown in Fig. 10. For exposure times of 3000 h and 5000 h, the structure of corrosion products at the interface between LBE and T91 matrix are similar, which both are three sub-layer structure. The outermost sub-layer is Fe_3O_4 with a slightly loose structure, and a few LBE has penetration into Fe_3O_4 sub-layer; the middle sub-layer is (Fe, Cr)$_3O_4$ with more compact structure and without LBE infiltration; the innermost sub-layer is IOZ, which belong to a diffusion transition zone. However, compared with the corrosion morphologies for 3000 h and 5000 h, the corrosion morphology for 8000 h is different. These difference mainly includes two aspects: (1) LBE has infiltrated the T91 substrate near IOZ layer; (2) From outside to inside, the oxide scale is divided into five layers, i.e., Fe_3O_4/(Fe, Cr)$_3O_4$/ Fe_3O_4/(Fe, Cr)$_3O_4$/IOZ. The formation of the complex structure is likely to be associated with severe LBE penetration.

TABLE 1. RATE CONSTANTS OF DIFFERENT STEELS IN THE LONG-TERM CORROSION TEST

Steel	Fe_3O_4 sub-layer	(Fe,Cr)$_3O_4$ sub-layer	IOZ sub-layer	Total Thickness
T91	0.0534	0.0408	0.00988	0.2804
15-15Ti	-	0.0000876	-	-
CLAM	0.0341	0.0191	0.00759	0.16478
316L	-	0.00138	-	-

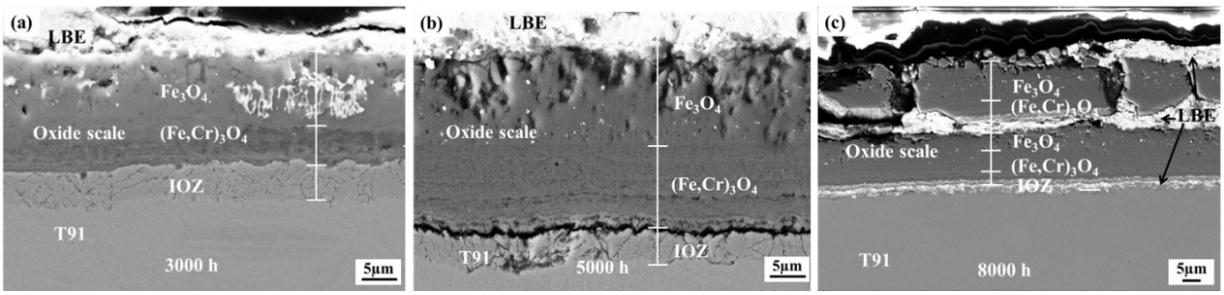

FIG. 10. Typical cross-section morphologies of T91 specimens with different exposure times: (a) 3000 h, (b) 5000 h, (c) 8000 h.

Typical cross-section morphologies for 15-15Ti steel with different exposure times were shown in Fig. 11. The morphologies are different from those of T91 steel: (1) A thin and dense oxide scale with the thickness of 0.5~2 μm formed in the interface between LBE and 15-15Ti substrate; (2) the corrosion morphologies for 3000 h, 5000 h and 8000 h are similar. The composition of oxide scale was determined to be (Fe, Cr)$_3O_4$, according to the EDX and XRD results. In addition, the phenomenon of oxide scale lamination did not happen, which is different from the morphology of static corrosion exposed to LBE with the oxygen concentration of 10^{-6} wt%.

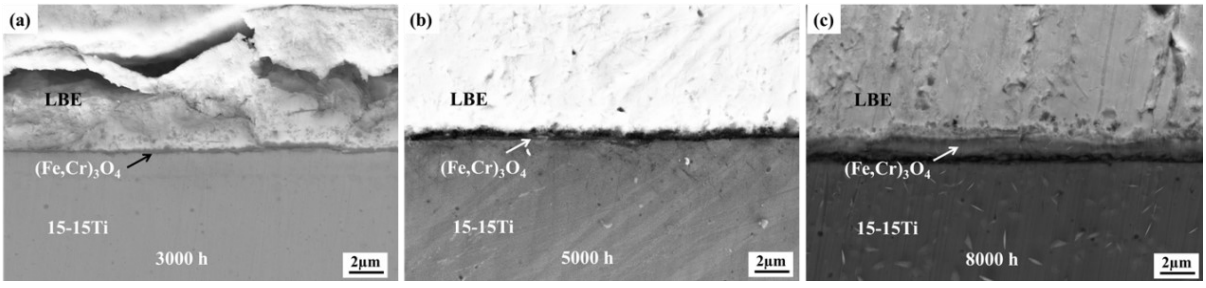

FIG. 11. Typical cross-section morphologies of 15-15Ti specimens with different exposure times: (a) 3000 h, (b) 5000 h, (c) 8000 h

5. RESEARCH AND DEVELOPMENT OF SI-CONTAINED STEEL

A new type Si-contained austenitic stainless steel has been developed based on the high-temperature reinforcement theory and a phenomenon that the addition of silicon element can enhance corrosion resistance of steel to LBE. The ratio of Ti/C and the contents of Si, Cr and Ni element were optimized based on composition of 15-15Ti. Figure 12 is typical cross-section morphologies for the Si-contained austenitic stainless steel and 15-15Ti steel exposed to oxygen-controlled LBE ($1\sim3\times10^{-6}$ wt%) with 1 m/s flow velocity at 500 °C for 2000 h. For both types of steels, a thin and dense $(Fe, Cr)_3O_4$ layer formed in the interface between LBE and steel substrate. However, compared with that of 15-15Ti, $(Fe, Cr)_3O_4$ layer of the Si-contained austenitic stainless steel is more even and thinner, which indicates considerable improvement of the corrosion resistance was attained. This phenomenon may be because many tiny SiO_2 particles which formed in $(Fe, Cr)_3O_4$ layer hinder the mass transfer between LBE and steel matrix.

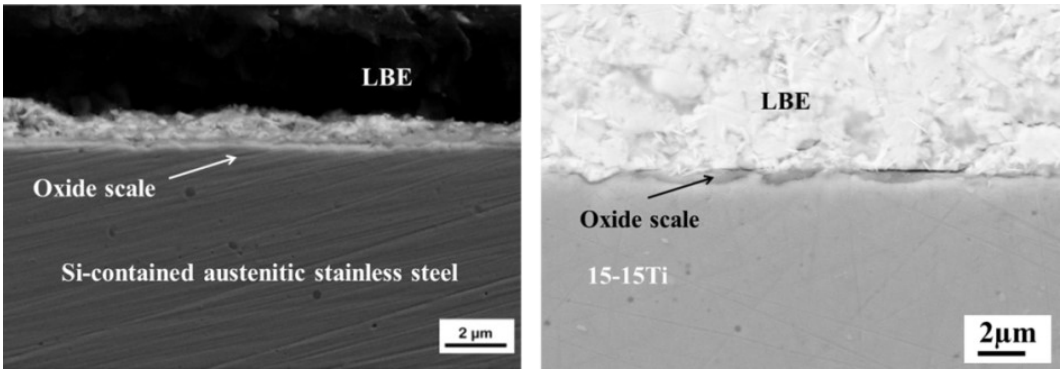

FIG. 12. Typical cross-section morphologies for Si-contained austenitic stainless steel and 15-15Ti steel

ODS steel is one of the candidate structural materials for lead-based reactors because of its excellent high temperature strength, high temperature creep performance and excellent radiation resistance. A new Si-containing ODS steel for lead-based reactor has been designed based on CLAM, and the corrosion behavior has been studied in static lead with 10^{-6} wt% oxygen concentration at 550 °C. As shown in Fig. 13, after exposure for 3000 h, an oxide film with a three-layer structure was formed on the surface of Si-containing ODS steel. The outermost layer was Fe_3O_4, the middle layer was composed of $(Fe, Cr)_3O_4$ with spinel structure and the innermost layer was a Cr-rich and Si-rich oxide layer. As shown in Fig. 14 and Fig. 15, the thickness of the oxide film on ODS steel after corrosion reduced with the increase of Si content. It is believed that the addition of Si can promote the formation of dense Cr-rich and Si-rich oxide layer and slow down the diffusion of oxygen into the substrate, and thus improve the corrosion resistance of ODS steel.

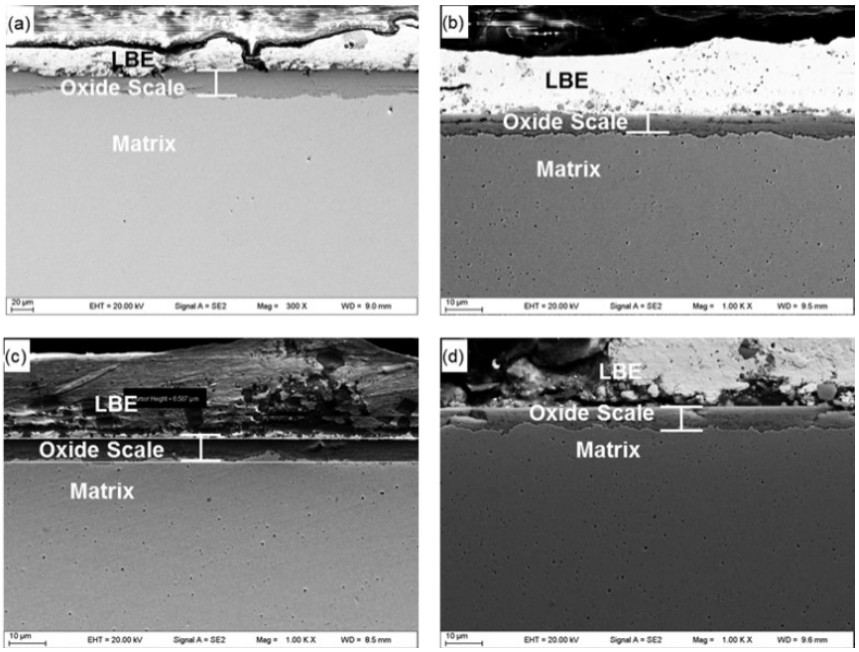

FIG. 13. Cross-section morphology of ODS steel with different Si content after exposure for 3000h: (a) without Si, (b) with 0.3 wt% Si, (c) with 0.5 wt% Si, (d) with 1 wt% Si [18]

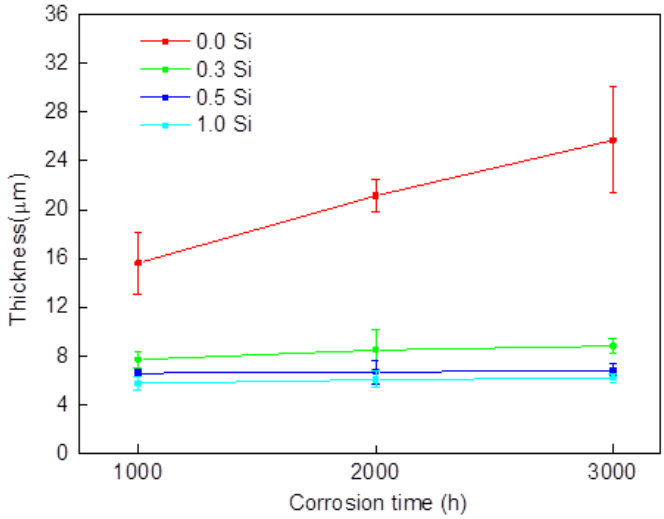

FIG. 14. Evolution of corrosion thickness of ODS steel with different Si content with time [18].

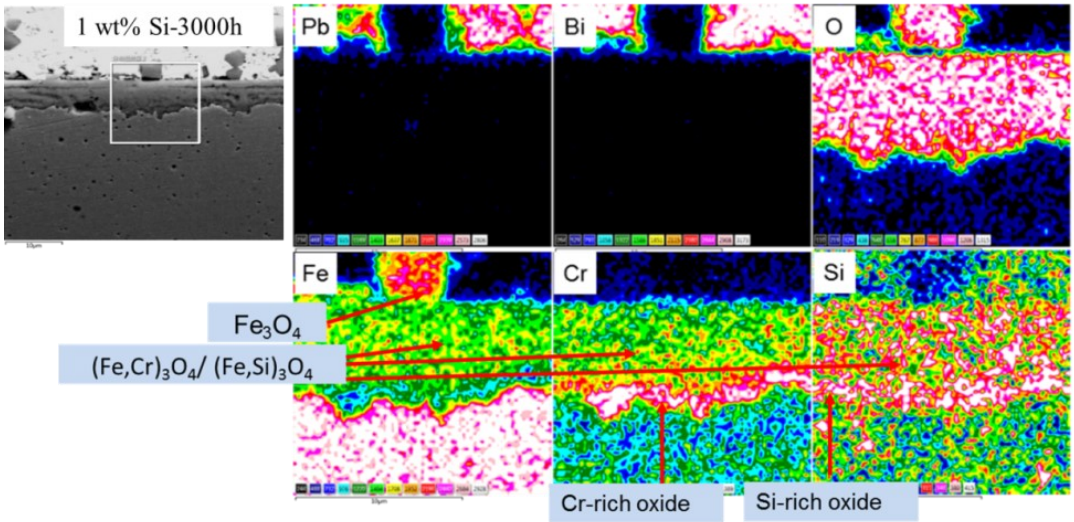

FIG. 15. Results of the EDS area scanning through the cross-section of the ODS containing 1 wt% Si after exposure for 3000 h [18]

6. CONCLUSIONS

A series of compatibility evaluations on structural materials has been carried out in oxygen controlled in LBE at 500 °C and 550 °C. The evaluations obtain the following important results:

(1) The oxygen content in LBE is a key factor in determining the corrosion behaviours of T91 steel and 15-15Ti steel and the dominant factor affecting the types and properties of corrosion interface products. As for T91, the oxide-scale structure changes from a three-layer magnetite/spinel/internal oxidation zone (IOZ) scale under the oxygen concentration of 10^{-6} wt%, to formation of a two-layer spinel/IOZ scale under the oxygen concentrations of 10^{-7} and 10^{-8} wt%. As for 15-15Ti, oxidation occurred, and a two-layer magnetite/spinel scale was formed under the oxygen concentration of 10^{-6} wt%.

(2) After long-term corrosion test, the whole oxide layers of T91 steel and CLAM steel from exterior to interior are magnetite/spinel/internal oxidation zone, respectively. However, the oxide scales of 15-15Ti steel and 316L steel consisted mainly of a Fe-Cr spinel layer. The growth kinetics curves of oxide layers for T91, 15-15Ti, CLAM and 316L steels follow a parabolic rule ($\Delta x^2=K_p t$), and the rate constant for 15-15Ti steel is lowest.

(3) Si-contained stainless steel and ODS-9Cr steel has been developed. Compatibility evaluation revealed that the corrosion resistances of the above steels have attained considerable improvement.

ACKNOWLEDGEMENTS

This work was funded with the National Magnetic Confinement Fusion Science Program of China with Grant Nos. 2018YFE0312200, the National Natural Science Foundation of China (nos. 51401204 and51501185) and the Natural Science Foundation of Anhui Province of China (1708085QE96).

REFERENCES

[1] WU Y. Neutronics of Advanced Nuclear Systems[M]. Springer, 2019.

[2] WU Y., BAI Y., SONG Y., HUANG Q., ZHAO Z., HU L.. Development strategy and conceptual design of China Lead-based Research Reactor [J]. Annals of Nuclear Energy, 2016, 87: 511-516.

[3] WANG M, LIAN C, LI Y, ET AL. Preliminary conceptual design of a lead–bismuth cooled small reactor (CLEAR-SR) [J]. International Journal of Hydrogen Energy, 2015, 40(44): 15132-15136.

[4] ALEMBERTI, A., CARLSSON, J., MALAMBU, E., ORDEN, A., STRUWE, D., AGOSTINI, P., MONTI, S., European lead fast reactor-ELSY[J]. Nucl. Eng. Des. 241 (2011) 3470-3480.

[5] WEISENBURGER, A., SCHROER, C., JIANU, A., HEINZEL, A., KONYS, J., STEINER, H., MULLER, G., FAZIO, C., GESSI, A., BABAYAN, S., KOBZOVA, A., MARTINELLI, L., GINESTAR, K., BALBAUD-CELERIER, F., MARTIN-MUNOZ, F.J., CRESPO, L.S., Long term corrosion on T91 and AISI1 316L steel in flowing lead alloy and corrosion protection barrier development: Experiments and models [J]. J. Nucl. Mater. 415 (2011) 260-269.

[6] LIU, J., JIANG, Z., TIAN, S., HUANG, Q., LIU, Y., Stress corrosion behavior of T91 steel in static lead–bismuth eutectic at 480 oC [J]. J. Nucl. Mater. 468 (2016) 299-304.

[7] HEINZEL, A., WEISENBURGER, A., MÜLLER, G., Corrosion behavior of austenitic steels in liquid lead bismuth containing 10−6 wt% and 10−8 wt% oxygen at 400-500 °C [J]. J. Nucl. Mater. 448 (2014) 163-171.

[8] KURATA, Y., FUTAKAWA, M., SAITO, S., Corrosion behavior of steels in liquid lead – bismuth with low oxygen concentrations [J]. J. Nucl. Mater. 373 (2008) 164-178.

[9] SCHROER, C., VOSS, Z., WEDEMEYER, O., NOVOTNY, J., KONYS, J., Oxidation of steel T91 in flowing lead bismuth eutectic (LBE) at 550 °C [J]. J. Nucl. Mater. 356 (2006) 189-197.

[10] SCHROER, C., WEDEMEYER, O., NOVOTNY, J., SKRYPNIK, A., Performance of 9% Cr steels in flowing lead-bismuth eutectic at 450 and 550 oC, and 10−6 mass% dissolved oxygen [J]. J. Konys, Nucl. Eng. Des. 280 (2014) 661-672.
[11] BARBIER, F., ET AL. (2001). "Compatibility tests of steels in flowing liquid lead–bismuth." Journal of Nuclear Materials 295(2–3): 149-156.
[12] MULLER, G., ET AL. (2004). "Behavior of steels in flowing liquid pbbi eutectic alloy at 420-600 degrees c after 4000-7200 h." Journal of Nuclear Materials 335(2): 163-168.
[13] SCHROER, C., ET AL. (2011). "Long-term service of austenitic steel 1.4571 as a container material for flowing lead-bismuth eutectic." Journal of Nuclear Materials 418(1-3): 8-15.
[14] TIAN, S. J., ET AL. (2016). "Oxidation behavior of t91 steel in flowing oxygen-containing lead-bismuth eutectic at 500 degrees c." Materials and Corrosion-Werkstoffe Und Korrosion 67(12): 1274-1285.
[15] MÜLLER G, SCHUMACHER G, ZIMMERMANN F. Investigation on oxygen controlled liquid lead corrosion of surface treated steels [J]. J. Nucl. Mater. 2000, 278(1): 85-95.
[16] MARTINELLI L, BALBAUD-CÉLÉRIER F, TERLAIN A, ET AL. Oxidation mechanism of an Fe–9Cr–1Mo steel by liquid Pb–Bi eutectic alloy at 470°C (Part II) [J]. Corrosion Science, 2008, 50(9): 2537-2548.
[17] SHUJIAN T., 2016. Corrosion Behavior and Mechanism of T91 and 15-15Ti Steels in Liquid Lead-Bismuth Eutectic under Oxygen Control at 500 ℃. PhD Thesis, University of Science and Technology of China.
[18] LIANGLIANG S., 2018. Design and Property Analyses on Silicon-containing 9Cr-ODS Steels. PhD Thesis, University of Science and Technology of China.

DEVELOPMENT OF ALUMINA FORMING MATERIALS FOR CORROSION MITIGATION IN HEAVY LIQUID METAL COOLED NUCLEAR REACTORS

Alfons Weisenburger
Karlsruhe Institute of Technology, Institute for Pulsed Power and Microwave Technology
Herman-von-Helmholtz-Platz1, 76344 Eggenstein-Leopoldshafen, Germany
Email: Alfons.weisenburger@kit.edu

Adrian Jianu
Karlsruhe Institute of Technology, Institute for Pulsed Power and Microwave Technology
Herman-von-Helmholtz-Platz1, 76344 Eggenstein-Leopoldshafen, Germany

Annette Heinzel
Karlsruhe Institute of Technology, Institute for Pulsed Power and Microwave Technology
Herman-von-Helmholtz-Platz1, 76344 Eggenstein-Leopoldshafen, Germany

Hao Shi
Karlsruhe Institute of Technology, Institute for Pulsed Power and Microwave Technology
Herman-von-Helmholtz-Platz1, 76344 Eggenstein-Leopoldshafen, Germany

Sabine Schlabach
Karlsruhe Institute of Technology, Institute for Applied Materials
Herman-von-Helmholtz-Platz1, 76344 Eggenstein-Leopoldshafen, Germany

Vinga Szabo
Karlsruhe Institute of Technology, Institute for Applied Materials
Herman-von-Helmholtz-Platz1, 76344 Eggenstein-Leopoldshafen, Germany

Georg Müller
Karlsruhe Institute of Technology, Institute for Pulsed Power and Microwave Technology
Herman-von-Helmholtz-Platz1, 76344 Eggenstein-Leopoldshafen, Germany

Abstract

Liquid Pb and PbBi are promising coolants for nuclear reactors operating in fast neutron spectrum. Beside its excellent neutronic properties, Pb and PbBi offer improved safety features. But, deficient compatibility of structural materials with the heavy liquid metals (HLM) especially at higher temperatures is a major challenge to be solved for the use of Pb and PbBi as coolant or heat storage material.

The major driving force for corrosion attack is the solubility of steel alloying elements like Ni, Fe and Cr in the HLM. Addition of oxygen to the HLM to provide in-situ formation of protective oxide scales is the mitigation mechanism of choice, but in a limited operating temperature window of up to 500°C. To enlarge the operation window of HLM cooled nuclear reactors advanced mitigation measures are under investigation since several years. Alloying of strong oxide formers like Al into steel surfaces can shift the operating temperature window to 600°C and even higher. FeCrAlY surface layers and bulk

materials are one further option to increase the corrosion resistance in oxygen-containing liquid metals. Both methods rely on the in-situ oxidation capability of such material. Recently, new classes of bulk materials, alumina-forming austenitic steels (AFA) and alumina forming high entropy alloys (HEA), are investigated. The paper will briefly discuss the involved corrosion (dissolution and oxidation) mechanisms and will then focus on the advanced mitigation strategies that rely on in-situ alumina formation (surface alloying and mainly the new advanced alumina forming bulk materials (HEA and AFA) required for reliable long term operation at higher temperatures for HLM cooled fast reactors.

1. INTRODUCTION

To limit global warming, a transition to low-carbon economy by reducing the CO_2 footprint of electricity production is required. However, most of the renewable energy sources have no base-load capability and are intermittent, like wind and PV. Therefore, as a base load capable energy source with low CO_2 footprint, nuclear energy, which contributes 11% of the world's energy supply today will be part of the energy mix in the future [1-2].

The research and design of the new nuclear reactor generation ("Generation IV International Forum") targets highly improved safety standards in combination with higher temperatures and advanced heat transfer fluids. According to the "Generation IV International Forum", six new types of reactors, including gas-cooled fast reactor, lead cooled fast reactor, molten salts reactor, sodium-cooled fast reactor, supercritical water-cooled reactor (SCWR), and very high-temperature gas reactor (VHTR) are selected as the next generation reactor designs [3-4]. These systems often involve high temperature, mechanical loads and high irradiation doses (500-1000 °C, neutron dose: 10-150 dpa) [5]. The compatibility between the structural materials (e.g. container, pipes, heat exchanger, cladding materials) and these aggressive mediums, in particular the high corrosiveness at elevated temperatures, challenge their commercial applications [6-11]. Therefore, developing advanced materials is essential to improve the high temperature compatibility between structural materials and aggressive heat transfer fluids.

Alumina-forming alloys (e.g. Ni-based, Fe-based) have received a great attention for high temperature applications because of their excellent oxidation resistance and improved mechanical properties [12-15]. By adding appropriate concentrations of Al and Cr, the alloys can form protective alumina-rich oxide scale in oxygen containing environmental conditions. Ferritic FeCrAl alloys have been successfully developed for use in liquid Pb environment. However, ferritic steels as well as ferritic FeCrAl alloys suffer from liquid metal embrittlement in liquid Pb [16-17], while AFA not. The high entropy alloy concept, which was first reported in 2004, has attracted attention to many research groups [18-19]. These alloys contain five or more principle elements in equal or near-equal atomic ratio to form solid solutions. Some of these combinations show superior mechanical, physical properties in comparison with the traditional materials. Recently, the high entropy alloys are proposed as candidates for high temperature structural materials considering their excellent corrosion resistance, structural stability and mechanical properties [20-21]. This paper will give an overview on the recent work at Karlsruhe Institute of Technology to develop corrosion resistant materials for liquid Pb cooled nuclear reactors [22].

2. CORROSION OF METALLIC MATERIALS IN LEAD ALLOYS AT ELEVATED TEMPERTAURES

The corrosion of metallic materials in liquid lead at elevated temperatures is mainly driven by the dissolution of steel alloying elements [6, 9, 11]. The dissolution of Ni, Fe and Cr results in material loss and microstructural changes. The solubility of alloying elements in molten Pb is ordered as follows: Ni>Al>Cr>Fe. In addition, solubility is positive temperature dependant, which results in a significant increase of solubility with increasing temperature. Therefore, large temperature gradients in a cooling system will result in dissolution attack at the hot part and deposition of corrosion products at the cold parts [9]. Liquid Pb can penetrate inside the steel matrix through cracks and grain boundaries, which can significantly accelerate the crack growth rate under mechanical load [8, 23]. Corrosion in flowing condition (velocity > 2 m/s) above 500 °C can even be accelerated due to the shear and frictional stress acting on the surface, changing oxygen conditions, mass transport between the hot and cold part, and erosion attack [9, 24, 25]. To prevent steels from dissolution attack, the addition of an appropriate amount of oxygen is considered as a strategy to minimize dissolution attack in liquid Pb cooled nuclear systems by the formation of protective, compact and adherent oxide scales in-situ [26 – 28]. However, above 500 °C, commercial austenitic steels of 316 type do not form a protective oxide scale, even at oxygen conditions that are sufficient for magnetite formation [6, 9]. Especially localized dissolution attack mainly at grain boundaries, imperfections and impurities are of concern. Use of austenitic steels in Pb at temperatures above 500 °C will result in dissolution attack, mainly dissolution of Ni, and phase transformation in the attacked surface region [6, 9]. Alumina forming austenitic steels were first developed at KTH and showed their potential of being one possible solution for advanced corrosion mitigation [29].

3. ADVANCED MITIGATION STRATEGIES

Several advanced corrosion mitigation strategies were developed at KIT based on the in-situ formation of thin protective Al_2O_3 rich oxide scale. The activities were started several years ago by introducing the concept of surface alloying of existing fuel cladding materials with Al containing alloys and enlarged over the years to alumina-forming bulk materials (AFA) and alumina-forming high entropy alloys (HEA).

3.1. **Surface alloying**

The development of new fuel cladding materials is a time and resource consuming process. To shorten this, a surface alloying process of qualified cladding tubes with alloys that can form in-situ protective Al_2O_3 scales was developed at KIT [30, 31]. The process consists of two major process steps. The first one is applying a dedicated coating followed by the 2nd step the alloying of this coating into the substrate without altering the general mechanical properties of the underlying fuel cladding material. The coating consists usually of a Fe-base alloy in composition similar to ferritic or also austenitic steel with the addition of Al and preferably also minor additions of reactive elements like Y or Zr. It is advised that the coating is oxygen free and stay in the range of the re-melting capabilities regarding the depth of the used GESA (Gepulste Elektronenstrahl Anlage)/pulsed electron beam facility) facility, which limits the thickness to 20 to 30 µm. The surface alloying is achieved by the pulsed electron beam facility GESA that allows by applying pulsed electron beams of 120keV for about 60 µs to alloy such coatings into the bulk substrate surface.

3.2. **AFA – alumina forming austenitic steels**

It is advisable that the design of AFA alloys consider the influence of the alloying elements on the structure and phase stability and the oxide scale formation. Al e.g. act as ferrite stabilizer and alumina layer former, Cr as ferrite stabilizer, chromia layer former and provider of the third-element effect, and Ni as an austenite stabilizer.

For a 1st generation of AFA steels [10] an Al concentration ranging between 2 and 4 wt.% was selected to ensure the formation of protective alumina scales and to avoid excessive ferrite formation and alloy embrittlement. Cr was varied between 12 and 16 wt. % to search for a strong third element effect on the alumina formation and to limit the formation of ferrite and Cr-rich phases. The Ni addition was varied between 20 and 29 wt.% to stabilize the austenite at the exposure temperature range and to limit its amount due to its high solubility in molten Pb and the high costs. Based on the corrosion results of this first generation, in a 2nd development step Y and Nb was added to prove their described positive effects on alumina scale formation and Laves phase formation, that can act as high temperature strengthening phase (Table 1).

TABLE 1. AFA OF 2ND GENERATION - DESIGN COMPOSITION AND MEASURED COMPOSITION

Code	Nominal Composition	*Al*	*Cr*	*Ni*	*Nb*	Y	Fe
AFA70	Fe-14Cr-2.5Al-18Ni-0.5Y	2.7	14.7	17.9	---	0.4	Balance
AFA71	Fe-15Cr-2.5Al-20Ni-0.5Y	2.5	15.4	19.9	---	0.5	Balance
AFA72	Fe-16Cr-2.5Al-22Ni-0.5Y	2.5	15.4	21.8	---	0.5	Balance
AFA73	Fe-15Cr-2Al-20Ni-0.5Y-1.5Nb	2.1	15.4	22.0	1.3	0.5	Balance
AFA74	Fe-15Cr-3Al-29Ni-0.5Y-1.5Nb	4.3	15.5	27.9	1.1	0.5	Balance
AFA75	Fe-16Cr-3Al-24Ni-0.5Y-1.5Nb	3.1	15.5	24.1	1.7	0.7	Balance

Phase-stability diagrams at 550°C and 600°C for the Fe-12Cr-xAl-yNi, Fe-14Cr-xAl-yNi, Fe-15Cr-xAl-yNi and Fe-16Cr-xAl-yNi +Y and Nb systems are calculated using the commercial software Thermo-Calc (TCFE7 database). As an example, the coordinates of the 2nd generation AFA alloys (Y and Nb addition) at 600°C are shown in Fig. 1-1. The calculated values of the selected alloy compositions are close to the separation lines between the stability domains of the austenite (γ) and austenite plus ferrit e(γ+α). The figure contains also the point corresponding to 316 austenitic stainless steel, which is located very close to the separation lines of γ and γ+α phases.

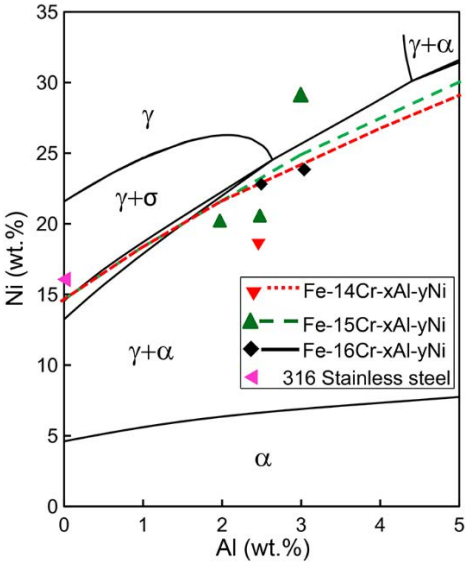

FIG. 1-1. Phase diagram of Fe-(14-16) Cr-(2-3) Al-(18-29) Ni-0.5Y-(1.5Nb) with the coordinates of the 2ndgeneration AFA model alloys, ▼ – AFA70; ▲- AFA71, AFA73, AFA74; ◆– AFA72, AFA75; ◄ - 316

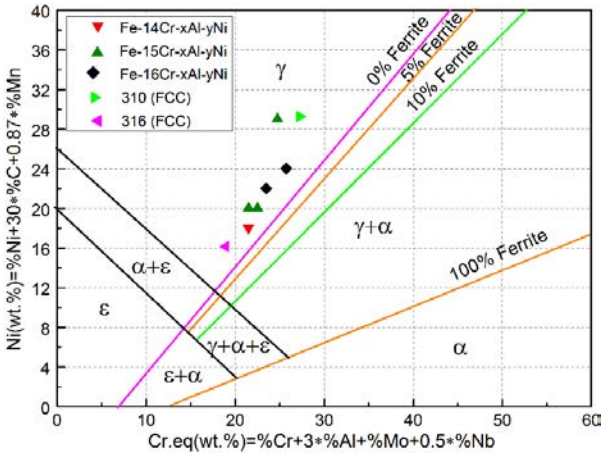

FIG. 1-2. Schaeffler constitution diagram including the coordinates of the Fe-Cr-Al-Ni-Y-Nb model alloys and two references: stainless steels AlSI 310 and AlSI 316 (γ- austenite, α - ferrite, ε - martensite)

The empirical Schaeffler diagram, which is developed by stainless steel industry to estimate the types of structural phases and their amounts as a function of the chemical composition of the steels allows a rough evaluation of the phase constitution of the stainless steels at ambient temperature, following the water cooling from liquid phase or from austenite domain (>1200 °C) . Figures 1-2 depicts the Schaeffler diagram where all the 2nd generation of the AFA model alloys should have an austenite structure at room temperature. The two commercial austenitic stainless steels (AISI 310 and AISI 316) are also marked in the diagram for comparison.

The alloys were produced using pure metal powder in an arc melter, followed by an annealing process in inert atmosphere and further quenching in a water bath. The X-ray diffraction pattern of the as produced AFA all show only austenitic phase (Fig. 2-1) with a grain size in the order of several 100 µm (Fig 2-2).

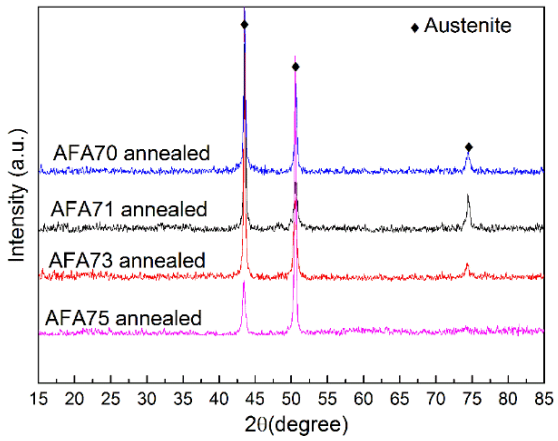

FIG. 2-1. Representative XRD patterns of AFA-2nd generation samples after annealing at 1250 °C for 2 h

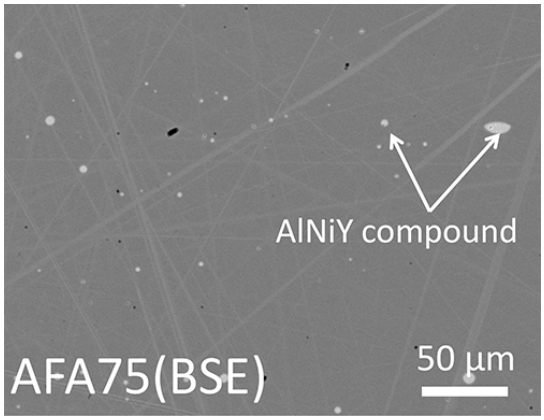

FIG. 2-2. Examples of microstructures of AFA-2nd generation alloys after annealing at 1250 °C for 2 h

3.3. **HEA – Alumina forming High Entropy Alloys**

The design of HEA focuses on several basic requirements: the corrosion resistance in molten Pb, stable FCC (face-centered cubic) structure, excellent high-temperature thermo-physical and mechanical properties, competitive costs, raw materials availability and to be made from low activation elements. However, not only single-phase FCC HEA, also dual-phase HEA (DP-HEA), which use solid solution strengthening by secondary phase precipitation like NiAl (B2 phase), L12-Ni3(AlTi) (γ' phase) and Fe2Nb (Laves phase) were considered. Based on these requirements the following seven elements are selected: **Al, Cr, Ni, Fe,** Nb, Ti, and Cu. The first four elements selected are also the basis for the AFA alloys.

To minimize the number of trial-and-error experiments, some empirical parameters have been applied to predict the formation of solid solution and intermetallic compounds; the enthalpy of mixing (ΔHmix), the difference in atomic radii (δr), the parameter $\Omega = \frac{\sum_i^n c_i Tm_i \cdot \Delta Smix}{|\Delta Hmix|}$ [32, 33], and the valence electron concentration (VEC). *VEC* can be used to quantitatively predict the stability of the solid-solutions with FCC and BCC (body-centered cubic) structures, formed in high-entropy alloys [34].

Six quaternary Al-Cr- Fe-Ni-based and three quinary Al-Cr-Fe-Ni-(Nb, Ti, Cu)-based high-entropy alloys were prepared by fulfilling the critical values of the following criteria: Number of alloy constituents: more than four principal elements; Element concentration between 5 and 35 at.%, -15 kJ/mol < $\Delta Hmix$ < 5 kJ/mol; 1% < δr < 6.6%; Ω > 1.1; VEC > 7.5. Multielement alloys can be considered as HEA if the Ω is above 1.1 [32].

The concentration of Al, which due to a VEC_{Al} = 3 may promote the formation of the BCC solid solution, was selected between ~6 and ~12 at. % to keep the VEC>7.5. The concentration of Nb (VEC_{Nb} = 5) and Ti (VEC_{Ti} = 4) was set at around 5 at.%. Cu (VEC_{Cu} = 11) stabilizes the FCC structure and shows a positive enthalpy of mixing with the other selected elements, except Al. Table 2 shows the design alloy compositions and their parameters values of $\Delta Hmix$, δr, VEC and Ω.

TABLE 2. DESIGN OF CANDIDATE HEA AND THEIR CORRESPONDING Δ*HMIX, VEC*, *ΔR, Ω*, AND PREDICTED PHASE.

Code	*Composition in at %*	Δ*Hmix*	*VEC*	*Δr*	*Ω*	Predicted Phase
HEA1	Al9.9Cr31.1Fe31.1Ni28.0	-8.62	7.56	4.44	2.28	SS+IM
HEA2	Al10.1Cr22.8Fe33.6Ni33.6	-8.29	7.75	4.41	2.31	SS+IM
HEA3	Al8.8Cr23.1Fe34.0Ni34.0	-7.87	7.76	4.22	2.43	SS+IM
HEA4	Al11.8Cr22.4Fe32.9Ni32.9	-8.87	7.62	4.74	2.18	SS+IM
HEA5	Al6.2Cr25.3Fe34.2Ni34.2	-6.84	7.89	3.54	2.76	SS (FCC)
HEA6	Al7.9Cr23.4Fe34.4Ni34.4	-7.55	7.85	4.02	2.52	SS (FCC)
HEA7	Al8.3Cr20.7Fe31Ni34.5Nb5.5	-10.92	7.71	4.83	1.98	SS+IM
HEA8	Al8.1Cr22.3Fe32.3Ni32.2Ti5.2	-11.18	7.62	5.27	1.89	SS+IM
HEA9	Al8.1Cr22.3Fe32.3Ni32.3Cu5.2	-5.45	7.95	4.02	3.82	SS (FCC)

SS - solid solution, IM - inter metallic, FCC – face centered cubic.

As described for the AFA alloys, the HEA were manufactured using pure metallic powders that are alloyed in an Arc-melter in some tens of gram. The HEA alloys were used in as cast state without any further heat treatment. The microstructure and the phase composition were revealed by SEM cross sections and XRD and is exemplarily shown in Fig. 3 and Fig. 4 and proves the phases as predicted mainly. XRD of HEA 7 shows that the dendrites (D in Fig. 3) are the FCC matrix phase and the inter-dendrites (ID in Fig. 3) are the Laves phase.

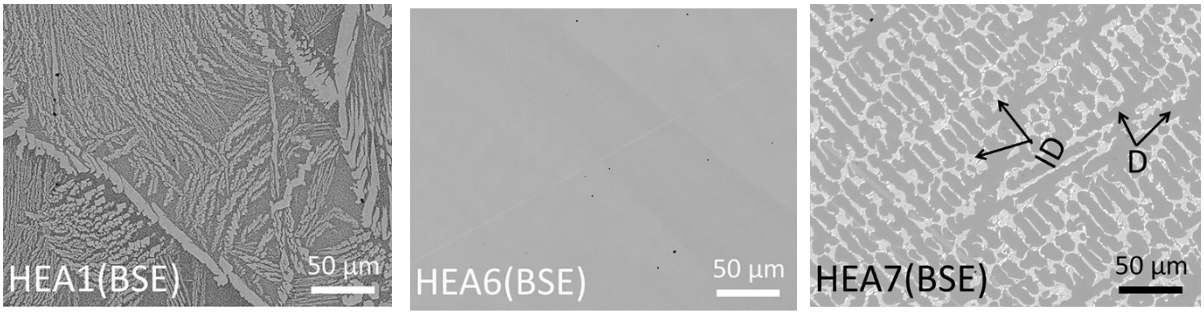

FIG. 3. SEM cross sections of as produced HEA showing the microstructure of the as produced HEA

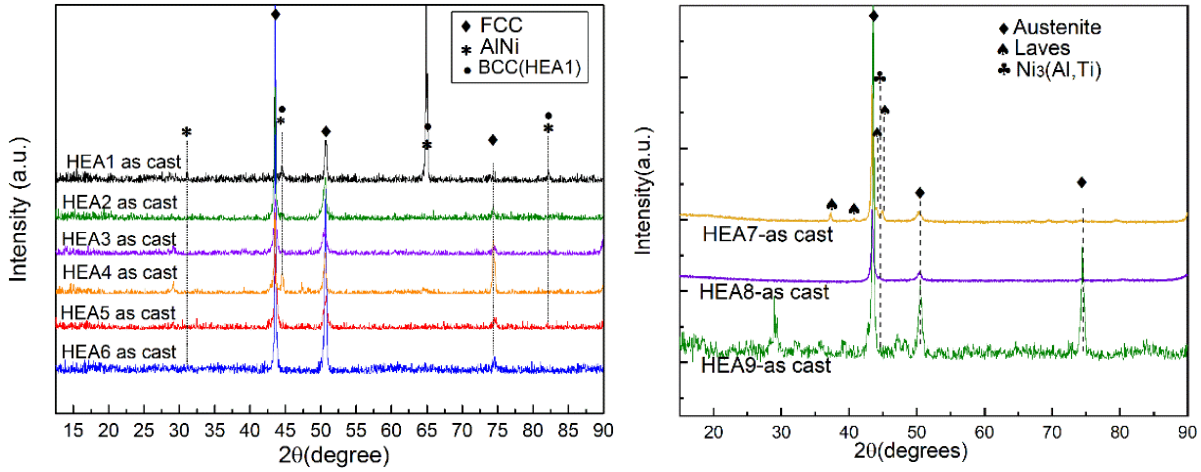

FIG. 4. XRD of HEA alloys after production in as cast state showing the different phases observed. Left: quaternary HEA, right: quinary HEA.

3.4. **Corrosion tests – Set-up and conditions**

The compatibility of the three different approaches with oxygen containing liquid Pb were all tested in the COSTA facilities at different temperatures at stagnant conditions [28]. Oxygen control was performed via the gas phase and the oxygen content of the furnace leaving gas was constantly monitored. The surface alloyed specimens based on FeCrAl+RE were tested in the last years in a large variety of temperatures from 450 to 650°C and oxygen contents between $<10^{-8}$ and 10^{-5} wt%. AFA steels of 1st generation and the HEA alloys are tested at two different temperatures (550°C and 600°C) in oxygen containing liquid Pb with 10^{-6} wt% oxygen addition for 1000h. AFA alloys of the 2nd generation containing Y and Nb were exposed to Pb with 10^{-6} wt% oxygen at 600°C for 1000h and 2000h.

4. RESULTS AND DISCUSSION

4.1. **GESA FeCrAl-surface alloys**

Corrosion tests for up to 10 000h in Pb with 10^{-6} wt% oxygen at 500°C and 600°C (Fig.5) showed formation of protective oxides scales. Depending on the concentration of Cr and Al thin protective oxide scale can be formed in a temperature range between 450 °C and 650°C [15].

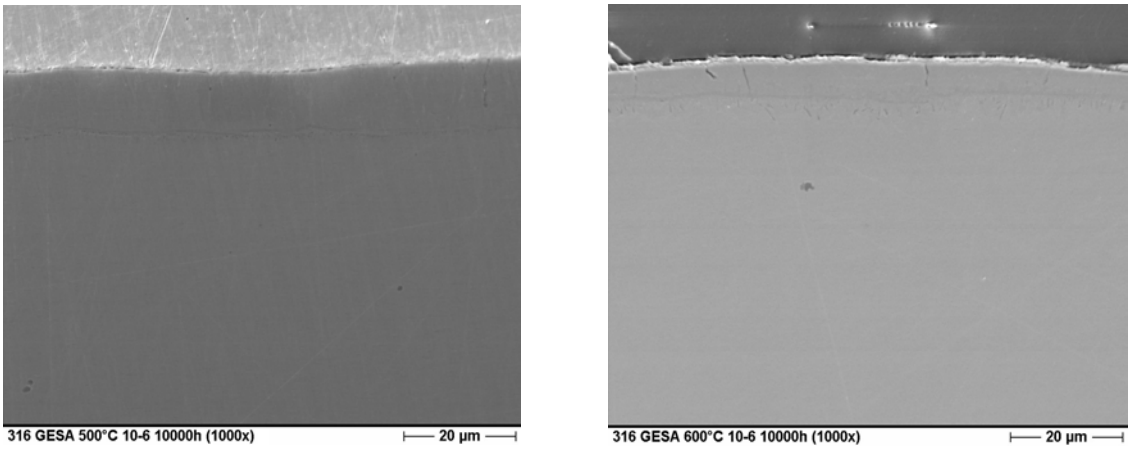

Fig. 5. Cross sections of FeCrAl surface alloyed 316 type steel after exposure to Pb for 10 000h. Left at 500°C and right at 600°C. Both specimens are protected against any attack by a thin alumina rich scale.

4.2. **AFA alloys after corrosion test**

At 550°C eight alloys with Cr content higher than 14 wt.% and at 600°C six of the AFA alloys with 15 wt.% Cr and 16 wt.% Cr are protected by oxide scales with a thickness of 100-200 nm. An outer scale consisting of Cr_2O_3 and an inner layer of Cr_2O_3-Al_2O_3 solid solution covers most of the surface while some spots of magnetite (<2%) were developed as well. On all the specimens a transitional layer (1-3µm thick with decreased Ni content) having B2(NiAl) and BCC solid solution precipitates was formed. The number of precipitates was slightly higher at 600°C exposed specimens compared with the same alloy exposed at 550 °C.

All AFA-2nd generation alloys have formed protective oxide scales after 2000h in oxygen containing molten Pb at 600 °C, after 1000h one alloy (AFA 72) exhibits oxide scale spallation after 1000h of exposure. Like the AFA without Y and Nb the oxide scales have a thickness lower than 200 nm that is based on Cr_2O_3 and Cr_2O_3- Al_2O_3 solid solution. The addition of Y homogenizes the distributions of Al and Cr in the oxide scale. Some spots of magnetite are formed in the vicinity of YNiAl-rich precipitates that are depleted in Al and Ni. Underneath the scale a Fe-, Ni-rich transitional layer, with a thickness of 0.5-2 µm has formed during the corrosion tests. Some B2 and Fe-, Cr-rich precipitates can be observed in the transitional layer of all samples (Fig. 6). XRD patterns of BCC originating from B2 and Fe-, Cr-rich precipitates become less prominent compared with the first generation AFA alloys. In case of Nb containing samples, the bright Laves particles coherent with B2 precipitates are also observed in the transitional layer.

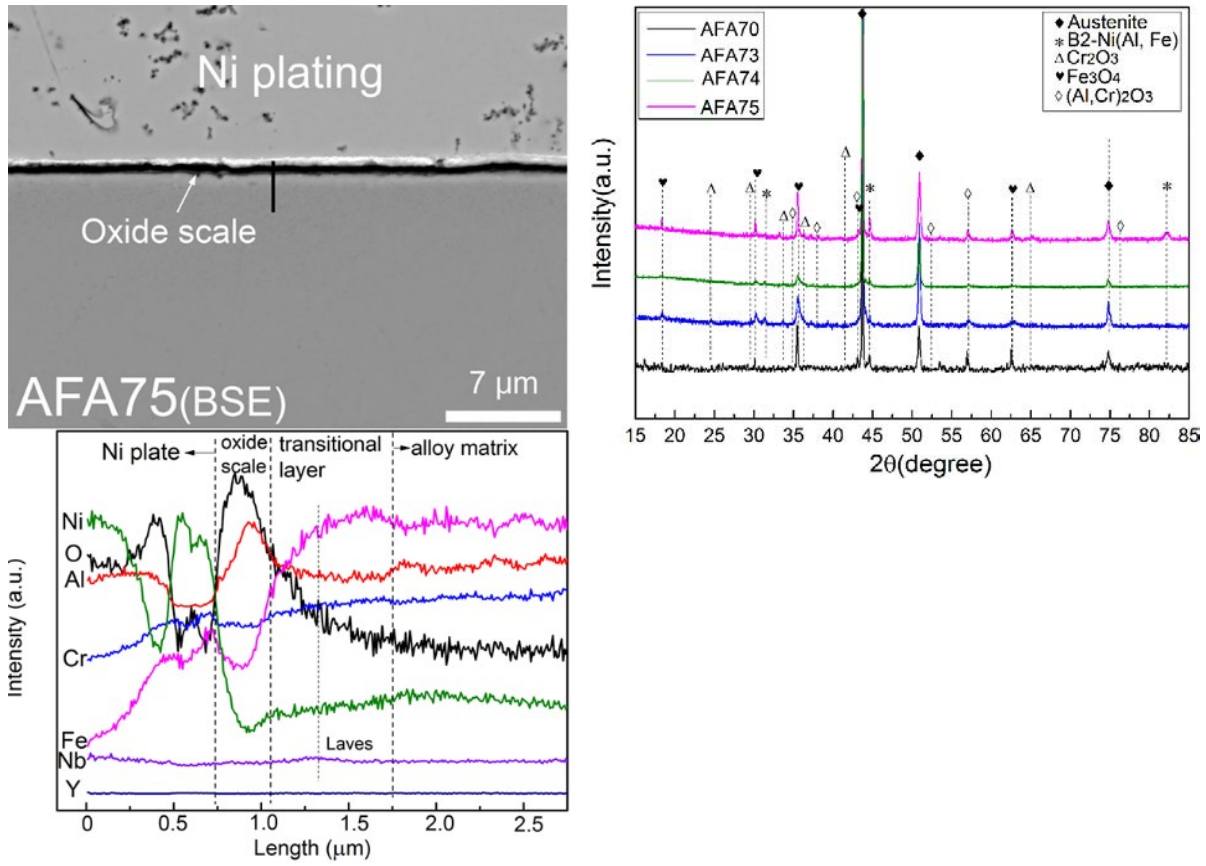

FIG. 6. left: SEM cross section and EDS line scans of AFA-2nd generation sample after 2000 h exposure to 10^{-6} wt.% oxygen containing molten Pb at 600 °C. right: XRD patterns of AFA-2nd generation samples after 2000 h exposure to 10^{-6} wt.% oxygen containing molten Pb at 600 °C.

Poly- and nano-crystalline oxides are observed in the scale after 2000 h corrosion test in low oxygen containing molten Pb using TEM investigation of AFA75 (Fe-15.7Cr-3.1Al-24.1Ni-0.7Y-1.68Nb). The thickness of the oxide scale is around 100 nm (Fig. 7-1). Nano-size grains of B2-NiAl (300-500 nm) and Laves (< 50 nm) phases in addition to the austenitic matrix are detected using TEM-EDS mapping and line scanning of the alloy matrix (Fig. 7-2).

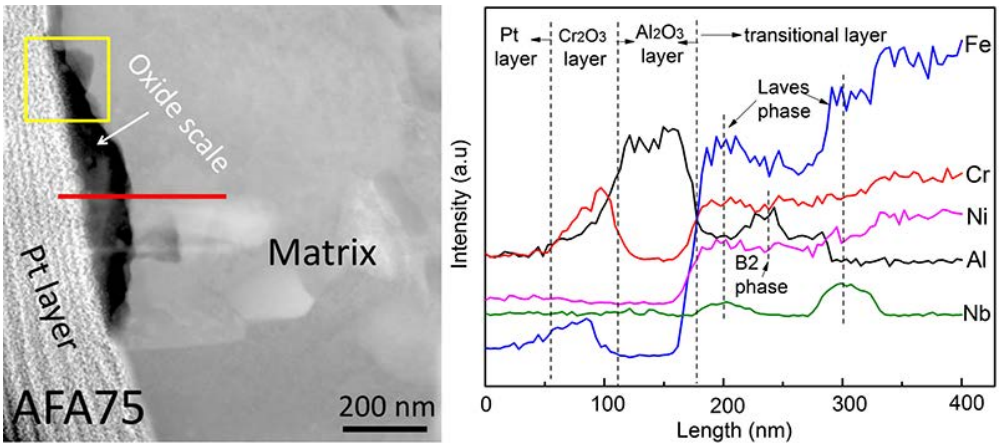

FIG. 7-1. STEM-image (left) and STEM-EDS line profile (right) of the cross section of the oxide scale formed on AFA75 after 2000 h exposure to 10^{-6} wt.% oxygen containing molten Pb at 600 °C.

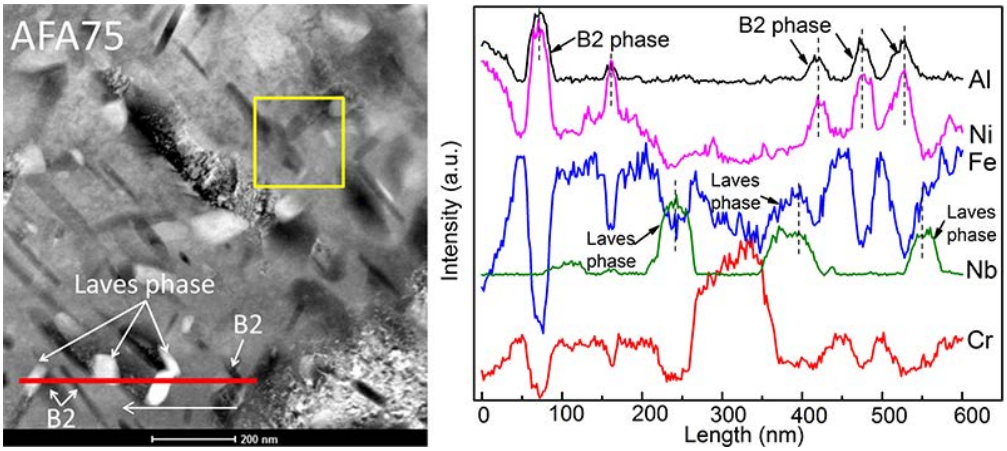

FIG. 7-2. STEM-image (left) and STEM-EDS line profiles (right) of the matrix of AFA75 after 2000 h exposure to 10-6 wt.% oxygen containing molten Pb at 600 °C.

4.3. **HEA alloys after corrosion test**

The four quaternary HEA alloys with dual-phase (HEA1, HEA2, HEA3 and HEA4) are all corrosion resistant to molten Pb at 550 °C and 600 °C for at least 1000 h. HEA2, HEA3 and HEA4 formed Cr_2O_3 and Cr_2O_3-Al_2O_3 solid solutions scales after 1000 h exposure in oxygen containing molten Pb at 550 °C and 600 °C. In addition, a discontinuous transitional layer was observed underneath the oxide scale after exposure at 550 °C but not at 600°C. Some dark precipitates enriched in Al and Ni and others enriched in Fe and Cr have been found in this transitional layer. HEA1 (see Fig. 8), with highest Cr content, formed at most of the surface a continuous thin layer (<200nm) of Cr_2O_3-Al_2O_3 solid solution, while at some part's thicker layers (400 to 700 nm) above the thin layer are observed. The thick oxide scale consists of (Fe, Cr)$_3O_4$. Both quaternary HEA alloys with single FCC phase (HEA5 (Fig. 8) and HEA6 (not shown in figure) are also corrosion resistant in oxygen containing molten Pb after 1000 h exposure at 550 °C and 600 °C. On both samples the oxide scales formed consist of Cr_2O_3 and

Cr_2O_3-Al_2O_3 solid solutions. A quasi-continuous transitional layer is observed on both samples after corrosion tests at 550 °C and 600 °C with some dark precipitates enriched in Al and Ni and others enriched in Cr and Fe. Two of the three quinary HEA alloys, the two dual-phase (HEA7, HEA8), formed stable protective oxide scales while the single phase (HEA9 with Cu)) exhibit oxide scale spallation without any sign of dissolution attack. Sample HEA7 (Fig. 9) with Nb formed a continuous oxide scale consisting Cr_2O_3 and α-Al_2O_3 at 550 °C, and α-Al_2O_3 at 600 °C. At 550 °C the thickness of the oxide scale formed is around 200 nm, while the thickness of the layer formed at 600 °C is 150 nm. Moreover, a dis-continuous transitional layer with some dark precipitates is underneath the oxide scale, at the Laves-phase free regions after exposure tests at 550 °C and 600 °C. The addition of Ti in HEA8 leads to the formation of an outer oxide layer of Cr_2O_3 and TiO_2, and an inner layer of $(Al, Cr)_2O_3$ at both temperatures.

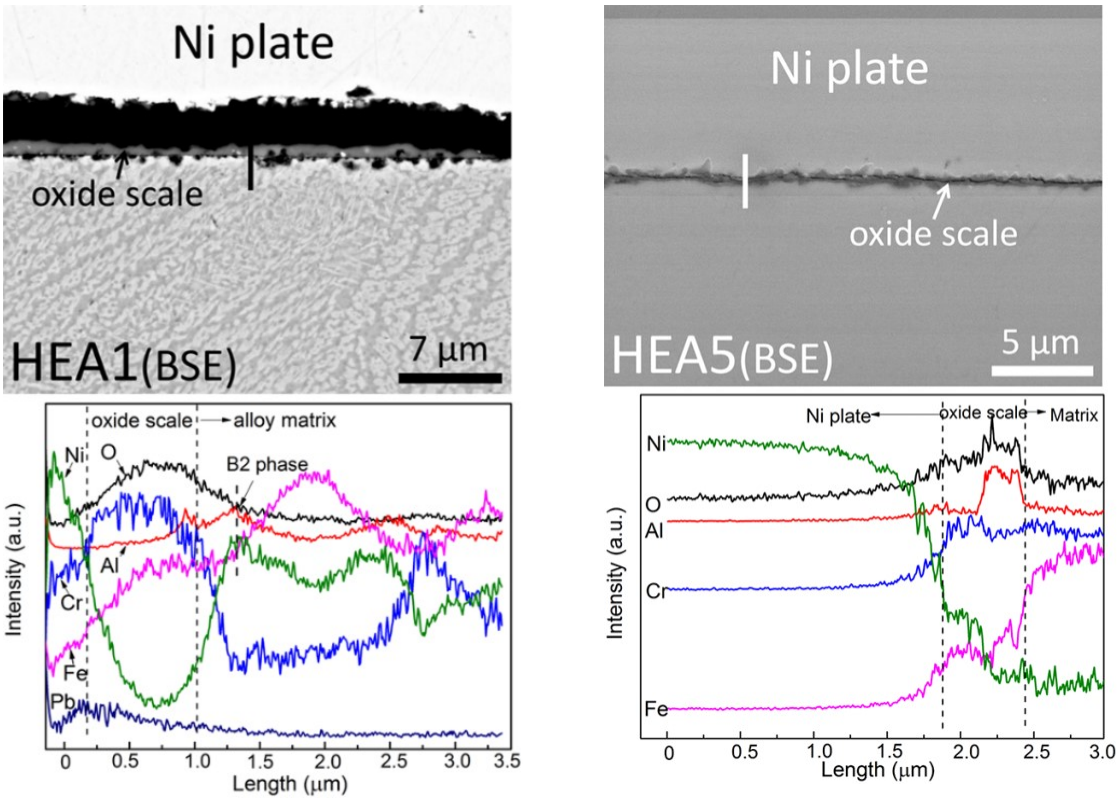

FIG. 8. EDS line scans of the cross sections of HEA1 and HEA5 after 1000 h exposure to 10^{-6} wt.% oxygen containing molten Pb at 600 °C.

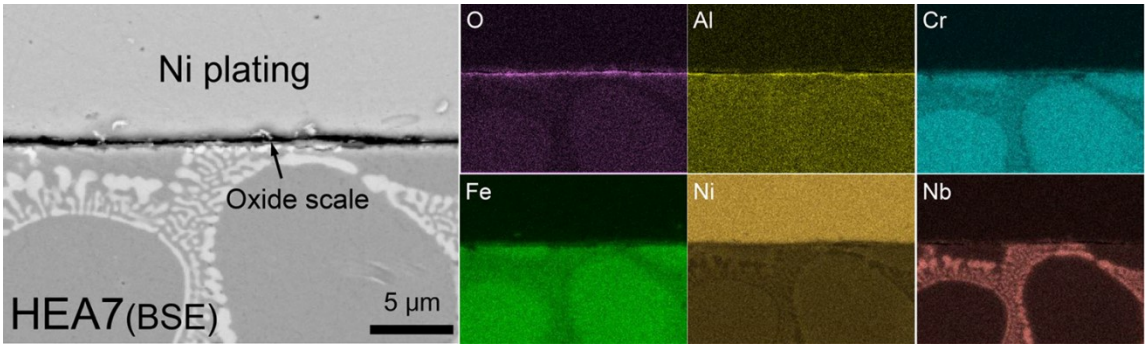

FIG. 9. SEM cross section and EDS mapping of HEA7 after 1000 h exposure to 10^{-6} wt.% oxygen containing molten Pb at 600 °C.

To investigate the structural stability the alloys matrix of all samples after the 1000 h exposure tests at 550 °C and 600 °C have been analyzed in comparing with the as-cast samples (table 3). According to the applied analysis, HEA1, HEA2, HEA4 and HEA7 maintain the phase compositions and microstructure stability after 1000 h exposure in 10^{-6} wt.% oxygen-containing molten Pb at 550 °C and 600 °C. HEA3 (at 550 °C) and HEA6 (at 550 °C) exhibit composition fluctuations by forming bright network structures in the alloy matrix after 1000 h exposure tests. HEA3, HEA5 and HEA6 formed B2(NiAl) precipitates at the grain boundaries. HEA8 alloyed with Ti undergoes phase transformations during the corrosion test at both 550 °C and 600 °C from FCC to sigma phase and from γ′ to η phase.

TABLE 3. PHASE EVALUATION OF HEA SAMPLES AFTER 1000 H EXPOSURE IN 10^{-6} WT.% OXYGEN CONTAINING MOLTEN PB AT 550 °C AND 600 °C

Code	Phase transformation	Second phase formation
HEA1	N	N
HEA2	N	N
HEA3	N	Y (at 600 °C)
HEA4	N	N
HEA5	N	Y
HEA6	N	Y (at 600 °C)
HEA7	N	N
HEA8	Y	Y

N: No; Y: Yes.

5. SUMMARY AND OUTLOOK

AFA and HEA model alloys, based on the backbone composition of Fe-Ni-Cr-Al are designed to search for the composition map of target materials that are compatible with molten Pb. AFA model alloys based on Fe-(20-29) Ni-(12-16) Cr-(2-4) Al (in wt.%) have been designed based on equilibrium phase calculations (Thermo-Calc) and the Schaeffler diagram. All the annealed alloys are single FCC phase. Nine alumina forming HEA alloys have been designed based on empirical parameters, including mixed enthalpy (ΔHmix), atomic size difference (δr), parameter Ω ((ΣciTm,i)ΔSmix/|ΔHmix|) and valance electron concentration (VEC). The designed alloys include four quaternary alloys with dual phase ($Al_{(0.26\text{-}0.36)}Cr_{(0.68\text{-}1)}FeNi_{(0.9\text{-}1)}$, FCC+B2 or BCC), two quaternary alloys with single FCC phase ($Al_{0.18\text{-}0.23}Cr_{0.68\text{-}0.74}FeNi$), and three quinary alloys alloyed with Nb/Ti/Cu ($Al_{0.24\text{-}0.25}Cr_{0.6\text{-}0.69}Fe_{0.9\text{-}1}NiNb_{0.15}/Ti_{0.16}/Cu_{0.16}$, FCC+Laves or γ' phase and single FCC).

Compatibility tests were performed in 10^{-6} wt.% oxygen containing molten Pb at 550 °C and 600 °C for 1000 h and 2000 h. The excellent corrosion resistance the AFA alloys to low oxygen containing molten Pb conditions is due to the formation of a protective oxide scale (<200 nm) based on an outer layer of Cr_2O_3 and an inner layer of Cr_2O_3-Al_2O_3 solid solutions. By adding yttrium, the uniformity in scale thickness and in Al and Cr distribution has been improved. In case of Nb containing samples, TEM evaluation of the alloy matrix indicates the formation of B2 (NiAl) and Laves (Fe_2Nb) phases in addition to the austenite phase. The mechanism of the oxide layer passivation on HEA alloys is almost identical to that of the AFA alloys. A continuous oxide scale based on Cr_2O_3 or $(Fe, Cr)_3O_4$ (in case of BCC phase) or TiO_2 (HEA alloyed with Ti), which acts as a first corrosion barrier, has formed before the formation of continuous alumina-rich scale. Then, alloys with sufficient Al addition form a protective oxide scale underneath the first corrosion barrier, based on oxides of Cr_2O_3-Al_2O_3 solid solution

(corundum structure) or α-Al_2O_3. Four HEA model alloys have shown their microstructure stabilities during exposure in low oxygen containing molten Pb at 550-600 °C. Three HEA alloys show precipitations of B2(NiAl) phases at the grain boundaries. Sample with Ti addition exhibits phase transformations, namely FCC→sigma and γ′→η phase.

Considering both test environments, a general formula of AFA alloys that are compatible with oxygen containing Pb at 550-600 °C can be given: Fe-(20-29) Ni-(15.2-16.5) Cr-(2.3-4.3) Al (wt.%). HEA alloys based on the backbone composition of Fe-Ni-Cr-Al, that are chemical compatible with oxygen containing molten Pb at 550-600 °C, and that are maintaining the FCC structure in the matrix, are defined as: (30.3-34.5)Fe-(32.6-35)Ni-(21.3-23.8)Cr-(6-11.7)Al (at.%). Elements like Nb or Y either act as a principle element (Nb in HEA) or as minor additions (AFA) can have a positive effect on the alumina scale formation in molten lead at elevated temperatures.

For further improvement of these alloys, small amounts of additional elements will be added to the base formula of AFA alloys to further optimize the properties, like stabilizing the austenitic structure (C, Mn, Cu), and improving the mechanical properties (Nb, Ti, W, Mo, B), and increasing the scale adherence (Y). It is advised to perform the long-term (>2000 h) corrosion test of optimized AFA alloys in stagnant and flowing molten Pb conditions to investigate the alumina scale durability in extreme conditions. Testing the mechanical properties (e.g. creep resistance, fatigue, strength-ductility) of AFA and HEA and exploring their weldability are the next steps in the development of these materials. Additionally, the irradiation behavior of AFA alloys is also essential to be known in case of nuclear applications. First AFA alloys will be irradiated in Petten reactor in the frame of the H2020 project GEMMA.

ACKNOWLEDGEMENTS

This work was supported by the Helmholtz program NUSAFE at the Karlsruhe Institute of Technology and has been carried out partially in the frame of EERA Point Programme of Nuclear Materials, partly funded by the European Commission HORIZON 2020 Framework Programme under grant agreement No. 755269. Hao Shi appreciates the PhD fellowship supported by the China Scholarship Council (CSC No. 201506230151).

REFERENCES

[1] Global energy statistical yearbook 2018. https://yearbook.enerdata.net.

[2] BP energy outlook-2018. https://www.bp.com/content/dam/bp-country/de_ch/PDF/Energy- Outlook-2018-edition-Booklet.pdf.

[3] IRSN, Overview of Generation IV (Gen IV) Reactor Designs, https://www.irsn.fr/EN/Research/ publications-documentation/Scientific-books/Documents/GENIV_texte_VA_241012a.pdf.

[4] LOCATELLI, G., MANCINI, M., TODESCHINI, N., Generation IV nuclear reactors: Current status and future prospects, Energy Policy. 61 (2013) 1503-1520.

[5] SARVGHAD, M., MAHER, S.D., COLLARD, D., TASSAN, M., WILL, G., STEINBERG, T.A., Materials compatibility for the next generation of Concentrated Solar Power plants, Energy Storage Materials. 14 (2018) 179-198.

[6] FAZIO, C., SOBOLEV, V.P., AERTS, A., GAVRILOV, S., LAMBRINOU, K., SCHUURMANS, P., GESSI, A., AGOSTINI, P., CIAMPICHETTI, A., MARTINELLI, L., GOSSE, S., Handbook on lead-bismuth eutectic alloy and lead properties, materials compatibility, thermal-hydraulics and technologies-2015 edition (No. NEA--7268). Organisation for Economic Co-Operation and Development. 2015.

[7] ASHER, R.C., DAVIES, D., BEETHAM, S.A., Some observations on the compatibility of structural materials with molten lead, Corrosion Science. 17 (1977) 545-557.

[8] JIANU, A., MÜLLER, G., WEISENBURGER, A., HEINZEL, A., FAZIO, C., MARKOV, V.G., KASHTANOV, A.D., Creep-to-rupture tests of T91 steel in flowing Pb–Bi eutectic melt at 550 C, Journal of nuclear materials. 394 (2009) 102-108.
[9] WEISENBURGER, A., SCHROER, C., JIANU, A., HEINZEL, A., KONYS, J., STEINER, H., MÜLLER, G., FAZIO, C., GESSI, A., BABAYAN, S., KOBZOVA, A., Long term corrosion on T91 and AISI1 316L steel in flowing lead alloy and corrosion protection barrier development: Experiments and models, Journal of Nuclear Materials. 415 (2011) 260-269.
[10] SHI, H., JIANU, A., WEISENBURGER A., TANG C.C., FETZER R., HEINZEL A., LANG F., STIEGLITZ R., MUELLER G., Corrosion resistance and microstructural stability of austenitic Fe-Cr-Al-Ni model alloys exposed to oxygen-containing molten lead, Journal of Nuclear Materials. 524 (2019) 177-190.
[11] WEEKS, J. R. Corrosion of steam generator tubing in operating pressurized water reactors (No. BNL-19158; CONF-741013-2). USAEC Directorate of Licensing, Washington, DC. 1974. AUTHOR, A., Book Title in Title Case, Series No. if applicable, Publisher, Place of Publication (Year).
[12] WALLWORK, G.R., The oxidation of alloys, Reports on Progress in Physics. 39 (1976) 401.
[13] YAMAMOTO, Y., BRADY, M. P., LU, Z. P., MAZIASZ, P. J., LIU, C. T., PINT, B. A., MORE, K.L., MEYER, H.M., PAYZANT, E. A, Creep-resistant, Al2O3-forming austenitic stainless steels, Science. 316 (2007) 433-436.
[14] PINT, B.A., The future of alumina-forming alloys: challenges and applications for power generation, In Materials Science Forum, Trans Tech Publications. 696 (2011) 57-62.
[15] WEISENBURGER, A., JIANU, A., DOYLE, S., BRUNS, M., FETZER, R., HEINZEL, A., DELGIACCO, M., AN, W., MÜLLER, G., Oxide scales formed on Fe–Cr–Al-based model alloys exposed to oxygen containing molten lead, Journal of Nuclear Materials. 437 (2013) 282-292.
[16] VAN DEN BOSCH, J., BOSCH, R.W., SAPUNDJIEV, D., ALMAZOUZI, A., Liquid metal embrittlement susceptibility of ferritic–martensitic steel in liquid lead alloys, Journal of Nuclear Materials. 376 (2008) 322-329.
[17] KOBAYASHI, S., TAKASUGI, T., Mapping of 475 C embrittlement in ferritic Fe–Cr–Al alloys, Scripta Materialia. 63 (2010) 1104-1107.
[18] YEH, J.W., CHEN, S.K., LIN, S.J., GAN, J.Y., CHIN, T.S., SHUN, T.T., TSAU, C.H., CHANG, S.Y., Nanostructured high-entropy alloys with multiple principal elements: novel alloy design concepts and outcomes, Advanced Engineering Materials. 6 (2004) 299-303.
[19] CANTOR, B., CHANG, I.T.H., KNIGHT, P., VINCENT, A.J.B., Microstructural development in equiatomic multicomponent alloys, Materials Science and Engineering: A. 375 (2004) 213-218.
[20] MIRACLE, D., MILLER, J., SENKOV, O., WOODWARD, C., UCHIC, M., TILEY, J., Exploration and development of high entropy alloys for structural applications, Entropy. 16 (2014) 494-525.
[21] MIRACLE, D. B. Critical assessment 14: High entropy alloys and their development as structural materials, Materials Science and Technology. 31 (2015) 1142-1147.
[22] HAO SHI, Alumina forming alloys (steels, high entropy materials) for the mitigation of compatibility issues with liquid metals and steam in energy related, high-temperature applications, Dissertation at KIT, submitted for proof.
[23] BALLINGER, R.G., LIM, J., An overview of corrosion issues for the design and operation of high-temperature lead- and lead-bismuth-cooled reactor systems, Nuclear Technology. 147 (2004) 418-435.
[24] HOJNA, A., DI GABRIELE, F., KLECKA, J., Characteristics and Liquid Metal Embrittlement of the steel T91 in contact with Lead–Bismuth Eutectic, Journal of Nuclear Materials. 472 (2016) 163-170.
[25] WEISENBURGER, A., HEINZEL, A., MÜLLER, G., MUSCHER, H., ROUSANOV, A., T91 cladding tubes with and without modified FeCrAlY coatings exposed in LBE at different flow, stress and temperature conditions, Journal of Nuclear Materials. 376 (2008) 274-281.
[26] MÜLLER, G., HEINZEL, A., KONYS, J., SCHUMACHER, G., WEISENBURGER, A., ZIMMERMANN, F., ENGELKO, V., RUSANOV, A., MARKOV, V., Behavior of steels in flowing liquid PbBi eutectic alloy at 420–600 C after 4000–7200 h, Journal of Nuclear Materials. 335 (2004) 163-168.
[27] MÜLLER, G., HEINZEL, A., SCHUMACHER, G., WEISENBURGER, A., Control of oxygen concentration in liquid lead and lead–bismuth, Journal of Nuclear Materials. 321 (2003) 256-262.
[28] LI, N., Active control of oxygen in molten, lead–bismuth eutectic systems to prevent steel corrosion and coolant contamination, Journal of Nuclear materials. 300 (2002) 73-81.
[29] EJENSTAM, J., SZAKÁLOS, P., Long term corrosion resistance of alumina forming austenitic stainless steels in liquid lead, Journal of Nuclear Materials. 461 (2015) 164-170.
[30] ENGELKO, V., MÜLLER, G., BLUHM, H-J., Pulsed electron beam facility (GESA) for surface treatment of materials, Vacuum 62 (2001) 211-216.

[31] MÜLLER, G., ENGELKO, V., WEISENBURGER, A., HEINZEL, A. Surface alloying by pulsed intense electron beams, Vacuum 76 (2005) 469-474.
[32] YANG, X., ZHANG, Y. Prediction of high-entropy stabilized solid-solution in multi-component alloys, Materials Chemistry and Physics. 132 (2012) 233-238.
[33] ZHANG, Y., ZHOU, Y. J., LIN, J. P., CHEN, G. L., LIAW, P. K., Solid-solution phase formation rules for multi-component alloys, Advanced Engineering Materials. 10 (2008) 534-538.
[34] GUO, S., NG, C., LU, J., LIU, C. T., Effect of valence electron concentration on stability of fcc or bcc phase in high entropy alloys, Journal of applied physics. 109 (2011) 103505.

CORROSION OF STEEL CLADDINGS OF FAST REACTORS FUEL ELEMENTS IN THE INTERACTION WITH URANIUM-PLUTONIUM NITRIDE FUEL

Alexander S. Ivanov
NRC "Kurchatov Institute"
123182 Kurchatov Sq., Moscow, Russia

Keywords: nitride nuclear fuel; thermodynamics; carbon and oxygen impurities; chemical interaction; carbide; intergranular corrosion; steel claddings; strength characteristics.

Abstract

The paper presents computational simulation of the effect of carbon and oxygen impurities on the chemical and phase composition of uranium-plutonium nitride fuel during irradiation performed with the IVTANTHERMO computer code. It is demonstrated that carbon present in the composition of the fuel can be dissolved in the fuel in the unbound form. The effect of unbound carbon on the steel cladding of a fuel element is most pronounced in the low-temperature part of the temperature range under consideration at maximum burn-ups and maximum concentrations of carbon and oxygen impurities, i.e. in the same areas of change of parameters at which the fraction of unbound carbon reaches its maximum values. It is shown that one of the possible ways to reduce the effect of carbon on the strength characteristics of steel shells of fuel rods is to block its penetration into the shell. Binding of free carbon in fuel by introducing into its composition a certain amount of effective carbide formers makes it possible to suppress intergranular corrosion of steel fuel cladding.

1. INTRODUCTION

Nuclear fuel and structural materials used in nuclear reactors are complex objects as far as thermodynamic modeling is concerned. Nuclear reactions proceeding during the reactor operation involve formation of new chemical elements that start interacting with the fuel and structural materials. From the standpoint of thermodynamics, the system under study represents a heterogeneous multicomponent object formed by hundreds of chemical compounds that can produce solutions. When the fuel is being burned, its elemental composition varies continuously, thus disturbing the equilibrium system. On the other hand, chemical reactions proceeding in the system aim at bringing the latter to equilibrium.

Strictly speaking, condensed solutions formed in the system cannot be considered as ideal, and the list of substances contained in various solutions is unknown. Hence, when developing a thermodynamic model of nuclear fuel, an assumption about substances capable of forming solutions shall be made, solution models shall be chosen, and model parameters defined.

An issue about the possibility to describe nuclear fuel properties using the mathematical apparatus of equilibrium thermodynamics deserves special consideration. Generally speaking, the thermodynamic equilibrium state suggests that there are not any flows (of mass, energy or momentum) in the system under study. It is quite possible to achieve such a state of the system in mixed nitride fuel fabrication processes. In operating conditions, however, heat transfer processes take place in fuel elements due to existing temperature gradients. Besides, strong temperature dependence of some chemical reaction constants will result in non-uniform distribution of fuel components and fission products over fuel pellets, giving rise to diffusion flows of substance. All this imposes significant constrains on applicability of thermodynamics to the object under study and calls for a thorough analysis of the range of applicability of thermodynamics in operating conditions.

Interest in studies of mixed uranium-plutonium nitride fuel for fast reactor has revived recently, inciting a number of researchers to investigate phase and chemical composition of the fuel in the process of its fabrication by various technologies and under irradiation in a nuclear reactor [1-8]. In particular, in [1] describes the method of thermodynamic modeling of manufacturing of nitride nuclear fuel in the temperature range of 1000-2500 K.

In the manufacturing process of the nitride fuel, it may be contamination of carbon and oxygen. The research results presented in the paper [3] indicate that the presence of oxygen impurities significantly affects the physical and chemical properties of the fuel. In particular, the presence of 1 wt. % Oxygen reduces its thermal conductivity by 9-13%. In [5, 6], the results of thermodynamic modeling of phase and chemical composition of the mixed U-Pu nitride fuel in the temperature range 900-1400K, analyzes the impact of fission products to the phase and chemical composition of the nuclear fuel. Thermodynamic analysis and experimental research carried out in [8] showed that the nitride fuel thermochemically stable up to 1700-2073K. At these temperatures the vapor pressure of nitrogen does not exceed 2.1 Pa.

Despite the performed studies, still much remains unclear about the nitride fuel behavior. Specifically, of particular interest is the effect of carbon and oxygen impurities on the phase and chemical composition of the fuel during its irradiation, considering the fact that the presence of the mentioned components in the mixed nitride nuclear fuel on the one hand may be due to the fuel fabrication process, and on the other hand may have a great impact on the fuel performance.

To improve the operational reliability of fuel rods of fast reactors with uranium-plutonium nitride (U,Pu)N fuel, a clear understanding of the phenomena that were observed after reactor tests is necessary. The purpose of this work is to identify mechanisms for reducing the mechanical characteristics of steel claddings of fuel elements when interacting with (U,Pu)N fuel and developing methods for stopping parasitic effects. The analysis [9] has demonstrated that equilibrium thermodynamic calculations can be used for evaluation of chemical and phase composition of the fuel.

This paper presents a thermodynamic analysis of some anomalies in behavior of the model system “(U, Pu) N fuel + cladding from austenitic steel ChS68-ID” by the IVTANTERMO code [10].

2. THE EFFECT OF THE CARBON AND OXYGEN IMPURITIES

Calculations of the equilibrium chemical and phase composition of the fuel were performed using the IVTANTHERMO software system [10]. Basic elements of the system were determined from neutronics calculations [11, 12]. This paper deals with the (U-Pu)N fuel composition containing 13.4 wt. % of plutonium. The geometric parameters of the calculation model are given in the table 1.

TABLE 1 - THE GEOMETRIC PARAMETERS OF THE FUEL ROD

Diameter of the fuel rod, mm	9,7
Thickness of the cladding, mm	0,5
Gas gap between fuel and cladding, mm	0,15
Diameter of the fuel column, mm	8,4
Cladding length, mm	1100

In the calculation model, it is assumed that the length of the cladding is equal to the height of the fuel column.

The condensed phase of the fresh fuel consists of the following elements and compounds: U, UN, $UN_{1.466}$, $UN_{1.54}$, $UN_{1.73}$, Pu and PuN. For calculation of the thermodynamic equilibrium, there was considered a system where all condensed components were divided into 2 solutions, while individual phases were used for the other components. All nitrogen, iodine and bromine compounds were included in the first solution. When there was oxygen, oxides were added to the composition of the first solution. The second solution contained all carbon and tellurium compounds, as well as uncombined elements. The heat of dissolution of the solution components was taken equal to zero, which corresponds to the ideal solution model. The calculations were done for the temperature range 873 – 1773K. Oxygen and carbon may be found in the fuel as impurities due to the fabrication process. The effect of the carbon and oxygen impurities on the phase composition of the fuel was evaluated for the fresh fuel and for the fuel irradiated to the burnup of 0; 4; 9.3 % and 12% FIMA (fissions per initial metal atom). The oxygen content of the system was taken as 0 - 0.3 wt.% and the carbon content – as 0 - 0.3 wt.%.

In the process of manufacturing a mixed nitride fuel it may be contaminated with carbon and oxygen. Results of researches [12] indicate that the presence of carbon and oxygen impurities has a significant effect on the phase and chemical composition of (U,Pu)N fuel.

According to the performed calculations, the majority of uranium atoms remains combined with nitrogen. As the burnup increases, the amount of UN reduces, going into $UN_{1.466}$, $UN_{1.54}$ and $UN_{1.73}$. The UN concentration is virtually independent of temperature. Uranium carbides are formed in minor quantities, mostly in the form of UC. At low burnup levels and high temperatures, uranium is also found in uncombined form. Plutonium forms such compounds as Pu, PuC, PuC_2, Pu_2C_3 and PuN in the system under study. Plutonium and uranium carbides are formed in minor quantities. Most of plutonium remains in the form of nitride PuN, while appreciable amounts of uncombined Pu are only found under low burnup and high temperature conditions.

Calculated temperature dependences of the uncombined uranium content in the original fuel are shown in Figures 1 and 2 below.

According to Figure 1, the presence of the oxygen impurities dramatically reduces the uncombined uranium content in the fresh fuel apparently due to formation of uranium dioxide. This may result in a substantial suppression of uranium transfer processes in the given fuel. Figure 2 presents unbound U content in the fuel irradiated to the burnup of 9.3% FIMA at various concentrations of oxygen impurity (0 - 0.3 wt.%) versus of temperature. It is interesting to note that the concentration of uncombined uranium reduces as the fuel burns up (Fig. 2).

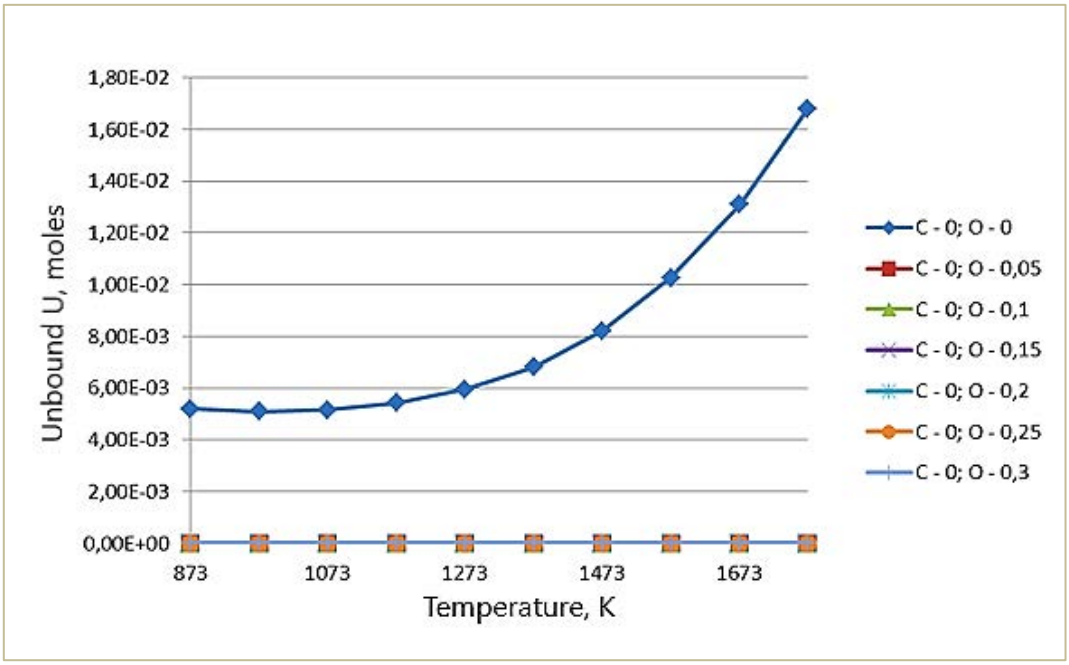

Fig. 1. – Unbound U content in the fresh fuel in the absence of carbon at various concentrations of oxygen impurity (0 - 0.3 wt.%) versus of temperature

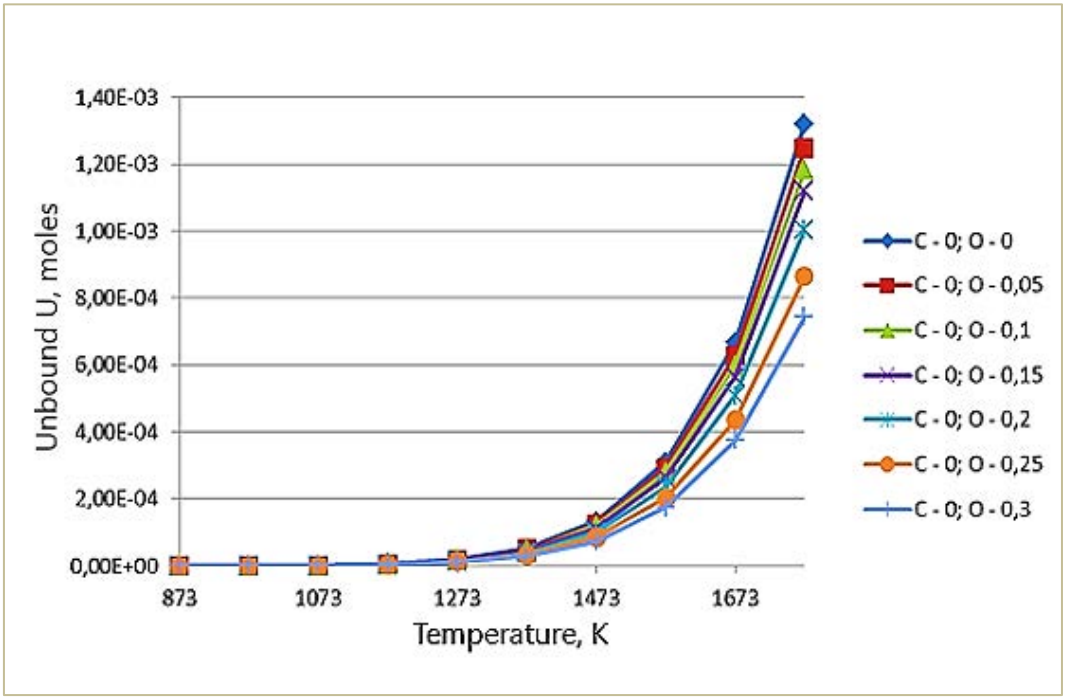

Fig. 2. – Unbound U content in the fuel irradiated to the burnup of 9.3% FIMA in the absence of carbon at various concentrations of oxygen impurity (0 - 0.3 wt.%) versus of temperature.

Uncombined plutonium demonstrates behavior similar to that of uncombined uranium in the system being studied, but its concentration is noticeably lower than the concentration of uncombined uranium.

Effect of impurities on the composition of nitride phase of (U, Pu) N fuel is shown in Figures 3 and 4. Figure 3 shows the amount of uranium nitride (UN) in the fresh fuel as a function of carbon concentration for various oxygen concentrations (0 - 0.3 wt.%).

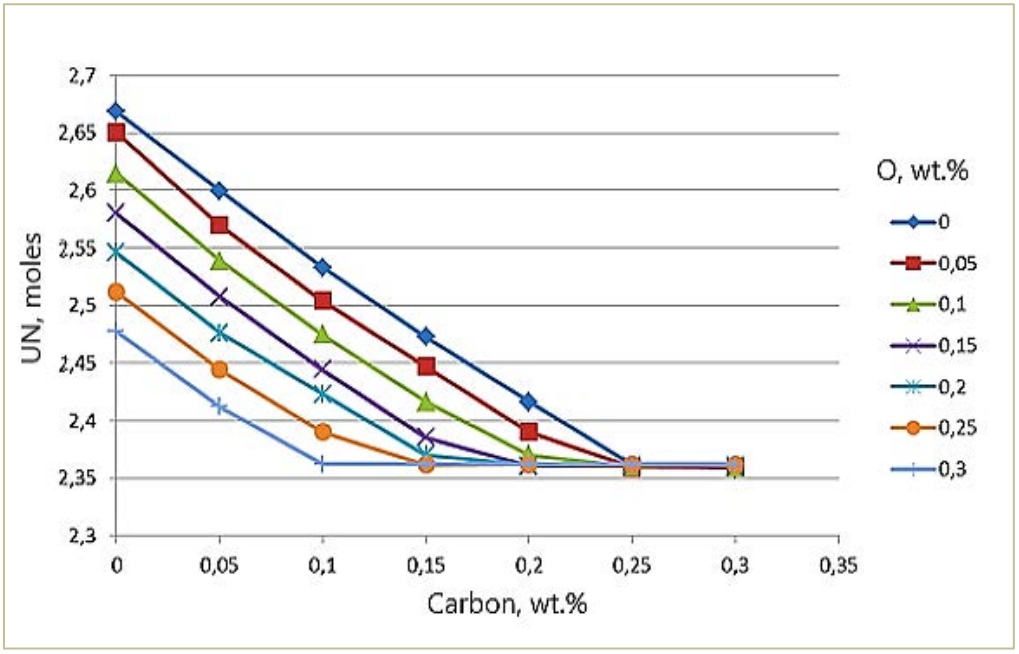

Fig. 3. – UN in the fresh fuel depending on the carbon concentration for various oxygen concentrations (0 - 0.3 wt.%) at a temperature of 873K

Figure 4 shows the same dependence of the amount of UN on the carbon impurity content in the fuel irradiated to the burnup of 9.3% FIMA.

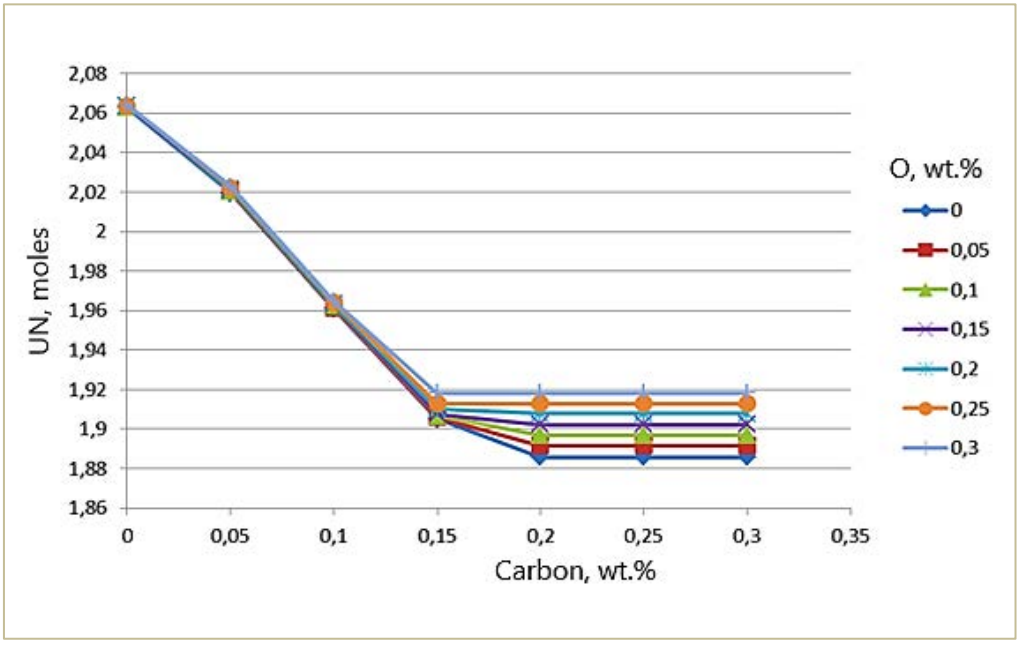

Fig. 4. – UN in the fuel irradiated to the burnup of 9.3% FIMA depending on the carbon concentration for various oxygen concentrations (0 - 0.3 wt.%) at a temperature of 873K

According to these figures 3 and 4 with increasing carbon concentration decrease in the number UN phase up to a certain limit is observed. Upon reaching this limit, a further increase in the concentration of carbon impurities does not affect the amount of UN in the fuel. In this case, the formation of uranium carbide stops, and the added carbon may remain in the unbound state. Thereby, it is of interest to study the dependence of the concentration of unbound carbon in the solid phase on its total content.

We have shown that the carbon present in the composition of the fuel can be under certain conditions, both in the bound state in the form of carbides, carbonates or other compounds of the components of the fuel with carbon and dissolved in the fuel in the unbound form.

For example, Figure 5 shows the dependences of the fraction of unbound carbon with respect to the total carbon impurity content in the fuel with different burnup depending on the mass fraction of oxygen impurity at 0.2 wt.% of carbon impurity and at temperature 873K.

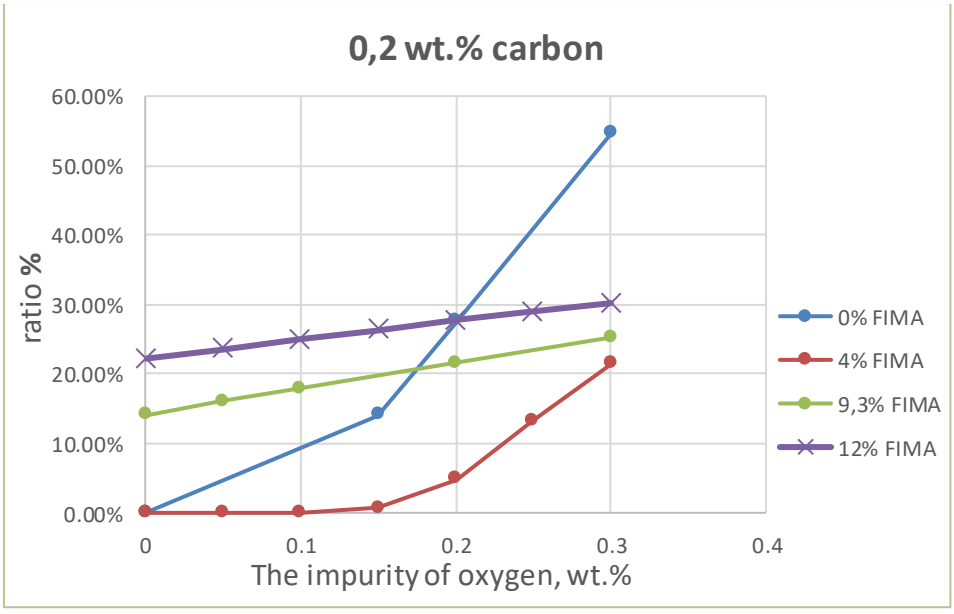

Fig. 5. – The fraction of unbound carbon with respect to the total carbon impurity content in fuel with different burnup, depending on the mass fraction of oxygen impurity at 0.2 wt.% of carbon impurity and at temperature 873 K

In this case, the fuel is a carbon source, which can directly affect the condition of the steel cladding of the fuel element and its mechanical characteristics. In this work, we studied the thermodynamics of the model system "(U, Pu) N fuel + cladding from austenitic steel ChS68-ID" by the IVTANTERMO code. It is shown that an increase of the carbon content in the initial fuel leads to a monotonic decrease in the average concentration of unbound chromium in the fuel cladding.

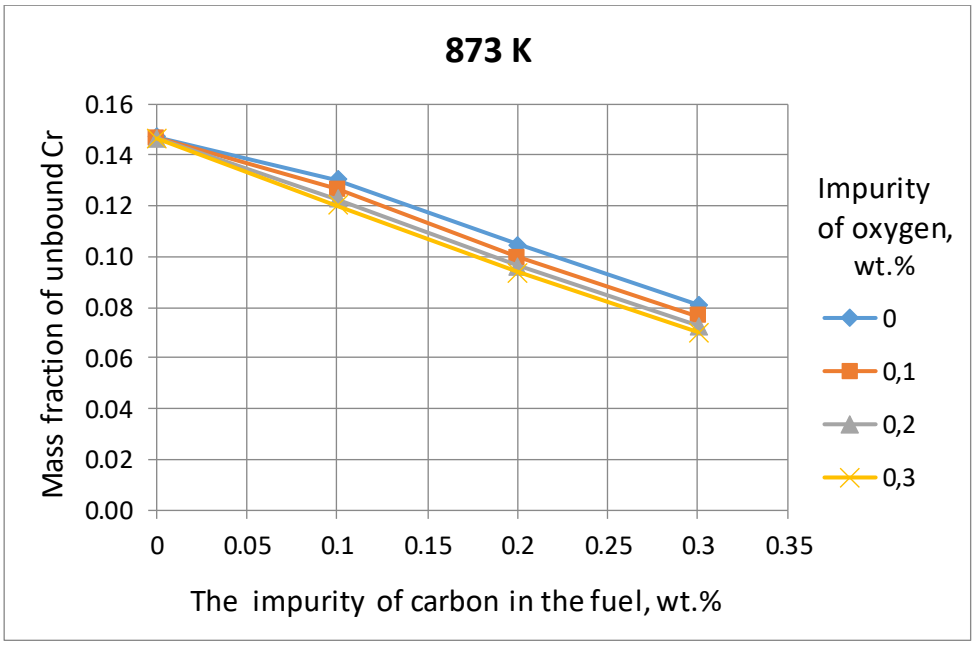

Fig. 6. – Mass fraction of unbound Cr (wt.%) in the cladding at a temperature of 873K, depending on the content of carbon impurities at different values of the concentration of oxygen impurities; 0% FIMA

All unbound carbon in the fuel goes into the fuel cladding and is associated mainly with chromium. The limit of passivity with respect to intergranular corrosion of austenitic steel (12 wt.% Cr) is reached at a temperature of 873K for all values of oxygen concentration and the mass fraction of carbon in the fuel is less than 0.15 wt.%. As the temperature rises, more unbound carbon binds to the components of the fuel. Therefore, the effect of carbon on the steel cladding decreases significantly with increasing temperature. For example, at a temperature of 873K in fresh fuel and in the absence of an oxygen impurity, the passivity limit for unbound chromium (12 wt.%) is reached at ~ 0.14 wt.% of a carbon impurity. However, at 1073 K this value is ~ 0.28 wt.% carbon impurities.

An increase in the oxygen content in the original fuel leads to a more rapid attainment of the passivity limit with respect to intergranular corrosion.

The effect of unbound carbon on the steel cladding of a fuel element is most pronounced in the low-temperature part of the temperature range under consideration (873 – 1073 K) at maximum burn-ups and maximum concentrations of carbon and oxygen impurities, i.e. in the same areas of change of parameters at which the fraction of unbound carbon reaches its maximum values.

One of the possible ways to reduce the effect of carbon on the strength characteristics of steel claddings of fuel rods is to block its penetration into the cladding.

Binding of free carbon in the fuel by introducing into its composition a certain amount of effective carbide formers makes it possible to suppress intergranular corrosion of steel fuel cladding. The calculation results show a rather low efficiency of both molybdenum and titanium as carbide-forming additives in the system under consideration, especially in burned (U, Pu) N fuel. However, the use of Cr as carbide former provides an encouraging result.

Three options for adding Cr to fuel: $\Delta Cr = 0$; 0.5 and 1 wt.% will be compared.

The dependence of the mass fraction of unbound chromium on the amount of carbon impurity for 3 variants of the addition of chromium to fuel at a temperature of 873 K and 0% FIMA is shown in Figure 7 for the system of "(U, Pu)N fuel with carbon impurities + carbide formers Cr + steel ChS68-ID". The horizontal line of 12% marks the limit of passivity with respect to intergranular corrosion of austenitic steel. The dashed lines indicate the intersection of the 12% level with the dependences of the Cr content on the amount of carbon impurity. These points characterize the concentration of carbon in the fuel to which the steel shell remains stable with respect to intergranular corrosion.

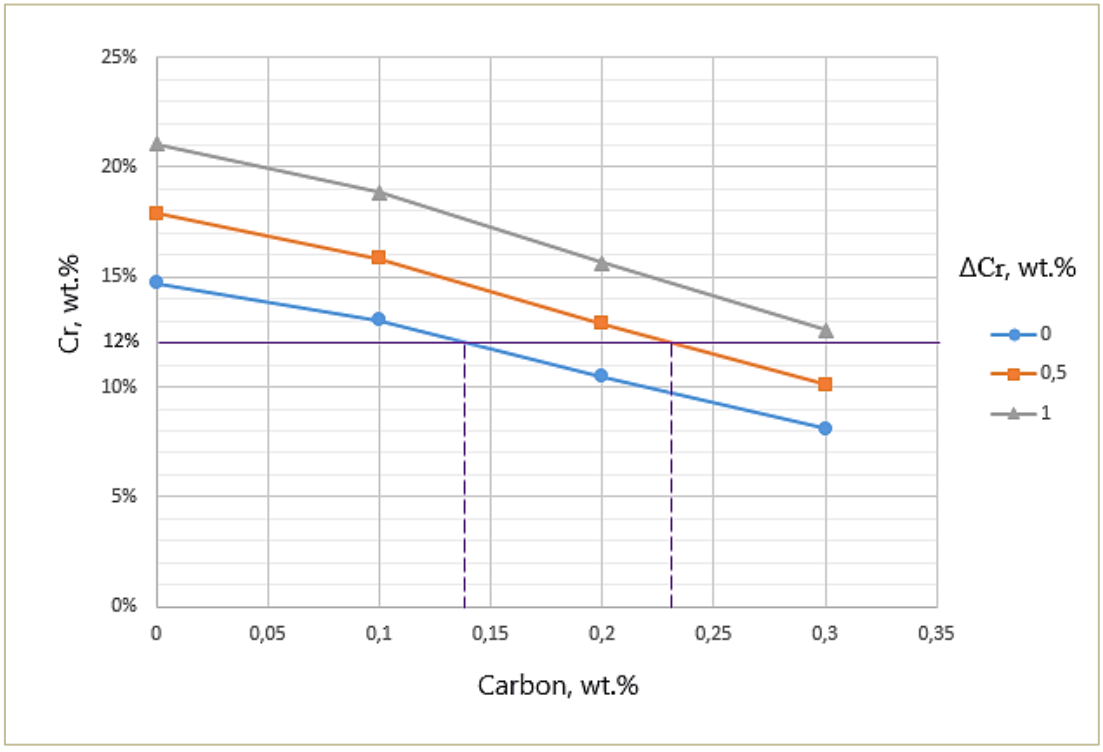

Fig. 7. - Mass fraction of unbound chromium (wt.%) versus on the amount of carbon impurity for 3 variants of chromium addition (0, 0.5 and 1 wt.%) to the fuel at a temperature of 873 K; 0% FIMA

Figure 8 shows the same lines in the system “(U, Pu)N fuel with carbon impurities + carbide formers Cr + steel ChS68-ID”, but for the fuel irradiated to the burnup of 9.3% FIMA.

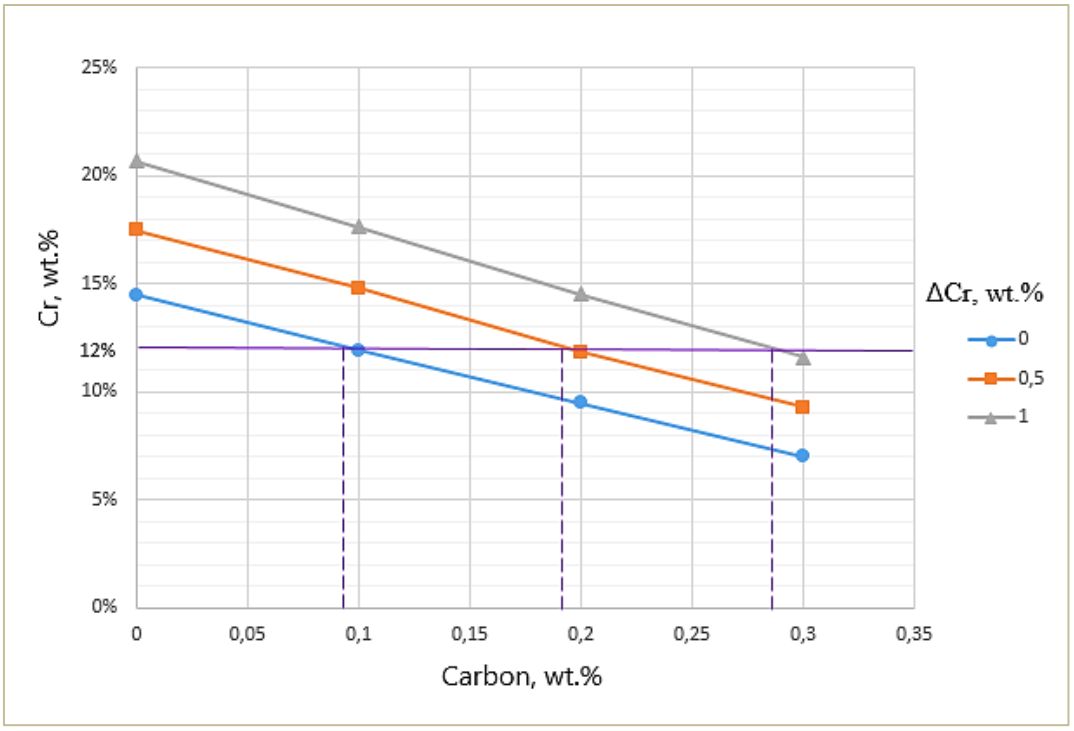

Fig. 8. - Mass fraction of unbound chromium (wt.%) versus on the amount of carbon impurity for 3 variants of chromium addition (0, 0.5 and 1 wt.%) to the fuel at a temperature of 873 K; 9,3 % FIMA

Detailed computational studies of the thermodynamics of the system “(U, Pu)N fuel with oxygen and carbon impurities + carbide formers Cr + steel ChS68-ID” showed that the introduction of 1 wt.% Cr into the fuel should ensure the stability of the steel cladding with respect to intergranular corrosion.

3. CONCLUSION

The paper presents an analysis of the effect of carbon and oxygen impurities on the chemical and phase composition of uranium-plutonium nitride fuel. The analysis was performed with the IVTANTHERMO software system. At low burnup levels and high temperatures, uranium is also found in uncombined form. The presence of the impurities dramatically reduces the uncombined uranium content of the unirradiated fuel, apparently due to formation of uranium dioxide. This may result in a substantial suppression of uranium transfer processes in the given fuel. It is interesting to note that the concentration of uncombined uranium reduces as the fuel burns up. Most of plutonium remains in the form of nitride PuN, while uncombined Pu is only found in low burnup, high temperature regions. The effect of the oxygen and carbon impurities involves a significant reduction in the concentration of uncombined plutonium in the fresh fuel and at low burnup levels.

Carbon present in the composition of the fuel can be under certain conditions, dissolved in the fuel in the unbound form. In this case the fuel is a carbon source, which can directly affect the condition of the steel cladding of the fuel element and its mechanical characteristics. The effect of unbound carbon on the steel cladding of a fuel element is most pronounced in the low-temperature part of the temperature range under consideration at maximum burn-ups and maximum concentrations of carbon and oxygen impurities, i.e. in the same areas of change of parameters at which the fraction of unbound carbon reaches its maximum values.

One of the possible ways to reduce the effect of carbon on the strength characteristics of steel claddings of fuel rods is to block its penetration into the shell. Binding of free carbon in fuel by introducing into its composition a certain amount of effective carbide formers makes it possible to suppress intergranular corrosion of steel cladding. Shown, that the introduction of 1 wt.% Cr into fuel should ensure the stability of the steel cladding with respect to intergranular corrosion. It should be noted that the introduction of 1wt.% Cr into the fuel may affect neutronic characteristics of the core and should be considered in reactor calculations.

In conclusion we would like to note that the observed effects of the oxygen and carbon impurities on the phase and chemical composition of the uranium-plutonium nitride fuel shall be considered when designing fuel elements based on this fuel.

REFERENCES

[1] JOLKKONEN M., STREIT M., WALLENIUS J. Thermo-chemical Modelling of Uranium-free Nitride Fuels // Journal of NUCLEAR SCIENCE and TECHNOLOGY, 2004.-Vol. 41, No. 4, p. 457–465.

[2] J.-O. ANDERSSON, T. HELANDER, L. HO¨GLUND ET AL., Thermo–Calc and DICTRA, computational tools for materials science // Calphad, 2002.-V.26. P. 273-312.

[3] ARAI Y., MORIHRA M., OHMICHI T. The effect of oxygen impurity on the characteristics of uranium and uranium-plutonium mixed nitride fuels // Journal of nuclear materials, 1993.-V. 202. P 70-78.

[4] ARAI Y., MAEDA A., SHIOZAWA K., OHIMICHI T. Chemical forms of solid fission products in the irradiated uranium-plutonium mixed nitride fuel // Journal of nuclear materials, 1994.-V.210.-P.161-166

[5] LUBIMOV D.YU., ANDROSOV A.V., BULATOV G.S., GEDGOVD K.N. Thermodynamic modeling of the phase composition of mixed uranium-plutonium mononitride under fast-neutron irradiation to the burnup of 80 GW·day/t at 900–1400 K // Atomnaya Energiya. 2013. V. 114. No. 4. Pp. 198-202.

[6] BONDARENKO G.G., BULATOV G.S., GEDGOVD K.N., LUBIMOV D.YU, YAKUNKIN M.M. The change in the chemical and phase composition of the uranium-plutonium fuel irradiated by fast neutrons as a result of electron decay of metallic fission products // Metals. 2011. No. 6. P. 59.

[7] SRIVASTAVA D., CARG S.P., GOSWAMI G.L. Thermodynamic analysis of mixture carbide, carbonitride and nitride fuels for fast breeder reactors // Journal of nuclear materials, 161 (1989), pp. 44-56

[8] ROGOZKIN B.D. ET AL. Thermochemical stability, radiation testing, fabrication, and reprocessing of mononitride fuel // Atomic Energy. 2003. Vol. 95, No. 6

[9] IVANOV, A. S., RUSINKEVICH, A. A., BELOV, G. V., IVANOV, YU. A. Analysis of the Range of Applicability of Thermodynamic Calculations in the Engineering of Nitride Fuel Elements. Physics of Atomic Nuclei, 2017, Vol. 80, No. 8, pp. 1464–1469.

[10] BELOV G.V. Calculation of equilibrium composition and properties of thermodynamic systems under elevated pressure. Mathematical modeling, 2001. V13, No.8.

[11] GLUSHKOV E.S., NAZARENKO I.P., PANEVIN I.G., PONOMAREV-STEPNOY N.N. Neutronics calculation methods for nuclear reactors. Moscow, MAI Publisher, 2000.

[12] RUSINKEVICH, A.A., IVANOV, A. S., BELOV, G. V., SKUPOV, M. V. Some Thermodynamic Features of Uranium–Plutonium Nitride Fuel in the Course of Burnup. Physics of Atomic Nuclei, 2017, Vol. 80, No. 8, pp. 1470–1475.

SESSION III: QUALIFICATION PROGRAMMES OF STRUCTURAL MATERIALS FOR HLM FAST REACTORS

QUALIFICATION PROGRAMME OF CANDIDATE MATERIALS FOR ALFRED

S. BASSINI, C. SARTORIO, A. FIORE, S. CATALDO, M. UTILI, M. ANGIOLINI, M. TARANTINO
ENEA FSN-ING
C. R. Brasimone, 40032 Camugnano (Bologna), Italy
Email: serena.bassini@enea.it

G. GRASSO
ENEA FSN-SICNUC
C. R. Bologna, Via Martiri di Monte Sole n°4, 40129 Bologna, Italy

M. VANAZZI, F. DI FONZO
Center for Nano Science and Technology @PoliMi, IIT
Via Giovanni Pascoli 70/3, 20133 Milano, Italy

A. ALEMBERTI, M. FRIGNANI
Ansaldo Nucleare S.p.A.
Corso Perrone 25, 16152 Genova, Italy

Abstract

The Advanced Lead-cooled Fast Reactor European Demonstrator (ALFRED) is intended to demonstrate the feasibility of the liquid lead technology applied to liquid metal fast reactor systems. Recently, the operation strategy of ALFRED was revised to take into account the need for a graded approach to licensing and operation. The operation strategy now includes new approach which implements different operating temperature windows. The first stage implements the low temperature conditions and with the further stages the core outlet temperature is progressively increasing. This approach will ensure faster return of experience due to the fact that it will eliminate the distance between the available technology and intended commercial performance. During this research the demonstration will provide a feedback about operation. To ensure the overall competitiveness of lead-cooled fast reactors the research and demonstration will continue in parallel.

Advanced anti-corrosion protection measures need to be developed and qualified for the high temperature operation. Conventional steels are sensitive to dissolution-based corrosion when in contact with lead melt and the temperature and the oxygen concentration dissolved in the melt are key parameters influencing the corrosion. It is known that the oxygen dissolved in lead can form a protective oxide layer on austenitic steels up to 450-480°C whereas above this limit severe corrosion is expected. Increasing the temperature, and so increasing the performance of LFR systems, will require new technological solutions (e.g. coatings or advanced materials) to face corrosion.

The first stage of ALFRED operation (primary cycle 390-430°C) is intended to provide operational feedback assessing the compatibility of structural materials with lead at low temperature and the irradiation performance of core components. Indeed, the combination of oxygen control and the choice of austenitic steels as structural materials (316L and 15-15Ti AIM1) have been shown to be compatible in the temperature range of stage 1. To the opposite, design conditions of the following stages will require protective solutions to address the HLM corrosion issues and their qualification before the implementation into the reactor, in particular for fuel cladding components exposed to the highest temperature and level of neutron irradiation. To overcome the shortage of fast irradiation facilities worldwide, cladding protective measure will be qualified under neutron irradiation during stage 1 in ALFRED itself.

Here, the main results obtained in the recent years about advanced mitigation strategies and materials for the later operational stages are presented. For cladding structures, amorphous nanoscale Al_2O_3 layer by Pulsed Laser Deposition (PLD) technique was selected as reference choice due to outstanding chemical compatibility with liquid lead, mechanical properties and irradiation resistance (up to very high doses although by heavy ions). FeCrAl aluminizing techniques are considered for the protection of components with complex geometry such as inner vessel components, heat exchangers, decay heat removal (DHR) and primary pump impellers. Also, AlTiN layer is considered for the protection of primary pump impellers for the outstanding wear resistance, and Al2O3 layer by Detonation Gun deposition considered as candidate coating for reactor vessel. Finally, alumina-forming austenitic (AFA) steels are promising bulk materials for their potential high corrosion resistance in lead.

1. INTRODUCTION

Lead Fast Reactors (LFRs) have been considered by the international community as one of the most promising technologies capable of meeting the Generation-IV goals [1]. The use of molten lead as a coolant offers many advantages thanks to the favorable chemical and physical properties [2], which allow for enhanced safety, sustainability and competitiveness. As an example, the LFR is considered to excel in safety, based on the very low potential energy density stored in the coolant system [3], once the thermal energy (including compression potential energy), the potential chemical energy (due to interaction with zirconium for LWR or water/air for SFR), and the potential chemical energy of interaction of consequently released hydrogen with air are taken into account. The limited potential consequences following a nuclear accident translate in design simplifications, as well as improved robustness and economic competitiveness.

Undeniable challenges require to be timely addressed for a successful commercial deployment of LFRs. Among the highest technological priorities for a safe and reliable operation, the corrosion of structural materials when exposed to molten lead needs to be addressed through further R&D efforts. The high solubility of the steel constituents in liquid lead alloys induces a progressive depletion of the surface exposed to the HLM, which translates into severe corrosion [2][4], if the dissolution of the constituents is not adequately prevented.

In Europe, the above aspect has been addressed in terms of basic and applied research producing a large collection of experimental data. Extensive collaboration between various research institutions and industrial partners, often supported by funding from European Commission or national initiatives, allowed the identification of promising solutions for the protection of steels in molten lead.

However, the low technology readiness of such solutions for industrial use in nuclear applications has fed a transversal consensus on the capabilities of ALFRED (namely, the Advanced Lead-cooled Fast Reactor European Demonstrator) to bridge the gap between the development of innovative technologies and their deployment in a nuclear reactor, through a staged approach and a rigorous qualification process [5]. FALCON, an international consortium Fostering ALFRED Construction, under the leadership of Ansaldo Nucleare (Italy), with ENEA (Italy) and ICN (Romania), is pursuing an R&D programme in support of the design, licensing and operation of the prototype of a viable competitive LFR commercial unit in the SMR segment by 2035-2040 [6].

The ALFRED staged approach is based on increasing progressively the coolant core outlet temperature, thus closing the gap between current technology and desired commercial performances. In Stage 1 of operation, two main areas of concern for the LFR technology will be addressed: (1) compatibility of lead with structural materials at low temperature and (2) lead chemistry control. Indeed, ALFRED operation is based on an oxygen concentration control in the coolant (10-6 to 10-8 wt. %) and on the use of nuclear grade structural materials (notably, 316 and 15-15Ti type austenitic steels), which have been shown to be compatible in the temperature range selected for the Stage 1 (390-430°C) and with oxygen control [2][7]. Entering Stage 2 (core outlet temperature of 480°C), some regions of the core will be subject to high temperatures where oxygen control cannot be effective anymore in protecting the steel surface via passivation [2][7]. Therefore, the qualification of protective measures will be necessary. Increasing further the core outlet temperature with Stage 3 (temperature of interest for commercial applications), all the components of the RCS exposed to the core outlet temperature will require special materials or protective measures.

The demonstrator will leverage on the R&D programme running in parallel, which will be aimed at qualifying technological solutions compatible with the design conditions of the following stages, providing the evidences for a licensing up-rate. As presented throughout the paper, different strategies (intending either innovative corrosion-resistant materials or specific coatings deposited by industrial techniques on bulk materials) are being considered and dedicated development and qualification is planned in separate experimental facilities. For cladding structures, Al_2O_3 layer by Pulsed Laser Deposition (PLD) technique was selected as reference choice for ALFRED due to outstanding chemical compatibility with liquid lead, mechanical properties and irradiation resistance (up to very high doses although by heavy ions). FeCrAl aluminizing techniques are considered for the protection of components with complex geometry such as inner vessel components, heat exchangers, DHR and primary pump impellers. AlTiN layer is considered for the protection of primary pump impellers for the outstanding wear resistance, and Al_2O_3 layer by Detonation Gun deposition considered as possible coating for reactor vessel. Finally, alumina-forming austenitic (AFA) steels are promising bulk materials for their potential high corrosion resistance in lead.

However, the shortage of neutron irradiation facilities and delays in the construction and operation of new ones is going to impair a short-term deployment of the technology, thereby making the demonstrator itself a necessarily integral part of the experimental and qualification programme. Design conditions of following stages will be reproduced in the ALFRED core through an in-pile section to qualify corrosion protective technologies or innovative materials for higher temperatures, before unlocking the following stage by implementing the qualified solution in the reactor.

2. MATERIAL CHOICE AND COOLANT CHEMISTRY STRATEGY

ALFRED is conceived as a pool-type reactor where all the main components are immersed in the coolant contained in the Reactor Vessel (RV) and hanging from the Reactor Cover (RC). A schematic sketch of ALFRED reactor and the temperature distribution inside the reactor vessel is reported in FIG. 1. The core is made of wrapped hexagonal fuel assemblies constrained by the core barrel, the lower diagrid and the upper diagrid (located in the cover gas space). Three primary pumps (mechanical of axial type) are located at the core outlet and feed a large pool in the upper part of the RCS (namely, Hot Pool - HP). The molten lead is cooled by Steam Generators (SG), or by immersed Heat Exchangers (HX) connected to a passive Decay Heat Removal (DHR) system. The DHR system is designed to deal with any accident condition and thus it is capable to reach large volume at the cold temperature (Cold Pool - CP). The HP is

separated from the CP by the Internal Structure (IS). Due to this the coolant, before it flows downward against the RV and re-entering the core, it is forced to flow upwards and around a baffle. The coolant stratification in the upper part of the RCS is eliminated. Also, this configuration eliminates any steam which could potentially be entrained in the coolant because of a SG tube rupture.

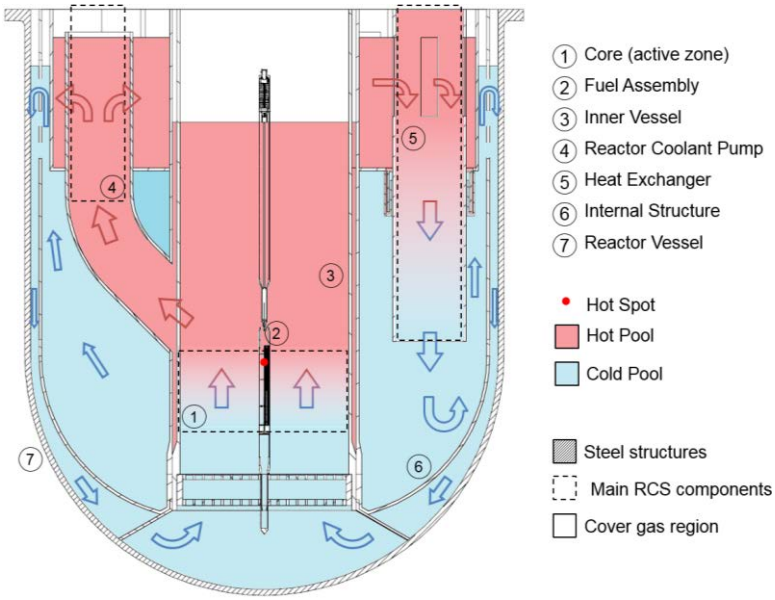

FIG. 1. Schematic sketch of ALFRED reactor and temperature distribution

The different regions of the RCS are exposed to different temperature conditions, which, in turn, influence the material selection. In addition, the temperature conditions for the reactor components will increase passing from Stage 1 to Stage 3 (see TABLE 9), except for the RV which is exposed approximately to the same low temperature (390°C in Stage 1 and 400°C in Stage 3).

TABLE 9: ALFRED TEMPERATURE PARAMETERS IN THE VARIOUS STAGES OF OPERATION [5].

Parameters	Stage 1 (Low T)	Stage 2 (Medium T)	Stage 3 (High T)
Core inlet T (°C)	390	400	400
Core outlet T (°C)	430	480	520
Hot Spot T (°C)	450	535	600
Core thermal power (MWth)	100	200	300

Based on the current state of knowledge about the protection offered by the Fe-Cr oxide layer on austenitic stainless steel in heavy liquid metals (mostly Pb-Bi eutectic), Stage 1 thermal cycle has been defined to ensure the chemical compatibility with the coolant for all the structures, which are made of bare austenitic steels. Indeed, concerning the corrosion behaviour, austenitic steels are corrosion resistant at temperature lower than 450°C if a sufficient oxygen concentration is dissolved in the coolant [7][8], whereas they undergo dissolution (selective leaching of Cr and Ni mainly) at higher temperature due to the loss of the protective feature of the oxide scale [4][7]. By considering that the nominal operating temperature in Stage 1 does not exceed 430 °C (450°C in the hot spot on fuel cladding tubes), austenitic steels such as AISI 316 and 15-15Ti (DIN 1.4970 or in the cold-worked state AIM-1) should not undergo significant corrosion and can be employed without trouble.

Considering instead the temperature conditions of Stage 2, the qualification of protective measures for the hot parts (fuel cladding, fuel assembly and HXs) will be necessary. Increasing further the core outlet temperature as for Stage 3, all the components of the RCS will require advanced materials or protective measures to face corrosion. RV, operating at low temperature in all the Stages, is basically considered as bare component, even if protection with coating can be considered to prevent large release of corrosion products in the coolant (which should be removed during the operation).

The candidate materials for the various stages of operation are enlisted in TABLE 10. Stage 1 will operate with low temperature (up to max. 450°C on fuel cladding tubes) with dissolved oxygen control in lead (10^{-6} - 10^{-8} % wt.) is expected to form a protective oxide layer on the steels preventing heavy dissolution. Conversely, in Stages 2 and 3 at higher temperatures non-protective oxidation and significant corrosion are expected for bare austenitic steels with the same oxygen concentration range. Thus, to face corrosion, Al_2O_3 coatings, FeCrAl diffusion layers or advanced materials such as AFA steels are foreseen in later Stages of ALFRED for all structures and components except for RV.

TABLE 10: CANDIDATE MATERIALS FOR ALFRED REACTOR AND PROTECTIVE MEASURES.

Component	**Materials (Stage 1)**	**Materials and/or Coatings**
Fuel cladding	15-15Ti 20% CW (AIM1)	15-15Ti AIM1 + Al_2O_3 by PLD
FA Structures	15-15Ti 20% CW (AIM1)	15-15Ti AIM1 + Al_2O_3 by PLD/ALD[a]
Internal structures	AISI 316LN (ASTM)	FeCrAl diffusion coating, or AFA steel
Steam Generator	AISI 316LN (ASTM)	AFA steel, or FeCrAl diffusion coating
DHR Heat Exchanger	AISI 316L (ASTM) 15-15Ti (DIN 1.4970)	FeCrAl diffusion coating, or AFA steel
Primary Pumps (Impellers)	AISI 300 series	FeCrAl diffusion coating, or AlTiN coating
Reactor Vessel	AISI 316LN (ASTM)	O-control (or Al_2O_3 by D-Gun)

[a] *ALD = Atomic Layer Deposition*

It is to be noted that, differently from the Pb-Bi eutectic case, there is a lack of experimental corrosion data for austenitic steels in pure lead and an indication about the maximum temperature at which corrosion is still acceptable under oxygen control, is not available. This temperature is around 450°C for Pb-Bi [8], considered more aggressive than lead due to the higher solubility of steel alloying elements for a given temperature [2]. Considering this lack of data, the limit valid for Pb-Bi is applied for ALFRED structural steels, waiting for new data better assessing the corrosion behavior in lead. This lack will be covered in some way during GEMMA H2020 European project (n°755269), where exposure tests in liquid lead will be performed in static and flowing conditions for 316L and 15-15Ti AIM1 austenitic steels at 480°C and 550°C.

3. MATERIALS QUALIFICATION AND RESULTS

3.1. Al_2O_3 by PLD

Concerning the development of protective solutions for ALFRED fuel cladding tubes and FAs, innovative Al_2O_3 coatings have been designed by Istituto Italiano di Tecnologia (IIT, Milan).

Amorphous/nano-crystalline films have been grown on several steel substrates (such as T91 ferritic/martensitic and 316L or 15-15Ti AIM1 austenitic steels) by means of PLD. This bottom-up approach allows the fabrication of high quality fully adherent films at room temperature, without requiring any post-deposition thermal treatment. At the time being, the PLD process has been exploited by IIT to cover realistic sample geometries such as fuel cladding-like tubes, up to 30 cm of total length.

The main features of these films depend on the peculiar structure of PLD-grown Al_2O_3. The presence of an amorphous matrix along with embedded nano-grains confers a unique assemble of remarkable properties:

- quasi-metallic mechanical behaviour and plastic deformability up to a few percentages [9];
- anti-diffusion and anti-permeation capability against several gaseous species. This feature is particularly relevant in relation to the tritium confinement, for either fission- or fusion-based systems [10][11][12];
- high radiation tolerance. Al_2O_3 films have been irradiated up to 450 dpa, showing neither cracking, nor delamination [13][14][15].

Concerning corrosion issues in heavy liquid metals, steel-coated specimens have been characterized. In order to decouple the liquid lead chemistry from the protective performance of alumina-based materials, exposure tests have been performed taking into account different environmental conditions: 1) oxidative regime (high oxygen concentration) and dissolutive regime (low oxygen concentration) to prove the advantages connected to a stable oxide film. Exposure tests have been conducted in collaboration with ENEA Brasimone. PLD-coated and uncoated 15-15Ti AIM1 specimens have been exposed to static lead at 550 °C for 1000 hours, with oxygen in lead of 10^{-3} wt. %, and 10^{-8} - 10^{-9} wt. % for the oxidative and dissolutive regime respectively. Exposed samples have been characterized, reporting no corrosive interaction, neither in the oxygen-rich environment, nor in the oxygen-free one. The superior stability of the Al_2O_3 coatings protects efficiently the underlying substrate, independently from the oxygen content inside the liquid metal.

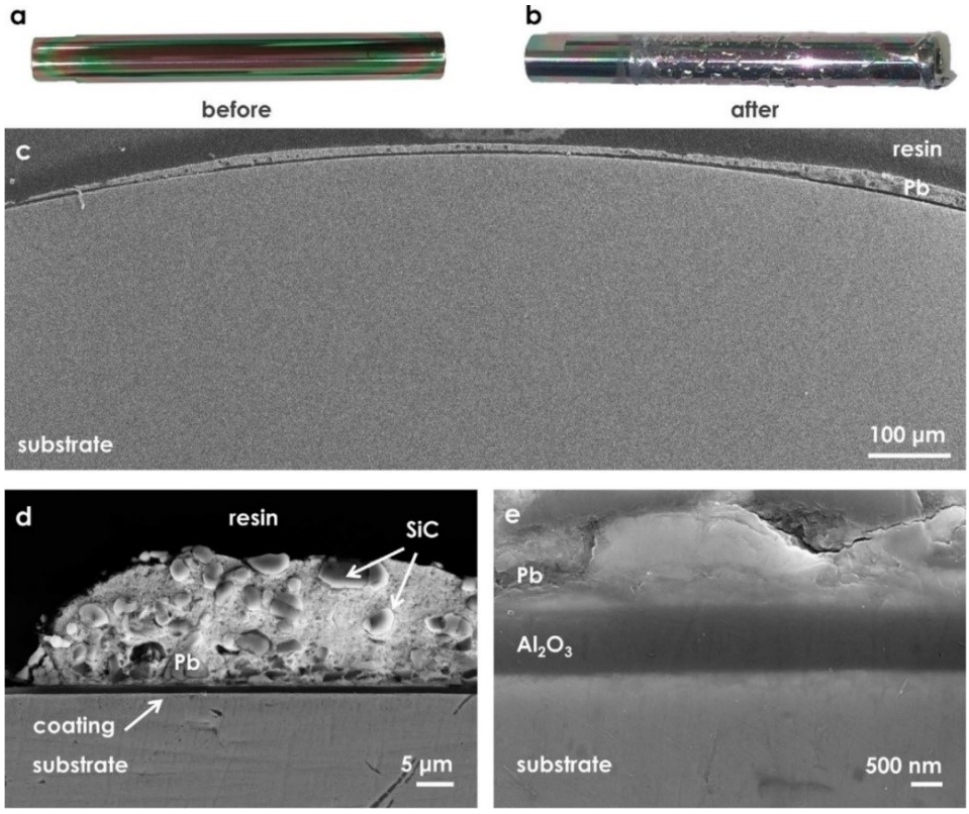

FIG. 2. Coated 15-15Ti AIM1 cylinders before (a) and after (b) corrosion test in static Pb (550°C, 4000 h, 10^{-8} wt. % O). Liquid Pb does not corrode the steel substrate, neither at the macroscopic (c) nor at the microscopic scale (d and e) [14]

After this preliminary investigation, longer tests in liquid lead have been conducted in low oxygen conditions up to 4000 hours (FIG. 2). This regime has been selected for two reasons: firstly, because of a conservative approach has been adopted (corrosion rates in dissolutive conditions are, in general, several times higher than in oxidative regime for austenitic steels). Secondly, the absence of oxygen inside lead (and thus the absence of related impurities such as PbO) would represents a huge improvement for the safe operation of the LFR system. Again, the results obtained showed that nano-ceramic films withstood the corrosive action of the liquid lead, confirming the effectiveness of PLD-Al_2O_3 in protecting steels for LFR applications (see FIG. 2).

Finally, long-term exposure tests of PLD-Al_2O_3 coatings in flowing lead will be performed in the framework of GEMMA H2020 European project.

Protective coatings of Al_2O_3 can be also obtained by the alternative technique Atomic Layer Deposition (ALD). This technique is among the most versatile and it is capable of coat complex geometries. For this reason, the technique is considered to coat FA's in ALFRED. In the ALD process, the steel substrate inside in a vacuum chamber is alternately exposed to two different precursors, e.g. $Al(CH_3)_3$ and H_2O to form Al_2O_3 [16][17]. By varying the number of cycles, for example, it is possible to finely tune the thickness of the final Al_2O_3 film. Presently this deposition method is under development at IIT in Milan for the application in heavy liquid metals.

3.2. **FeCrAl Aluminizing**

Diffusion alloying method such as pack cementation is considered to coat complex component such as HXs, DHR, pump impellers and internals. The method involves Al diffusion into the steel bulk and it is obtained by thermal decomposition at high temperature of powder mixtures containing Al and other alloying elements of the surface treatment with an activator salt (halide salts, generally chlorides and fluorides) and an inert filler (usually Al_2O_3) (the pack) [18]. In the pack, the activator creates halides vapors that reacts with the substrate to be coated releasing the Al and the other alloying elements: the gaseous products of the reaction are halide vapors that are recycled and restart the process. The process forms a coating and a diffusion layer on the substrate with features that depend on the Al activity and temperature of the process. The method requires an accurate control of the Al content in the layer. Indeed, brittle and less-protective Al-enriched phases (e.g. Al_5Fe_2) are prone to form when Al content in the outer layer is high. Here, heat treatment after the deposition can be applied to complete Al incorporation into the steel matrix and transforming the Fe_2Al_5 phase into the more protective Fe-Al and α-Fe(Al) phases [19]. Then, Al/Fe/Cr powder ratio requires optimization to have a low enough Al activity in the final layer [18]. The thickness of the Al layer is usually in the range 40-120 μm.

FeCrAl diffusion coating, deposited by pack cementation on 15-15Ti, were tested in ENEA laboratories at Brasimone at 550°C for 1500 hours in static liquid lead with high and low oxygen concentration. The coated specimens were prepared and optimized by RINA-CSM S.p.a. (Centro Sviluppo Materiali, Rome).

SEM images in FIG. 3 illustrate the morphology of FeCrAl-coated 15-15Ti steel. The layer consists of a broader interfacial/interdiffusion layer and an outer layer with lower thickness. The outer and the interdiffusion layers are ~17 μm and 59 μm thick respectively and a compact layer covers the entire surface.

The elemental distribution across the coating layer determined by EDX indicates that Al content in the interfacial zone was less than that in the outer zone, corresponding then to different phases. Going deep, Al decreases from ~47 % at. to ~11 % at. and reaches a value < 1 % at. at about 80 μm of depth, while Fe and Cr increase from 35 % at. and 5 % at. to 58 % at. and 16 % at. respectively. Considering the atomic ratios, the outer layer consists mostly of FeAl phase, as typical for pack cementation and aluminide coatings with high Al activity. Between the outer and the interdiffusion layers a Ni-rich area, depleted of Fe and Cr, is detected.

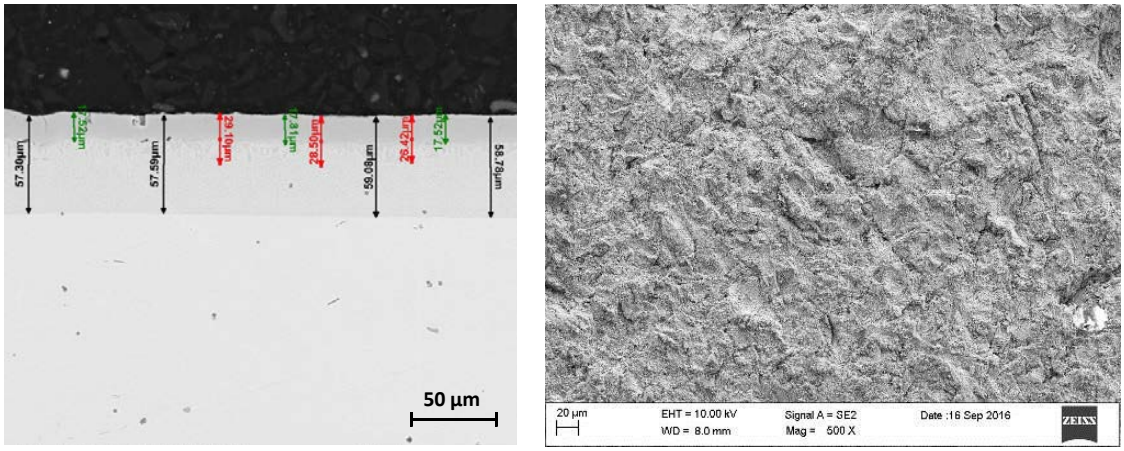

FIG. 3. SEM images of FeCrAl diffusion coating by pack cementation on 15-15Ti steel showing the cross-sectional view (left) and the longitudinal view (right)

Higher-magnification SEM images (FIG. 4) reveals other microstructural features, such as small precipitates appearing as needles and flower-like structures at the interface between the two layers. The black needles (see white arrows), observed underneath the outer layer, could be ascribable to AlN, usually detected in pack cementation coating. The flower-like structures are instead AlNi precipitates, exhibiting in whole interdiffusion layer but mainly concentrated near the interface between the two layers.

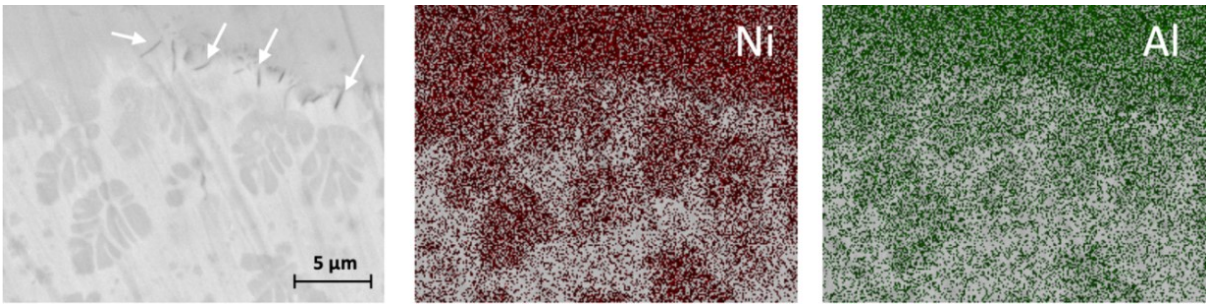

FIG. 4. SEM image of outer layer/interdiffusion layer interface and corresponding EDX distribution map of Ni and Al

FIG. 5 shows SEM images of diffusion coated 15-15Ti after the exposure in static Pb for 1500 hours at 550°C with high (10^{-3} % wt. O, cross-sectional view) and low oxygen concentration (10^{-8} % wt. O, longitudinal view). The specimens do not show any evidence of dissolution attack and Pb penetration in both cases: the overall thickness of the coating is nearly unchanged (left) and shows poor interaction with liquid lead (right), since lead droplets remain isolated along the whole surface.

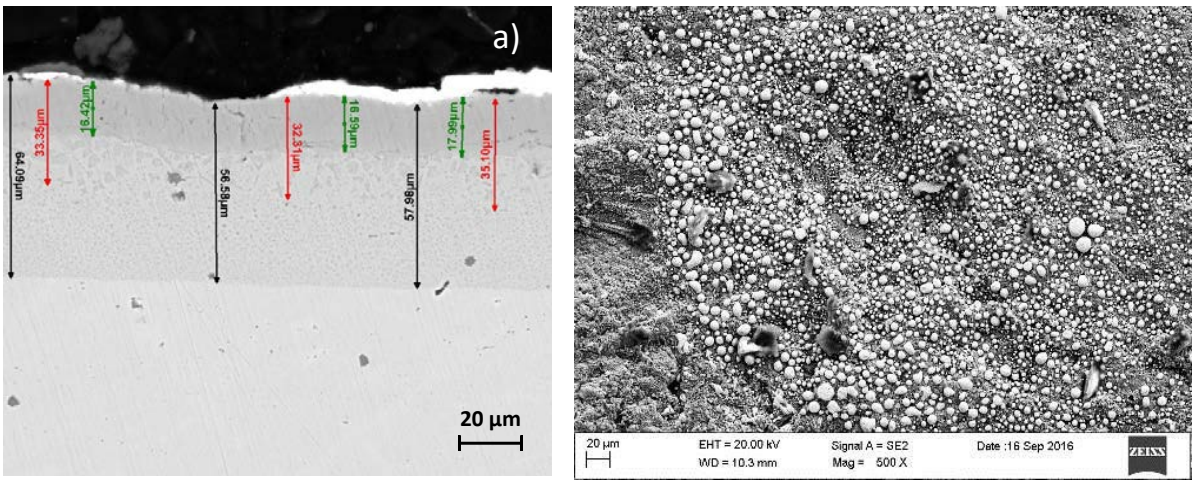

FIG. 5. SEM images of pack cementation coating on 15-15Ti steel after exposure to static liquid Pb at 550°C for 1500 h, as cross-sectional view for the test at high oxygen (left) and as longitudinal view for the test at low oxygen (right)

Pack cementation technique is industrially available for austenitic steels. Indeed, although good optimization of the diffusion coating was obtained by CSM, there will be the need to use industrial equipment allowing the coating of large parts for the protection of components such as HX and DHR. Thus, in the frame of GEMMA project, exposure tests in liquid lead of pack cementation diffusion coating by an industrial supplier [20] will be performed in flowing conditions.

3.3. AlTiN coating by Physical Vapor Deposition (PVD)

AlTiN coating as well as TiN coating are industrial coatings having high hardness and wear resistance and they are usually employed in the production of mechanical parts and tools subjected to wear/erosion [21]. Based on these features, they are good candidate material for the protection of pump impellers, which are subjected to significant wear/erosion due to the high lead flow velocity (up to 20 m/s).

In ENEA Brasimone, both TiN and TiAlN coatings on different substrates were tested in liquid lead to assess the protection feature against liquid metal corrosion. The main difference between the two coatings stands in the presence of Al, which should improve the oxidation resistance of the layer in oxidative environment (such as oxygen-saturated liquid metals) [22].

The coatings were produced by RINA-CSM with arc-Physical Vapor Deposition (PVD). Both coatings were compact and adherent, with thickness of 6-10 µm for TiN layer and 1-2 µm for TiAlN layer.

The behavior of TiN and TiAlN layers in liquid lead are shown in

FIG. 6 and FIG. 7 respectively. TiN layer is subjected to oxidation after exposure to lead at 480°C for 1000h at high oxygen concentration, whereas TiAlN does not show evidence of oxidation after 1500h in lead at 450°C and high oxygen concentration.

Although the tests were conducted with different parameters, AlTiN layer shows higher oxidation resistance and can be considered a good candidate for the protection of pump impellers.

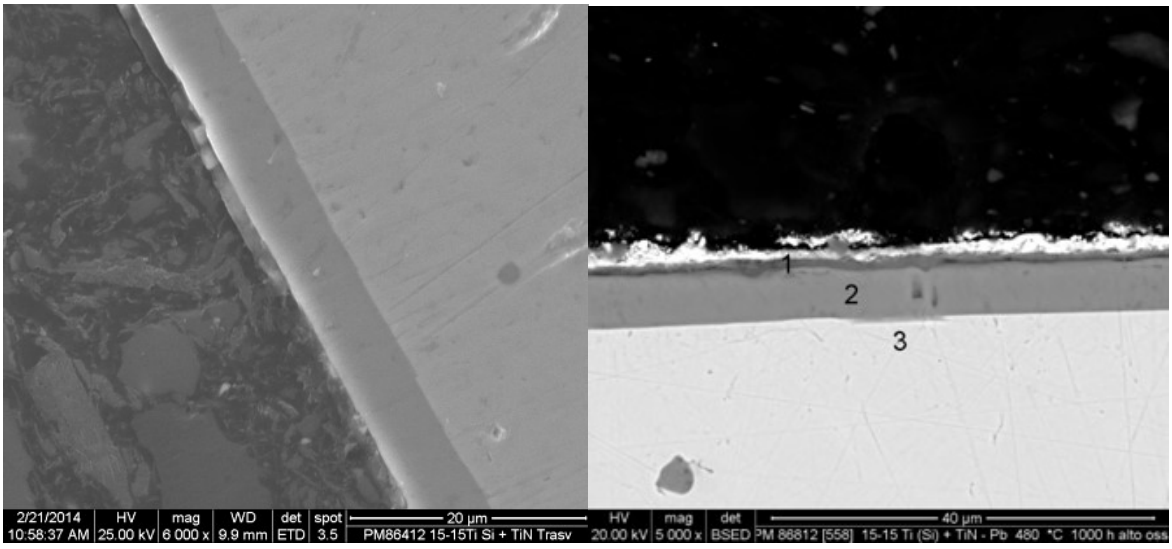

% wt.	1	2	3
N	13.6	31.8	-
O	41.0	-	-
Si	-	-	0.8
Ti	42.1	67.8	1.9
Cr	-	-	14.1
Mn	-	-	1.6
Fe	0.4	0.4	64.8
Ni	-	-	15.1
Mo	-	-	2.0
Pb	2.9	-	-

FIG. 6. TiN layer as deposited on 15-15Ti steel substrate (left) and TiN layer after exposure in liquid Pb at 480°C, 1000h, 3·10-4 %wt. O (center) with point elemental composition by EDX of the layer after the test (right)

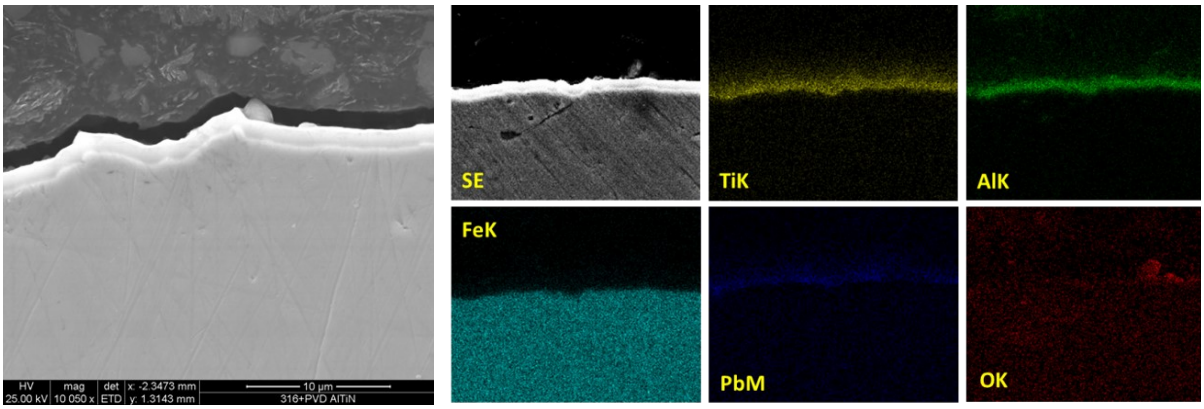

FIG. 7. TiAlN layer as deposited on AISI 316 steel (left) and EDX map of TiAlN layer after exposure in liquid Pb at 450°C, 1500h, $2 \cdot 10^{-4}$ %wt. O (right)

3.4. Al_2O_3 by Detonation Gun Spray

D-gun spray process is a thermal spray coating process which gives an extremely good adhesive strength, low porosity and coating surface with compressive residual stresses [23].

The coating is realized by a hot powder that travels down the barrel of the detonation gun at a high velocity thanks to a controlled explosion created in the first part of the gun (see FIG. 8). A precisely measured amount of the combustion mixture, consisting of oxygen, nitrogen and acetylene, are feed through a tubular barrel closed at one end. Simultaneously, a predetermined amount of the coating powder is feed into the combustion chamber. The process heats and accelerates the particles to a plasticizing stage with velocity of 1200 m/sec. The gas mixture inside the chamber is ignited by a simple spark plug. The combustion of the gas mixture generates high-pressure shock waves (detonation wave), which then propagate through the gas stream. The gun is cooled with water and a chiller system. The Detonation Gun Spray apparatus at ENEA Brasimone is shown in FIG. 9.

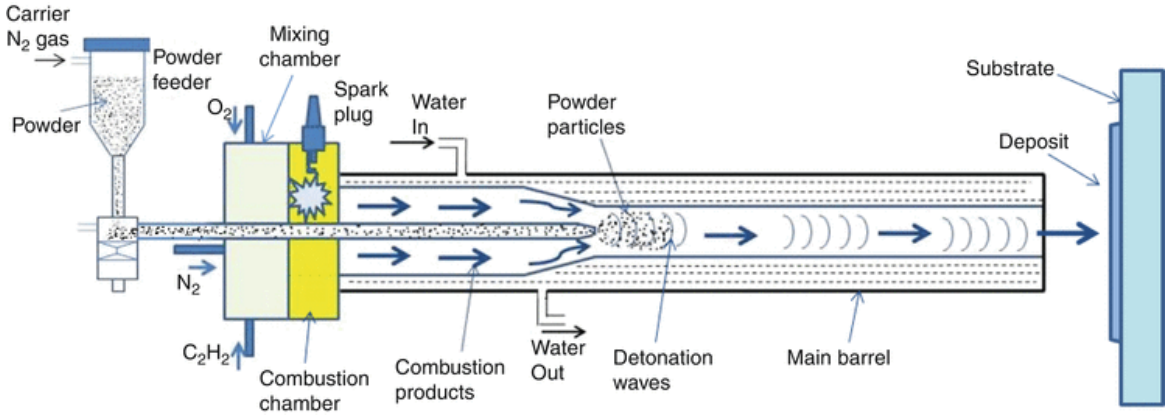

FIG. 8. Schematic sketch of the Detonation Gun Spray technique

FIG. 9. Picture of Detonation Gun Spray installed at ENEA Brasimone

Detonation spraying is performed using a Computer-Controlled Detonation Spraying facility CCDS 2000 (STPC, Siberia). The explosive charge was kept within 50-70% of the barrel volume and different O_2/C_2H_2 ratios and nitrogen as a carrier gas.

Due to the features of coating process, it is not possible to reduce the thickness of the coating lower than 20 µm, therefore this technique can be used to coat big components such as reactor vessel or internals.

Al_2O_3 coatings were deposited on AISI 316L stainless steel (see FIG. 10) and other substrate (such as AISI 304, 15-15Ti AIM1) and they were preliminarily investigated in liquid lead showing no corrosion damage. The mechanical fatigue tests have shown also good adhesion after the test at 500°C. In the frame of GEMMA project, the qualification of this coating will go on, with long-term exposure tests in lead in flowing conditions.

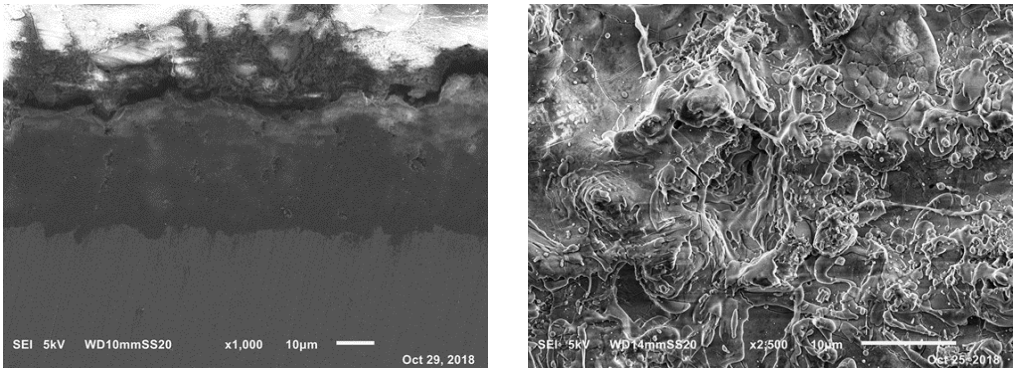

FIG. 10. Cross section SE-SEM image (left) and longitudinal SE-SEM image (right) of Al_2O_3 coating manufactured with Detonation Gun on AISI 316L

3.5. **AFA steels**

Although few studies exist about neutron irradiation damage, AFA steels can be considered as structural materials for LFR components thanks to their high creep and corrosion resistance [24] where neutron irradiation level is low or negligible. For these reasons, AFA steels are taken into consideration for ALFRED internals, SG and DHR in the operational Stages 2 and 3.

Several AFA steels with different amounts of Al, Cr and Ni were investigated in recent years to identify the concentrations at which the steels are corrosion resistant and, at the same time, preserve the austenite structure. Indeed, Ejenstam et al. found that AFA steel with ~ 2.5 % wt. Al, 14 % wt. Cr and low amount of Ni (14 % wt.) exhibited excellent corrosion resistance due to thin Al_2O_3 protective layer, but a phase transition from austenite to ferrite occurred during long-term exposure [25]. On the contrary, by increasing Ni concentration in the matrix (up to 20 % wt.), AFA steel preserved the austenite phase but displayed localized dissolution attacks [25].

Since both Al and Cr are stabilizing elements of ferrite in steels, their concentration should be balanced together with Ni (austenite stabilizer) to avoid austenite-ferrite transition as well as well to have an Al concentration sufficient to ensure Al_2O_3 (+Cr_2O_3) surface passivation. Based on the experimental results, some authors have found a general formula guarantee these two requirements (wt. %): Fe-(20-29)Ni-(15.2-16.5)Cr-(2.3-4.3)Al [26]. Similar results were obtained by Yamamoto et al. who noted that protective Al2O3 scale can be formed at 650-800°C with little amount of Al (~ 2.5 wt.%), when Nb (carbide former) is added up to 1 % wt. and Ti, V and N are minimized in the matrix [24].

In ENEA two AFA steels with different chemical composition were preliminary investigated with short-term tests at 550°C for 1000 hours in static liquid lead at high and low oxygen concentration. The materials were delivered by ORNL in plate shape produced by VIM-VAR technique followed by homogenization, hot-rolling and annealing treatments. Plate specimens with Ra ~ 0.02-0.04 μm were used for the corrosion tests. The chemical composition of the two AFA steels is reported in TABLE 11.

TABLE 11: NOMINAL COMPOSITION (IN WT. %) OF AFA OC-Q (LOW NI) AND OC-E (HIGH NI) PROVIDED BY ORNL.

AFA	C	Cr	Ni	Mn	Al	Cu	Nb	Si	V	Ti	B
12Ni (OC-Q)	0.2	14	12	4	2.5	3	0.6	0.15	0.05	0.05	0.01
25NI (OC-E)	0.2	14	25	2	4	0.5	2.5	0.15	0.05	0.05	0.01

After the exposure to lead with high oxygen concentration (10-3 % wt.), both AFA steels undergoes oxidation but in different ways and with different magnitude. In the case of OC-Q 12Ni, most of the surface is unaffected after the exposure. However, in some area the AFA exhibited non-protective Fe-rich oxide layer (0.5-1 μm thick) and oxidation spots (depth up to 20 μm) with single or double structure composed of internal Fe-Cr-Ni-Al mixed oxide and external Fe_3O_4 magnetite (see FIG. 11, left). It is possible to note that the matrix is enriched with globules (white little spots), which correspond to Nb carbides. To the opposite, OC-E 25Ni shows strong oxidation with formation of large and flat oxidation area composed of Fe-Cr-Ni-Al mixed oxide (depth up to 70 μm) together with oxidation spots (similar to that of AFA 12Ni) with depth up to 10-15 μm (FIG. 11, right).

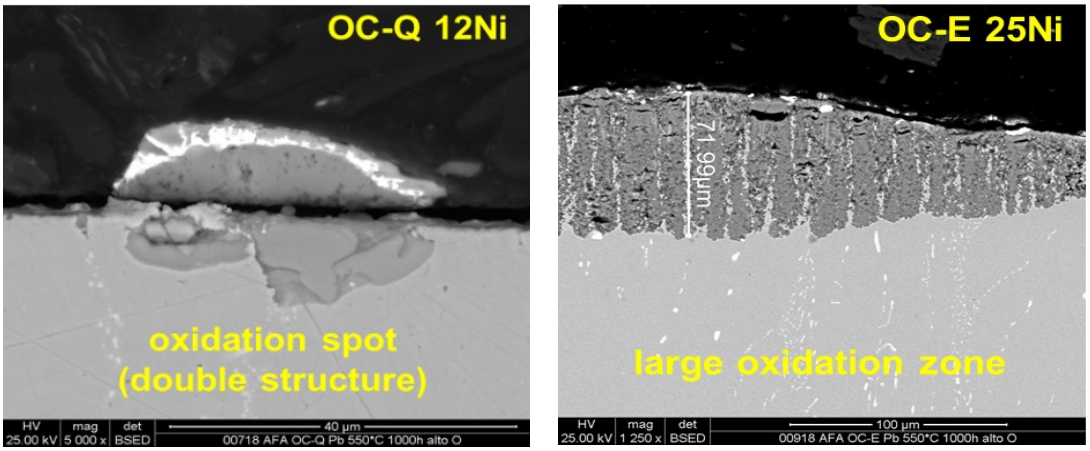

FIG. 11. BSE-SEM images showing oxidation spots for AFA OC-Q 12Ni (left) and large oxidation area for OC-E 25Ni (right) after exposure to static liquid Pb at 550°C, 1000h and 10^{-3} %wt. O

On the other hand, the two materials exhibit very good corrosion behavior after exposure in liquid lead with low oxygen concentration (10-8 % wt.). Observing SEM images in Figure 12, the surface is unaffected for both AFA steels as no significant oxidation or dissolution attacks is detected. Al_2O_3 layer was not clearly identified from SEM pictures since too thin for the resolution of the microscope, but Al and O peaks were detected by EDX line-scan on the outer surface suggesting the presence of external protective Al_2O_3 layer.

After the exposure, XRD analysis was performed to check possible phase transitions. Specifically, the formation of FexAly was detected in 12Ni AFA samples, ascribable to the phase transition from austenite to ferrite as the test goes by.

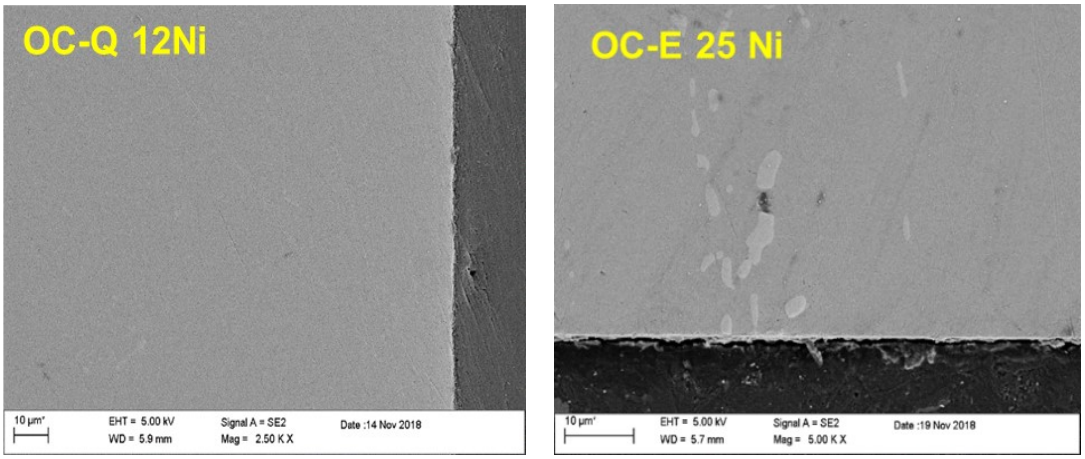

FIG. 12: SE-SEM images showing unaffected surface for AFA OC-Q 12Ni (left) and OC-E 25Ni (right) after exposure to static liquid Pb at 550°C, 1000h and 10^{-8} %wt. O.

Corrosion mitigation strategies such as coatings and advanced materials are under development and qualification in liquid lead to support the operation of ALFRED LFR reactor in the later stages, where the primary cycle temperatures will be high enough to hinder the use of bare steels due to corrosion issues.

For fuel cladding structures, Al_2O_3 coating by PLD is the reference choice thanks to the excellent corrosion resistance in static liquid lead, the metal-like mechanical properties and the good performance under heavy ions irradiation. Long-term qualification in lead flowing conditions will be performed in the frame of GEMMA project to further validate this mitigation solution for fuel cladding structures, as well as mechanical tests in liquid lead will be performed. Similarly, also Al_2O_3 layer from Detonation Gun, potentially considered as protective coating for reactor vessel, will be qualified from the point of view of the long-term corrosion in lead.

FeCrAl aluminizing such as pack cementation is considered for the protection of components with complex geometry. Although good results were obtained in recent years on aluminized steel substrates produced with small-scale pack cementation process, the need to coat large and complex components such as HXs or DHR requires the investigation of solution from industrial methods. About that, the qualification of industrial pack cementation process will be performed in liquid lead during GEMMA project.

AlTiN coating is considered for the protection of primary pump impellers for the high wear/erosion resistance, and it is industrially available. Preliminary exposure tests in liquid lead showed no evidence of corrosion but testing and qualification on prototype impeller component should be performed to assess finally the suitability for the protection of primary pumps.

Finally, short-term exposure tests of AFA steels showed that these materials are promising for their high corrosion resistance in liquid lead. Long-term corrosion tests will be performed in the future to fully qualify these materials and to investigate the need for optimizing the composition, which has to respect the requirements of corrosion resistance and preservation of the austenite structure.

ACKNOWLEDGEMENT

The results here described were obtained in the frame of several founded projects. The authors are grateful to the Italian Framework Program between ENEA and the Ministry of Economic Development (AdP MiSE-ENEA, B.3.1-LP2), the European project MATISSE (EURATOM FP7, n°604862) and the EUROFUSION Breeding Blanket project (n°633053) for the financial support.

The authors wish to thank also Dr Y. Yamamoto and Dr M. Brady from Oak Ridge National Laboratory (ORNL, USA) for providing AFA materials for corrosion tests in liquid lead.

REFERENCES

[1] ALEMBERTI, A., SMIRNOV, V., SMITH, C.F., TAKAHASHI, M., "Overview of lead-cooled fast reactor activities", Prog. Nucl. Energ. 77 (2014) 300-307.

[2] Handbook on Lead-bismuth Eutectic Alloy and Lead Properties, Materials Compatibility, Thermal-hydraulics and Technologies, OECD/NEA No. 7268 (2015).

[3] TOSHINSKY, G.I., KOMLEV, O.G., TORMYSHEV, I.V., PETROCHENKO, V.V., "Effect of Potential Energy Stored in Reactor Facility Coolant on NPP Safety and Economic Parameters", World Journal of Nuclear Science and Technology 3 (2013) 59-64.

[4] SCHROER, C., WEDEMEYER, O., NOVOTNY, J., SKRYPNIK, A., KONYS, J., "Selective leaching of nickel and chromium from type 316 austenitic steel in oxygen-containing lead-bismuth eutectic (LBE)", Corros. Sci. 84 (2014) 113-124.

[5] FRIGNANI, M., ALEMBERTI, A., TARANTINO, M., GRASSO, G., "ALFRED staged approach", International Congress on Advances in Nuclear Power Plants ICAPP 2019, May 12-15 Juan-les-pins.

[6] FRIGNANI, M., ALEMBERTI, A., VILLABRUNA, G., ADINOLFI, R., TARANTINO, M., GRASSO, G., PIZZUTO, A., TURCU, I., VALECA, S., "ALFRED: a Strategic Vision for LFR Deployment", Trans. of ANS 117 (2017) 1468-1471.

[7] MULLER, G., HEINZEL, A., KONYS, J., SCHUMACHER, G., WEISENBURGER, A., ZIMMERMANN, F., ENGELKO, V., RUSANOV, A., MARKOV, V., "Behavior of steels in flowing liquid PbBi eutectic alloy at 420-600°C after 4000-7200h", J. Nucl. Mater. 335 (2004) 163-168.

[8] KLOK, O., LAMBRINOU, K., GAVRILOV, S., LIM, J., DE GRAEVE, I., "Effect of Lead-Bismuth Eutectic oxygen concentration on the onset of dissolution corrosion in 316 austenitic stainless steel at 450°C", Journal of Nuclear Engineering and Radiation Science, Vol. 4 (2018) 031019-1/7.

[9] GARCÌA FERRÉ, F., BERTARELLI, E., CHIODONI, A., CARNELLI, D., GASTALDI, D., VENA, P., BEGHI, M.G., DI FONZO, F., "The mechanical properties of a nanocrystalline Al_2O_3/α-Al_2O_3 composite coating measured by nanoindentation and Brillouin spectroscopy", Acta Mater. 61 (2013) 2661-2670.

[10] IADICICCO, D., BASSINI. S., VANAZZI, M., MUÑOZ, P., MOROÑO, A., HERNANDEZ, T., GARCÍA-CORTÉS, I., SÁNCHEZ, F.J., UTILI, M., GARCÍA FERRÉ, F., DI FONZO, F., "Efficient hydrogen and deuterium permeation reduction in Al_2O_3 coatings with enhanced radiation tolerance and corrosion resistance", Nucl. Fusion 58 (2018) 126007 (7pp).

[11] MUÑOZ, P., HERNANDEZ, T., GARCÌA-CORTÉS, I., SANCHEZ, F.J., MAIRA, A., IADICICCO, D., VANAZZI, M., UTILI, M., DI FONZO, F., MOROÑO, A, "Radiation effects on deuterium permeation for PLD alumina coated Eurofer steel measured during 1.8 MeV electron irradiation", J. Nucl. Mater. 512 (2018) 118-125.

[12] IADICICCO, D., VANAZZI, M., GARCÍA FERRÉ, F., PALADINO, B., BASSINI, S., UTILI, M., DI FONZO, F., "Multifunctional nanoceramic coatings for future generation nuclear systems", Fus. Eng. Des. 146 (2019) 1628-1632.

[13] GARCÌA FERRÉ, F., MAIROV, A., CESERACCIU, L., SERRUYS, Y., TROCELLIER, P., BAUMIER, C., KAÏTASOV, O., BRESCIA, R., GASTALDI, D., VENA, P., BEGHI, M.G., BECK, L., SRIDHARAN, K., DI FONZO, F.., "Radiation endurance in Al_2O_3 nanoceramics", Sci. Rep. 6:33478 (2016) 1-9.

[14] FERRÉ, G., MAIROV, A., IADICICCO, D., VANAZZI, M., BASSINI, S., UTILI, M., TARANTINO, M., BRAGAGLIA, M., LAMASTRA, F.R., NANNI, F., CESERACCIU, L., SERRUYS, Y., TROCELLIER, P., BECK, L., SRIDHARAN, K., BEGHI, M.G., DI FONZO, F., "Corrosion and radiation resistant nanoceramic coatings for lead fast reactors", Corros. Sci.124 (2017) 80-92.

[15] GARCÍA FERRÉ, F., MAIROV, A., VANAZZI, M., SERRUYS, Y., LEPRETRE, F., BECK, L., VAN BRUTZEL, L., CHARTIER, A., BEGHI, M.G., SRIDHARAN, K., DI FONZO, F., "Extreme ion irradiation of oxide nanoceramics: Influence of the irradiation spectrum", Acta Mater. 143 (2018) 156-165.

[16] JARVIS, K.L., EVANS, P.J., NELSON, A., TRIANI, G., "Comparisons of alumina barrier films deposited by thermal and plasma atomic layer deposition", Materials Today Chemistry 11 (2019) 8-15.

[17] ZAZPE, R., PRIKRYL, J., GÄRTNEROVA, V., NECHVILOVA, K., BENES, L., STRIZIK, L., JÄGER, A., BOSUND, M., SOPHA, H., MACAK, J.M., "Atomic Layer Deposition Al_2O_3 Coatings Significantly Improve Thermal, Chemical, and Mechanical Stability of Anodic TiO_2 Nanotube Layers", Langmuir 33 (2017) 3208-3216.

[18] DELOFFRE, PH., BALBAUD-CÉLÉRIER, F., TERLAIN, A., "Corrosion behaviour of aluminized martensitic and austenitic steels in liquid Pb-Bi", J. Nucl. Mater. 335 (2004) 180-184.

[19] GLASBRENNER, H., KONYS, J., VOSS, Z., WEDEMEYER, O., "Corrosion behaviour of Al based tritium permeation barriers in flowing Pb-17Li", J. Nucl. Mater. 307-311 (2002) 1360-1363.

[20] https://www.turbocoating.com/

[21] SANTECCHIA, E., HAMOUDA, A.M.S., MUSHARAVATI, F., ZALNEZHAD, E., CABIBBO, M., SPIGARELLI, S., "Wear resistance investigation of titanium nitride-based coatings", Ceramics International Vol. 41, No 9, Part A (2015) 10349-10379.

[22] CHIM, Y.C., DINGB, X.Z., ZENG, X.T., ZHANG, S., "Oxidation resistance of TiN, CrN, TiAlN and CrAlN coatings deposited by lateral rotating cathode arc", Thin Solid Films 517 (2009) 4845-4849.

[23] SINGH, L., CHAWLA, V., GREWAL, J.S., "A Review on Detonation Gun Sprayed Coatings", Journal of Minerals and Materials Characterization and Engineering Vol. 11, No 3 (2012) 243-265.

[24] YAMAMOTO, Y., BRADY, M.P., SANTELLA, M.L., BEI, H., MAZIASZ, P.J., PINT, B.A., "Overview of strategies for high-temperature creep and oxidation resistance of alumina-forming austenitic stainless steels", Metallurgical and Materials Transactions A 42 (2010) 922-931.

[25] EJENSTAM, J., SZAKÁLOS, P., "Long term corrosion resistance of alumina forming austenitic stainless steels in liquid lead", J. Nucl. Mater. 461 (2015) 164-170.

[26] SHI, H., JIANU, A., WEISENBURGER, A., TANG, C., HEINZEL, A., FETZER, R., LANG, F., STIEGLITZ, R., MÜLLER, G., "Corrosion resistance and microstructural stability of austenitic Fe-Cr-Al-Ni model alloys exposed to oxygen-containing molten lead", J. Nucl. Mater. 524 (2019) 177-190.

SOME NEW R&D FOCUS IN STRUCTURE MATERIALS LICENSING FOR THE SVBR-100 REACTOR FACILITIES

A.V.DEDUL
JSC "AKME-engineering"
Moscow, Russian Federation
Email: A.Dedul@SVBR.org

O.G.Komlev
JSC "AKME-engineering"
Moscow, Russian Federation

A.V.Kondaurov
JSC "AKME-engineering"
Moscow, Russian Federation

Abstract

Development and justification of service properties for materials used in reactor design and specific design solutions are inextricably connected. Special steels with increased corrosion resistance in the lead-bismuth coolant have been created and industrially mastered in Russia. A distinctive feature of these steels is the increased content of silicon as an alloying element that contributes to the stabilization of protective oxide films, limiting their diffusion permeability. Implementation of the fast neutron reactor SVBR-100 with lead-bismuth coolant required an extended study of the characteristics of radiation and corrosion resistance of the materials used. In the frame of R & D on materials substantiation, samples of reactor materials were irradiated to damage doses up to 25 dpa. As a result of performed researches the limits of the damage dose, beyond which the materials become unacceptably embrittled were determined. The basic mechanisms of radiation embrittlement and their regularities are established. Necessary measures were implemented to ensure the radiation resistance of materials for the entire design life (400 thousand hours). The second important result was the successful completion of corrosion resistance studies for the fuel rod cladding materials for a full lifetime (50 thousand hours). At the same time, an important conclusion of the R&D program on substantiation of materials and works on project licensing was made. New focus formed on the need to expand the scope of necessary research to the field of extreme states of materials. These works are necessary to justify the project in area of severe accidents associated with beyond design basis core damage accidents.

1. INTRODUCTION

The development of the SVBR-100 reactor is based on the following basic principles:

— the project uses lead-bismuth coolant and mastered technology of dissolved oxygen control in the coolant to ensure corrosion resistance of materials;
— this is generation IV technology that can demonstrate, among other, how the inherent safety characteristic of fast neutron heavy liquid metal cooled (HLMC) reactors can be converted into cost savings;
— this technology is based on industrially available materials and technologies that have clear limits, including temperature limits, thus, design elements, materials, technological schemes, parameters and modes of operation have been optimized to exclude redundant systems and equipment, the volume of construction and finally – capital costs for plant construction.

At the initial stage of the project development the main structural materials were selected:

— EP-823 steel of ferritic-martensitic class;
— EP-302 steel of austenitic class;
— 08X18H10T steel of austenitic class.

These materials meet the necessary requirements in terms of their characteristics, have been mastered by industry and tested in real operating conditions. Significant experience in BN reactors and the amount of experimental data on the characteristics of austenitic and ferritic-martensitic steels, including data on the effect of irradiation, are fully applicable to the SVBR project. Corrosion resistance and the possibility of using steels of these classes under certain temperature restrictions confirmed by both Russian and foreign studies [1,2,3].

At the same time, the existing practical experience and the volume of experimental studies performed (at the beginning of the SVBR project development) did not fully cover the new requirements for equipment lifetime and damaging factors typical for a fast neutron reactor [4]. The key issues that required confirmation at the initial stage of the project were:

— long-term corrosion resistance of fuel rod cladding materials;
— radiation resistance of reactor materials exposed to increased radiation damages.

These issues were solved at the first stage of the materials research program. The main results are presented below.

2. MAIN RESULTS OF MATERIALS CORROSION RESISTANCE JUSTIFICATION FOR SVBR-100 REACTOR

Longtime corrosion tests of cladding materials were made in the SM-1 and CU-2M test facilities in SSC RF – IPPE in conditions corresponding to the maximum temperature of the fuel rod cladding – 600 °C and the value of oxygen concentration of $1 \div 4 \times 10^{-6}$ % wt. The oxygen concentration level is chosen to avoid potentially dangerous processes of lead oxide deposition during rapid transition to the cooling mode and, at the same time, to avoid the potential for destruction of oxide films under extreme heating of the circuit above the nominal parameters (see Fig. 1, below). During the development of the project, a detailed analysis of the parameters of the reactor plant in all operating modes, including standby, start-up, and operation at different power levels, planned and emergency shutdown was performed. The key designs limits are determined considering the transients and uncertainties.

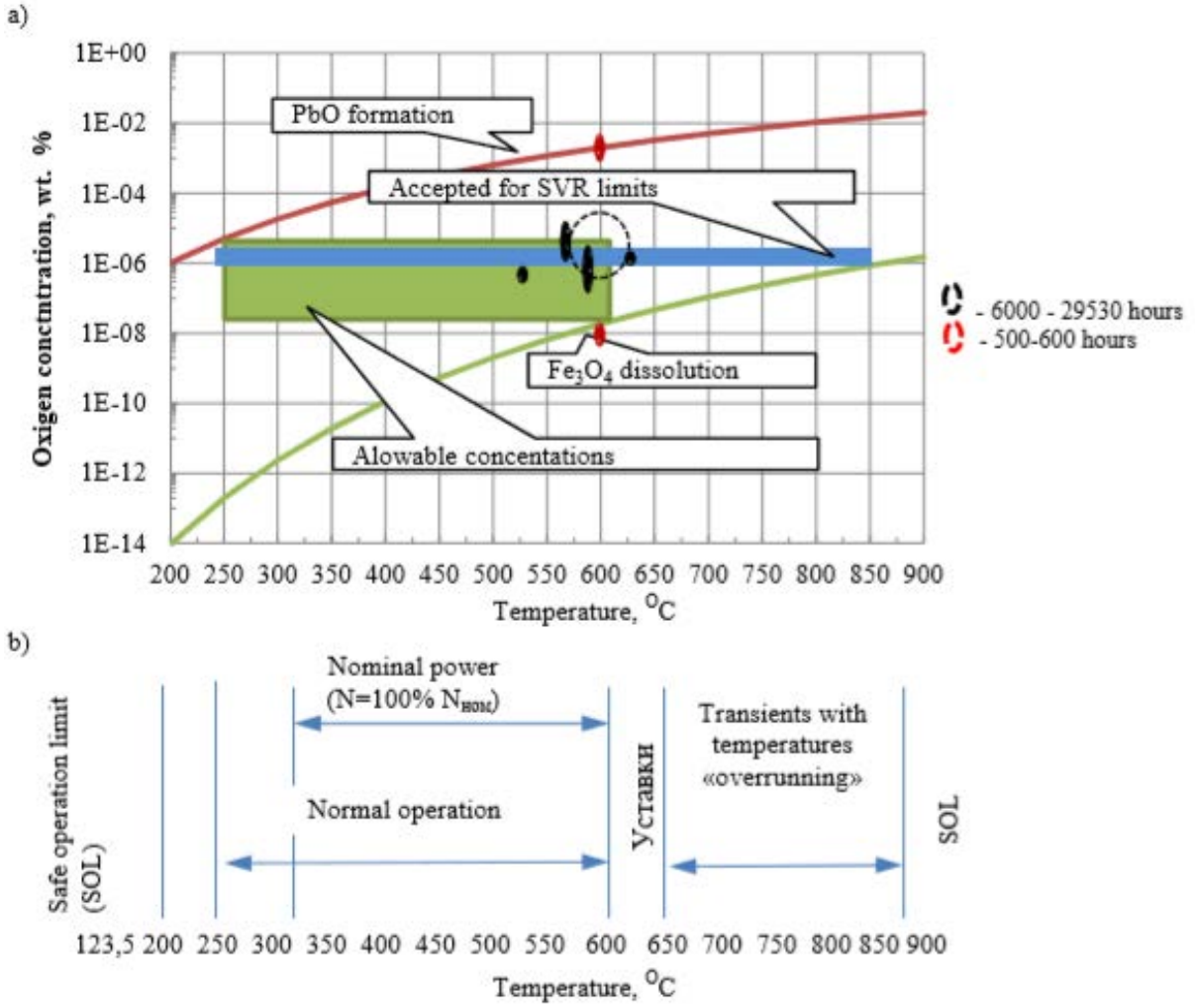

FIG. 1. The range of permissible values of oxygen concentration in the lead-bismuth coolant (a) and temperatures on the fuel rod claddings (b)

Results of sample studies (see Fig. 2) showed that the thickness of the oxide film at the end of the test does not exceed 14 μm. There were no cases of local corrosion. It was been noted:

— the growth rate of the oxide film slows down over time;
— the structure of the oxide film, its increase in time are the same, both for the case of pre-oxidized samples, and for samples without pre-treatment;
— there were no found mass change for any specimen.

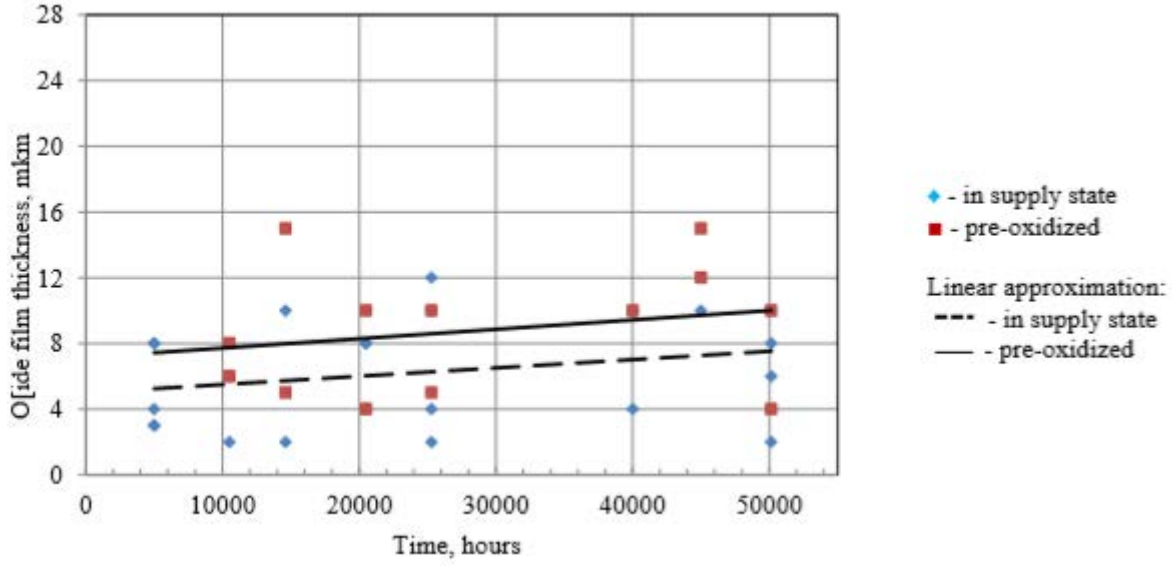

FIG. 2. Dependence of oxide film layer thickness at the surface of ferritic-martensitic steel from time of corrosion testing (T=600°C)

FIG. 3. Appearance of sample and microstructure of material after tests in flow of Pb-Bi:
A) 50 135 hours at 600 °C
B) 2 895 hours at 620 – 630 °C

The results of metallographic studies have shown that steel retains high structural stability under prolonged exposure to high temperatures (Fig. 3). The influence of the coolant on the change of mechanical properties of the metal is not noted.

3. MAIN RESULTS OF MATERIALS REACTOR TESTING

The temperature levels characterizing the working conditions of SVBR reactor materials are given in TABLE 1, the values of damaging doses on metal structures are shown in Fig. 4.

TABLE 1. TEMPERATURE LEVELS FOR THE MAIN COMPONENTS OF SVBR-100 IN THE MAIN OPERATING CONDITIONS

Title and dimensions	Parameter value at corresponding power level				
	100 % N_{nom}	70 % N_{nom}	50 % N_{nom}	30 % N_{nom}	0 % N_{nom}
Thermal power (MW_t)	280	196	140	84	0
Coolant temperature (°C)					
- at core inlet;	339	321	380	298	
- at core outlet;	484	465	453	443	200 – 250
- at steam generator inlet;	478	459	447	437	
- at steam generator outlet (top/bottom)	333/335	313/316	299/304	285/292	
Maximum (with «overheating factors») temperature of fuel rod cladding (°C)	620	602	589	579	250 – 300

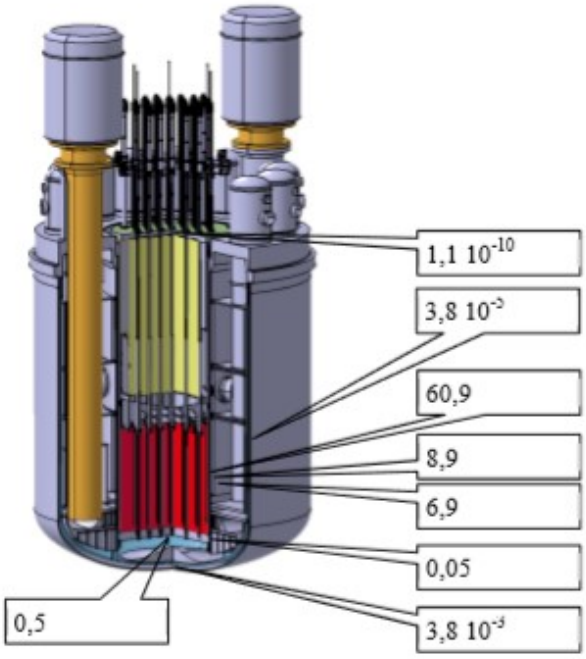

Fig. 4. The values of typical damage dose (in dpa) on the SVBR-100 reactor elements (reproduced from ref. [5])

A preliminary analysis of the available data and available materials made in the late 2000s [4] showed that the choice of materials for the project is very limited. Acceptable corrosion resistance in lead-bismuth coolant can provide only steels with a high content of silicon. The main prerequisites for the successful solution of material science problems of the project based on available experimental data were justified at the initial stage of the project [4, 6].

It is clear that the presence of silicon admixtures in steels has a negative impact on the mechanical characteristics of steels and especially on the radiation resistance of austenitic steels. The use of silicon steels is a compromise solution and requires careful study of their properties and justification of acceptable conditions for their use.

The experimental data available at that time (see Table 2) showed that the irradiated EP-302 steel is completely brittle and has a low level of brittle strength at room temperature of the test. At a test temperature equal to the irradiation temperature, the steel retains a reserve of plasticity at high strength properties. However, reliable characteristics were available for limited temperatures and damaging doses.

TABLE 2. MECHANICAL PROPERTIES OF EP-302 STEEL IRRADIATED IN A REACTOR WITH SVT [4]

No.	Dose, dpa	T_{clad}, °C	T_{test}, °C	R_m, MPa	$R_{p0.2}$, MPa	A, %
1	10	260	25	707	-	0
2	11	265	25	102	-	0
3	11	265	25	730	680	0
4	12	270	270	1200	1035	4.3
5	12	280	280	2305	1140	4.7
6	12	280	25	1058	865	0.67
7	11	280	25	130	-	0
8	10	290	250	1560	1320	6.4
9	10	290	290	1230	1025	2.4
10	10	290	25	135	-	0

The first phase of extended irradiation tests performed in 2008 - 2010 in the framework of the SVBR project showed the danger of unacceptable embrittlement at doses 11 - 22 dpa at irradiation temperatures of 315 - 470 °C.

In the second stage, the performed studies of mechanical properties in a narrow region at low damage doses and at temperatures up to 400 °C and at elevated dose of radiation at temperatures up to 550 °C.

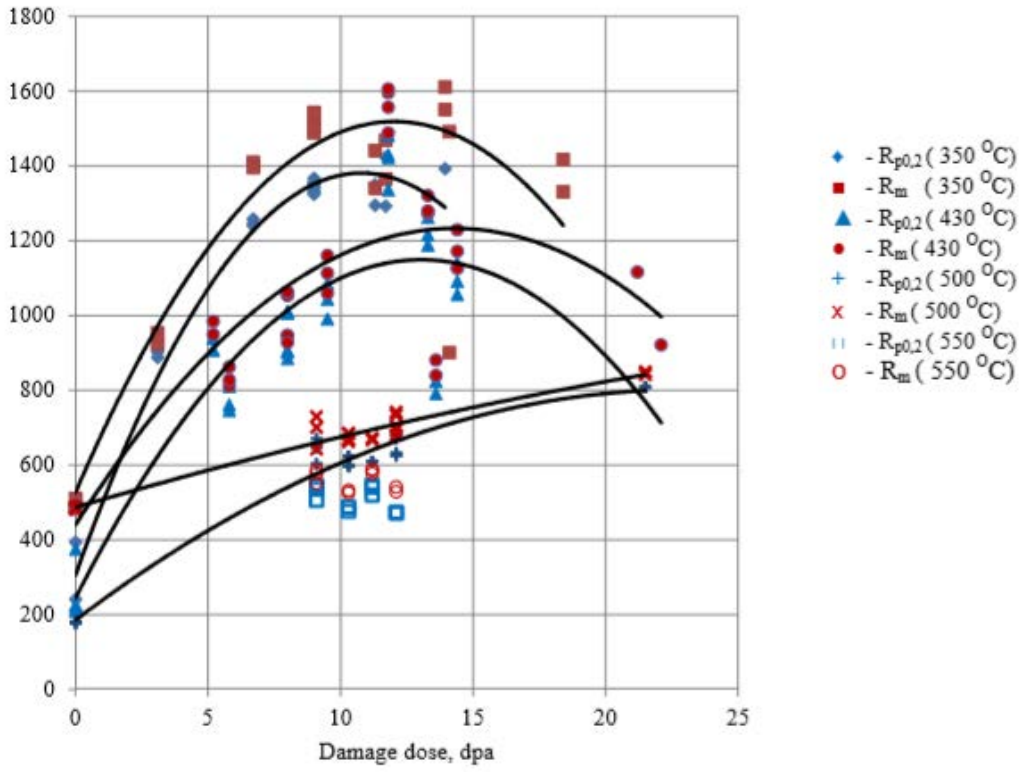

Fig. 5. Dependence of the tensile strength and yield strength of steel and welded joints on the test temperature and the damaging dose

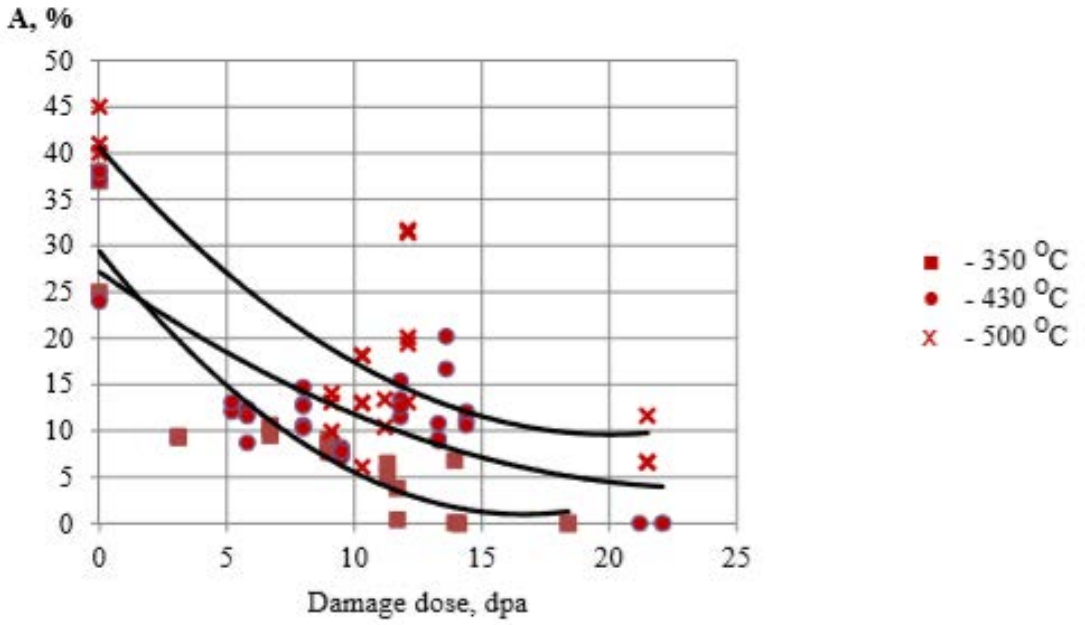

Fig. 6. Dependence of elongation of EP-302 steel and its welded joints on temperature and damaging dose

The new results mainly confirmed the preliminary characteristics and features of the influence of radiation on the mechanical properties of steel EP-302.

Studies were carried out on a large number of samples obtained from two melts with a variation in the composition of steel components within the technical specifications. The studies were carried out not only directly on steel samples, but also on weld samples. The characteristics of steel and welds showed similar values and presented in Fig. 5 and 6 without separation. The data are presented for samples at test temperatures approximately equal to the irradiation temperatures.

There is a general characteristic dependence - sufficiently rapid hardening of the steel and embrittlement up to zero values of relative elongation.

The rise of the irradiation temperature and test temperature shifts the boundary of embrittlement to the area of high damaging dozes.

Comparison of the obtained data with similar data for the well-studied 08X18H10T steel showed that:

— radiation resistance of steel EP-302 are slightly worse than those of steel 08H18H10T, and the mechanisms and dependencies of the changes of mechanical properties are somewhat different from similar mechanisms for steel 08X18H10T;
— the values of radiation swelling for steel EP-302 are located in the field of variation the same data for steel 08X18H10T.

For the purpose of a deeper analysis of the characteristics of radiation embrittlement of EP-302 steel, a complex of studies of the fracture resistance of steel and welded joints on samples with pre-applied cracks was carried out.

The studies correspond to ASTM E399-90 and GOST 25.506-85 standards [7]. The studies showed acceptable characteristics of fracture toughness of steel EP-302 in the initial state, comparable with the characteristics of steel 08X18H10T. There is a fairly rapid drop characteristics and stabilization of them after about 10-15 dpa at the level of the critical stress intensity factor K_{1C} = 50-25 MPa.m$^{1/2}$. Where K_{1C} is defined in accordance with ASTM E399-90 and GOST 25.506-85 standards.

The criteria for the acceptability of austenitic steel properties are similar to those developed for VVER and BN reactors.

— value of relative elongation A ≥ 1% and reduction of area ≥ 50%;
— fracture toughness K_{1C} ≥ 50 MPa.m$^{1/2}$.

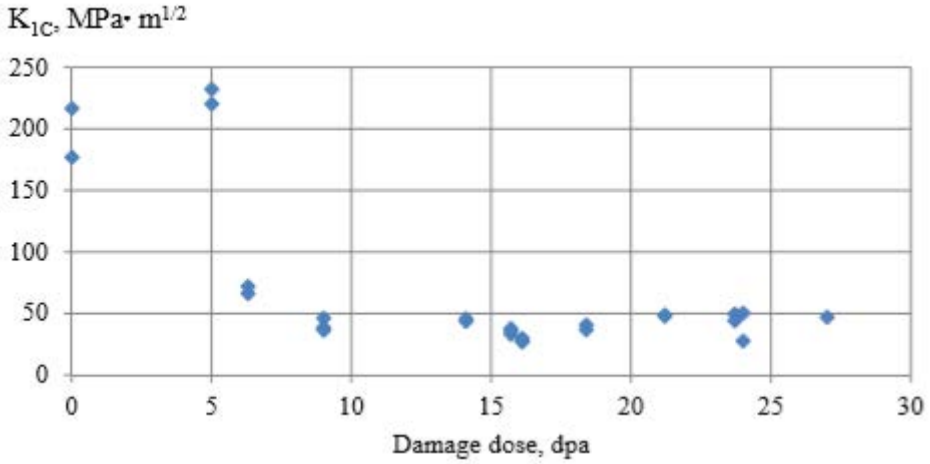

Fig. 7. The values of the critical stress intensity factor K_{1C} for steel EP-302 and welded joints, depending on the damaging dose

Under such criteria, the damaging dose to the materials of reactor internals should be limited to the value of 6÷8 dpa. To meet the accepted criterion, the design of the reactor was modified with changes in both the design of the reactor and the use of materials for its elements.

4. RESEARCH PROGRAM ON COMPLETION OF JUSTIFICATIONS FOR THE USE OF MATERIALS

The approximate scope of work that is yet to be performed to fully justify the use of materials in the reactor plant in accordance with Russian legislation is determined by regulatory documents. According to the content of the work, it is determined by the already canceled document, PNAE G-7-008-89 (ANNEX 11) [8], which despite the changing in current licensing process, can be used as a guide.

In substantiation of service properties of structural materials scheduled:

— study of long-term strength, plasticity and creep;
— study of cyclic strength and kinetics of crack growth during cyclic tests of steel and its welded joints in presence of coolant;
— radiation studies of steel in a narrower area corresponding to normal operation to increase statistics;
— annealing conditions of steel and its characteristics after annealing mode. The future R & D program will focus on the following pilot activities:
— irradiation tests of fuel rods in BOR-60 and BN-600 reactor plants;
— resource tests of models of steam generators (on the first and second circuits);
— primary pumps resource tests;
— creation of an experimental facilities for the study of physical and chemical processes in the conditions of destruction of the core elements.

One of the key directions of the R & D program implemented in support of the SVBR-100 reactor design is the definition and justification of safety and design limits of the core elements.

In accordance with the General provisions on the safety of nuclear power plants (NP-001-15) : "the design of a NPP should provide limits and conditions for safe operation and technical means and organizational measures aimed at preventing violations of limits and conditions of safe operation ..." For new projects, which include the project SVBR-100, the project should be justified by basic safety criteria, including the values of design safety limits (clause 1.1.2). The main focus of future R & D for the qualification of materials for SVBR-100 will be:

— in-depth study of extreme states of materials;
— damage mechanisms for specific structures and processes under the influence of damaging factors;
— study of the chemical interaction of structural materials, fuel and coolant at extreme temperatures corresponding postulated severe accidents.

ACKNOWLEDGEMENTS

In conclusion the authors express their gratitude to the large team of specialists of SSC RF – IPPE, JSC EDO "GIDROPRESS", SSC RF RIAR, CRISM “Prometey”, all employees took part in preparing and holding such a large-scale and labor-intensive long-term work on research materials for SVBR-100 project. The authors express special gratitude to Dr. A. E. Rusanov, Dr. A. D. Kashtanov, Dr. V. M. Troyanov who made an invaluable contribution to the organization of works and obtaining a large amount of new results.

REFERENCES

[1] FROGHERI, M., ALEMBERTI, A., MANSANI, L. The Advanced Lead Fast Reactor European Demonstrator (ALFRED) // The 15th International Topical Meeting on Nuclear Reactor Thermal - Hydraulics, NURETH-15, Pisa, Italy, May 12-17, 2013

[2] OECD NEA, Handbook on Lead-bismuth Eutectic Alloy and Lead Properties, Materials Compatibility, Thermal-hydraulics and Technologies. 2015 Edition. // OECD NEA. No. 7268

[3] AGEEV, V.S., TSELISHCHEV, A.V., SHKABURA, I.A., BUDANOV, YU.P., LEONTYEVA-SMIRNOVA, M.V., MITROFANOVA, N.M., IOLTUHOVSKIY, A.G. Structural Materials for Russian Fast Reactors Cores. Status and Prospects // International Conference on Fast Reactors and Related Fuel Cycles – Challenges and Opportunities, Kyoto, Japan, December 711, 2009/ (https://www-pub.iaea.org/MTCD/ meetings/PDFplus/2009/ cn176 /cn176_Presentations/ parallel_ session_4.2/ 04-09.Ageev.pdf)

[4] BESPALOV A.G., KONOBEEV YU.V., POROLLO S.I., RUDENKO V.A., KHABAROV V.S., SHULEPIN C.V. Problems of radiation resistance of structural materials of reactors with lead-bismuth coolant.// Collection of reports of the conference "Heavy liquid metal coolants in nuclear technologies". In 2 volumes. - Obninsk: SSC RF - IPPE, 1999.-Volume 2. – 450 p.

[5] http://www.akmeengineering.com/svbr.html

[6] RYZHOV, S. B., ZUBCHENKO, A. S., STEPANOV, V. S., KLIMOV, N. N., RUSANOV, A. E., PEVCHIH, YU. M., KARZOV, G. P., KASHTANOV, A. D., YAKOVLEV, V. A., STARCHENKO, E. G., NOSOV, S. I. Structural materials of the core elements of the primary circuit of the SVBR-100 reactor installation //VANT/ Series: "Nuclear power plant safety". Scientific and technical collection. Edition 24. Reactor installation SVBR. Podolsk, 2009. ISBN 978-5-94883-089-8 // http://www.gidropress.podolsk.ru/files/ vant/vant24.pdf

[7] GOST 25.506-85 Calculations and strength tests. Methods of mechanical testing of metals. Determination of fracture toughness (fracture toughness) characteristics under static loading.

[8] Rules for the design and safe operation of equipment and pipelines of nuclear power plants. , PNAE G-7-008-89. Approved by the resolution of gosatomenergonadzor of the USSR from 26.04.1989, No. 5. Introduced on 1 January 1990 with Change No. 1 of 27 December 1999

STATUS OF HLMC TECHNOLOGY AND RELATED MATERIALS RESEARCH IN CHINA INSTITUTE OF ATOMIC ENERGY

B. LONG[1], B. QIN[1], X.G. FU[1], J.Q. ZHANG[1], Z.S. RUAN[1], H.R. MA[1], L.X.REN and Y.Y. QIAN[1]
Z.H. WANG[2], J.Y. SHI[2], W.H. ZOU[2], H.J. CHANG[2]
1. China Institute of Atomic Energy, P.O.BOX, 275(34), 102413, Beijing, China
2. Nuclear Industrial Engineering Research and Design Co., Ltd., No. 58, Block B, Shunkang Road, Xilin River Economic Development Zone, Shunyi District, Beijing, China

Abstract

China Institute of Atomic Energy (CIAE) is the earliest research institute to start the lead-bismuth eutectic technology studying in China. With the support of national projects, the accelerator driven system (ADS) was developed, a serials studies focus on the compatibility and irradiation properties of domestic structural materials in liquid lead and lead-bismuth eutectic (LBE) were performed. Nowadays, the Lead or LBE cooled fast reactor is attracted more attention, more research on liquid metal technology and materials selection are carrying out to meet the requirements of reactor design. This present paper will give brief information on the relevant research facilities and some experimental results obtained, such as thermal-hydraulic loop, LBE corrosion loops, oxygen control systems etc. While some corrosion results of structural materials in LBE will also be discussed.

1. INTRODUCTION

With the development of economy, the demand for energy is increasing gradually. Nuclear fission energy is one of the important suppliers in China. To combat worsening greenhouse-gas emissions and pollution, China aims to raise its nuclear capacity to 200 gigawatts by 2030. While, it is expected that the cumulated spent fuel generated by nuclear plants will reach to ~10,000 tons at that time. How to properly handle the spent fuel, especially the long-life and high-level radioactive waste, is a major issue for the sustainable development of nuclear power.

Accelerator-driven system (ADS) is proposed for high-level radioactive waste transmutation. ADS use an accelerator to provide high-energy and high-current protons to bombard heavy liquid target to produce high-flux spallation neutrons as the external neutron source for the sub-critical reactors, transforming long-lived high-radionuclides into short-lived radionuclides or stable nuclides. Heavy liquid metals (HLM) such as lead (Pb) or lead-bismuth eutectic (LBE) were proposed as target material and coolants for spallation target and sub-critical fast reactor, respectively, due to its good neutron and physical properties [1, 2].

The LBE is the main candidate materials for spallation target in ADS demonstrator because of its advantage on neutron properties: heavy elements with a low neutron capture cross-section induce a high neutron production. The LBE is also used as a coolant for ADS subcritical reactor and Gen IV fast reactors because it has good thermal properties, low melting temperature (~125 ºC) and high boiling point (~ 1670 ºC). But, LBE is known to be very corrosive to structural material at elevated temperatures. Oxygen control is a very important issue for the ADS system when LBE is used as the coolant or the target materials. It could affect the corrosion resistance of structural materials and the operation of the facilities.

CIAE is the earliest research institute to start the lead-bismuth eutectic technology studying in China. With the support of national projects, the accelerator driven system (ADS) was developed, a serials studies focus on the compatibility and irradiation properties of domestic structural materials in liquid lead and lead-bismuth eutectic (LBE) were performed. Several LBE related facilities were established. This present paper will give brief information on the relevant research facilities and some experimental results obtained, such as thermal-hydraulic loop, LBE corrosion loops, oxygen control systems etc. While some corrosion results of structural materials in LBE will also be discussed.

2. LBE DYNAMIC CORROSION TEST LOOP

2.1. **Characteristic of loop design**

The LBE dynamic corrosion test loop is one of the key facilities for carrying out the compatibility test of structural materials in LBE for ADS and LFR (Lead-cooled Fast Reactor). It can simulate the corrosion properties of structural materials in LBE at high temperature and high flow rate under in-reactor operating conditions other than irradiation conditions.

- The loop consists of two test sections (the high temperature test section and the low temperature test section). The high temperature test section is at the highest temperature of the system and the low temperature test section is at the lowest temperature of the system to simulate the ambient temperature of the heat transfer components in the high and low temperature regions of the LFR.
- The structure of loop is typical "8" shaped. The whole system consists of main circuit (including high temperature zone, intermediate heat exchanger and low temperature zone), LBE supply and discharge circuit, oxygen control and magnetic purification trap, covering gas and vacuum system. The LBE storage tank is at the lowest position of the system, so that the LBE can be discharged by gravity in emergency conditions. The LBE pump is in the cold zone of the system to improve its efficiency and safety.
- The loop adopts frame-type bench structure, the lower part is LBE system, and the upper part is covering gas supply and vacuum system. Sample operating platform is used to ensure safe operation.
- The main components and pipes of the system are manufactured by 316S.S. with the same batch to avoid or reduce the effect of mass transfer effects due to the different materials. For some components made of non-316S.S. materials, such as flow meter or LBE valves, should be positioned at the downstream of high and low temperature sections, respectively, to reduce the impact of corrosion products.
- The sampling device of the loop adopts a fully sealed glove box. The sample sampling and mounting both for high test section and low temperature section are all performed in inert gas glove boxes to avoid contamination of the LBE system.

2.2. **Main parameters**

The flow chart of the LBE dynamic corrosion test loop is shown in Fig. 1. Its main parameters are as follows:

- Total power: ~ 70 kW
- Total capacity ： ～0.150 m^3
- T of high temp. test section: 400 ˚C~550 ˚C
- T of low temp. test section: 300 ˚C~450 ˚C
- Maximum T difference ΔT: 250 ˚C
- LBE flow rate: 0.576 m^3/h
- LBE speed on the sample surface: 1~5 m/s
- Pressure of system: 0.03~0.06 MPa
- LBE inventory: 1500 kg

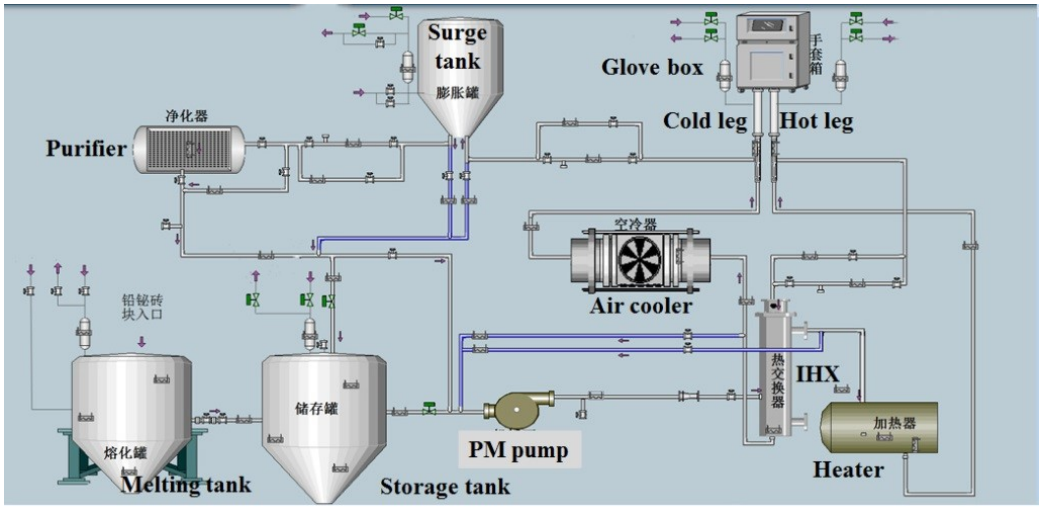

FIG. 1. The flow chart of the LBE dynamic corrosion test loop

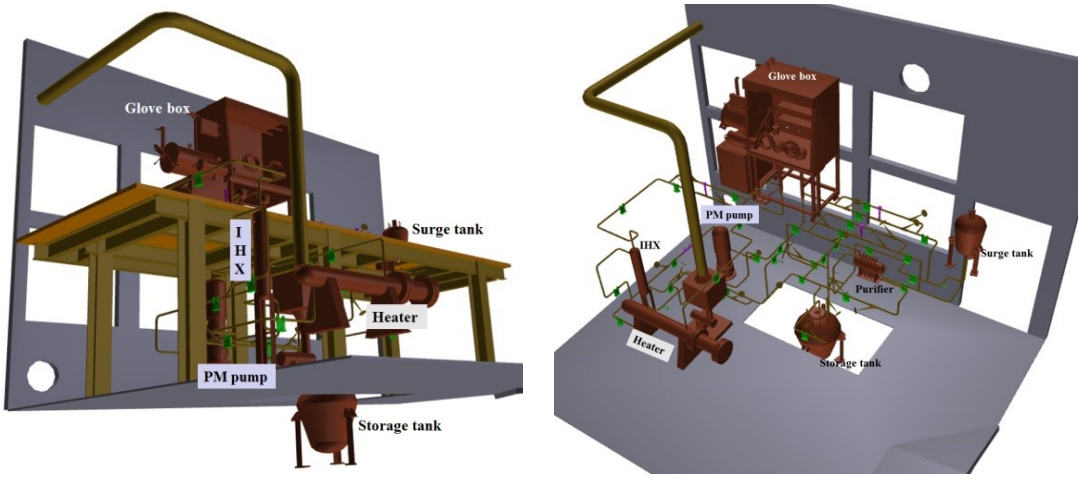

FIG. 2. Drawing of the LBE dynamic corrosion test loop

FIG. 3. The picture of the LBE dynamic corrosion test loop

2.3. **Main components and auxiliary system**

The LBE dynamic corrosion test loop consists of as following:

(1) Main circuit;

(2) Storage tank and LBE supply system;

(3) Covering gas and vacuum system;

(4) Sampling system;

(5) Instrumentation control system

2.3.1. *Main circuit*

Main circuit system includes; high and low temperature test sections, permanent magnet LBE pump, surge tank, air cooler, electric heater, flow meter, intermediate heat exchanger (IHX), purifier etc.

High and low temperature test sections

The test sections are used for mounting the test samples in the highest and lowest temperature range of the loop, respectively. The structural sketch of the test section is shown in Figure 4. The test section is made of 316 stainless steel pipes with a length of about 0.6 meters. The lower part is the test sample mounting area. The surface of liquid LBE is covered with high purity argon-hydrogen mixture. The upper part of the test section is connected with inert glove box by sealing cover to keep the LBE system free from contamination. In order to keep the oxygen content in LBE at a certain level during the experiment, the two test sections are connected with the gas phase oxygen control system.

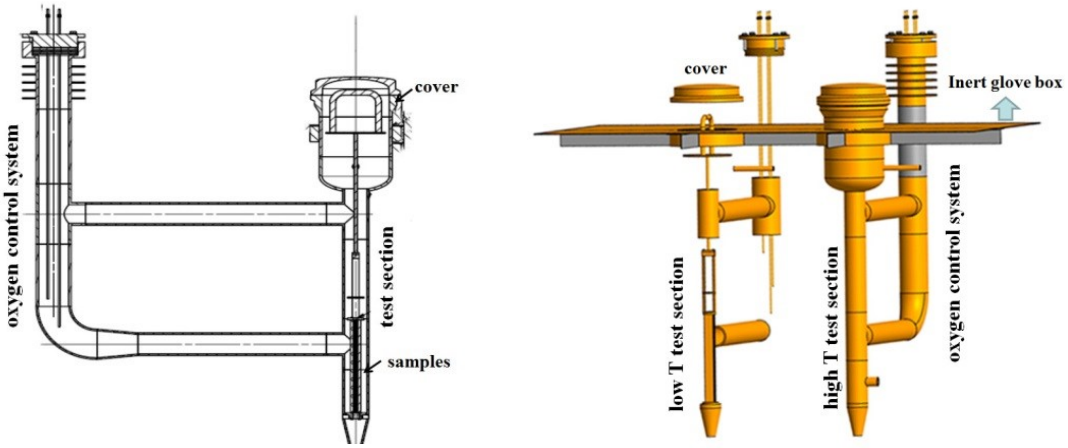

FIG. 4. Sketch of test sections

Surge tank

The LBE has a certain volume expansion after melting, so it is necessary to design an expansion tank to provide the free expansion space for the whole system during heating. Surge tank is located at the highest position of the loop, its main functions are providing enough free expansion space for liquid LBE and stabilizing system pressure. The structure of the surge tank is shown in Figure 5. The tank is pear-shaped, the upper dimension is ϕ426mm, and the lower dimension is ϕ325mm. The total volume of the tank is about 0.056m^3. The material is 06Cr17Ni12Mo2 stainless steel.

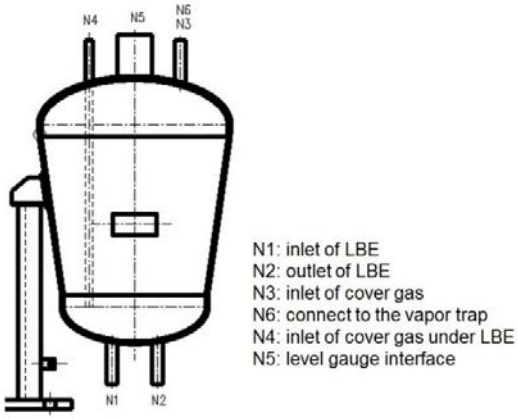

FIG. 5. Sketch of surge tank

Heater

The heater is used to heat the LBE in the loop and adjust the operating temperature to meet the needs of the experiment. In order to ensure sufficient temperature in the high temperature test section, the heater is located upstream of the high temperature test section. Figure 6 shows the structure of the heater. It is a cylinder with a dimension of ϕ360 mm x 5 mm x 1700 mm. Its material is 316 S.S. here are 12 heating rods are inserted into the container. The material is S32168 seamless stainless steel, and the total rated power is about 34 kW. To ensure the LBE temperature in high temperature test section can reach 550 ˚C, a 4 kW flange heater is installed. The LBE inlet pipe of heater is at the lowest point, and the outlet is at the highest point to ensure that the LBE in the container can be refluxed back to the pipeline by its own gravity. The baffles are installed in the container to increase turbulence and ensure the LBE reflux as clean as possible. The flow rate of LBE in the container is about 0.42 kg/s~1.66 kg/s.

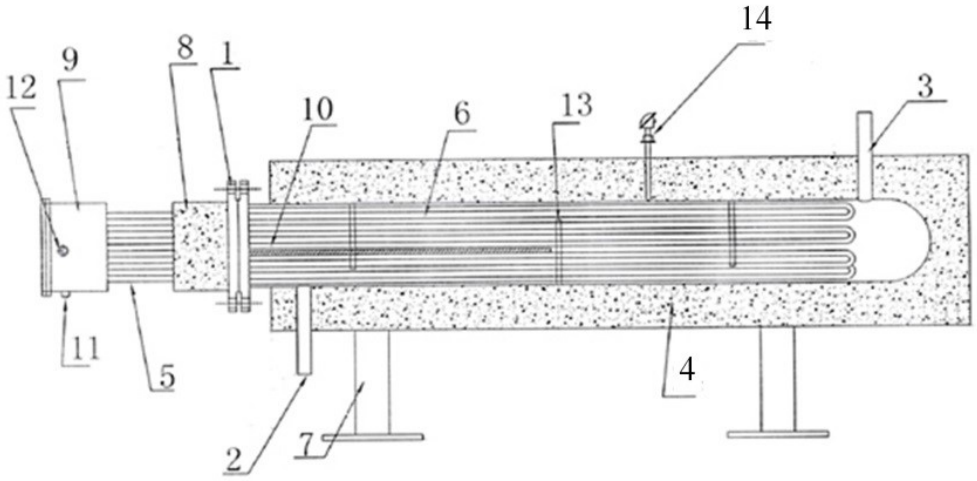

FIG. 6. Sketch of heater
1. Heater Flange; 2. LBE inlet 3.LBE outlet 4. Insulation 5. Heat dissipation area for heat rod
6. Heat container 7. Support frame 8, heat insulation 9. Junction box 10. Internal thermal-couple casing 11. Entrance hole for power supply 12. Outlet hole of thermal-couple 13. Baffles
14. Thermal-couple for outer wall of container

IHX

The IHX in this loop adopts shell-and-tube heat exchanger with vertical structure (see Fig. 7). The structural material is 06Cr17Ni12Mo2 stainless steel. It is used for heat exchange between cold and hot LBE. Hot LBE goes pipe path, while cold stream by shell path. The mass flow rate is 0.42kg/s~1.66kg/s, heat transfer area is 1.5m^2, inlet temperature of pipe path is 550 ˚C, outlet temperature is 360 ˚C, inlet temperature of shell path is 300 ˚C, and out shell temperature is 509 ˚C.

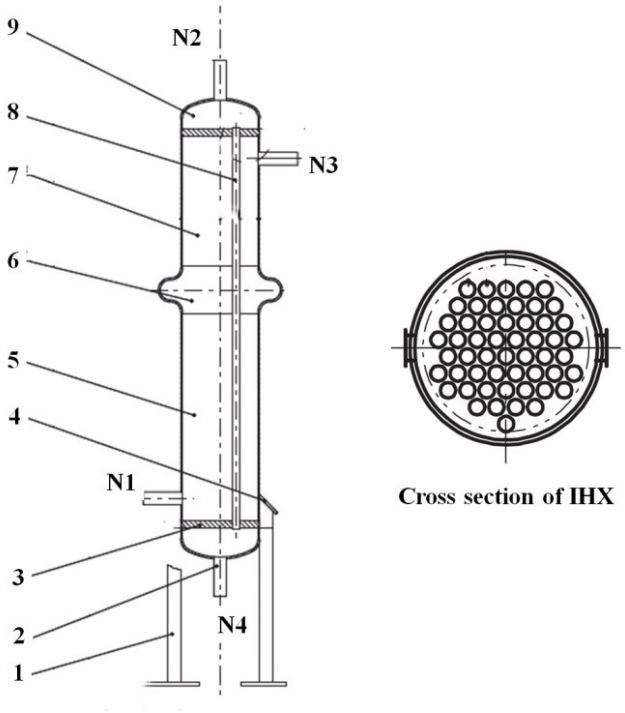

FIG. 7. Sketch of IHX
1. Support 2. Nozzle 3. Tube-sheet 4. Steel plate 5. Cylinder 6. Expansion joint 7,8. Steel tubes 9. Head
N1. Inlet of cold LBE N2. Outlet of cold LBE N3. Inlet of hot LBE N4. Outlet of hot LBE

LBE pump

LBE permanent magnet pump (PMP) is the heart of the loop. The overall structure of the pump is permanent magnet drive vertical pump (see Fig. 8), which is mainly divided into two parts: electric motor and magnetic drive. The magnetic drive adopts high temperature resistant permanent magnet with isolation sleeve made of 316 stainless steel and the base of internal and external magnetic rotors made of 316 stainless steel. Because the temperature resistance of samarium cobalt material is 350 ˚C, while LBE temperature in pump is 480 ˚C, therefore, it is necessary to set up the heat dissipation, air cooling and heat insulation structures in the outer rotor, so that the magnetic drive can operate normally within the required temperature range of magnetic materials. The main parameters of this pump are listed as following:

— Inlet pressure: 0.4 MPa
— Outlet pressure: 1.2 MPa
— Flow rate: 0.1~ 0.6 m^3/h
— Pressure head: 1.2 MPa
— Working temperature: 480 ˚C
— Sealing requirements: it should be no leakage in any working conditions within the working temperature range

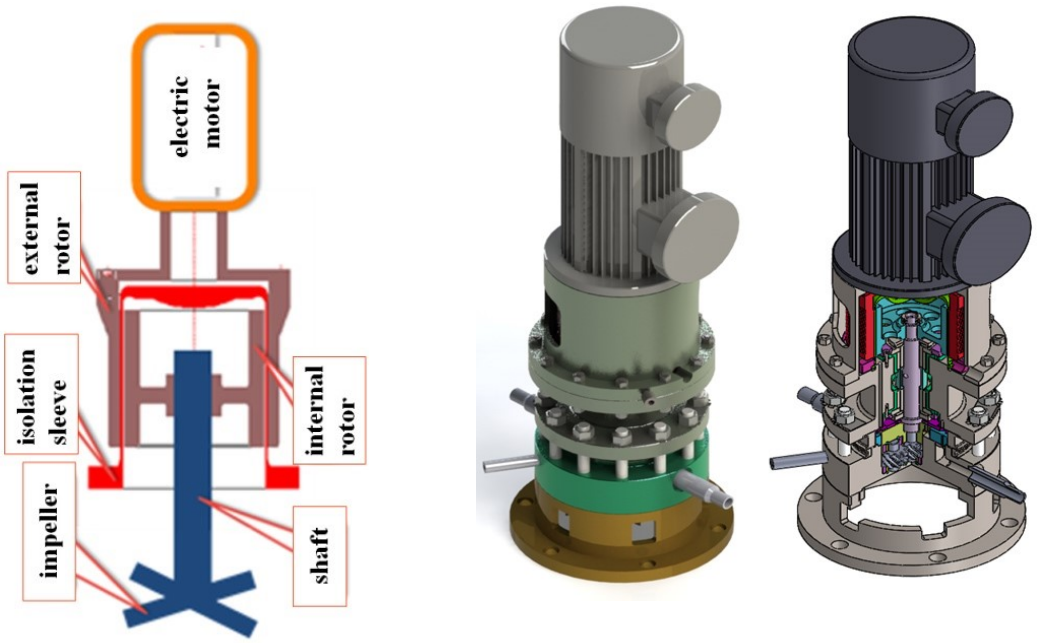

FIG. 8. Sketch of PMP (left: planar structure; right: 3D diagram)

Air cooler

The LBE temperature is still high after flowing through the IHX from the high temperature test section. The air cooler plays such a role to cool the LBE before it enters the low temperature test section to achieve the temperature difference of 200 ˚C between the cold leg and hot leg. The LBE pipeline has a U-shaped structure in the outer shell, and copper fins are welded on the pipeline (see Fig. 9). When the temperature of the outlet LBE pipe exceeds the design value, the fan opens automatically to increase the cooling ability.

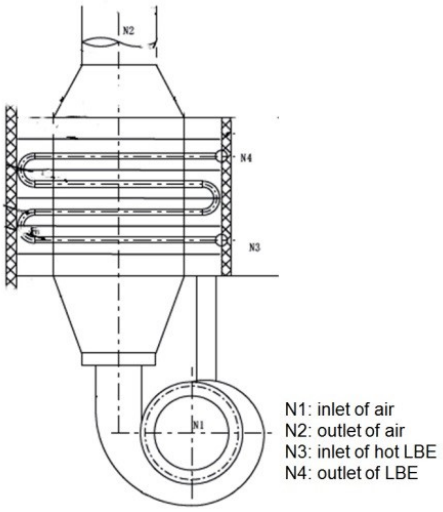

FIG. 9. Sketch of air cooler

Flow meter

Venturi flow meter is used to measure the LBE flow in the loop pipeline (see Fig. 10). The parameters of flow meter are as follows:

— Medium: LBE, Ar gas
— Structural material: 06Cr17Ni12Mo2
— Temperature: 480 ˚C
— Design Pressure: 1.5 MPa
— Measuring range: 0~1 m^3/h
— Measurement accuracy: 1 %

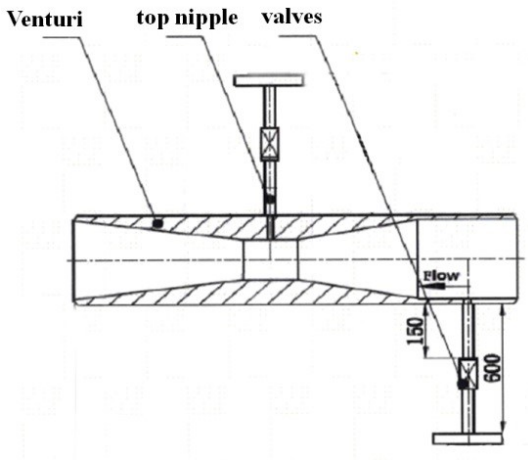

FIG. 10. Sketch of flow meter

Purifier

The purifier is used to remove the impurities such as Ni, Fe and lead bismuth oxide produced by corrosion during the loop operation. It is a magnetic trap for impurities in LBE. The purifier head is elliptical with cylinder-shaped barrel (see Fig. 11). 06Cr17Ni12Mo2 stainless steel is used as structural material. The inner part of the purifier is filled with stainless steel wire, which occupied 60% of the volume, and the wire mesh is fixed in the middle position. The purifier barrel is inserted in AlFeCo permanent magnet steel. When the LBE flow through the purifier, impurities in LBE are absorbed to realize the purifying effect.

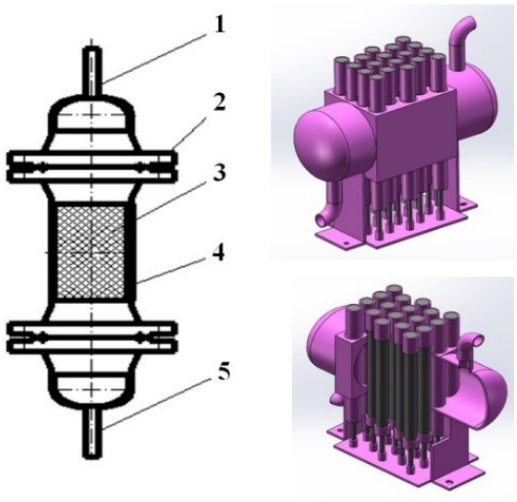

FIG. 11. Sketch of purifier (left: planar structure; right: 3D diagram)
1. Inlet of LBE 2. Flange 3. Stainless steel wire meshes 4. Barrel 5. Outlet of LBE

2.3.2. *Storage tank and LBE supply system*

The function of the LBE storage tank is more like a stomach for a person. It is a container that provides LBE to the loop. In order to drain the liquid metal totally, the tank is placed in the lowest position of the whole loop system. The sketch of the tank is shown in Fig. 12. The tank is pear-shaped similar as surge tank, with the upper dimension of 800mm, and the lower dimension of 500mm. The total volume of the tank is about 0.27m3. The material is 06Cr17Ni12Mo2 stainless steel.

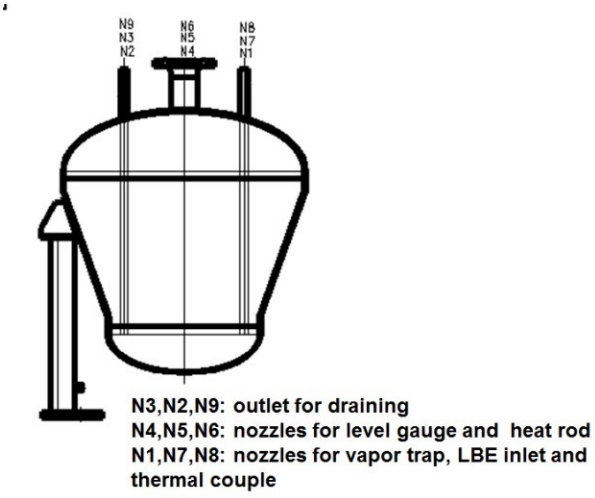

FIG. 12. Sketch of flow meter

2.3.3. *Covering gas and vacuum system*

In order to prevent impurities such as water and air into the loop, the system should be evacuated by vacuum pump before its running. When the loop is in operation, all free surface of liquid LBE should be covered with inert gas. These functions are realized by covering gas supply and vacuum system.

Covering gas system consists of two independent lines: one is to supply argon as cover gas at normal operating conditions; the other is to supply argon-hydrogen mixture to provide the gas for the oxygen control system (OCS), so it is in fact belonging to a part of the OCS. Figure 13 shows the flow chart of this system. The pressure of cover gas is slightly higher than atmospheric pressure to ensure that air, water and other impurities do not leak into the system. The cover gas should be cleaned by passing through the cleaning tank before it is vented.

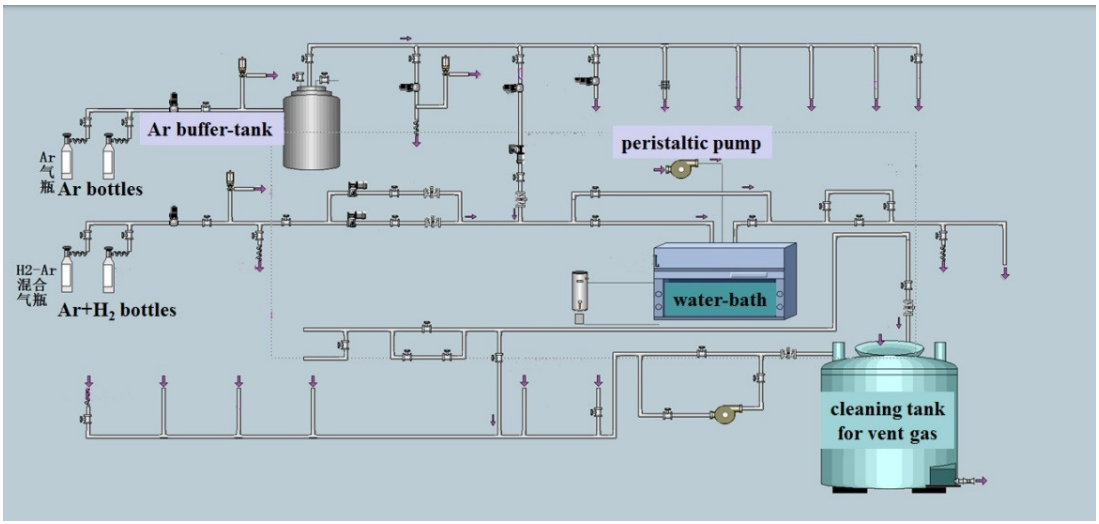

FIG. 13. Flow chart of covering gas and vacuum system

2.3.4. *Sampling system*

In LBE system, the influence of LBE oxidation on the test results and the possible contamination of the system should be avoided as far as possible when the test samples are taken and placed. The sampling system of this loop adopts inert gas glove box combined with sealed flange cover structure.

The samples are mounted in a sample holder (see Fig. 14), then the sample holder could be set down into the test sections as showing in Fig. 4. The flow velocity of LBE on the surface of sample can be modified both by adjusting the LBE flow rate in loop or by adjusting the width of sample row spacing.

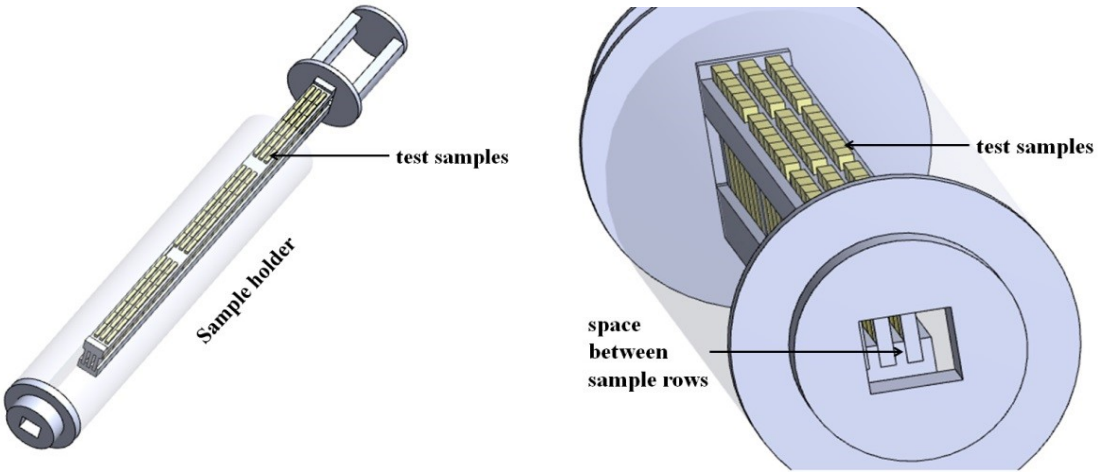

FIG. 14. Sketch of the sample holder

2.3.5. *Instrumentation control system*

The stability of instrumentation control system is the guarantee of stable and reliable operation of LBE dynamic corrosion test loop. The main functions of the control system are as follows:

- Control and display of temperature;
- Control and display of LBE flow rate;
- Display of gas pressure;
- Pressure and liquid level alarm of LBE.

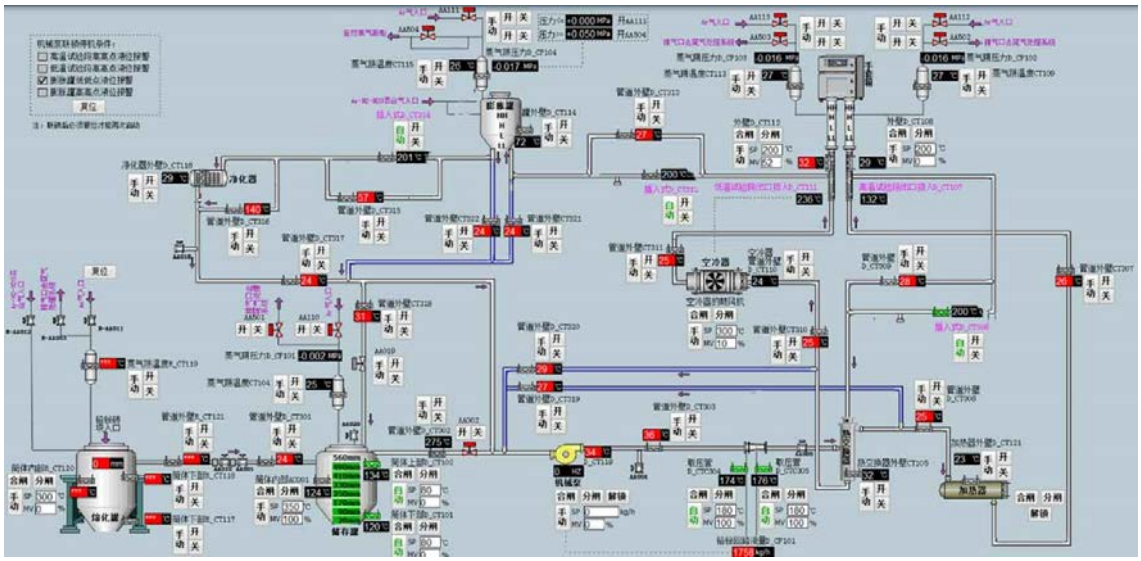

FIG. 15. Chart of instrumentation control system

Fig. 15 is the chart of the instrumentation control system. All symbols marked with heating in this figure are controlled by an instrument program. When the heating reaches to the value of set temperature, the heating wire or heating rod is stopped, or the input power decreases.

The liquid LBE levels in the high and low temperature sections are controlled by argon pressure. When the liquid level shows higher than L level, the test sections will be filled with argon by cover gas system automatically; when the liquid level shows lower than L level, the gas in test sections will be discharged.

The PM pump can be stopped automatically by the interlock system according to the following operating conditions:

(a) When the liquid level exceeds the highest liquid level HH in the high temperature section.
(b) When the liquid level exceeds the highest liquid level HH in the low temperature section.
(c) When the liquid level is lower than the lowest liquid level LL of the surge tank.
(d) When the liquid level exceeds the highest liquid level HH of the surge tank.

The heater can be stopped automatically by the interlock system according to the following operating conditions:

(a) When the running rate the PM pump drops to 0.5 HZ;
(b) When the outlet temperature of the high temperature section is 20 ˚C higher than the set value;
(c) When the outer surface temperature of the heater exceeds the set value.

2.4. **Current state of the loop**

At present, the loop has been installed and debugged, and operated safely and steadily for 168 hours under 550 ˚C. The research work to be carried out on this circuit is as follows:

- Corrosion behaviour of austenitic stainless steel (including 316SS, 316LSS, 304SS and 15Cr-15NiTi SS) in LBE at high temperature and high velocity;
- Corrosion properties of ferrite/martensitic steels (including T91, HT9, Si-added FM steel and Al-added FM steel) in LBE at high temperature and high velocity;
- Corrosion behaviour of coating materials in LBE at high temperature and high velocity

3. LBE THERMONVECTION LOOP

3.1. **Characteristics of loop**

LBE thermal convection loop is one of the important equipment for the compatibility test of structural materials with high temperature LBE. The equipment is mainly used for preliminary screening test of structural masteries by its corrosion property in low-velocity LBE for ADS system or LFR. The corrosion rate of specimens, the surface-layer structure, the dissolution and migration of the materials elements and the effect of the LBE on the internal structure and microstructure of the material can be evaluated and measured by experiments. The effect of LBE environment on the mechanical properties of the material can also be obtained by testing the mechanical properties after exposed to LBE in this loop.

The main characteristics of the loop are as follows:

- The main components (for example, high and low temperature sections) and pipelines are made of 316 SS to avoid or reduce the influence of the different materials of the system on the test results.
- The sampling system of the loop consists of a sample transfer cylinder, a vacuum ring sealing and a high vacuum gate valve. The device can guarantee that the sample mounting in the inert atmosphere to avoid the contamination of the system by air.
- The oxygen content in LBE is monitored by installed electrochemical sensors with yttria-stabilised zirconia (YSZ)/Pt (air) reference electrode both at hot leg and cold leg.
- The loop is equipped with a gas-phase oxygen control device to control the oxygen content in LBE during its operation.

3.2. **Main parameters**

The diagram of LBE thermal convection loop is shown in Fig 3.1, and the photo of this facility is shown in Fig. 16. The main parameters of the loop are as follows:

- Temperature of hot leg: 400 ˚C~550 ˚C
- Temperature of cold leg: 300 ˚C~400 ˚C
- Maximum T difference ΔT: 250 ˚C
- LBE speed on the sample surface: 0.03 m/s～0.05 m/s
- Pressure of system: 0.03~0.06 MPa
- LBE inventory: 150 kg
- Total power: 12 kW

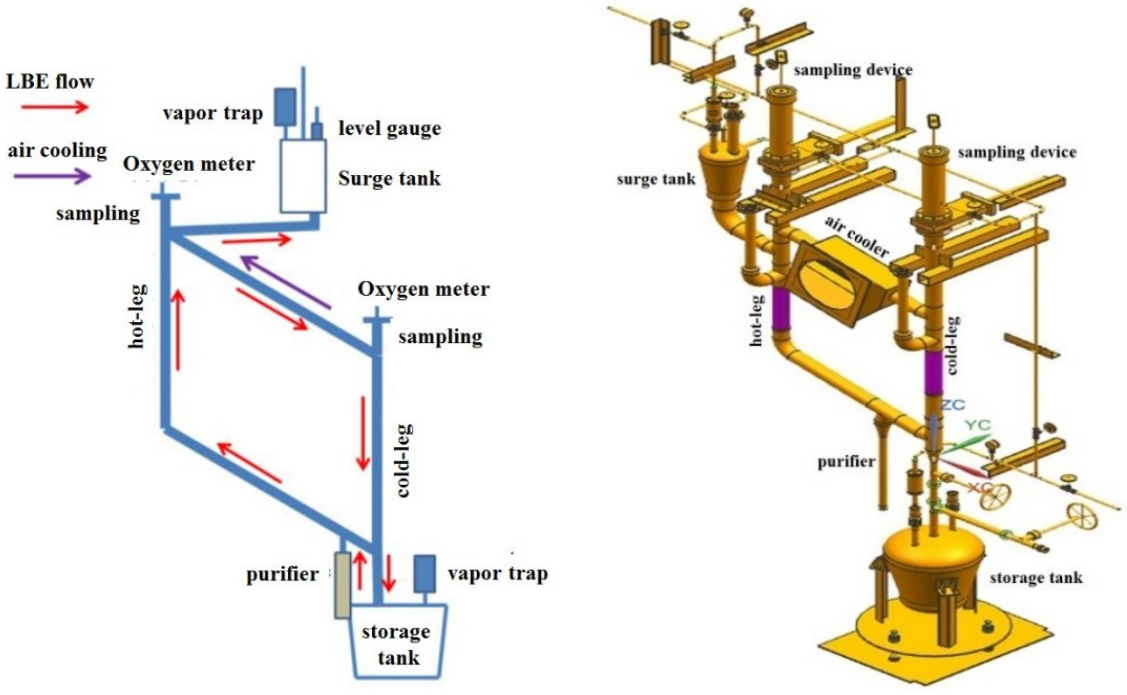

FIG. 16. Diagrams of LBE thermal convection loop (Left: plane diagram; Right: 3D diagram)

FIG. 17. Photo of LBE thermal convection loop

3.3. **Current studies performing in the loop**

At present, the thermal convection loop is in a long-term operation. The ongoing and planned research in this loop includes:

- Studies on the corrosion properties of candidate structural materials, including CN15-15, 316Ti, 316L, 304 stainless steel, FM steel T91, HT9, etc., in LBE for CiADS and LFR.
- Corrosion behaviour of coating materials in LBE.
- R&D on high-entropy alloy with radiation resistance and LBE corrosion resistance.

4. LBE STATIC CORROSION TEST APPARATUS

4.1. **Characteristic of the apparatus**

The static corrosion tests of materials in LBE could be performed in this LBE static corrosion test apparatus, which is mainly conducted to understand basic corrosion mechanism and make screening of materials.

The main characteristics of the facility are as follows:

- The apparatus is divided into gas control unit and high temperature test unit (see Fig. 18 and Fig. 19).
- Gas control unit adopts gas phase oxygen control device. Ar and Ar+5%H_2 are used as gas sources, and gas mass flowmeters are used to control the flow rates of the two gas sources. Ar+H_2 mixed gas flows through a water bath with certain temperature, which brings out water vapor, thus forming Ar+H_2+H_2O mixed gas. Then dew point mixed gas is measured by dew point meter to obtain the molar ratio of hydrogen peroxide in the mixed gas. The mixture of Ar+H_2+H_2O was injected into the liquid LBE or the liquid surface of LBE in the high temperature furnace, and the equilibrium of the reaction was adjusted by the oxidation-reduction reaction of PbO+H_2→Pb+H_2O and the proportion of hydrogen in the mixed gas. The partial pressure of oxygen in the exhaust gas was measured to determine whether the oxygen content in the LBE reached the expected value.
- For high temperature test unit: LBE test furnaces have two different types: one is horizontal heating vessel, the other is vertical heating pot. The test inner tube of horizontal vessel is made of quartz glass or stainless steel, LBE is held in a small quartz crucible cup, and the test samples can be corroded in quartz crucible. A certain proportion of Ar+H_2+H_2O mixed gas flows in quartz tube or stainless-steel tube, thus realizing oxygen content control in LBE. The container of the vertical heating pot is made of stainless steel. The inner surface of the container is nitride to reduce the dissolution of the elements of stainless steel to LBE. The mixture of Ar+H_2+H_2O is filled into liquid LBE to control oxygen content in LBE.

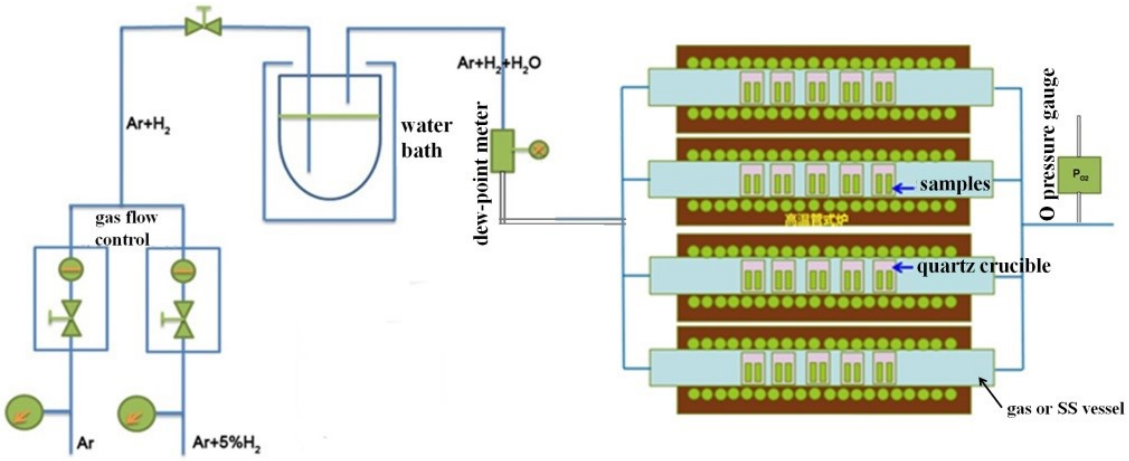

FIG.18. LBE static corrosion test apparatus (type1)
upper: flow chart of apparatus; lower: photo of apparatus

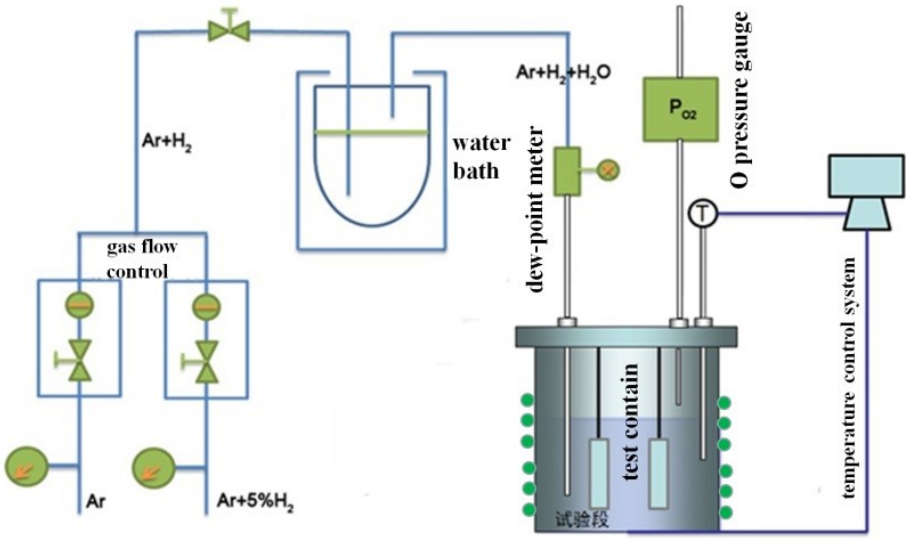

FIG. 19. LBE static corrosion test apparatus (type2)

4.2. **Main parameters**

The main parameters of the apparatus are as follows:

- Maximum test temperature: 800 ˚C
- Oxygen content in LBE: from saturated to 1×10^{-8} wt.%

4.3. **Studies performed in the apparatus**

The researches that have been carried out and are being carried out on this device are as follows:

- Corrosion properties of austenitic stainless steel (including 316SS, 316LSS, 304SS and 15Cr-15NiTi SS) in LBE at different oxygen contents;
- Corrosion behaviours of ferrite/martensitic steels (including T91, HT9, Si-added FM steel and Al-added FM steel) in LBE at different oxygen contents;
- Corrosion behaviour of high entropy alloy coatings on austenitic steels in static LBE;

5. CORROSION TESTS IN LBE

In order to select qualified fuel assembly materials and key components materials for CiADS (China initiative Accelerator Driven System) and LBE-cooled fast reactor, the compatibility of FM steels and austenitic stainless steels with LBE was studied. FM mainly uses modified 9Cr-1Mo (T91 steel), austenitic stainless steels include 316Ti, CN1515, 316L and 304 stainless steels, among which CN1515 is the cladding material for fuel assembly of sodium-cooled China Experimental Fast Reactor (CEFR). The composition of the above materials is listed in Table 1.

TABLE 1 CHEMICAL COMPOSITION OF TESTED MATERIALS

	C	Si	Mn	P	S	Cr	Ni	Mo	Ti	V	Nb	N	Fe
T91	0.1	0.4	0.4	<0.02	<0.01	9.0	0.1	1.0		0.2	0.08	0.05	Bal.
CN1515	<0.08	0.3~0.9	1.3~2.0	<0.03	<0.01	15.5~17.0	14~15.5	1.9~2.5	0.2~0.6				Bal.
316Ti	<0.08	<1.0	<2.0	<0.035	<0.03	18	12	2.0	0.7				Bal.
316L	<0.035	<1.0	<2.0	<0.045	<0.035	16-18.0	10-14.0	2.0-3.0					Bal.
304	<0.08	<1.0	<2.0	<0.045	<0.035	18-20.0	8-10.5						Bal.

5.1. **Parameters for corrosion test**

Tests conditions and parameters are as follows:

- Sample size: 20 mm x 10 mm x 2 mm
- Test temperatures were 450, 500, 550 and 600 ˚C
- Test time was 1000h, 3000h and 6000h
- Oxygen content in LBE: 10^{-6}-10^{-7} wt.%

The tests were performed in the static corrosion apparatus (see Fig. 18).

Our experimental results are consistent with those of most previous researchers [3, 4, 5, 6]. For ferrite/martensitic steel and austenitic stainless steels, the corrosion behavior is different with the change of corrosion time and temperature.

In the following sections, we will give the test results and discuss it by comparing two kinds of materials. It should be noted that, in order to facilitate comparison, we only have selected 316Ti and 15-15 stainless steels from austenitic stainless steel, while T91 is as FM steel.

5.2. **Test results**

At 450°C

As shown in Fig. 20a and b, the protective oxide layers can be formed on the surface of austenitic stainless steel CN1515 and ferritic/martensitic steel T91 after exposure in LBE at 450 ˚C for 3000 hours. The formed oxide on the surface has a double layer structure, the inner layer is Fe-Cr oxide, and the outer is iron oxide. XRD analysis indicates that the oxides are spinel $(Fe, Cr)_3O_4$ and Fe_3O_4, respectively. The total thickness of the oxide layer is about 10-15μm, in which the Fe-Cr spinel layer is generally less than 5μm, while the thickness of the outer Fe_3O_4 oxide layer varies greatly, which can exceed 10μm. Or it could be peeled off, and only the inner $(Fe, Cr)_3O_4$ is observed in some cases. Anyway, the oxide layer formed on the surface of steels (no matter F/M steel T91 or austenitic steel CN1515) could still play a role to protect the inner matrix from elements dissolution and corrosion by LBE.

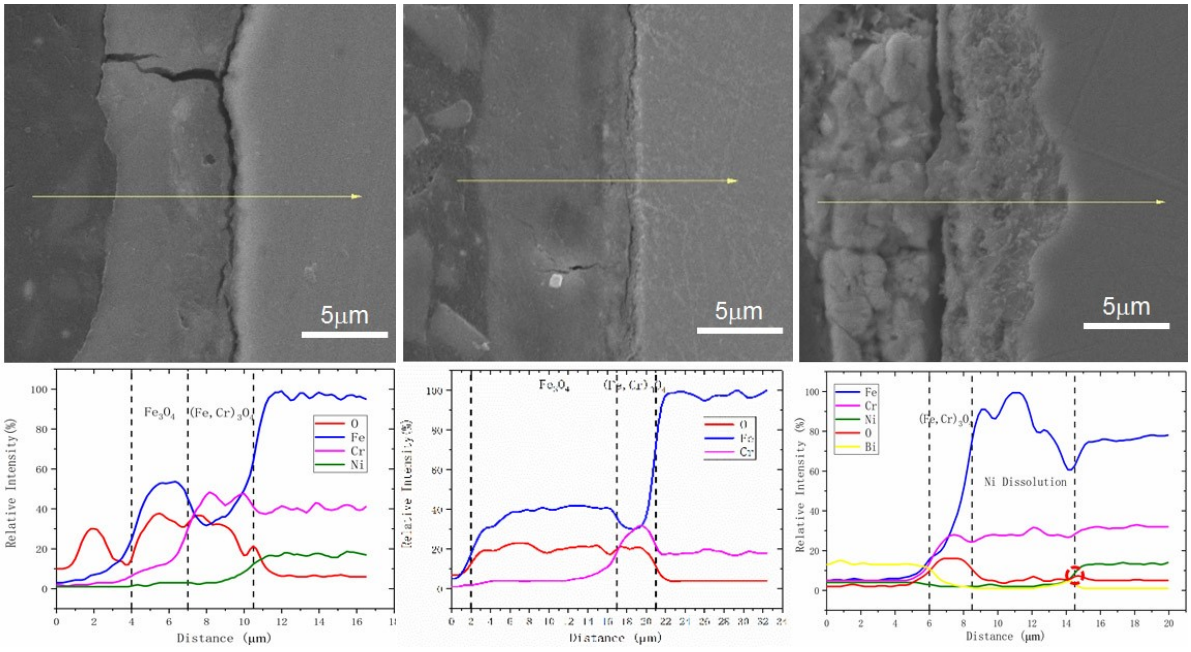

a) CN1515, 3000h b) T91, 3000h c) CN1515, 6000h

FIG. 20. Morphologies and line scan of specimens after exposure to LBE at 450oC

After 6000 hours exposure in LBE, a relatively complete Fe-Cr oxide layer on the surface of CN1515 austenitic stainless steel can still be observed, and its thickness is about 2μm. But it has lost its protective effect. The dissolution of Ni and enrichment of Fe were detected in the matrix under the oxide layer. The dissolution layer is about 5μm. EDS analysis indicates that a small amount of lead and (or) bismuth were found at the interface between the dissolution layer and the matrix, as shown in Fig 5.1c. For T91, a thin oxide layer about 1μm formed on the surface of specimens at the same test conditions, no dissolution of steel elements is observed in matrix.

At 500~550 ˚C

With the increase of test temperature, serious Ni dissolution was observed for austenitic stainless-steel specimens, and the corrosion depth varied greatly at different locations. The maximum corrosion depths of specimens for different austenitic stainless steels were generally 30-80μm after 6000 hours. Among them, 304 SS exhibited very strong corrosion at 550 ˚C, its corrosion depth reached 210μm after 6000 hours. Discontinuous oxide layers were observed on the surface of some specimens. A lot of cracks and voids in matrix were observed under those discontinuous layers which resulting of a large amount of lead and bismuth penetration. Figure 21 shows the test results of 316Ti SS at 500 ˚C, the corrosion depth of 316Ti SS specimen is about 40μm after 6000 h in liquid LBE. The EDS line scanning showed there was no Ni detected in the surface layer, which indicated that the corrosion mechanism was elements of steel (especially Ni) dissolution. Attention should be paid to the presence of a lead and (or) bismuth penetration layer of about 3μm near the 316Ti substrate under the corrosion layer (see EDS line scanning in Fig. 21).

In this temperature range, slight dissolution of Fe and Cr occurred in T91. The microstructure analysis results showed that there was a thin Cr-rich layer on the surface of the specimen, which may be a Cr_2O_3 oxide. It is probably the formed protective Cr_2O_3 oxide layer prevented the further dissolution of the steel elements, but the formation mechanism of Cr-rich layer is still unclear and needs further study. Figure 22 depicts the morphology observation and EDS line scanning results of T91 after exposed to LBE at 500 ˚C for 6000 hours. It can be seen that the thickness of the Cr-rich layer on the surface is about 3 μm. In addition, no lead and (or) bismuth penetration in the matrix was observed at this temperature.

The above experimental results showed that the corrosion resistance to LBE of F/M steel is better than that of austenitic stainless steel in this temperature range.

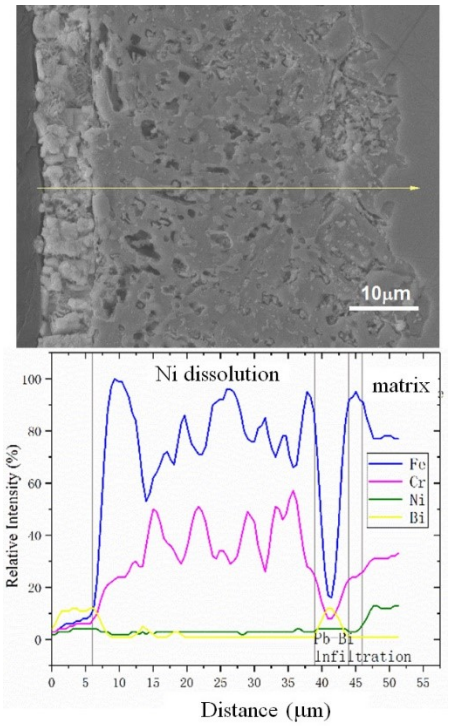

FIG. 21. Morphology analysis and line scan of austenitic steel 316Ti after corrosion in LBE (500 °C, 6000 hours)

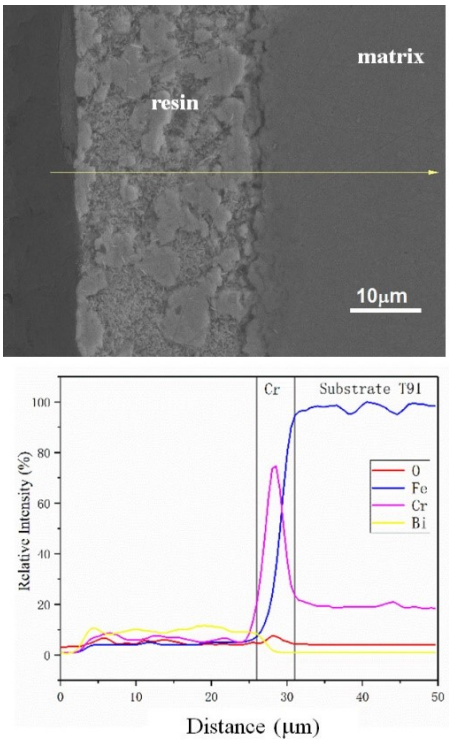

FIG. 22. Morphology analysis and line scan of FM steel T91 after corrosion in LBE (500 °C, 6000 hours)

At 600 °C

No protective oxide layer was observed on the surface of austenitic stainless steel in LBE at 600 °C. Serious Ni dissolution occurred, and lead or bismuth penetration was obvious. With the increasing of immersion time, the corrosion depth of specimens increased significantly. The maximum corrosion depth of CN1515 steel for 1000h, 3000h and 6000h was 80, 190 and 234 microns, respectively (see Fig. 23). The corrosion becomes more and more serious with the increase of time. Only a small amount of lead or bismuth penetrated into matrix at 1000 h, and intergranular corrosion phenomena with fewer cavities was observed. After 3000h, lead and bismuth in matrix increased obviously, and a large number of holes appeared, but the matrix composed of iron and chromium in the nickel depletion layer remains intact. After 6000 hours, the penetration of lead and bismuth increased dramatically, and the dissolved corrosion layer (i.e. Ni-depletion layer) was separated by the invaded lead and (or) bismuth.

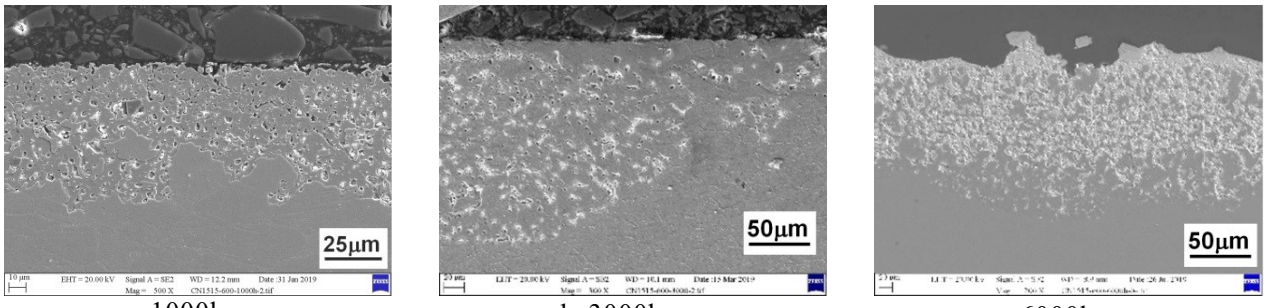

a. 1000h b. 3000h c. 6000h

FIG. 23. Morphologies of CN1515 steel after corrosion in LBE at 600 °C

For F/M steel T91, no protective oxide layer was observed on the surface of specimens after exposure to LBE at 600 ˚C for 6000h, but there was no obvious corrosion was observed on most of the specimens' surfaces. A Cr-rich layer of about 5 μm was detected, as shown in Fig. 24.

The phenomenon of dissolution and corrosion in local area was still obvious. The penetration of lead and bismuth can be observed. The maximum corrosion (penetration) depth is about 35 μm (see Fig 25).

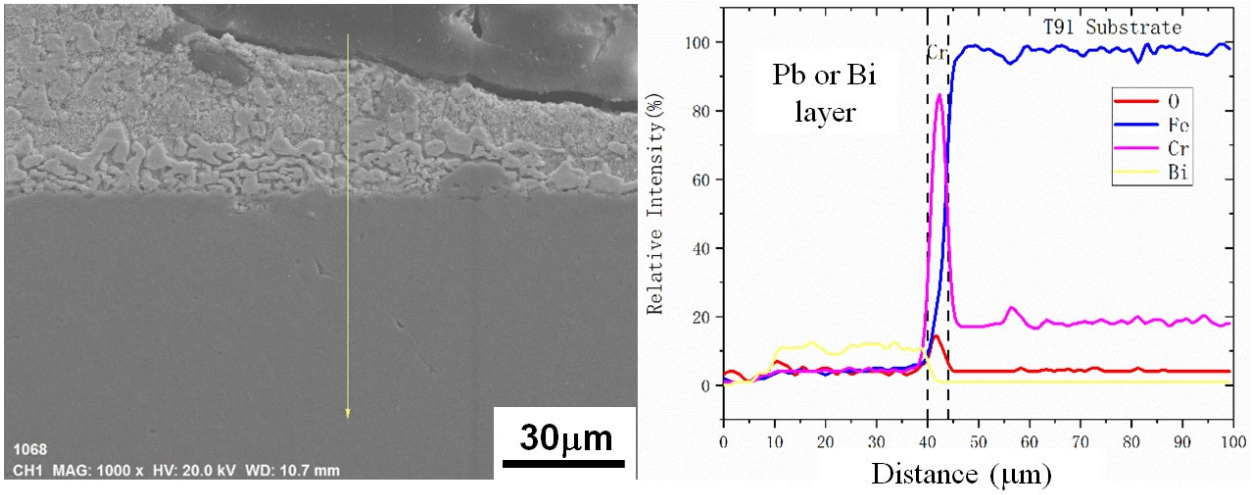

FIG. 24. Morphology analysis and EDS line scan of FM steel T91 after exposure in LBE (600 ˚C, 6000 hours)

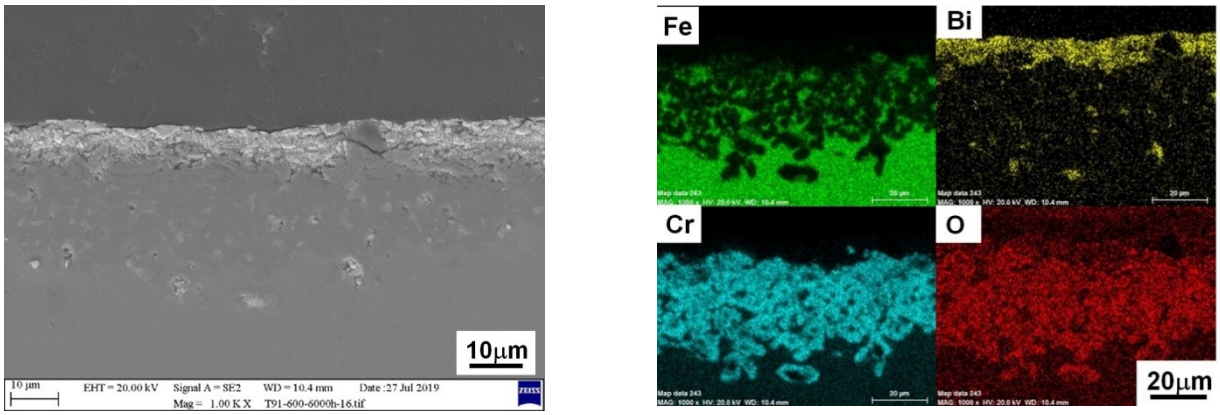

FIG. 25. Morphology analysis and EDS element mapping of T91 after exposure to LBE (600 ˚C, 6000 hours)

5.3. **Summary**

- For austenitic steels in static LBE: all specimens exposed to LBE for a long time exhibited un-resistant to LBE attack in the test temperature range (from 450 ˚C to 600 ˚C). The obvious corrosion of austenitic stainless steel occurs at the test temperature greater than 450 ˚C. The corrosion mechanism of austenitic stainless steel is the diffusion and dissolution of steel elements in LBE. Figure 26 shows the EDS mapping scan results on main elements of CN1515 steel after 1000 hours exposure to LBE at high temperature. As shown in the figure, the corrosion of the steel at 500, 550 and 600 ˚C is mainly due to the diffusion and dissolution of Ni into the LBE, which induced microstructure modification on two issue: one is that the austenite structure of FCC was unstable due to the loss of Ni resulting on the transformation from austenite of FCC to ferrite of bcc structure. On the other hand, the loss of Ni leads to corrosion voids on the surface of austenitic stainless steel. The liquid Lead-bismuth eutectic (mainly Bi element) will move along the grain boundary to the matrix of the steel. Diffusion of lead and (or) bismuth causes further dissolution and corrosion of the matrix.

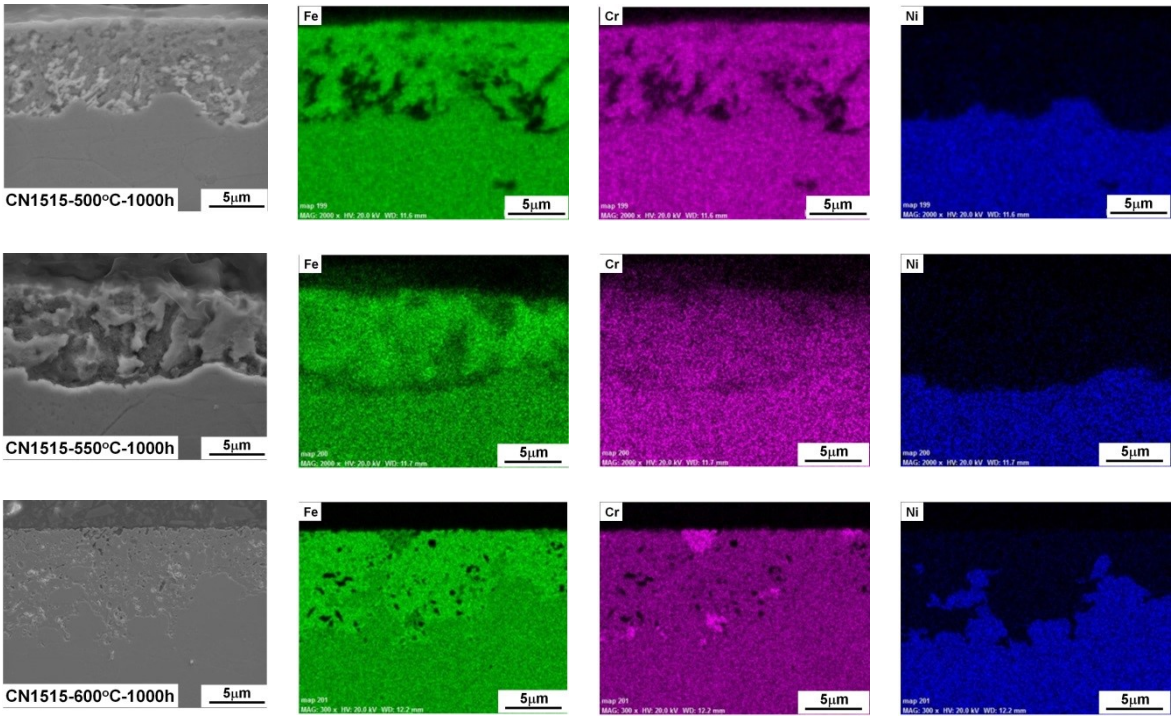

FIG. 26. Morphologies and EDS element mapping of austenitic steel CN1515 after corrosion in LBE

- For T91 in static LBE: when test temperature is less than 450 ˚C, a thin oxide layer about 1μm formed on the surface of specimens which could prevent the dissolution of steel elements into the liquid LBE. When the temperature was greater than 500 ˚C, the steel began to dissolve locally, especially iron dissolution (see Fig. 27). The element dissolution in LBE was obvious at 600 ˚C, accompanied by the penetration of lead or bismuth to the matrix of steel.

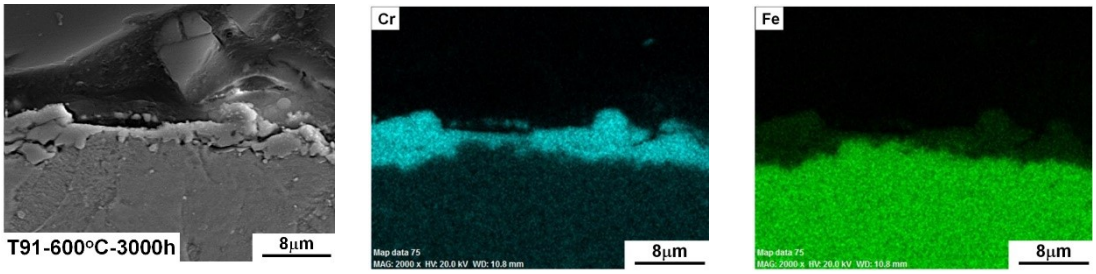

FIG. 27. Morphologies and EDS element mapping of FM steel T91 after corrosion in LBE

6. LME EFFECTS ON FM STEEL T91

Liquid metal induced embrittlement (LME) is an important compatibility issue in many applications where solid metals are in contact with liquid metals. Due to LME effects, the mechanical properties of solid metals can be severely degraded and structural components can fail through sudden brittle fracture during operation. Therefore, LME is a very important materials research topic studied since a long time [7, 8, 9, 10].

Because T91 steel does not contain Ni, its corrosion resistance to liquid LBE normally is better than that of austenitic stainless steel which has high nickel content. However, because T91 steel belongs to the ferritic martensitic steel with BCC structure, this kind of steel is sensitive to low temperature embrittlement, which may be sensitive to the embrittlement effect induced by contact with liquid LBE. Therefore, the embrittlement effect of liquid metal on T91 steel was studied. The composition of the T91 is listed in Table 2.

TABLE 2. CHEMICAL COMPOSITION OF FERRITIC-MARTENSITIC STEEL T91 (WT.%, FE, BALANCE)

elements	Cr	Ni	Mn	Mo	Ti	V	Si	P	Nb	W	Ta	C
T91	8.63	0.23	0.43	0.95	0.001	0.21	0.31	0.002	0.09	<0.01	----	0.1

6.1. **Parameters for SSRT test**

Slow-strain-rate-tensile (SSRT) tests on T91 steel were performed both in the inert argon and in stagnant liquid LBE environment to study the LME effect of T91 steel.

The LME test facility was used for SSRT tests. The facility consists two parts: one is a tensile test machine; the other is the test section which is connected to the tensile machine to perform the test inside the liquid LBE. We call this test section as LME test station.

The set-up of LME test section consists three vessels to melt and condition the appropriate LBE melt, in which the specimen of steel will be exposed. Figure 28 shows the flow diagram of the LME test station. The main components of this station are: 1) test section (named as DUT tank); 2) storage vessel (named as PRE tank); 3) filling vessel (named as FILL tank); 4) pneumatic

LBE valve which connects the DUT and PRE tanks; 5) cover gas and vacuum system; 6) LBE drain pipe; 7) temperature control unit.

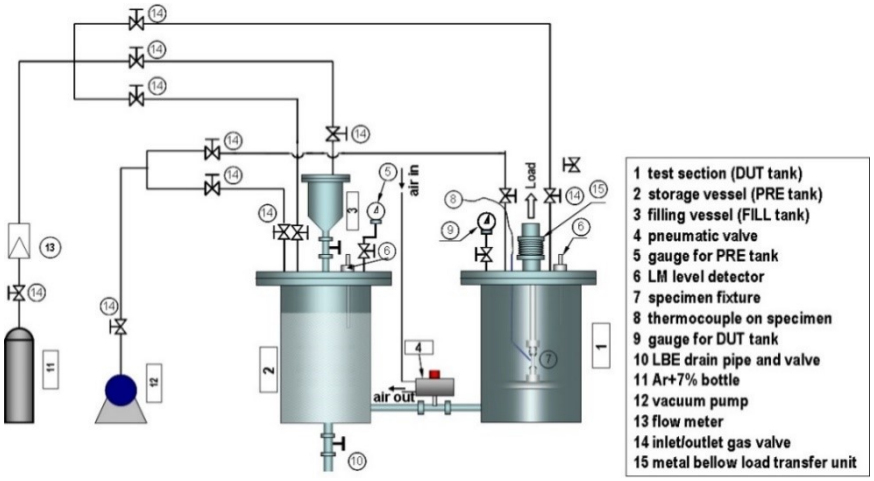

FIG. 28. Flow sketch of the LME test station

Tests conditions and parameters are as follows:

- Sample size: 20mm x 10mm x 2mm
- Test temperatures: 150, 200, 250, 300, 350, 400, 425, 450 and 500 ˚C
- Test environments: in Ar and in LBE
- Strain rate: $1\times10^{-5}s^{-1}$
- Oxygen content in LBE: 10^{-6}-10^{-7} wt.%

6.2. **Test results**

Specimens were tested at eight temperatures between 150 and 500 ˚C in a step of 50 ˚C. Figure 29 shows the results of the selected specimens tested at these temperatures in LBE, for comparing, one test performed in argon also involved as well. It can be seen that the embrittlement phenomenon clearly appeared in a temperature range from 300 ˚C to 400 ˚C. The tensile curves of the specimens tested in this temperature range (300 ˚C to 400 ˚C) show fast failure of specimens just after necking started, which suggests that the LBE promoted the crack propagation. Although the total elongation was significantly reduced for these specimens, their yield and ultimate tensile strength were not affected.

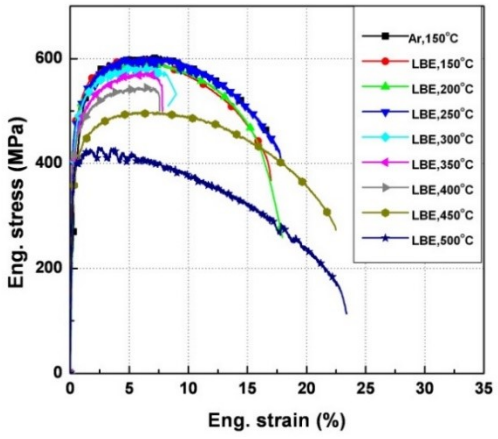

FIG. 29 Tensile stress-strain curves of selected T91 steel specimens tested in liquid LBE at different temperatures. For comparing, specimen tested in argon at 150oC also presents in this figure. Tests conditions: in LBE, ε̇=1x10-5s-1.

The typical morphologies of embrittled specimens after tested in LBE are showed in Fig. 30. For comparing, specimens without embrittlement are also presented in this figure. It can be seen clearly that specimens tested in LBE in the temperature range of 300-400 ˚C showed a very clear brittle rupture feature, there was just little necking before the specimen broken. While, when the test temperature is higher than 450 ˚C, specimens broke after fully necking and exhibited ductile feature. It means ductility get recovered.

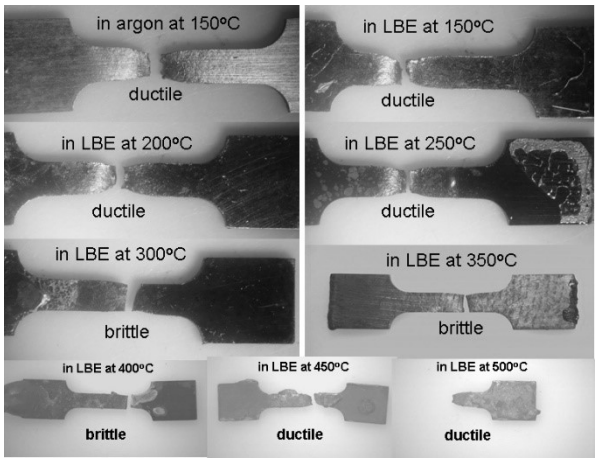

FIG. 30. The morphologies of T91 specimens after tested both in argon and LBE. In the temperature range of 150 to 250 ˚C in LBE, specimens show ductile brittle as it tested in argon; in the temperature range of 300 to 400 ˚C, LME observed; T ≥ 450 ˚C, ductility get recovered.

The SEM observations were performed on some broken specimens to identify the fracture mode. The examination indicated that fracture mode of specimens tested in Ar at all temperatures was ductile. Fracture of T91 steel in argon occurs by nucleation and growth of equiaxed micro-voids, presumably associated with intermetallic precipitates and inclusions. A typical fractograph illustrating dimpled rupture is shown in Fig. 31a.

The fracture surfaces of the specimens tested in LBE, which illustrated the embrittlement effect, showed generally brittle fracture, as can be seen from Fig. 31 b and c. The fractographies were changed, the dimples disappeared, fracture surfaces exhibited as flat facets. The fracture path is propagating along the martensitic lath boundaries.

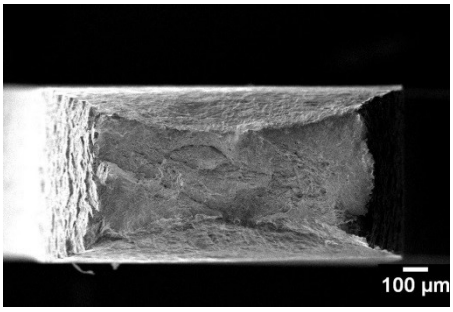

a. in Ar at 300 °C

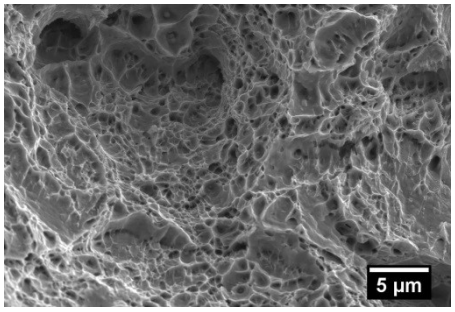

in Ar at 300 °C

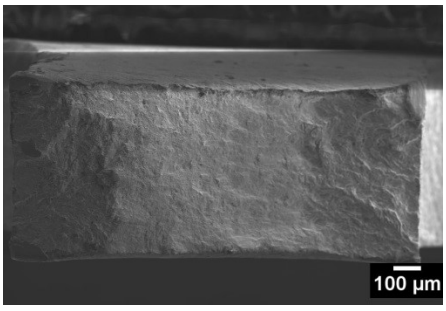

b. in LBE at 300 °C

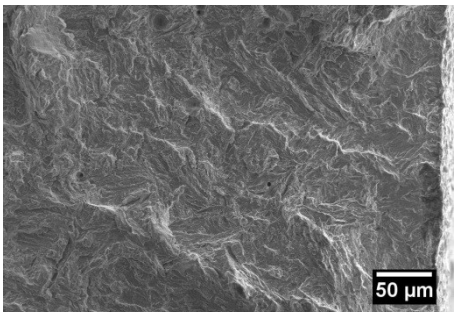

in LBE at 300 °C

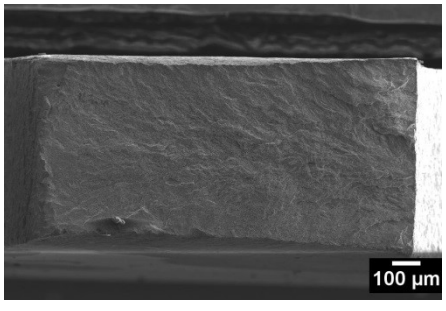

c. in LBE at 400 °C

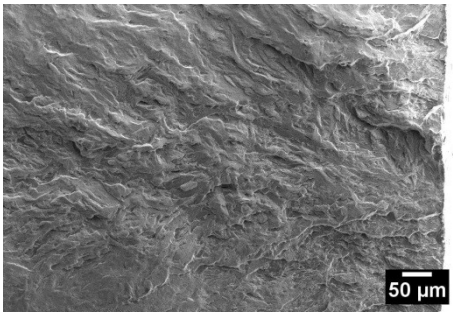

in LBE at 400 °C

FIG. 31. SEM on fracture surfaces of specimens after SSRT tests both in Ar and LBE at different test temperatures with strain rate of $1x10^{-5}s^{-1}$

6.3. **Summary**

Fig. 32 is a summary on the tendency of the total elongation versus the test temperature. It shows the on-set of ductile trough for the T91 steel is around 300 ˚C, while when temperature is increased to 450 ˚C, the ductility of specimen gets recovered. It indicated that the T91 FM steel may exhibit LBE embrittlement in the temperature range of 300 to 425 ˚C. In this temperature range, the ductility of the T91 steel can be drastically reduced from 15% down to less than 5%. Meanwhile, the fracture mode changes from ductile micro void coalescence in inert Ar environment to brittle trans granular cleavage in liquid LBE environment. The obtained results well-define a “ductility trough” for the FM steel – liquid LBE system.

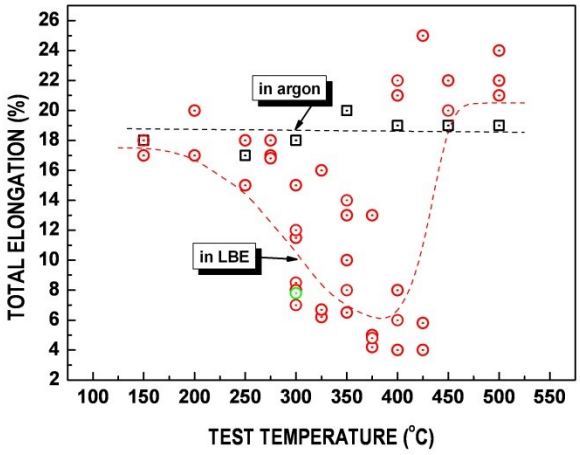

FIG. 32. Total elongation versus testing temperature for T91 steel tested in argon and in LBE.

7. CONCLUSIONS

- In order to meet the requirements of structural materials for CiADS and LBE-cold fast reactor, a series of LBE devices and platforms have been established for compatibility studies between LBE and structural materials and thermal hydraulic experiments.
- Preliminary test results show that austenitic stainless-steel exhibits better corrosion resistance under 400 ˚C in liquid LBE environment, while FM T91 steel exhibits slightly better corrosion resistance comparing with austenitic stainless steel, and it has excellent resistance to lead and bismuth corrosion below 550 ˚C.
- The embrittlement effect induced by liquid metal, namely LME, should be considered in the application of T91 steel. Our experimental results give the "ductility trough" of T91 steel in LBE environment.
- With the improvement of design parameters of CiADS and LBE-cold fast reactor, the existing materials cannot meet the requirements of the system and equipment for their corrosion resistance. Therefore, the following studies are suggested:
  1) R&D on new structural materials with resistant to LBE corrosion and neutron irradiation damage;
  2) R&D on anti-corrosion coating technology on structural materials with resistant to irradiation damage;
  3) Study on OCS of LBE for industrial application

ACKNOWLEDGMENTS

The authors wish to acknowledge the continuous support of the Ministry of Science and Technology with name of 973 projects, to acknowledge Chinese Academy of Sciences for the support by the Strategic Leading Scientific Research Program. We thank the Institute of modern physics of CAS for its cooperation. The authors also thank Dr. Peter Hosemann for his revision of this paper.

REFERENCES

[1] CINOTTI, L., B. GIRAUD (2004). Journal of Nuclear Materials 335(2): 148-155.

[2] WAGNER, W., DAI, Y. (2007). Journal of Nuclear Materials 361(2-3): 274-281.

[3] Yuji Kurata, Masatoshi Futakawa, Shigeru Saito, Journal of Nuclear Materials 373 (2008) 164-178.

[4] YACHMENYOV, G.S., RUSANOV, A.YE., GROMOV, B.F., BELOMYTSEV, YU. S., SKVORTSOV, N.S., DEMISHONKOV, A.P. Proceedings of Heavy Liquid Metal Coolants in Nuclear Technology, HLMC'98, October 5–9, 1998, Obninsk, Russia, 1999, p. 133.

[5] BENAMATI, G., FAZIO, C., PIANKOVA, H., RUSANOV, A., Journal of Nuclear Materials. 301 (2002) 23.

[6] AIELLO, A., AZZATI, M., BENAMATI, G., GESSI, A., LONG, B., SCADDOZZO, G., Journal of Nuclear Materials 335 (2004) 169.

[7] LONG, B., DAI, Y., BALUC, N., Journal of Nuclear Materials, Volume 431, Issues 1–3, December 2012, Pages 85-90.

[8] LONG, B., DAI, Y., Journal of Nuclear Materials, 376 (2008) 341-345

[9] GONG X, MARMY P, QIN L, ET AL. Journal of Nuclear Materials, 2016, 468:289-298.

[10] FEYZAN Ö. E., GAVRILOV S, VERBEKEN K. Journal of Nuclear Materials, 2016, 472:171-1

Appendix

MEETING PROGRAMME

A.1. MEETING ORGANIZATION

General Chair	Elena Daniela GUGIU
Scientific Secretaries	Vladimir Kriventsev Chirayu Batra

A.2. METING SESSIONS

The contributions to the meeting are classified into three major areas, and the meeting was divided into following three session:

Session I: HLM Compatibility with Structural Materials: Phenomena, Modelling and Operational experience (Kamil Tucek)

Paper ID	Title	Presenter	Country	Org
3	Kinetics and Mechanism of Crack Initiation of Liquid Metal Embrittlement	Ms Anna Hojna	Czech Republic	CV REZ
6	RATEN ICN Status on Mechanical Properties Investigation of 316L Generation IV Candidate Material	Mr Alexandru Nitu	Romania	RATEN ICN
7	Simulations of some Structural Materials Behavior under Neutron Irradiation	Ms Elena Daniela Gugiu	Romania	RATEN ICN
11	Vacancy Type Defects Behavior in Materials Foreseen for Liquid Metal Cooled Fast Reactors	Mr Vladimir Slugen	Slovakia	Slovak Univ. of Technology
12	Research of Corrosion Behavior of Steam Generator Tubes for Lead-cooled Power Unit	Mr Kirill Shutko	Russia	NIKIET
18	Tensile Testing of Sub-sized T91 Steel Specimens in Liquid Lead	Mr Kamil Tucek	EC	JRC

Session II: Corrosion Mitigation Measures: Coating, New Structural Materials, Environmental Conditioning (Peter Szakalos, Alfons Weisenburger)

Paper ID	Title	Presenter	Country	Org
1	Corrosion Behaviours of Austenitic Steel and Ferritic Steel in LBE with Oxygen Controlled Conditions	Mr Bo Qin	China	CIAE
13	Corrosion and Mechanical Testing of a Low Alloyed Alumina Forming Austenite for Liquid Lead Applications	Mr Peter Dömstedt	Sweden	KTH
14	Alumina Nanoceramic Coatings: An Enabling Technology for Heavy Liquid Metal-Cooled Fast Reactors	Mr Fabio Di Fonzo Mr Matteo Vanazzi	Italy	CNCT
8	Evaluation of the High-entropy Cr-Fe-Mn-Ni Alloys Compatibility with a Liquid Lead Coolant	Mr Viktor Voyevodin	Ukraine	KIPT
19	Design and Material Selection for Leak-before Break Nature of Double Walled Once Through Steam Generators in Lead-Bismuth Cooled Fast Reactors	Mr Jung Hwan Lee	Republic of Korea	UNIST
20	Compatibility Evaluation on Structural Materials for Clear in Oxygen Controlled Lead-Bismuth Eutectic at 500 °C and 550 °C	Mr Zhizhong Jiang	China	INEST
21	Development of Alumina Forming Materials for Corrosion Mitigation in Heavy Liquid Metal Cooled Nuclear Reactors	Mr Alfons Weisenburger	Germany	KIT
22	Corrosion of Steel Claddings of Fast Reactors Fuel Elements in the Interaction with Uranium-Plutonium Nitride Fuel	Mr Alexander Ivanov	Russia	Kurchatov Institute

Session III: Qualification Programmes of Structural Materials for HLM Fast Reactors (Bin Long, Erich Stergar)

Paper ID	Title	Presenter	Country	Org
10	Qualification programme of candidate materials for ALFRED	Ms Serena Bassini	Italy	ENEA
16	Some new R&D focuse in structure materials licensing for the SVBR-100 reactor facilities	Mr Alexander Dedul	Russia	AKME-Engineering
2	Status of HLMC technology and related research in China Institute of Atomic Energy	Mr Bin Long	China	China Institute of Atomic Energy

A.3. GROUP DISCUSSIONS

Group Discussion	*Title*	*Chair*
Group Discussion I	Outstanding Research Challenges	Kamil Tucek Matteo Vanazzi
Group Discussion II	New Materials and Coating Techniques	Peter Szakalos Alfons Weisenburger
Group Discussion III	Industrialization	Erich Stergar

LIST OF PARTICIPANTS

BELGIUM

Stergar, E.	SCK•CEN
Gendebien, A.	Bel V

CHINA

Long, B.	China Institute of Atomic Energy (CIAE)
Qui, B.	China Institute of Atomic Energy (CIAE)
Fu, X.	China Institute of Atomic Energy (CIAE)
Qian, Y.	China Institute of Atomic Energy (CIAE)
Wang, Z.	Institue of Modern Physics, Chinese Academy of Sciences (IMP CAS)
Jiang, Z.	Institute of Nuclear Energy Safety Technology, Chinese Academy of Science (INEST CAS)
Zhao, X.	China Nuclear Power Technology Research Institute

CZECH REPUBLIC

Rozumova, L.	Centrum výzkumu Rez s. r. o.
Kosek, L.	Centrum výzkumu Rez s. r. o.
Hojna, A.	Centrum výzkumu Rez s. r. o.

EUROPEAN COMMISSION

Tucek, K.	Joint Research Centre, European Commission (EC/JRC)

GERMANY

Weisenburger, A.	Karlsruher Institut für Technologie, (KIT)

ITALY

Bassini, S.	ENEA FSN-ING
Angiolini, M.E.	ENEA FSN-ING
Di Fonzo, F.	Center for Nano Science and Technology
Vanazzi, M.	Center for Nano Science and Technology

REPUBLIC OF KOREA

Kim, J.H.	Ulsan National Institute of Science and Technology (UNIST)
Lee, J.H.	Ulsan National Institute of Science and Technology (UNIST)
Lee, J.	Ulsan National Institute of Science and Technology (UNIST)
Hwang, I. S.	Ulsan National Institute of Science and Technology (UNIST)
Noh, S.	Korea Atomic Energy Research Institute (KAERI)

LUXEMBOURG

Cinotti, L.	Hydromine Nuclear Energy Sàrl

ROMANIA

Nitu, A.	Technologies for Nuclear Energy State Owned Company - Institute for Nuclear Research
Gugiu, D.	Technologies for Nuclear Energy State Owned Company - Institute for Nuclear Research

RUSSIAN FEDERATION

Kondaurov, A.	JSC “AKME-engineering”
Dedul, A.	JSC “AKME-engineering”
Komlev, O.	JSC “AKME-engineering”
Shutko, K.	NIKIET JSC
Ivanov, A.	NRC “Kurchatov Institute”

SLOVAKIA

Slugen, V.	Institute of Nuclear and Physical Engineering, Slovak University of Technology

SWEDEN

Dömstedt, P.	Royal Institute of Technology (KTH)
Szakalos, P.	Royal Institute of Technology (KTH)

UNITED KINGDOM

Green, R.	Office for Nuclear Regulation

UKRAINE

Voyevodin, V.	National Science Center “Kharkiv Institute of Physics and Technology”

IAEA

Kriventsev, V.	International Atomic Energy Agency (IAEA)
Batra, C.	International Atomic Energy Agency (IAEA)
Monti, S.	International Atomic Energy Agency (IAEA)
Veshchunov, M.	International Atomic Energy Agency (IAEA)
Tung Nguyen, D. C.	International Atomic Energy Agency (IAEA)

CONTRIBUTORS TO DRAFTING AND REVIEW

Angiolini, M.E.	ENEA FSN-ING
Bassini, S.	ENEA FSN-ING
Batra, C.	International Atomic Energy Agency
Cinotti, L.	Hydromine Nuclear Energy Sàrl
Dedul, A.	JSC “AKME-engineering”
Di Fonzo, F.	Center for Nano Science and Technology
Dömstedt, P.	KTH, Royal Institute of Technology
Fu, X.	China Institute of Atomic Energy
Gendebien, A.	Bel V
Green, R.	Office for Nuclear Regulation
Gugiu, D.	Technologies for Nuclear Energy State Owned - Institute for Nuclear Research
Hojna, A.	Centrum výzkumu Rez s. r. o.
Hwang, I. S.	Ulsan National Institute of Science and Technology
Ivanov, A.	NRC “Kurchatov Institute”
Jiang, Z.	Institute of Nuclear Energy Safety Technology
Kim, J. H.	Ulsan National Institute of Science and Technology
Kim, K. S.	International Atomic Energy Agency
Komlev, O.	JSC “AKME-engineering”
Kondaurov, A.	JSC “AKME-engineering”
Kosek, L.	Centrum výzkumu Rez s. r. o.
Kriventsev, V.	International Atomic Energy Agency
Lee, J.	Ulsan National Institute of Science and Technology
Lee, J.H.	Ulsan National Institute of Science and Technology
Long, B.	China Institute of Atomic Energy
Mahanes, J.	International Atomic Energy Agency

Nitu, A.	Technologies for Nuclear Energy State Owned- Institute for Nuclear Research
Noh, S.	Korea Atomic Energy Research Institute
Qian, Y.	China Institute of Atomic Energy
Qui, B.	China Institute of Atomic Energy
Rozumova, L.	Centrum výzkumu Rez s. r. o.
Shutko, K.	NIKIET JSC
Slugen, V.	Institute of Nuclear and Physical Engineering, Slovak University of Technology
Stergar, E.	SCK•CEN
Szakalos, P.	KTH, Royal Institute of Technology
Tucek, K.	Joint Research Centre, European Commission
Tung Nguyen, D. C.	International Atomic Energy Agency
Vanazzi, M.	Center for Nano Science and Technology
Veshchunov, M.	International Atomic Energy Agency
Voyevodin, V.	National Science Center "Kharkiv Institute of Physics and Technology"
Wang, Z.	Institue of Modern Physics, Chinese Academy of Sciences
Weisenburger, A.	Karlsruher Institut für Technologie, Institute for Pulsed Power and Microwave Technology
Zeman, M.	International Atomic Energy Agency
Zhao, X.	China Nuclear Power Technology Research Institute

Consultants Meeting
Vienna, Austria: 12–13 June 2019

IAEA
International Atomic Energy Agency

No. 26

ORDERING LOCALLY

IAEA priced publications may be purchased from the sources listed below or from major local booksellers.

Orders for unpriced publications should be made directly to the IAEA. The contact details are given at the end of this list.

NORTH AMERICA

Bernan / Rowman & Littlefield

15250 NBN Way, Blue Ridge Summit, PA 17214, USA
Telephone: +1 800 462 6420 • Fax: +1 800 338 4550

Email: orders@rowman.com • Web site: www.rowman.com/bernan

REST OF WORLD

Please contact your preferred local supplier, or our lead distributor:

Eurospan Group

Gray's Inn House
127 Clerkenwell Road
London EC1R 5DB
United Kingdom

Trade orders and enquiries:

Telephone: +44 (0)176 760 4972 • Fax: +44 (0)176 760 1640
Email: eurospan@turpin-distribution.com

Individual orders:

www.eurospanbookstore.com/iaea

For further information:

Telephone: +44 (0)207 240 0856 • Fax: +44 (0)207 379 0609
Email: info@eurospangroup.com • Web site: www.eurospangroup.com

Orders for both priced and unpriced publications may be addressed directly to:

Marketing and Sales Unit
International Atomic Energy Agency
Vienna International Centre, PO Box 100, 1400 Vienna, Austria
Telephone: +43 1 2600 22529 or 22530 • Fax: +43 1 26007 22529
Email: sales.publications@iaea.org • Web site: www.iaea.org/publications

International Atomic Energy Agency
Vienna